DOI: 10.18154/RWTH-2021-02093

Aachener Verfahrenstechnik

RWTH AACHEN UNIVERSITY

Continuous Flow-Electrode Capacitive Deionization

Alexandra Rommerskirchen

Aachener Verfahrenstechnik Series
AVT.CVT – Chemical Process Engineering
Volume 12 (2021)

Alexandra Klara Elisabeth Rommerskirchen

# Continuous Flow-Electrode Capacitive Deionization

# Continuous Flow-Electrode Capacitive Deionization

## Kontinuierliche fließ-kapazitive Deionisierung

Von der Fakultät für Maschinenwesen der Rheinisch-Westfälischen Technischen Hochschule Aachen zur Erlangung des akademischen Grades einer Doktorin der Ingenieurwissenschaften genehmigte Dissertation

vorgelegt von

Alexandra Klara Elisabeth Rommerskirchen

Berichter:
Univ.-Prof. Dr.-Ing. Matthias Wessling
apl. Prof. Dr.-Ing. Matthias Franzreb

Tag der mündlichen Prüfung: 17.09.2020

Diese Dissertation ist auf den Internetseiten der Universitätsbibliothek online verfügbar.

**Titel:** Continuous Flow-Electrode Capacitive Deionization
Kontinuierliche fließ-kapazitive Deionisierung

**Autor:** Alexandra K. E. Rommerskirchen

**Reihe:** Aachener Verfahrenstechnik Series
AVT.CVT - Chemical Process Engineering
Volume: 12 (2021)

**Herausgeber:** Aachener Verfahrenstechnik Series
Forckenbeckstraße 51
52074 Aachen
Tel.: +49 (0)241 8097717
Fax.: +49 (0)241 8092326
E-Mail: secretary.cvt@avt.rwth-aachen.de
http://www.avt.rwth-aachen.de/AVT

**DOI:** 10.18154/RWTH-2021-02093

To

My family

My guides along the way

# Acknowledgements

Mit dem Abschluss dieser Arbeit neigt sich für mich ein Lebensabschnitt dem Ende zu. Die letzten Jahre bedeuten mir sehr viel. Ich habe mich persönlich weiterentwickelt, konnte viele fachliche Erfahrungen sammeln und hatte große Freude an einem so spannenden Thema zu arbeiten. Den Abschluss dieser Arbeit habe ich der Unterstützung vieler zu verdanken.

Mein besonderer Dank gilt meinem Doktorvater, Prof. Dr.-Ing. Matthias Wessling. Ich danke ihm sehr für die Möglichkeit, an diesem Thema forschen zu dürfen, und die Freiheiten, diverse Ideen zu verfolgen, von denen ein Teil in dieser Dissertation festgehalten ist. Ich bin froh und stolz darauf, dass ich Teil seines Teams sein durfte, in dem Teamgeist und Kooperation so wertgeschätzt wird.

Ein herzliches Dankeschön möchte ich auch an Prof. Dr.-Ing. Matthias Franzreb aussprechen. Ich danke ihm sowohl für die Begutachtung meiner Arbeit als Koreferent, als auch für die vorangegangene Zusammenarbeit im BMBF-Kooperationsprojekt ElektroWirbel. Durch seine gezielten Fragen hat er mich das ein oder andere Mal zum Nachdenken gebracht und einen wertvollen Beitrag zu dieser Arbeit geleistet.

A sincere thank you to Dr. Youri Gendel, who had the original idea to pursuit this topic in Aachen. I am grateful for the opportunity to work on this topic, and thank him for the many fruitful discussions, brainstorming sessions and lab sessions over the years, and the following successful collaboration.

Ich danke dem Bundesministerium für Bildung und Forschung (BMBF) für die finanzielle Unterstützung im Rahmen des Kooperationsprojektes *ElektroWirbel* und des BMBF-MOST Kooperationsprojektes *SepIon*. Vielen Dank an alle Projektpartner aus Industrie und Wissenschaft, die an diesen Projekten mitgewirkt haben. Vielen Dank für die regen fachlichen Diskussionen und das kritische Hinterfragen. Gerade diese Fragen sind es doch, die die Forschung besonders voranbringen und die besten Ideen hervorbringen. Besonders hervorheben möchte ich hier die Beiträge von Yuliya Schießer, Matthias Woyciechowski und Thomas Klicpera im Rahmen des Projektes *ElektroWirbel*.

Thank you to all the members of the scientific community, especially in the field of membrane technology and capacitive deionization, whom I have been in contact with over the years. Thank you for all the critical questions and scientific discussions, which have been a great driver for my research. I have greatly enjoyed the exchange during conferences and other meetings.

Vielen Dank an Susanne Offermann für die Hilfsbereitschaft, das große Engagement und die Unterstützung während meiner gesamten Zeit am Lehrstuhl und der Promotion.

Ich danke den Teams der mechanischen und elektronischen Werkstätten der AVT, vor allem Heinz-Jürgen Bouge, Jacek Schmidt, Joachim Schornstein, Herbert Thelen und Florian Metzler. Auch phantasievolle Zelldesigns und Bestellungen einer größere Anzahl an Bauteilen für FCDI Zellen wurden durch die mechanische Werkstatt immer zeitnah in fertige Bauteile umgesetzt und haben so diese Arbeit erst ermöglicht. Vielen Dank den Mitarbeitern der mechanischen Werkstatt des DWI für die häufig kurzfristige Unterstützung bei kleineren oder größeren "mechanischen Notlagen".

Vielen Dank an die Analytiklabore der AVT und des DWI für die Durchführung, die

Beratung und die Unterstützung bei zahlreichen durchgeführten Laboranalysen. Besonders danken möchte ich Sandra Gelbach, Sybille Hanisch, Gerd Spalding und Karin Faensen.

Vielen Dank an Markus Reichelt und Timo Linzenmeier für die Unterstützung im DWI Erdgeschoss Labor.

Mein Dank gilt den unermüdlichen Teams des Einkaufs, des Controllings, der Buchhaltung und der Personalabteilung des DWI. Besonders danke ich Hans Hamacher, Corinna Steimel und für die jahrelange Unterstützung. Ohne die Verwaltung der Projekte, Beschaffung von Materialien, Einstellung von wissenschaftlichen Hilfskräften und so weiter wäre wohl kaum ein Forschungsprojekt durchzuführen. Mein Dank gilt außerdem den Teams der IT und Buchhaltung der AVT für die Unterstützung.

Vielen Dank an alle Kolleginnen und Kollegen an der CVT, die mir in besonderer Erinnerung bleiben werden. Die vielen gemeinschaftlich verbrachten Stunden, sowie die regen fachlichen Diskussionen, werden mir immer in Erinnerung bleiben. Mein besonderer Dank geht an Christian Linnartz, Anna Kalde, Dana Kaubitzsch, Hannah Roth, Michael Alders, Korcan Percin, Florian Roghmans, Robert Sengpiel, Robert Femmer, Burkhard Ohs, Johannes Lohaus, Sebastian Bannwarth, Serafin Stiefel, Benedikt Aumeier, Theresa Rösener, Tao Luo, Tim Femmer, Suzana Djeljadini, Daniel Felder, Sarah Armbruster, Elizaveta Evdochenko und Stefanie Kriescher. Vielen Dank an Süleyman Yüce für den regelmäßigen Input und die fachlichen Diskussionen. A sincere thank you to Oana David for the fruitful discussions during lab sessions. Many thanks to Woyciech Ogieglo and Oded Nir for the scientific discussions during the time as office colleagues.

Ein herzliches Dankeschön an alle Studentinnen, Studenten und Hiwis, mit denen ich zusammenarbeiten durfte. Deren Engagement hat einen essentiellen Beitrag zu dieser Arbeit geleistet. Abgesehen davon, hat mir die Zusammenarbeit und Betreuung immer sehr viel Freude bereitet. Auf die hervorragende Kollaboration und das tolle Arbeitsklima im "Team FCDI" bin ich besonders stolz und ich hoffe, dass alle Beteiligten diese Zeit in genauso guter Erinnerung behalten werden wie ich. Mein besonderer Dank für die Arbeiten und Vorarbeiten, die schlussendlich diese Arbeit ermöglicht haben, gilt vor allem: Franziska Egidi, Sefkan Kendir, Leon Bongers, Jonas Rabe, Marc Decker, Lisa Willenberg, Karl Hepp, Philippe Brasseur, Florian Wiesner, Jingyu Xie, Nora Grütering, Daniel Müller, Faras Brumand-Poor, Yannik Fels, Jan Keil, Kristina Heesen, Nadine Schmidt, Martin Steinbach, Christopher Sauer, Nora Heinrich, Nils Weber, Zhaowei Zou, Max Düppenbecker, Yue Pan, Christian Kneppeck, Francesco Scalogna, Niklas Köller, Michael Wirz, Rachel Krupp und Marilyn Padua.

Mein ganz besonderer Dank gilt meiner Familie. Meinen Eltern, Peter und Petra, und meinem Bruder, Matthias. Ihr habt mich zu dem Menschen gemacht, der ich bin und habt mich immer unterstützt. Thank you to my family in India for the support over the years and especially for supporting me during the last days while finishing this thesis. Zu guter Letzt mein herzliches Dankeschön an meinen Mann Enoch, mit dem ich inzwischen schon so viele Jahre den Lebensweg gemeinsam beschreite, der mich unentwegt unterstützt und ermuntert.

# Abstract

Flow-electrode capacitive deionization (FCDI) is a relatively young technology, which is promising for the desalination of and salt recovery from aqueous solutions with a wide range of salinities. FCDI is related to electrodialysis and capacitive deionization processes, and profits from existing literature and ongoing research regarding these technologies. However, the combination of ion-exchange membranes with capacitive flow electrodes, also termed slurry electrodes, leads to complex interactions and especially the physico-chemical mechanisms within capacitive flow electrodes are not yet fully understood.

This thesis discusses the state of the art of FCDI and related technologies and, based on this, presents experimental and theoretical studies, which advance the field of FCDI. Topics investigated in this thesis range from the investigation of (1) fundamental mechanisms, such as the charge transfer in carbon flow electrodes, over the (2) module and process design, culminating in the presentation of (3) a newly developed, improved process model, which can facilitate the further advancement of FCDI processes on all scales from membrane materials to system design. The overall focus of this thesis lies on the application of FCDI for the treatment of high salinity solutions.

# Kurzfassung

Die fließ-kapazitive Deionisierung (FCDI) ist eine recht junge Technologie, welche vielversprechend für die Entsalzung von und Salzrückgewinnung aus hochkonzentrierten, wässrigen Salzlösungen ist. FCDI ist verwandt mit Elektrodialyse- und kapazitiven Deionisierungsprozessen. Sie profitiert von vorhandener Literatur und laufender Forschung bezüglich dieser Technologien. Die Kombination von Ionenaustauschermembranen mit kapazitiven, fließfähigen Elektroden, auch Slurry-Elektroden genannt, führt jedoch zu komplexen Interaktionen. Vor allem die physikalisch-chemischen Vorgänge in solchen fließfähigen Elektroden sind noch nicht abschliessend verstanden.

Diese Arbeit diskutiert den aktuellen Stand der Technik von FCDI und verwandten Technologien. Basierend darauf werden experimentelle und theoretische Studien präsentiert, welche das Verständnis der Technologie voranbringen. Hauptthemen dieser Arbeit spannen von der Untersuchung (1) fundamentaler Mechanismen, z.B. dem Ladungstransfer in fließfähigen Elektroden, über (2) Modul- und Prozessdesign, bis hin zu der Beschreibung eines (3) neu entwickelten, verbesserten Prozessmodells für kontinuierliche FCDI Prozesse, welches die gezielte Weiterentwicklung von FCDI Technologien auf allen Größenskalen fördern kann, vom Membranmaterial zum Systemdesign. Der generelle Fokus dieser Arbeit liegt auf der Anwendung von FCDI zur Behandlung konzentrierter Salzlösungen.

# Previous publications and student theses

Parts of this thesis have been published preliminary in form of the research articles listed in the following. Text passages from these articles have been adopted for this thesis. Large parts of Chapters 4 and 5 have been published previously, as mentioned at the beginning of the respective chapters. By now, parts of Chapter 7 and 8 have also been been published.

- [Rom2015] Alexandra Rommerskirchen, Youri Gendel and Matthias Wessling. "Single module flow-electrode capacitive deionization for continuous water desalination" in: *Electrochemistry Communications* 60 (2015), pp. 34-37. https://doi.org/10.1016/j.elecom.2015.07.018
- [Rom2018a] Alexandra Rommerskirchen, Christian J. Linnartz, Daniel Müller, Lisa Kathrin Willenberg and Matthias Wessling. "Energy Recovery and Process Design in Continuous Flow-Electrode Capacitive Deionization Processes" in: *ACS Sustainable Chemistry & Engineering* 6/10 (2018), pp. 13007-13015. https://doi.org/10.1021/acssuschemeng.8b02466
- [Rom2018b] Alexandra Rommerskirchen, Burkhard Ohs, Karl Arturo Hepp, Robert Femmer and Matthias Wessling. "Modeling continuous flow electrode capacitive deionization processes with ion-exchange membranes" in: *Journal of Membrane Science* 546 (2018), pp. 188 - 196. https://doi.org/10.1016/j.memsci.2017.10.026
- [Rom2019] Alexandra Rommerskirchen, Anna Kalde, Christian J. Linnartz, Leon Bongers, Georg Linz and Matthias Wessling. "Unraveling charge transport in carbon flow electrodes: Performance prediction for desalination applications" in: *Carbon* 145 (2019), pp. 507-520. https://doi.org/10.1016/j.carbon.2019.01.053
- Alexandra Rommerskirchen, Christian J. Linnartz, Franziska Egidi, Sefkan Kendir and Matthias Wessling. "Flow-electrode capacitive deionization enables continuous and energy-efficient brine concentration" in: *Desalination* 490 (2020) 114453. https://doi.org/10.1016/j.desal.2020.114453
- Alexandra Rommerskirchen, Michael Alders, Florian Wiesner, Christian J. Linnartz, Anna Kalde and Matthias Wessling. "Process model for high salinity flow-electrode capacitive deionization processes with ion-exchange membranes" In: *Journal of Membrane Science* 616 (2020) 118614. https://doi.org/10.1016/j.memsci.2020.118614

Some of the experiments and a preliminary version of the process model presented in Chapter 8 are based on work presented and conducted in the following student theses:

- Franziska Egidi, Master thesis, 27th March 2019, Module and process design of flow-electrode capacitive deionization processes (FCDI) for salt recovery.
- Florian Wiesner, Bachelor thesis, 20th December 2018, Modeling of a flow-electrode capacitive deionization process.
- Yannick R. Fels, Research internship, 21st November 2018, Investigation of the current-voltage behavior in electrodialysis applications for water desalination.
- Sefkan Kendir, Master thesis, 06th August 2018, Application of capacitive flow electrodes and their influence on electrically driven salt recovery.
- Leon Bongers, Master thesis, 23rd March 2018, Charge percolation in flow-electrode capacitive deionization for process water treatment.
- Daniel Müller, Bachelor thesis, 30th September 2016, Development of an energy efficient system for continuous water desalination via flow-electrode capacitive deionization.
- Lisa K. Willenberg née Becker, Master thesis, 21st April 2016, Investigation and development of regeneration methods with integrated energy recovery in continuous flow-electrode capacitive deionization (FCDI).
- Karl A. Hepp, Master thesis, 16th December 2015, Modeling flow-electrode capacitive deionization.

# Contents

# 1

# Introduction and motivation

Water is the basis for life on earth. Water is also essential for many processes-domestic, agricultural, industrial. Energy efficient, reliable and economical water desalination and water treatment processes are required to face today's and tomorrow's water-related challenges. Such processes already exist for many applications. For other applications, however, there are no energy efficient, reliable and economical solutions available yet. In many cases, available solutions still have room for improvements [Eli2011; And2010; Por2013].

Significant attention has been focused on capacitive deionization (CDI) technologies in the last decade. In CDI processes, an applied electrochemical potential gradient leads to the transport of dissolved ions towards the oppositely charged electrodes. The ions are then bound within the electrode material via electrostatic adsorption of ions in the electrical double layer formed at the electrode-solution interface. High surface areas, and hence high ion adsorption capacities, are usually achieved by employing solid, porous carbon electrodes [Por2013].

CDI processes can be operated in a variety of configurations. A widely-applied configuration is the operation in flow-by mode using static film electrodes. However, various new configurations have been proposed including flow-through electrodes [Sus2012] and wire-shaped electrodes [Por2012]. Ion-exchange membranes (IEM) can improve the performance of CDI processes regarding their desalination performance and energy efficiency, when placed in between electrodes and treated solution. These beneficial properties of membrane capacitive deionization (MCDI) processes result from the ion-exchange membrane's ability to efficiently block the back-diffusion of coions into the water channel, especially at low salinities [Por2013; Sus2015].

Apart from the configuration, many studies aim at improving the performance of CDI processes by improving the applied electrode materials. While most CDI processes are based on static carbon-based electrodes, several studies in the recent years also investigated the possibility of so-called pseudo-capacitive electrodes to increase the salt adsorption capacity. All static, solid electrodes, however, are fixed in place and are saturated with ions with increasing operation time. Consequently, the electrodes need to be regenerated in a desorption step. Therefore, CDI and MCDI processes are usually operated discontinuously

in charge-discharge cycles, and their practical applicability is limited to relatively low salinities [Ore2008; And2010; Por2013; Sus2015; AlM2014].

Flow-electrode capacitive deionization (FCDI) [Jeo2013], on the other hand, is based on flow electrodes. In case of FCDI, the flow electrodes, also termed slurry electrodes, usually consist of carbon particles suspended in an aqueous electrolyte solution. Flow electrodes are pumpable and can be regenerated in a separate module or compartment, which enables a fully continuous operation, as demonstrated by our work group in a two-module configuration [Gen2014] and single-module configuration [Rom2015], and by Doornbusch et al. in a sedimentation configuration [Doo2016]. In these configurations, the electrodes are continuously regenerated and a diluate and concentrate is produced continuously with more or less constant salt concentrations.

All in all, the high salt adsorption capacities [Sus2015; Gen2014; Sha2016], good desalination performance, the ability to desalinate high salinity solutions [Jeo2013], and the possibility of fully continuous operation [Gen2014; Rom2015; Doo2016] makes FCDI a promising technology. Thus, FCDI is a growing research field [Hat2015a]. Next to process configuration studies, several groups investigated the influence of coated or otherwise modified carbon materials on the performance of FCDI processes [Hat2015b; Xu2017]. Recently, a study regarding Faradaic reactions in FCDI electrodes was published [Nat2017].

Based on the characteristics of FCDI, four potential application areas seem adequate: (1) desalination of higher salinity brackish water, (2) brine treatment, (3) treatment of water streams with a high fouling and scaling potential (e.g. food industry, similar to ED [Str2010]) and (4) "special" applications such as salt metathesis [Lin2017] or (selective) removal of specific ionic species other than sodium chloride [Zha2018b].

This thesis focuses on the treatment of high salinity solutions (brines) using FCDI processes. The findings can, of course, be transferred to other potential application areas of FCDI processes. Next to the exploration of the practical potential of continuous flow-electrode capacitive deionization (FCDI) processes, the fundamental principles governing their performance are investigated.

Relevant information on state-of-the-art technologies and the theoretical background is given in Chapter 2. Based on this, an overview of the topics and aims of the following chapters and this thesis in general is given in Chapter 3.

# 2

# Background and fundamentals

## 2.1. Water desalination and brine concentration technologies

Water treatment processes can be aimed at a range of applications, such as the production of drinking water, the treatment of wastewater effluents, water desalination, water softening, and the pre- and post-treatment of industrial water streams. This includes domestic, agricultural, industrial and mining application areas. Hence, the requirements of a water treatment facility and the available types of water treatment processes are manifold and depend on the specific application. In the following, a short overview of available technologies is given, which does not aim at being complete: a range of good application-specific reviews and research articles exist for further study by the interested reader [Eli2011; Thi2015; Al-2013; Sha2013; Por2013].

Desalination and water treatment technologies can be categorized in different ways. Often, these processes are categorized by their main driving force or main characteristics. In the following, these processes are categorized into: (1) Temperature- and pressure-driven distillation processes, (2) (osmotic) pressure-driven membrane processes, and (3) ion-exchange and electrically driven processes.

### 2.1.1. Temperature- and pressure-driven distillation processes

The main temperature- and pressure-driven processes are multi-stage flash evaporation (MSF), multi-effect distillation (MED), and thermal and mechanical vapor compression (TVC/MVC) [Al-2013; Fri2007].

**Multi-stage flash evaporation (MSF).** In multi-stage flash evaporation units, heated seawater is flash evaporated in a series of stages with succesively lower temperature and pressure. The brine remains, while the evaporated water is condensed at heat exchangers. Fresh seawater flows through the heat exchangers and is preheated by the condensation energy, while the condensate is collected as freshwater. The preheating of the seawater reduces the required amount of external thermal energy. This process requires thermal energy for heating the

seawater feed, as well as for the generation of vacuum in the different unit sections. Additionally, electrical energy is required for the operation of pumps. MSF units require periodic cleaning due to the formation of deposits and scaling of the tubes. After reverse osmosis, the MSF technology is currently the most common desalination technology applied worldwide. The total energy demand for seawater desalination is usually in the range of 19-28 kWh/m$^3$ [Al-2013; Fri2007].

**Multi-effect distillation (MED).** The general principle of multi-effect distillation is similar to MSF. Seawater is preheated by the condensation energy of the produced freshwater. In this case, the preheated seawater is sprayed onto heated tubes to produce vapor. The water vapor produced in the first stage is supplied to the tubing system of the second stage to produce more vapor in the second stage. This way, vapor can be produced from seawater in a series of stages. While MED units are slightly more energy efficient than MSF units, MSF units have a slightly lower cost and lower scaling tendency. MED processes usually require energy of around 14-22 kWh/m$^3$ water [Al-2013; Fri2007].

**Thermal and mechanical vapor compression (TVC/MVC).** Similar to MSF and MED, the feed seawater is preheated in a heat exchanger in vapor compression units. In the evaporator, vapor is generated from the feed seawater and compressed to raise its temperature to serve as a heat source for the evaporation of water within the evaporator. The vapor is compressed by either thermal energy in case of thermal vapor compression (TVC), or by a compressor based on electrical energy in case of mechanical vapor compression (MVC). While TVC requires around 16 kWh/m$^3$ water for seawater desalination, MVC requires only around 7-12 kWh/m$^3$ water [Al-2013].

While MVC is all in all the most energy-efficient distillation process, it relies purely on electrical energy. In some cases, waste heat may be available from other processes, which can be applied to reduce the additional energy required in case of other distillation processes. However, MVC is currently the established state-of-the-art technology for the treatment of high salinity water streams, such as industrial wastewater and produced water [Thi2015; Sha2013].

**Membrane distillation (MD).** Membrane distillation (MD) is a membrane-based desalination process, which uses a temperature gradient across a microporous, hydrophobic membrane. MD is, so far, not really energy efficient in comparison to established thermally driven desalination technologies. Advantages of MD, however, are the ability of producing concentrates of high salinities and the possibility to exploit the energy present in low temperature industrial streams or

other waste-grade heat sources, as well as energy from renewable sources. A main challenge MD processes need to face before becoming viable for practical application is membrane wetting, which is often caused by membrane fouling, which stands for the deposition of matter on the membrane surface. Membrane wetting leads to a leakage of the saltwater feed through the membrane, which leads to a contamination of the permeate. Different approaches for fouling mitigation are being investigated, focusing on the membrane material (e.g. superhydrophobicity) and the system design and operation (e.g. air gaps, air backwashing, sweep gas) [Dri2015; Amy2017; Sha2013].

### 2.1.2. Pressure-driven membrane processes

Pressure- and osmotic pressure-driven membrane processes can be distinguished by the type of membrane applied. They range from microfiltration processes, which are based on porous membranes, to reverse osmosis processes, which are based on dense membranes [Mel2007]. Only reverse osmosis (RO) and nanofiltration (NF) are described further in the following, due to the focus of this thesis on the FCDI technology, and hence on desalination.

**Reverse osmosis.** The heart of a reverse osmosis (RO) unit or plant are the membrane modules, which in most cases consist of flat-sheet membranes with a dense active layer, which are packed into spiral-wound modules. For desalination, pressurized seawater is fed to such membrane modules. The permeating water is desalinated, while the retained water contains an increased salt concentration. Such systems can be operated in a multitude of configurations, depending on the feed water, the desired water recovery, product concentrations, flow rates, trace substances and so on. Next to the number of stages and the choice of the membrane material, the application of energy recovery devices really makes the difference. Thanks to the introduction of energy recovery technologies, modern RO plants can reach energy consumptions of as low as 1 kWh/m$^3$ diluate. Depending on the feed salinity and water recovery rate, even lower values are reachable. This is possible due to the avoidance of a phase transition, which allows RO to reach values close to the thermodynamic minimum energy of separation. Due to this, RO is currently the most energy efficient and most widely applied technology for seawater desalination [Eli2011; Fri2007; Pet2019; Amy2017].

Limitations of the RO technology are the feed water salinity and reachable water recovery rate. The higher the feed water salinity and water recovery rate, the higher is the required pressure of the feed stream. This leads to structural and material limitations [Pet2019]. The brines produced by seawater RO plants are usually in the range of 60 g/L salinity and are often directly discharged into the environment, with negative effects on the environment. Brine disposal also

contributes significantly to the total cost of desalination. To avoid membrane fouling and scaling, RO feed water needs pretreatment. The chemicals required for pretreatment of the feed water add to the environmental hazard. Due to the low water recoveries, RO processes require feed water volumes significantly larger than the resulting product, which need to be handled and pretreated [Amy2017; Pet2019].

To overcome the limitation of classical RO setups, novel approaches such as forward osmosis (FO) and osmotically-assisted reverse osmosis (RO) are being investigated [Bar2017; Tog2019; Pet2019; Sha2013].

**Osmotically assisted reverse osmosis.** Osmotically assisted reverse osmosis (OARO) aims at extending the applicability of RO processes towards the desalination and concentration of higher salinity feed water (brines). By using a sequence of stages, similar to the trays of a rectification column, the concentration difference across each membrane is reduced, and hence the osmotic pressure difference. Theoretical calculations show promising results regarding the ability to desalinate and concentrate brines and regarding the achievable energy efficiency and water recovery of OARO processes [Bar2017; Tog2019; Pet2019].

**Forward osmosis.** Forward osmosis (FO) processes rely on osmosis. A draw solution with high osmotic pressure extracts pure water from a feed solution with a lower osmotic pressure across a membrane with a dense active layer. The advantage of FO is the lower fouling tendency, due to the different driving force compared to RO. While in RO the feed is pressed through the membrane, in FO the water phase is drawn from the feed. Hence, FO has lower requirements for the feed water quality. Additionally, the requirements for the mechanical stability of the membrane is lower compared to RO. Recent developments, such as membranes containing aquaporin, enable high flux RO and FO membranes. [Amy2017] FO processes can theoretically treat water streams with a very wide range of salinities and qualities. Practically, the applicability depends on the energy demand and overall economic feasibility of the process including the dewatering of the draw solution back to its orignial state [Sha2015; Akt2015; Amy2017].

**Nanofiltration.** Similar to RO, nanofiltration (NF) processes are pressure driven. NF membranes have properties in between ultrafiltration and RO membranes, with a relatively dense, often charged, active layer. These properties allow the separation of inorganic salts, even the separation of mono- and multivalent ions, and small organic molecules. Compared to RO membranes, NF membranes allow a higher flux [Moh2015]. This mixture of characteristics makes NF interesting for many specialized applications in fields such as biotechnology, chemical and

pharmaceutical industry, water and wastewater treatment, food processing, and drinking water production. To achieve fractionation of mixtures or potentially a better separation performance, membrane cascades have been suggested also for NF processes, similar to distillation processes and OARO [Van2008].

### 2.1.3. Ion-exchange and electrically driven processes

Examples for processes based on an electrical potential gradient as driving force or based on ion-exchange materials are electrodialysis, capacitive deionization and ion-exchange processes. In many cases, electrically driven water treatment processes rely on ion-exchange materials, such as ion-exchange resins and ion-exchange membranes, described in the following.

**Ion-exchange membranes and resins.** Ion-exchange materials, such as ion-exchange resins (IER) and ion-exchange membranes (IEM), consist of polymers with a high number of charged functional groups. While cation-exchange membranes (CEM) contain fixed anionic groups, anion-exchange membranes (AEM) contain fixed cationic groups, as illustrated in Figure 2.1. [Str2004; Mel2007]

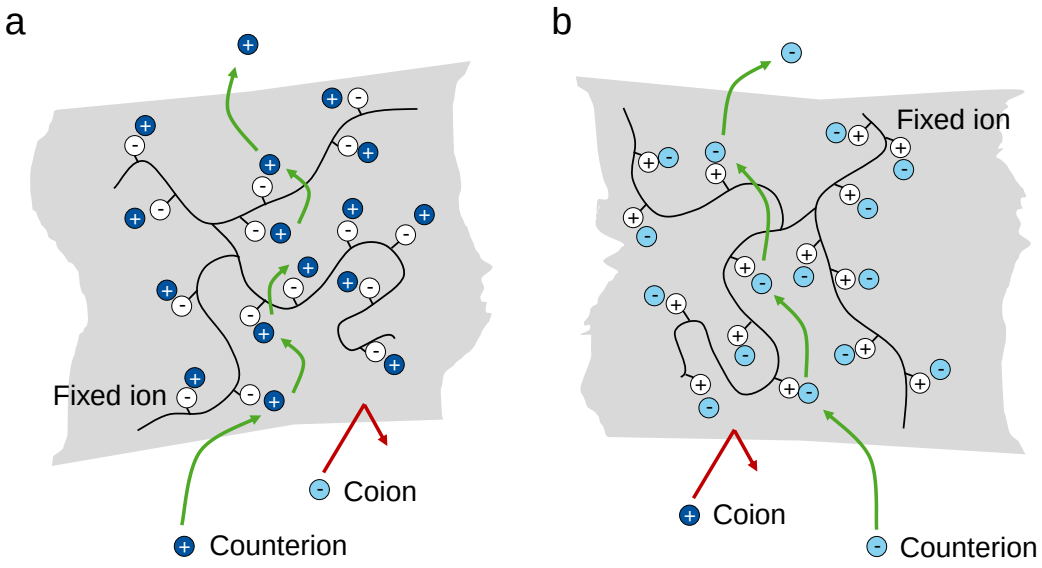


**Figure 2.1.:** Principle of ion-exchange membranes; (a) Cation-exchange membrane and (b) anion-exchange membrane.

The fixed charges (”fixed ions”) are countered by mobile charges (”counterions”) to achieve electroneutrality. Mobile ions of the same charge as the fixed ions are referred to as ”coions”. The actual coion concentration within an ion-exchange material depends on the material and solution properties. The high

charge density within IER and IEM usually leads to a nearly complete exclusion of coions. Depending on the degree of dissociation of the functional groups, ion-exchange materials can be classified as strong acid/weak acid and strong base/weak base material. In case of IEM, there is a further distinction depending on the structure of the membrane. In case of heterogeneous IEM, ion-exchange resin particles are dispersed in a binder polymer, while homogeneous IEM consist fully of ion-exchange polymers [Str2004; Mel2007]. For better mechanical stability, some homogeneous IEM are additionally reinforced by woven or non-woven polymeric fibers. Depending on the process, the desired ion-exchange material properties can vary. It is usually desired to achieve low electrical resistance, high permselectivity and good mechanical, chemical and thermal stability at low cost [Str2004; Mel2007].

Apart from ion-exchange membranes, ion-exchange resins can directly be used for desalination or the treatment of aqueous and non-aqueous solutions. Especially for the production of purified water, ion-exchange resins are often applied. In this case, a mixed bed of IER in $OH^-$ and $H^+$ form is used, meaning the counterions are $OH^-$ and $H^+$. Other ions present in the feed stream are then adsorbed into the ion-exchange resin and exchanged for $OH^-$ and $H^+$, as illustrated in Figure 2.2 (c) at the example of sodium chloride. Once most of the $OH^-$ and $H^+$ ions are released and exchanged to different ions, the IER need to be disposed of or regenerated using strong acids and bases. Hence, this type of water treatment is relatively material or chemical intense. Generally, many varieties of ion-exchange resin materials are commercially available for a multitude of applications.

**Electrodialysis.** Electrodialysis (ED) processes are based on ion-exchange membranes. In the conventional ED layout, AEM and CEM are arranged alternatingly between a pair of electrodes. Spacers, which are placed in between the membranes, or incorporated into the membranes [Bal2010], form water flow channels. When an electrical field is applied, the ions present in the electrolyte solutions migrate towards the oppositely charged electrodes and are either selectively transported through or retained by the encountered IEM. This leads to the formation of alternating desalinated and concentrated streams in between the membranes, as illustrated in Figure 2.2 [Str2004; Mel2007].

At the electrodes, the ionic current forming withing the membrane stack is converted into an electrical current by electrochemical reactions. Depending on the chosen electrode rinse solution, the nature of the electrochemical reactions can vary. The results of electrode reactions in ED can also be the formation of gases [Mel2007].

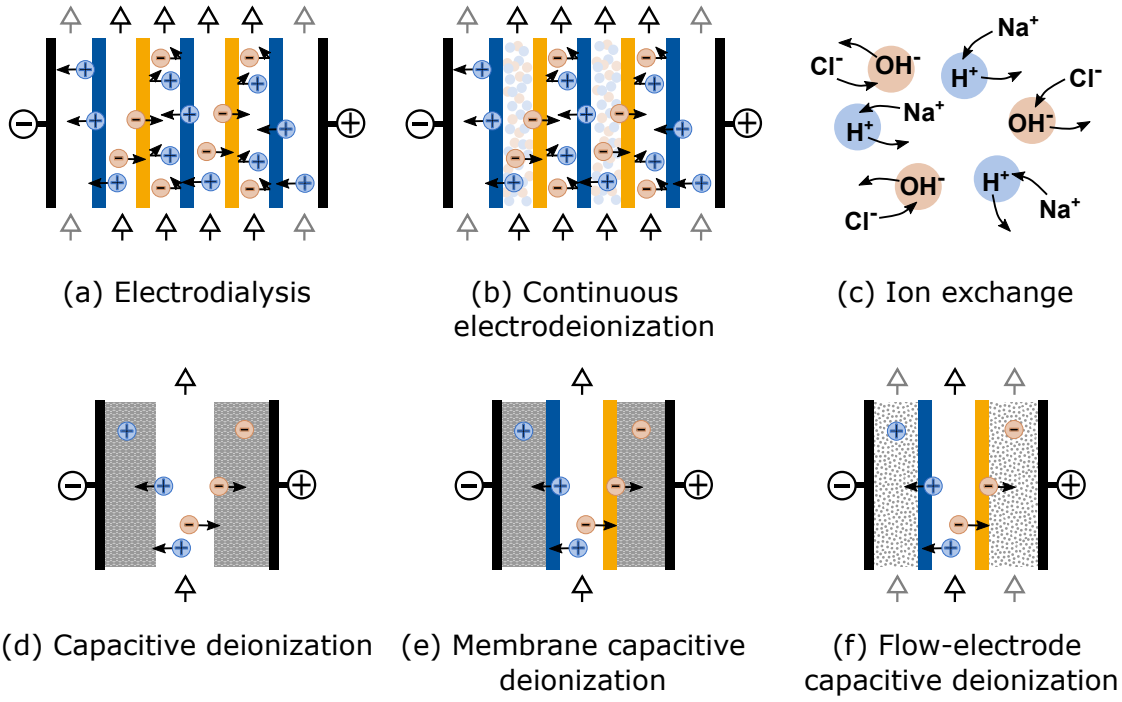


**Figure 2.2.:** Illustration of the working principles of major electrically driven and ion-exchange processes.

Electrodialysis was originally developed in the 1950s. In the beginning, ED often competed with RO in projects, until the development of thin film composite membranes led to a breakthrough of the RO technology. While nowadays RO dominates the desalination market, ED is mostly used for niche applications. Over the years, many varieties of ED processes have been developed. Among them are electrodialysis reversal, electrodialysis with bipolar membranes and continuous electrodeionization. For the interested reader, a multitude of books and articles exist about electrodialysis and related processes [Yam1969; Str2004; Mel2007; Str2010; Cam2018].

**Capacitive deionization.** Similar to ED, capacitive deionization (CDI) relies on an electrical field as driving force to evoke the migration of ions towards the oppositely charged electrodes. In case of CDI, however, the electrical potential is applied to a pair of porous carbon electrodes. The ions are adsorbed electrostatically on the electrode surface, which act as an electrical double-layer capacitor. When the electrode is saturated with ions, it can be regenerated by changing the electrode potential and, thus, releasing the ions into the water stream to form a concentrate [Por2013]. The process is comparable to the concept of parametric pumping, which can be driven by different intensive parameters, such as pressure, pH or the electric field, as is the case in CDI [Pet2018]. Thermodynamic

cycle analyses were applied as a helpful tool for further systematic improvement and investigation of CDI processes [Bie2009; Hat2018]. In case of membrane capacitive deionization (MCDI), ion-exchange membranes are added in front of the electrodes, which leads to improved salt removal and energy efficiencies [Bie2010]. A comprehensive review of the history and background of CDI technology was published by Porada et al. [Por2013] in 2013. A range of further reviews exist, which focus on different aspects of CDI technologies and their application [Ore2008; And2010; Sus2015; AlM2014; Zha2018a; Rat2019].

## 2.2. Flow-electrode capacitive deionization (FCDI)

Bringing together the fields of (membrane) capacitive deionization and flow capacitors [Pre2012; Hat2013], the first article mentioning flow-electrode capacitive deionization (FCDI) was published by Jeon et al. in 2013 [Jeo2013]. Since then, FCDI is a rapidly growing field with a continuously increasing number of articles being published every year.

In FCDI processes, the static (carbon) electrodes of CDI processes are replaced by flowing, pumpable carbon suspensions, termed flow electrodes or slurry electrodes [Hat2015a]. While CDI processes are operated in semi-continuous [Kim2018] or discontinuous [Por2013] manner, charge-discharge cycles can be avoided in case of FCDI. The charged electrodes can be pumped from the desalination module and continuously regenerated in a different location, for example a second module [Gen2014]. Continuous operation or replacement of charged flow electrodes by fresh, uncharged flow electrodes allows the treatment of high salinity solutions [Jeo2013; Jeo2014; Yan2016a].

In the following, an abstract overview of the developments over the last few years in the relatively young field of FCDI is given. The focus of each subsection lies on one of the four sides of the FCDI story: The flow-electrode materials and fundamental mechanisms, the module design, the process design, and research focusing on possible applications.

### 2.2.1. Flow-electrode materials

Early FCDI works published in 2013 and 2014 [Jeo2013; Jeo2014; Hat2014; Gen2014] mostly applied activated carbon powders as active material for the preparation of the flow-electrode suspensions. In the beginning, the suspensions often contained only low carbon mass fractions, which leads to a lower viscosity and better pumpability. Porada et al. [Por2014] soon showed how the desalination performance can be improved by the use of increased activated carbon contents. Hatzell et al. [Hat2015b] then demonstrated how the rheological char-

acteristics of flow electrodes can be improved by increasing the amount of oxygen containing functional groups at the carbon surface using nitric acid, which enables the use of increased carbon mass loadings. In the following years, more and more research studies focused on improving the charge percolation within and the general characteristics of flow electrodes by investigating different carbon and non-carbon materials and treatments. A review focusing on materials for flow-electrode applications was published in 2015 by Hatzell et al. [Hat2015a].

Park et al. synthesized and tested spherical activated carbons functionalized with ion-selective groups for use in FCDI processes [Par2016]. Xu et al. investigated an asymmetric FCDI system based on an activated carbon and manganese dioxide suspension as positive electrode and an activated carbon suspension as negative electrode with the aim to increase the operation voltage window to 1.8 V [Xu2017]. Ma et al. developed a redox-active flow anode for use in FCDI processes with improved desalination performance [Ma2016]. Liang et al. demonstrated improved conductivity and electrical charge transfer, and an increased viable voltage window due to the addition of carbon black into flow electrodes [Lia2017]. Yang et al. investigated the impact of different conductive additives for use in FCDI flow electrodes, including carbon black and different graphite materials. Plate-shaped graphite was identified as promising due to its larger size compared to carbon black and the resulting flow electrodes having no increased clogging tendency due to the alignment of the particles in flow direction [Yan2017]. In 2018, both Tang et al. [Tan2019] and Cho et al. [Cho2019] published studies demonstrating a significant enhancement of the desalination performance by the addition of carbon nanotubes into FCDI flow electrodes. Recently, Chang et al. [Cha2019] presented an FCDI system based on two non-identical flow electrodes. While the anode was based on activated carbon, the cathode was based on copper hexacyanoferrate. This enabled the use of a wider voltage window and hence an improved salt removal rate. A drawback is the more significant change of the concentrate pH value compared to the AC-AC system [Cha2019].

Apart from this, several studies aimed at extending the understanding of charge percolation within flow electrodes. In 2017, Hatzell et al. published a study using synchrotron X-ray tomography to reconstruct and visualize agglomerations within flow electrodes. This technique demonstrated increasing cluster volumes at increasing carbon contents and may be useful for further investigations regarding influences on the the dynamic formation of percolation networks [Hat2017]. A continuation of this research was recently published. [Dix2019] In 2018, Hoyt et al. developed an electrochemical impedance spectroscopy (EIS) model for describing the behaviour of capacitive flow electrodes [Hoy2018]. Later, Tang et al.

[Tan2019], as well as our own workgroup [Rom2019], published two independent EIS models aiming at the description of capacitive flow electrodes under dynamic conditions. The latter work is described further in Chapter 4.

All these studies have one thing in common: All demonstrate the importance of the quality of the flow-electrode material on the overall performance and efficiency of FCDI processes. The published research studies form a good foundation and an initial toolbox for the further development of flow-electrode materials and compositions. The ideal flow electrode might differ depending on the application case.

**Other general mechanisms and influencing factors of FCDI processes.** Several FCDI studies investigated general influences on FCDI processes and mechanisms apart from the charge transfer within slurry electrodes. Yang et al. [Yan2016a] demonstrated the positive effect of increased salinities within the flow electrodes on the overall system performance. Moreno et al. [Mor2018] investigated the impact of concentration gradients in FCDI systems on the water transfer in cyclically operated batch mode systems. Nativ et al. [Nat2017] investigated the occurence of faradaic reactions in cyclically operated FCDI processes. The study indicates a significant contribution of electrodialytical desalination mechanisms, meaning the conversion of ionic into electrical currents by means of faradaic reactions within the flow electrodes, in cyclically operated FCDI processes [Nat2017]. This may to a certain extent explain the high apparent salt adsorption capacities observed in the first FCDI study published by our workgroup [Gen2014]. However, I believe this to be of limited importance to continuous FCDI processes. As discussed in the research article presenting a first, simplified FCDI process model published by our workgroup in 2018 [Rom2018b], there are no significant changes of the flow electrode pH value observed in continuous FCDI processes, in contrast to cyclically operated FCDI processes. Further results supporting this hypothesis are presented in Chapter 5.

### 2.2.2. Module design and membrane materials

Some of the FCDI cells used in early articles [Jeo2013; Gen2014], including the first FCDI study published by Jeon et al., were made of stainless-steel current collectors with carved, meandering flow channels. Porada et al. [Por2014] used titanium plates and platinum wire as current collectors. The stainless steel current collectors have one disadvantage: They tend to corrode at the anode side, especially in case of the treatment of chloride salts. Hence, the community quickly adapted graphite plates as the current collector material of choice [Jeo2014; Hat2014; Rom2015].

Ion-exchange membranes designed for electrodialysis processes were used for the separation of feed stream and flow electrodes in most cases, as for example Neosepta IEM produced by the Astom Corporation or fumasep IEM produced by fumatech BWT GmbH [Jeo2013; Jeo2014; Por2014; Gen2014]. In 2018, Nativ et al. [Nat2018] also presented a study on FCDI cells utilizing nanofiltration membranes to achieve separation between divalent and monovalent ions. Apart from the most common approach of using IEM in FCDI systems, Hatzell et al. [Hat2014] presented a concept for an FCDI process without ion-exchange membranes in beginning of 2014. In this case, a porous separator was used to separate two flow electrodes. The particles within the flow electrodes adsorbed each one type of ions (anions/cations) and were in the following step separated from the continuous liquid phase by filtration. As an alternative, settling was suggested for the separation step.

The geometric design of flow channels, inlets, outlets and distribution of liquid flow streams to the respective flow channels varied from work to work. Various materials were used to form flow channels for the feed water in between the membranes, such as polymeric flannel spacers, mesh spacers or simply silicone gaskets which were cut in shape [Jeo2013; Jeo2014; Por2014; Gen2014]. While most FCDI cells were based on a planar architecture, Porada et al. [Por2014] also presented an architecture based on tubular IEM in 2014. In the first FCDI studies published by our workgroup, we used stainless steel fleece [Gen2014] or titanium fleece [Rom2015] in between the current collectors with carved flow-electrode channels and the ion-exchange membranes. Recently, Yang et al. [Yan2019] adapted this concept and investigated the use of titanium meshes in different locations within an FCDI cell as a replacement for voluminous and rigid current collector plates with carved flow channels.

The early FCDI systems were mainly based on a desalination module. In all initial studies, the regeneration step was performed either at a different time (charge-discharge cycles) [Jeo2014], in a separate module [Gen2014], separate vessel [Jeo2014] or a separate treatment step [Hat2014]. In 2015, our workgroup presented the first continuous system based on a single module and single flow electrode, which combined desalination and regeneration step. The module concept is based on three IEM and two spacers placed between a pair of current collectors, similar to an electrodialysis system with one cell pair. While on one side, anions or cations are adsorbed onto the carbon particles within the flow electrode, the same flow electrode gets into contact with an oppositely charged current collector on the other side of the cell and is hence regenerated and the ions discharged. A diluate stream and a concentrate stream is continuously produced within one cell, while the flow electrode is continuously recirculated and

regenerated [Rom2015].

Another interesting concept introduced by Doornbusch et al. in 2016 [Doo2016] and in the following continued by the workgroup of Matthew Suss [Coh2016] is the concept of fluidized bed electrodes in FCDI. Such fluidized bed FCDI cells make use of the dominating gravitational effect on relatively large carbon beads within an upright flow cell. Due to the high settling velocity compared to the flow rate of the continuous aqueous phase, the particles experience an increased residence time within the module, which leads to an increased concentration of carbon particles within a fluidized bed FCDI module. On the other hand, the concentration of carbon particles withing the tubing and overall system can be kept lower, which facilitates pumping. [Doo2016]

The workgroup of Donk Kook Kim, who had presented the first FCDI study in 2013 [Jeo2013], presented first concepts for upscaling FCDI processes in the following: In 2016, Yang et al. [Yan2016b] presented a first FCDI stack design, which is based on the simple stacking of FCDI cells with one pair of IEMs by milling flow channels on both sides of a current collector. In another concept presented in 2017, Cho et al. [Cho2017a] utilize a "honeycomb-shaped" porous substrate for the manufacturing of a 3D FCDI cell, which could be used in a repetitive manner for upscaling. The insides of the flow-electrode channels within the 3D structure were coated with ion-exchange materials, to provide selectivity, and a graphene layer, which functions as current collector or distributor. While the system offers good scalability, the achieved current densities were significantly lower than in conventional FCDI cells [Cho2017a].

### 2.2.3. Process design

The pumpability of flow electrodes makes FCDI processes flexible. It allows the relocation of the regeneration step out of the desalination module, and hence enables a multitude of possible process layouts. While the first FCDI study was performed with a simple FCDI desalination module in single-pass mode regarding both saline feed water and flow electrodes [Jeo2013], soon new regeneration concepts were published, as illustrated in Figure 2.3.

**Energy recovery from flow electrodes.** The same workgroup who published the first FCDI paper was also the first to investigate the regeneration of flow electrodes [Jeo2014]. They demonstrated the possibility to recover energy from flow electrodes in a separate regeneration step similar to the charge-discharge cycles of CDI processes (Figure 2.3 (b)). Later, our workgroup demonstrated

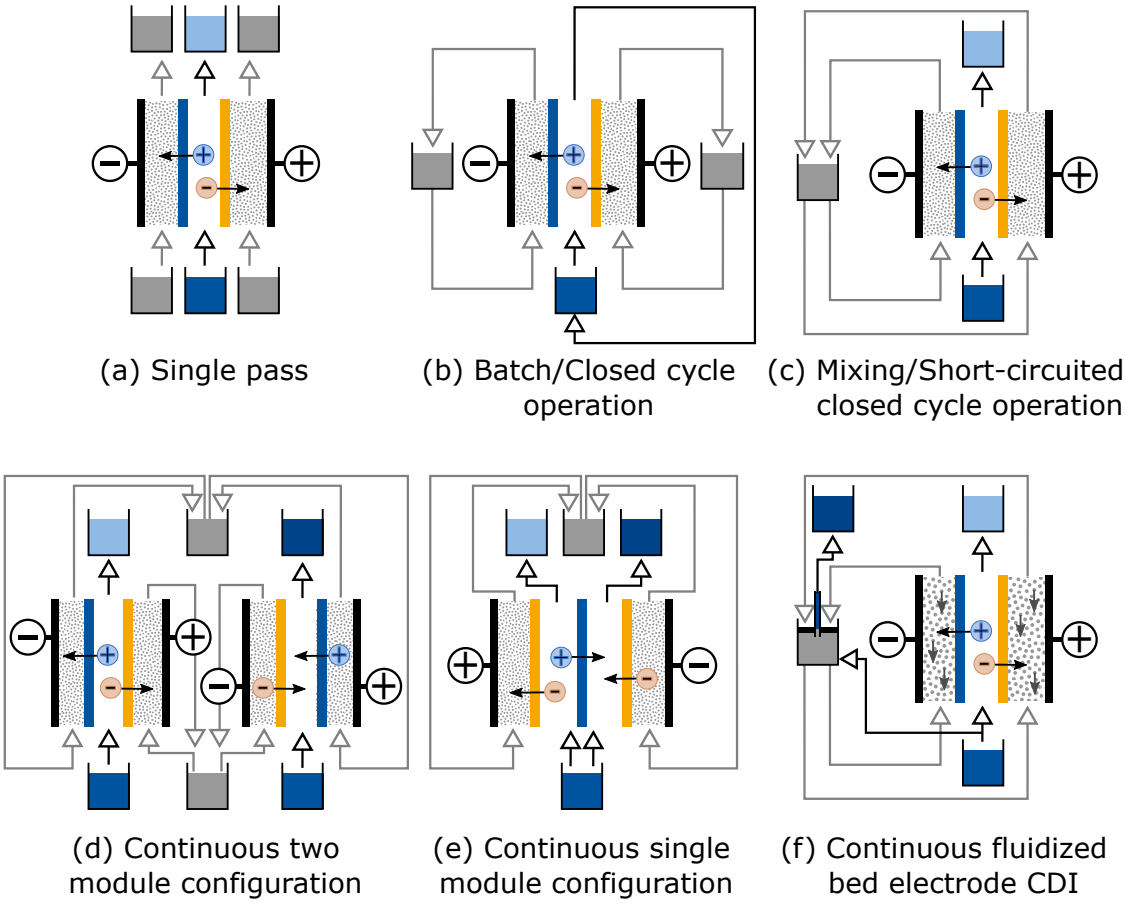


**Figure 2.3.:** Illustration of major FCDI process designs: (a) Single pass FCDI system [Jeo2013], (b) batch/closed cycle operation/cyclic operation [Jeo2014; Por2014; Gen2014], (c) mixing/short-circuited closed cycle operation [Jeo2014], (d) continuous two-module configuration [Gen2014], continuous single-module configuration [Rom2015], (f) continuous fluidized bed electrode capacitive deionization process [Doo2016].

the fully continuous energy recovery from flow electrodes in FCDI processes in two different process layouts, as described in Chapter 5 and the corresponging research article published in 2018 [Rom2018a].

**Flow-electrode regeneration by mixing.** Apart from the demonstration of energy recovery from flow electrodes in charge-discharge cycles, Jeon et al. [Jeo2014] demonstrated the possibility to discharge two oppositely charged flow electrodes by simple mixing (Figure 2.3 (c)). When two oppositely charged flow electrodes come into contact with each other, the oppositely charged particles can interact. Hence, they are electrically discharged and the adsorbed ions are desorbed from the carbon surface to form a salt in solution. As a result, the carbon particles can again acquire charge upon contact with current collectors or charged parti-

cles, and ions can again be adsorbed to the carbon surface. This process can be operated for an extended time period, during which the salinity of the continuous phase constantly increases. Consequently, the process can appear continuous for a certain amount of time, while it is not. However, this approach is very convenient for lab scale studies and is usually termed short-circuited closed cycle (SCC) operation. It allows the semi-continuous operation for an extended amount of time with very little technical effort, and was therefore adopted for many following FCDI studies [Lia2017; Fan2018; Ma2019].

This approach also allows a fully continuous operation, in case the salt concentration within the flow electrodes is kept constant by continuous removal of concentrated saline solution from the flow electrode and the continuous replacement of the liquid flow electrode by fresh feed water. This was first demonstrated in the fluidized bed FCDI study published by Doornbusch et al. [Doo2016]. Here, the increased settling velocity of the carbon spheres was harnessed to separate the carbon particles from the concentrated saline solution present in the flow electrodes by an ascending tube (Figure 2.3 (f)). A similar approach was employed by our workgroup in a two-step regeneration process, which includes a dedicated energy recovery module and a filtration module for retaining the carbon particles within the flow electrodes, as described in Chapter 5.

**Regeneration by electrical charge transfer via current collectors.** The possibility of flow-electrode regeneration by electrical charge transfer via current collectors was introduced by our workgroup in 2014 [Gen2014]. In this case, two identical FCDI cells were connected by flow-electrode circuits and hence formed a process, in which water can be continuously desalinated in the first FCDI cell. In the second FCDI cell, saline water is concentrated and at the same time the flow electrodes are continuously regenerated, as illustrated in Figure 2.3 (d). This approach was pursued and further improved by the introduction of the single-module FCDI concept (Figure 2.3 (e)) by our workgroup in 2015 [Rom2015], as described above. A comparison of different FCDI process layouts is presented in Chapter 5, a corresponding research article was published in 2018 [Rom2018a]. The research presented in Chapter 7 continues this research and introduces multiple cell pairs into an FCDI module, which leads to a reduced energy demand and cost.

Recently, Chang et al. [Cha2019] presented a promising study based on the two-module FCDI structure [Gen2014] with two non-identical flow electrodes using activated carbon and copper hexacyanoferrate, as described above.

The general advantage of regeneration by electrical charge transfer via current collectors is the operation stability. Such stability is significantly harder to achieve

in continuous process layouts based on the mixing approach, which have to rely on settling or cross-flow filtration for retaining the carbon particles within the flow electrodes.

**Capacitive neutralization deionization.** Another desalination approach based on flow electrodes, called capacitive neutralization deionization, was demonstrated by Wang et al. in 2016 [Wan2016]. In this case, the flow electrodes are not prepared with the usual salt solutions, but instead with an acid on one side and an alkaline solution on the other side. The cells applied for this approach were identical to classical FCDI cells. Similar to ion-exchange processes, the $H^+$ and $OH^-$ ions both diffuse into the saline water feed chamber in the middle and are therefore neutralized. Similar to ion-exchange resins, the $H^+$ and $OH^-$ ions in the flow electrodes are replaced by the salt present in the feed solution, which is therefore desalinated. While this process presents an interesting concept, which requires the addition of acidic and alkaline chemicals instead of the application of an external voltage, the regeneration and general operation strategy remains unclear.

### 2.2.4. Towards application

Apart from the above described layouts and operation strategies for FCDI processes, many studies focused on the development of FCDI processes towards specific applications. The collaboration of our workgroup with the workgroup of Youri Gendel resulted in the publication of a study presenting an FCDI metathesis process authored by Linnartz et al. [Lin2017]. In this work, the possibility of conducting a double displacement reaction in a salt metathesis FCDI process was demonstrated. The principle was performed with the example of magnesium chloride and potassium sulphate as feed streams and magnesium sulphate and potassium chloride as product streams, but can potentially be extended to all kinds of salt combinations. This approach is promising for many kinds of salt recovery processes, as it allows the simultaneous recombination and concentration of salts to generate product streams with increased value.

Zhang et al. [Zha2018b] presented an FCDI process aimed at ammonia recovery from dilute wastewaters in 2017. An FCDI process was combined with a membrane module submerged into the flow cathode, by which ammonia can be stripped directly from the flow electrode. The process allows the selective removal of ammonia and preconcentration within the flow cathode. However, the same workgroup recently presented another study on ammonia recovery from wastewaters by use of a simple FCDI process relying on charge-discharge cycles

[Zha2019a]. Another study focusing on ammonia recovery was presented by Fang et al. in 2018 [Fan2018], in which a good concentration factor was achieved in the recovery of ammonia from synthetic wastewater in SCC mode.

The ever-increasing number of FCDI related studies published in the recent years demonstrates the versatility and high potential of the technology. Apart from the above described examples, FCDI processes have by now been investigated for nitrogen and phosphorous recovery [Bia2019], nitrate removal [Son2019], copper removal [Zha2019b], and uranium removal including the uncharged Ca-$U0_2$-$C_3$ ternary complex [Ma2019]. Apart from a multitude of pure FCDI processes, many combinations with established processes are imaginable, such as the FCDI-NF combination published by Choi et al. in 2017 [Cho2017b].

## 2.3. Modeling electrically driven membrane processes

In the following, the basic theoretical background for the mathematical description of FCDI processes based on ion-exchange membranes is described. This requires equations for the (1) description of ionic transport, e.g. in an electrolyte solution or an ion-exchange membrane, (2) distribution of components between two adjacent phases, e.g. an IEM and the adjacent solution, as well as equations for the (3) capacitive adsorption of ions in the electrical double layer at the surface of carbon particles. The conductivity of salt solutions varies depending on the concentration. Hence, a relation is needed for the description of the (4) ohmic resistance of solutions depending the salinity. The focus of this thesis lies on the investigation of FCDI processes for the treatment of high salinity solutions. Due to this, importance is given to the (5) non-ideal effects such as water and coion transport across ion-exchange membranes, which occur at high salinities. Finally, (6) electrochemical impedance spectroscopy is discussed as valuable electrochemical characterization method and alternate modelling approach for electrochemical systems.

Differences in the chemical potential $\mu_i = \mu_i^0 + RTln(a_i)$ are the driving force for physical and chemical reactions and processes. In this equation, $\mu_i^0$ is the chemical potential at a reference state, $R$ is the ideal gas constant, $T$ the temperature and $a_i$ the activity of each component. When assuming ideal activity coefficients of $\gamma_i = \frac{a_i}{c_i} = 1$, the activity $a_i$ can be replaced the concentration $c_i$. In case of electrochemical processes, the total driving force also depends on the electric field. The sum of the chemical potential and electrostatic potential are usually termed electrochemical potential $\bar{\mu}$ [Boc1998]:

$$\bar{\mu}_i = \mu_i + z_i F\varphi = \mu_i^0 + RTln(c_i) + z_i F\varphi \tag{2.1}$$

In which $z_i$ the ion valence, $F$ the Faraday constant, and $\varphi$ the electrical potential.

### 2.3.1. Ionic flux

The driving force for the movement of ions in an electrochemical system is the electrochemical potential gradient. Based on this, the ionic flux can be described mathematically as $j_i = -u_i c_i \nabla\mu_i$. Hence, gradients in concentration ("diffusion") and the electrical potential ("migration") can cause the transport of ions. Additionally, the convective transport of ions $c_i \cdot v$ can be considered, $v$ being the velocity within the flow channel, which is left out in this case for simplicity. The result is the Nernst-Planck equation, which is usually written based on three-dimensional gradients for concentration and potential [Boc1998; Sch2012; Bar2001]:

$$j_i = -D_i \nabla c_i - u_i c_i \nabla\varphi \tag{2.2}$$

In this, $D_i$ is the Fick diffusion coefficient of a species $i$, and $u_i$ the ion mobility. $u_i$ can be determined via the Nernst-Einstein relation:

$$u_i = \frac{z_i F}{RT} D_i \tag{2.3}$$

When describing the flux in an electrochemical system, it is often sufficient to consider one-dimensional transport towards an electrode. In this case, the Nernst-Planck equation can be simplified as follows [Boc1998; Sch2012; Bar2001]:

$$j_i = -D_i \frac{dc_i}{dx} - u_i c_i \frac{d\varphi}{dx} \tag{2.4}$$

### 2.3.2. Distribution of an electrolyte between two phases: The Donnan potential

In electrochemical systems, interfaces between two phases can exist in several locations. In FCDI systems, examples for such phase boundaries are the interface between an ion-exchange membrane and the adjacent solution, or between a carbon micropore and the surrounding solution. Depending on the conditions, the ion concentrations in two adjacent phases can differ from each other. This leads to the development of an electrical potential across the phase boundary in case of charged species (ions), which is also referred to as (Gibbs-)Donnan effect.

When assuming electrochemical equilibrium between two adjacent phases, the electrochemical potential of phase $a$ and phase $b$ should be equal:

$$\bar{\mu_i}^a = \bar{\mu_i}^b \tag{2.5}$$

$$\mu_i^{0,a} + RTln(c_i^a) + z_i F\varphi^a = \mu_i^{0,b} + RTln(c_i^b) + z_i F\varphi^b \tag{2.6}$$

Using the equation for the thermal voltage $V_t = \frac{RT}{F}$ and simple mathematical operations, this equation can be converted to the following expression [Mac1955b]:

$$c_i^a = c_i^b \cdot exp(\frac{-z_i(\varphi^b - \varphi^a)}{RT}) = c_i^b \cdot exp(-\frac{z_i F \Delta\varphi_{Don,k}}{V_t}) \tag{2.7}$$

As can be seen from this equation, $\varphi_{Don,k}$, also referred to as Donnan potential, is actually a potential difference or potential jump across a phase boundary [Sch2012].

### 2.3.3. Electrosorption and electrical double layer modelling

At the interface between a charged surface and the surrounding electrolyte solution, a region with increased concentration of oppositely charged species is formed. Originating from the original conception (Helmholtz model) of this region being a condensed layer opposed to the surface charge, the term electrical double layer (EDL) was established [Boc2002]. EDLs form at any charged surface, including electrodes and charged polymeric membrane materials. Only in case the potential applied to an electrode leads to the achievement of the point of zero charge, EDLs are not formed at an electrode surface [Sch2012].

According to the Gouy-Chapman model for diffuse double layers, the concentration of the species with an opposite charge to the electrode, anions or cations, decreases exponentially within an EDL. Analogous to the equilibrium and resulting ion distribution between two phases, EDLs can also be described by an electrochemical equilibrium. The result is the Boltzmann equation, which describes the ion concentration in an EDL depending on the bulk concentration $c_i^0$:

$$c_i = c_i^0 \cdot exp(\frac{-z_i F\varphi}{RT}) \tag{2.8}$$

The expansion of EDLs depends on the charged surface and the salt concentration in the surrounding solution. A measure for the expansion of EDLs is the Debye length $\lambda_D$, which describes the distance from the electrode, at which the potential within the EDL is decreased to a value of 1/e (e being Euler's number):

$$\lambda_D = \sqrt{\frac{\epsilon_0 \epsilon_r kT}{2N_A e^2 I}} \tag{2.9}$$

In this equation, $\epsilon_0$ is the electrical field constant, also called vacuum permittivity, $\epsilon_r$ the relative permittivity of the medium, $k$ the Boltzmann constant, $N_A$ the Avogadro constant, $e$ the elemental charge of an electron and $I$ the ionic strength of the electrolyte, which depends on the concentration and valence. The expansion of EDLs is usually in the nanometer range.

The Gouy-Chapman-Stern model (GCS) merges two individual theories, the Helmholtz theory describing a rigid double layer, and the Gouy-Chapman theory for diffuse double layers. However, when considering porous materials, such as activated carbons, the Gouy-Chapman-Stern (GCS) model would account for two simultaneously occurring double layers, which may overlap in case of small pores. A newer, simplified model commonly used in CDI literature is the modified Donnan (mD) model [Jeo2011; Bie2010], which is more suitable to model overlapping EDLs. It describes strongly overlapping EDLs in micropores by assuming a constant potential within the pore. It describes the EDLs in porous electrodes by the combination of a Stern layer and a Donnan equilibrium between micropores and macropores carbon electrodes [Bie2011; Zha2012]. This modelling approach is applied in this thesis and further described in Chapter 8.

### 2.3.4. Ohmic resistance of salt solutions

Based on Ohm's law, the potential drop over a flow channel filled with saline water can be determined as follows [Sch2012; Mel2007]:

$$\Delta\varphi = \frac{h}{\kappa} \cdot i \tag{2.10}$$

The specific conductivity $\kappa$ is the reciprocal value of the specific resistance, while $h$ denotes the height of each channel, and $i$ denotes the current density. $\kappa$ strongly depends on the ion concentration:

$$\kappa_{sol} = \sum_{i=1}^{n} c_i \cdot \lambda_i + \kappa_{water} \tag{2.11}$$

Here, $\lambda_i$ is the molar conductivity of each ion species. $\kappa_{water}$ denotes the specific conductivity of distilled water without any dissolved ions. The molar conductivity of each ion species can be obtained using Kohlrausch's law [Sch2012]. Kohlrausch's law (Equation 8.8) is an empirical, non-linear correlation between conductivity and concentration, which can be used to determine the molar conductivity for strong electrolytes:

$$\lambda_i = \lambda_i^{\infty} - K \cdot \sqrt{c_i} \tag{2.12}$$

In this equation, $\lambda_i$ denotes the molar conductivity of a fluid containing dissolved ions, $\lambda_i^{\infty}$ the molar conductivity at infinite dilution, which can be obtained experimentally or from literature, and $c_i$ the ion concentration. $K$ is called Kohlrausch coefficient and depends on the stoichiometry of each salt in solution. The parameters can be obtained from literature or by fitting to experimental data for the conductivity of salt solutions depending on the concentration.

Friedrich Kohlrausch determined this originally empirical equation in the 19th century. However, the validity of the equation was later proven by theoretical derivations of Debye, Hückel and Onsager based on the theory of ionic clouds [Boc1998].

### 2.3.5. Ion and water transport in ion-exchange membranes

The field of ion and water transport through charged membranes and within ion-exchange materials is a vast field. A tremendous amount of literature has been published regarding this topic over the years. A nice and concise review was recently published by Kamcev and Freeman [Kam2016a], which may be of interest to some readers. Also, Kingsbury et al. [Kin2018] published a great research article, which contains experimental data for 20 commercial IEMs and further discussions on water and salt permeation in IEM.

The choice of input parameters for process models is often vital, as is discussed further in Chapter 8 of this thesis. An in-depth discussion of available models for different effects and review of typical data obtained for IEM processes such as electrodialysis, including data regarding osmotic and electroosmotic effects, is out of the scope of this thesis. However, when investigating the sensitivity of the process model presented in Chapter 8 on the choice of Fick diffusion coefficients, a strong dependence of the results of the simulations on the concentration on both sides of the membrane was observed. A possible explanation is the expansion of EDLs in solutions of low concentrations, which may lead to a "constriction" of salt channels within IEM, and hence reduced diffusion coefficients. It was chosen to model this with a simplified approach presented in Chapter 8.

## 2.4. Electrochemical impedance spectroscopy (EIS) and equivalent circuit models

Electrochemical impedance spectroscopy (EIS) is an electrochemical characterization method, which, as the name suggests, investigates the dependence of the impedance on a wavelength/frequency. During an EIS measurement, alternating potentials (or currents) of varied frequencies and usually low amplitudes are applied to any electrochemical or material system, while the current (or voltage) response is recorded. Similar to circuits operated with direct current, circuits operated with alternating current exhibit a resistance, which is called impedance $Z$. The time-dependent potential $U(t)$ and the current $I(t)$ determine the impedance, analogous to Ohm's law [Boc2002; Bar2005; Rom2019]:

$$Z(t) = \frac{U(t)}{I(t)} \tag{2.13}$$

A sinusoidal current or voltage of small amplitude is applied and hence a linear response is assumed. The change of amplitude and the phase shift $\varphi$ of the measured response allows to draw conclusions regarding chemical and physical processes dominating the system. EIS allows the study of frequency-related phenomena, such as the behaviour of electrical double layers and the distribution of their relaxation times, or electrochemical reactions. Generally, EIS will allow conclusions about rate-determining steps in electrochemical systems, which can for example be diffusion or electron transfer. EIS is a usually non-destructive analytical method, which makes it a powerful tool for material characterization. The applied frequencies are varied in a range suitable for the intended application and the phenomena which are to be observed. In most cases, the applied frequencies lie in the range of 0.01 Hz to 100 kHz [Boc2002; Bar2005; Dłu2010; Sus2013; Ban2015; Rom2019].

To describe the behaviour of the phase shift and change in amplitude mathematically, impedance is usually described by complex numbers with polar coordinates in the complex plane, and hence has the form of a vector. An applied sinusoidal potential can be described by:

$$U(t) = U_0 \cdot (cos(\omega t) + i \cdot sin(\omega t)) \tag{2.14}$$

In this, $U_0$ indicates the amplitude and $i$ the unit imaginary number $\sqrt{-1}$. The resulting steady state current can be described as:

$$I(t) = I_0 \cdot (cos(\omega t + \varphi) + i \cdot sin(\omega t + \varphi)) \tag{2.15}$$

By using Equation 2.13 and transforming the equation into Eulers form, e.g. $I(t) = I_0 \cdot \exp[i(\omega t + \varphi)]$, one can arrive at:

$$Z(t) = Z_0 \cdot cos(\varphi) + i \cdot Z_0 \cdot sin(\varphi) \tag{2.16}$$

Accordingly, the impedance of a system can be resolved into two components, the "real" part of the impedance, which is in phase with the stimulating signal, and the "imaginary" part of the impedance, which has a 90° phase shift to it. The real part of the impedance is equal to the ohmic resistance during the application of a direct current. Based on this are also the two most commonly applied types of diagrams for the analysis of EIS results: Bode plots and Nyquist plots. In case of Bode plots, the impedance (either the magnitude, the real, or the imaginary part) and the phase angle are plotted over the applied frequency. In case of Nyquist plots, the negative imaginary part of the impedance is plotted over the real part of the impedance [Boc2002; Bar2005].

### 2.4.1. Basic circuit elements and combinations

A prevalent way of modelling electrochemical systems is the derivation of equivalent circuits. An equivalent circuit, in the "electrochemists way of speaking" [Fle2014], is the arrangement of simple, linear electrical circuit elements, which in combination exhibits the same impedance behaviour as the studied electrochemical system. Based on the expected physical properties of the investigated system, equivalent circuit models can be developed to represent the governing phenomena. The best circuit element values are usually chosen based on the best fit, characterized by the minimized sum of the squared residuals between the experimental results and the theoretical impedance function based on the equivalent circuit. Such models can help to understand the physico-chemical mechanisms limiting an electrochemical process and develop ways to overcome such limitations [Fle2014]. Most elements used for the description of EIS behaviour are actual electrical circuit elements, such as resistors, capacitors and inductors. An overview of major EIS circuit elements and combinations is given in Figure 2.4 [Bar2001; Boc2002; Bar2005].

The simplest circuit element is probably the resistor R ((1) in the illustration). It only exhibits an ohmic resistance, which results in a change of amplitude of the applied signal, but no phase shift. Hence, it only exhibits a real impedance value, which is represented in a Nyquist diagram by a single dot on the x-axis, in which the x-axis value is the value of the resistance. The value of the impedance equals the resistance [Boc1998; Bar2005]:

$$Z = R \tag{2.17}$$

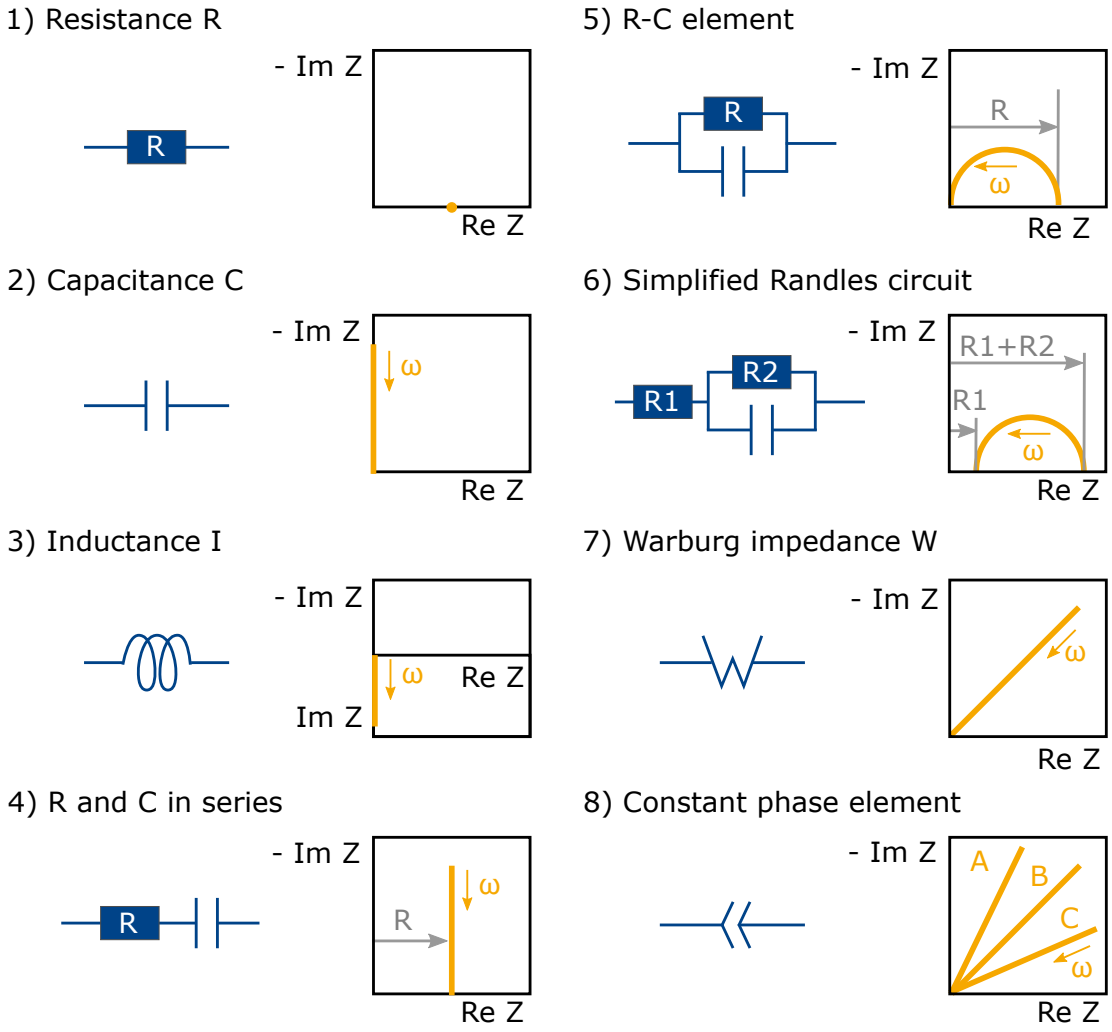


**Figure 2.4.:** Illustration of major EIS circuit elements and combinations, including typical circuit diagram representations and typical, schematic Nyquist plots.

Another common circuit element is the capacitor C ((2) in the illustration), which exhibits a frequency-dependent behaviour, resulting in only an imaginary impedance. At decreasing applied frequencies, the imaginary impedance increases, going towards infinity when the applied frequency goes towards zero. This makes sense: When a direct current is applied to a capacitor, the electrical circuit is basically disconnected, and hence the resistance infinite. Mathematically, this can be expressed by:

$$Z = \frac{1}{i\omega C} \tag{2.18}$$

$C$ is the value of the capacitance. The presence of $i$ already indicates the occuring phase shift, which goes hand in hand with the expression as imaginary

impedance [Boc1998; Bar2005].

While inductors ((3) in the illustration) are common electrical circuit elements, they do not often appear in EIS results and are not of high importance for the work at hand, and hence will not be discussed further. They sometimes appear at high frequencies in electrochemical systems, usually due to the connections and electrical wiring [Bar2001; Boc2002; Bar2005].

Three combinations of R and C are illustrated in Figure 2.4 to facilitate the understanding of the study described in Chapter 4. The illustrated combinations are R and C in series ((4) in the illustration), R and C in parallel (usually termed R-C element, (5) in the illustration), and an R-C element in series with another resistance R ((6) in the illustration). The first, R and C in series, behaves similar to a normal capacitor. The addition of an additional resistance R in series leads to a shift of the line along the x-axis, resulting in a line parallel to the y-axis in a Nyquist plot [Bar2001; Boc2002; Bar2005].

The combination of R and C in parallel ("R-C element") exhibits a more interesting behaviour. At low frequencies, the imaginary impedance, and hence the overall resistance, is so high that most of the current is conducted mostly by the the resistance R. Hence, at low frequencies the curve in the Nyquist plot intersects the x-axis, or is very close to the x-axis, at the value equalling the value of the ohmic resistance R. At increasing frequencies the resistance of the capacitor decreases. Hence, an increasing fraction of the AC current will be conducted via the capacitor, and the impedance will exhibit a stronger imaginary part. At further increasing frequencies, the AC resistance of the capacitor as well as the overall impedance goes towards zero, as discussed above. All in all, a semicircle forms in a Nyquist plot [Bar2001; Boc2002; Bar2005].

In case of the R-C element and the resistance in series, also often termed as simplified Randles circuit, the same kind of semicircle appears shifted along the x-axis. At low frequencies, the curve in the Nyquist plot intersects the x-axis, or is very close to the x-axis, at the value equalling the sum of the ohmic resistances, $R1 + R2$. At high frequencies, the semicircle ends at the x-axis at the value of resistance $R1$. This type of circuit element is valuable for the description of many physical and chemical processes, as most interfaces between two phases can be described by an R-C element, representing a charge transfer through the interface (represented by R) and an electrical double layer (represented by C) [Bar2001; Boc2002; Bar2005].

The above-mentioned R-C circuit elements usually have a simple, undistributed time constant $\tau$, which, in this case, can be determined as:

$$\tau = R \cdot C = \frac{1}{\omega} = \frac{1}{2\pi f} \tag{2.19}$$

$\tau$ depends on the resistance $R$ (in Ohm) and capacitance $C$ (in Farad) of an R-C element. The appearance of semicircles in Nyquist plots usually indicates characteristic time constants, of which there can be more than one in electrochemical systems. The investigation of time constants can help to identify the physicochemical cause of a specific observed behaviour, due to each mechanism having typical characteristic frequency ranges, in which they can be observed. The time constants of individual R-C elements can differ by orders of magnitude, depending on the resistance and capacitance. A small resistance and a small capacitance lead to a small time constant, which will be observable at high characteristic frequencies $f$. While most classical plate capacitors have a very low capacitance in the pF or nF range, electrical double layer capacitors, for example, have a very large surface area due to high porosity, and hence a large capacitance. This can be understood when considering the following equation for the capacitance of a parallel plate capacitor [Bar2001; Boc2002; Bar2005]:

$$C = \epsilon_0 \cdot \epsilon_r \cdot \frac{A}{d} \tag{2.20}$$

In this equation, $\epsilon_0$ is the electrical field constant, also called vacuum permittivity, $\epsilon_r$ the permittivity, $A$ the area of the condensator plates and $d$ the distance between the condensator plates. In case of EDL capacitors, the capacitance often lies in the range of $\mu F$ or $mF$, sometimes even $F$, e.g. in cases of so-called "pseudo-capacitance", which involves electrochemical reactions and hence faradaic charge transfer. In such cases, the resulting time constants are very high, and hence the related phenomena are usually observable at very low frequencies [Fle2014].

### 2.4.2. Physical and chemical phenomena and their EIS response

Many actually occuring physical and chemical processes exhibit behaviour which can be modelled only by a combination of many electrical circuit elements. In most real systems, the electrode surface is not uniformly active or accessible, which leads to a dispersion or distribution of the time constants. Examples for such processes are diffusion and porous supercapacitors or capacitive deionization electrodes, depending on the electrosorption of ions in EDLs [Ora2008].

**Porous capacitive electrodes.** As mentioned above, an obvious way to increase the capacitance of an electrode is to increase its surface area by increasing the

porosity, for example by reducing the pore size. However, this also leads to an increased resistance, as charged species (ions) have to penetrate the pore to make use of the additional surface area. Porous electrodes can, for example, be described by ladder structures of R and C elements, so-called transmission lines, as introduced by Robert de Levie [Lev1963; Lev1965] for modelling rough and porous electrodes. An illustration of such a ("horizontal") transmission line model is given in Figure 2.5 (a).

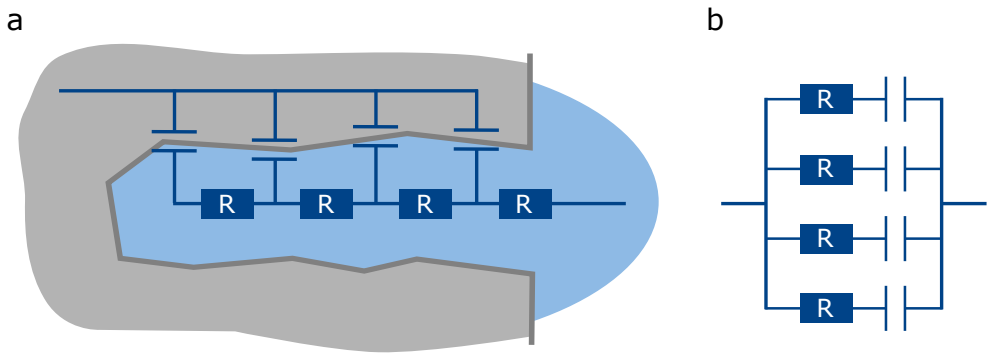


**Figure 2.5.:** Illustration of (a) a transmission line model with distributed resistances and capacitances representing a pore at an electrode surface, immersed in an electrolyte solution, also referred to as "horizontal ladder network", and (b) an example for a "vertical ladder network" [Lev1963; Köt2000; Ora2008; Fle2014].

Real materials, such as the activated carbons mostly applied in this thesis, do not have a uniform pore size, but rather a pore size distribution. Fletcher et al. [Fle2014] showed that such systems can be described by universal equivalent circuits consisting of "vertical" ladder networks, which are degenerate with horizontal ladder networks with the right choice of R and C values. Such vertical ladder networks (Figure 2.5 (b)) consist of a multitude of parallel sets of R and C elements in series. Each R-C series has its own time constant, representing the distributed resistances and characteristic frequencies of real materials, such as activated carbons. These time constants are often distributed over many orders of magnitude [Fle2014].

**Constant phase elements.** While such model approaches can generally represent any kind of porous, capacitive behaviour, the choice of values for the R and C elements can be challenging. For simplification, artificial circuit elements, which do not originate directly from real electrical circuit elements, have been introduced to model effects occuring in physico-chemical processes. An example for such a circuit element is the constant phase element (CPE), which basically

represents an infinite ladder network, and hence an infinite distribution of time constants [Fle2014]. The representation and typical plots of constant phase elements are illustrated in Figure 2.4, example (8). Mathematically, CPEs can be described as follows:

$$Z_{CPE} = \frac{1}{T(i\omega)^P} \tag{2.21}$$

At first glance, the equation looks similar to the equation representing the impedance of a capacitor. The difference makes the exponent $P$, which leads to a change of the angle of the line representing a CPE in a Nyquist plot, as illustrated by A, B and C in Figure 2.4 (8). In case of $P = 1$, the equation is identical to a capacitor equations, and hence will be represented by a vertical line in a Nyquist plot. In case of $P = 0.5$, the resulting line will have a 45° angle, which can also be used to reproduce an infinite length Warburg element, which is described below [Bar2005].

In real systems, an exponent close to 1 usually represents an electrode with a smooth surface. A decreasing exponent $P$ usually indicates a rough electrode, as can be seen in experimental results presented by de Levie for smooth and roughened electrode surfaces [Lev1965]. With increasing surface roughness or porosity, the exponent will decrease further.

**Warburg impedance.** Different physico-chemical phenomena can exhibit similar appearances in Nyquist plots, as indicated in Figure 2.4 (7) and (8). The infinite Warburg element is another example for an artificial equivalent circuit element introduced by Warburg in 1899 for the interpretation of EIS results involving diffusion. At an exponent $P$ of 0.5, the behaviour of a CPE element and a Warburg element is basically indistinguishable. Warburg elements can be represented by the following mathematical expression [Boc2002; Bar2005]:

$$Z_W = \frac{\sigma}{\sqrt{\omega}} - \frac{i\sigma}{\sqrt{\omega}} \tag{2.22}$$

$\sigma$ is a constant often called the Warburg coefficient, which depends on the concentration, diffusion coefficient and charge of the diffusing species. The infinite Warburg element represents the semi-infinite diffusion of a charged species towards an electrode. At increasing frequencies, the Warburg impedance becomes small in comparison to other typical impedances at electrode/solutions interfaces, as diffusion does not have enough time to establish and become a limiting factor. Hence, diffusion limitations usually dominate at low frequencies, while at higher frequencies other limitations, such as charge transfer, may be limiting. Various

modifications of Warburg elements exist, which can be applied for modelling different settings. An example is the diffusion in a finite flow channel with reflective boundary, or open-circuited behaviour ("finite length Warburg - open circuit" or just "open Warburg"), resulting in capacitive behaviour at sufficiently low frequencies. In this case, no direct current can flow in the system, the diffusing species accumulates at the boundaries [Bar2001; Boc2002; Bar2005; Ora2008].

**ED and CDI process models based on equivalent circuits.** Equivalent circuit models and EIS analyses are not limited to the above discussed circuit elements and examples for modelling approaches. Equivalent circuit modelling is frequently applied for modelling capacitive deionization [Ore2008; Qu2015] and electrodialysis [Cam2019] processes, or for the analysis of transport through ion-exchange membranes [Dłu2010], just to mention some examples.

# 3

# Overview: Understanding and advancing FCDI processes

In the following chapters I share with you the last few years of understanding and progress I achieved together with fellow researchers and students in the field of continuous flow-electrode capacitive deionization (FCDI) processes for potential application in desalination and brine concentration.

The concept of FCDI is, at a first glance, strikingly simple. However, many interlinking chemical and physical mechanisms have an effect on the process performance. Figure 3.1 illustrates some major phenomena, which have a major influence on FCDI processes. The illustration does not aim at being complete, but rather illustrates a selection of mechanisms relevant to FCDI processes. A short overview of the content of the core chapters of this thesis is given in the following.

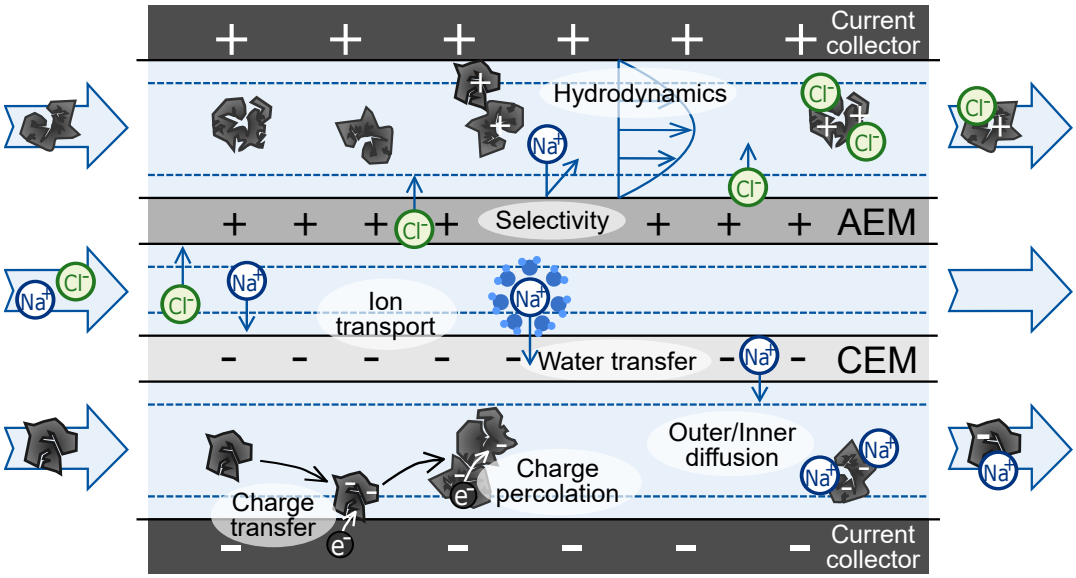


**Figure 3.1.:** Illustration of major mechanisms governing FCDI processes.

## Chapter 4 - Unraveling charge transfer in carbon flow electrodes using EIS

The flow-electrodes are the heart, or rather the blood, of an FCDI system. Effective electronic and ionic charge transfer and transport, as well as effective mass transport, are vital for flow-electrode based systems. The work presented in this chapter aims at extending the understanding of factors influencing the charge transfer and transport in suspension-based flow electrodes.

Additionally, this chapter aims at establishing a foundation for an application of EIS as predictive characterization method for flow-electrode materials, e.g. for incoming goods inspection. The performance of FCDI systems relies heavily on the quality of the active material, which is activated carbon in case of this work. In this chapter, it is demonstrated that it is possible to predict and match the desalination performance of flow electrodes based on two completely different activated carbon types using EIS.

## Chapter 5 - System design and energy recovery

In a system based on the capacitive/electrostatic adsorption of ions, it is self-suggesting to investigate the possibility of energy recovery. The possibility to recover energy from CDI electrodes has been demonstrated in several works [And2010; Dłu2013; Wel2005]. Jeon et al. [Jeo2014] also demonstrated the possibility recover energy in FCDI processes in a discontinuous manner.

The research presented in this chapter demonstrates continuous energy recovery in FCDI processes for the first time. Additionally, the performance and specific energy demand of FCDI systems in different process layouts, including the energy required for pumping flow-electrodes, is investigated. A first intermediary comparison to other desalination methods is attempted, which at the time served as a guidepost for further works aiming at developing a better understanding of FCDI processes and at making it competitive.

## Chapter 6 - Water and ion transfer in FCDI processes for the treatment of high salinity solutions

A short experimental study is presented, which focuses on developing a further understanding of salt and water transfer in the treatment of high salinity solutions using continuous FCDI processes. Two continuous FCDI process layouts, the two-module and single-module configuration, are directly compared regarding the water and salt transfer within the system. The results give an indication of the contribution of osmotic and electroosmotic effects to the overall water transfer.

## Chapter 7 - Influencing the energy demand

Based on the observations made in the previous studies, concepts for achieving a further reduction of the energy demand of FCDI processes are presented and tested in this chapter. It is shown that the energy demand of FCDI processes can be reduced significantly without energy recovery in the regeneration step, for example by introducing additional cell pairs into an FCDI module.

## Chapter 8 - Modeling FCDI processes at high salinities

The use of a process model can help to extend the understanding of the main influencing factors of a technology, as well as reduce the need for time consuming experimental studies. To address this, a first, strongly simplified, model was published in 2018 [Rom2018b]. The model presented a great help in recent years in developing a further understanding of the physical dependencies and main influencing parameters of FCDI processes and lead to accelerated advancements. However, this model is only suitable for simulating the treatment of low salinity solutions due to simplifying assumptions. FCDI may be a good candidate for brine treatment and concentration, in which case the previous assumptions are not valid.

To overcome this limitation, an improved process model is presented in this chapter, which is suitable for the simulation of continuous FCDI processes for the treatment of high salinity solutions.

## Chapter 9 - FCDI- the new alternative for water treatment? A compendium.

This chapter presents an attempt at evaluating the potential of FCDI technologies in the context of established technologies and new developments. The main findings presented in this thesis are summarized, and possible topics for further research and development are outlined.

# 4

# Unraveling charge transfer in carbon flow electrodes using EIS

Parts of this chapter have been published:

Alexandra Rommerskirchen, Anna Kalde, Christian J. Linnartz, Leon Bongers, Georg Linz and Matthias Wessling. "Unraveling charge transport in carbon flow electrodes: Performance prediction for desalination applications" in: *Carbon* 145 (2019), pp. 507-520.

## 4.1. Introduction

Effective electronic and ionic charge transfer and transport, as well as effective mass transport, are vital for flow electrode based systems. In case of capacitive systems, a high salt uptake capacity is preferred, whereas in case of flow-capacitors, a high capacitance is preferred. This chapter aims at extending the understanding of factors influencing the charge transfer and transport in suspension-based flow electrodes. All technologies based on pumpable (slurry-) electrodes rely heavily on the quality of the conductive material used to prepare the slurries. In most cases, these are carbon materials in various shapes and sizes [Hat2015a; Yan2017]. In case of applications with redox-active electrodes, materials with a comparably low surface area may be of advantage. In this case, adsorption is not desired, but rather a swift transport of the reacting components to the (flow-)electrode particle surface and a rapid transport of the products away from the surface [Per2018; Par2017]. In case of technologies based on adsorption of components in the EDL, a high surface area is desirable [Ore2008]. Many different physical and chemical processes influence the performance of flow electrodes in these processes, whose interactions are not yet fully understood. An increasing number of studies are investigating these physical and chemical interactions in flow electrodes by means of modelling [Hoy2016; Hoy2018], imaging methods [Hat2017] and electrochemical characterization methods [Pre2012; Hat2013; Den2014b; Den2014a; Pet2015b; Pet2015a; Hoy2018]. However, the influence of parameters and material characteristics on the performance as flow electrode for specific applications still needs further investigation. In most studies which focus on the investigation of slurry electrodes by electrochemical methods, such

as cyclic voltammetry (CV) or electrochemical impedance spectroscopy (EIS), the flow electrodes have been investigated in a static manner. The slurries were filled into cells with various designs and analyzed [Fan2014; Hat2015a; Cho2017c; Aku2017]. In some studies, electrochemical methods have been combined with rheological measurements performed in rheometers ("electro-rheology") [Blo1988; Hat2015a; You2015] and thus investigated dynamically. Only very few measurements were actually performed in a flow cell at dynamic conditions ("pumped flow electrodes") [Lia2017; Hoy2018]. However, these measurements were mostly applied for qualitative comparisons and not analyzed and interpreted in depth. Hoyt et al. recently developed a first electrochemical impedance spectroscopy model, which matches experimental data of capacitive flow electrodes [Hoy2018]. They developed a new circuit element, "$Z_{EFC}$", which simulates the suggested quasistatic behaviour of slurries at high frequencies.

**Motivation and objectives.** The impact of specific material characteristics on the performance of an FCDI process is not yet fully understood. Working on FCDI systems, significant differences in the performance of activated carbon (AC) material supposedly of the same type, but provided by the manufacturers in different vessels, were observed. The reason for this is that the actual rheology and desalination performance of a flowable electrode depends on a sum of parameters, encompassing the particle size distribution, particle shape [Boo2014], particle conductivity [Lia2017], pore size distribution [Tia2017], carbon surface chemistry [Hat2015b] and redox-activity [Yoo2015]. These parameters can change drastically from batch to batch, depending on the carbon material. Most commercial carbons are not intended for use as flowable electrodes, and hence the standard specifications are often insufficient. Due to the focus on specific characteristics, most classical physical and chemical characterization methods have only limited significance for the evaluation of a carbon material for application in FCDI. Additionally, many of these methods, such as gas adsorption measurements, are very time-consuming. Hence, for an actual application, a swift and reliable method for the evaluation of the overall performance of a carbon material as flowable electrode is required.

Electrochemical impedance spectroscopy (EIS) is an electrochemical characterization method, which applies an alternating potential (or current) of different frequencies, as described in Chapter 2. The hypothesis behind this work is that EIS measurements can predict the desalination performance of slurries accurately when performed at dynamic conditions. EIS measurements allow conclusions regarding the most important material characteristics required for FCDI when combined with classical physical and chemical characterization methods. While

Hoyt et al. [Hoy2018] took a first step and developed a model providing detailed physical understanding using a new circuit element, a more application oriented approach is applied here, which is based on standard elements used in EIS models.

The aim of the work presented in this chapter is to establish a foundation for an application of EIS as predictive characterization method for flow-electrode materials, e.g. for use as method for incoming goods inspection. This includes:

- The investigation of the influence of different system parameters on the EIS response. (Section 4.3)
- The development of a simple equivalent circuit model, which matches all obtained experimental results. (Section 4.4)
- An examination of the carbon characteristics and their influence on the FCDI performance. (Section 4.5)
- A demonstration of the possibility to predict and match the desalination performance of flow electrodes based on two completely different activated carbon types using EIS. (Section 4.6)

## 4.2. Materials and methods

The design of the FCDI cells used for the experiments described in this thesis is in principle the same for all chapters, and identical to the design described in recent FCDI-related publications by our workgroup [Rom2018a; Rom2019]. The FCDI cells consisted of polyethylene end plates, flat gaskets, epoxy-impregnated graphite electrodes (Müller & Rössner GmbH & Co. KG, 180x180x10 mm) with flow channels for the flow electrodes (3 mm width, 2 mm depth, 200 cm overall length), a pair of cation and anion exchange membranes (Fumasep FKB-PK-130/ED-100 and Fumasep FAB-PK-130/ED-100, Fumatech BWT GmbH) with an effective surface area of 121 $cm^2$ and a 0.5 mm mesh spacer (Fumatech BWT GmbH, ED-100). In all experiments described in this chapter, the cells were operated in co-flow. Changes from this standard layout are described in the respective chapters. In all experiments described in this thesis, there were no titanium or stainless steel fleeces placed between the graphite current collectors and ion-exchange membranes. This is the main difference to the modules described in the earlier works of our workgroup [Gen2014; Rom2015], which also provided the data for the simulations described in our publication regarding the first FCDI process model [Rom2018b]. A section of the FCDI cell applied for this study is depicted in a cross-sectional view in Figure 4.1.

The feed water was supplied to the FCDI cells by a peristaltic pump (Ismatec Reglo ICC peristaltic pump with two independent channels). The salt solutions

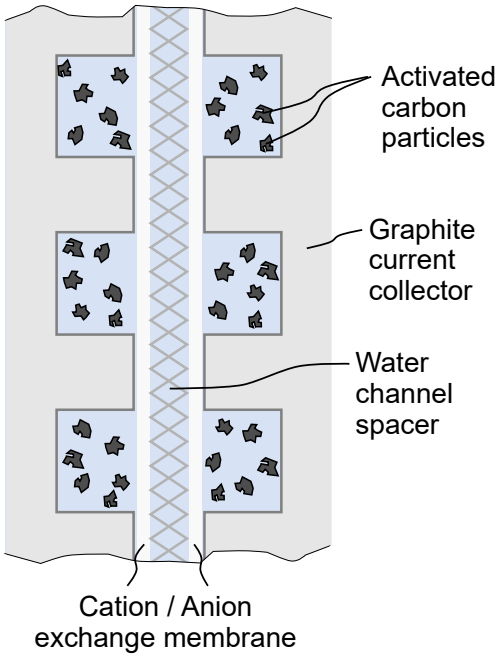


**Figure 4.1.:** Section of the FCDI cell applied for EIS measurements and desalination measurements in cross-sectional view.

used as feed water and for the slurry preparation were prepared with purified water and 60 g/L sodium chloride (VWR Chemicals, >99.8 %). The flow electrodes were recirculated through the FCDI systems using a second peristaltic pump (Ismatec MCP process drive, Masterflex two-channel pump head Easy-Load II, Norprene tubing).

**Table 4.1.:** Overview of activated carbons applied in this study. Information provided by the suppliers.

| | | Carbopal SC11PG | Carbopal CCP1400 spezial | NoritD10 -*Batch*1 | NoritD10 -*Batch*2 |
|---|---|---|---|---|---|
| abbreviations | | SC | CCP | N-*B*1 | N-*B*2 |
| **BET surface** | **$m^2/g$** | 950 | 1400 | 600 | 600 |
| **particle size** | **d90** | 64 $\mu$m | 80 $\mu$m | 140 $\mu$m | 140 $\mu$m |
| | **d50** | 16 $\mu$m | - | 30 $\mu$m | 30 $\mu$m |
| **pH value** | - | 4.5 - 6.5 | 6 - 8 | alkaline | alkaline |
| **type** | - | charcoal | coconut shell | - | - |

All in all, four different activated carbon powder samples were applied in this work: (1) Carbopal SC11PG, (2) Carbopal CCP1400 spezial (both provided by Donau Carbon GmbH, Germany) and (3)/(4) Norit D10 (Alfa Aesar), of which two different samples (hereafter termed "*Batch* 1" and "*Batch* 2") were analyzed,

which were purchased in two different vessels, but had the same LOT number. Table 4.1 gives an overview of the activated carbon sample properties according to conventional characterization techniques, as provided by the manufacturers. In addition, a set of experiments was performed using graphite powder (synthetic, <20 $\mu$m, 20 $m^2/g$, Sigma Aldrich, Germany) for the preparation of the slurry-electrode with varied electrolyte concentrations.

### 4.2.1. Sieving experiments

The activated carbon was sieved at low amplitude in a sieving tower assembled of stackable sieves (Retsch GmbH, Germany) with mesh widths (in $\mu$m) of 20, 32, 40, 63, 80, 112, 125, 160, 230 and 350. The vibrating unit (Retsch AS200 digit) was set to 1.5 for the duration of each sieving interval. The mass of the particle fractions was measured at regular time intervals, sieving was stopped when no significant changes were observed in the mass of the particle fractions.

### 4.2.2. Microscopic imaging

Microscopic images of the standard activated carbon and samples taken from the two sieve fractions $< 20$ $\mu$m and 40-50 $\mu$m were taken using a Olympus BH-2 light microscope, with an Olympus DP25 camera and an SPlan 40PL Objective (0.70, 160/0.17, 40x zoom). The activated carbon samples were mixed with glue to fix the particles on the sample slide to avoid agglomeration and sedimentation during the microscopy.

### 4.2.3. BET/Gas sorption

The activated carbon samples (about 0.1 g each) were analyzed regarding their surface and porosity characteristics via $N_2$ gas adsorption/desorption measurements (ASAP 2020, Micromeritics). The samples were pretreated at 90 °C and 10 mbar for 24 h and degassed for 6 to 8 hours before the adsorption/desorption analysis.

### 4.2.4. Rheological measurements

The rheological measurements were performed with a modular compact rheometer (MCR) from Anton Paar with the PP50 plate-plate measuring system at 25 °C. Shear rates between 10 1/s and 1000 1/s were applied.

### 4.2.5. Electrochemical impedance spectroscopy measurements

The electrochemical impedance spectroscopy (EIS) measurements were performend in two-electrode configuration with one FCDI cell through which two flow electrodes were continuously recirculated from small glass beakers, which were continuously stirred. The experimental settings are summarized in Table 4.2. In case of the EIS measurements for the prediction of the desalination performance of a specific flow electrode, the slurry was recirculated through both the desalination and concentration cells, as illustrated in Figure 4.2. The impedance measurements were performed with the desalination cell only. The EIS measurements were performed with a potentiostat with inbuilt frequency response analysis (FRA)-module (Reference 3000, Gamry). Frequencies between 0.009 and 10000 Hz were applied with an amplitude of 10 $mV$, experiments were performed without potential bias. In most measurements, the imaginary part was negative at high frequencies (above 1000 Hz), likely due to inductive effects of the cables. These effects were not considered in this work.

**Table 4.2.:** Overview of parameter settings for EIS experiments.

| | **Slurry** | | | **Feed water** | |
|---|---|---|---|---|---|
| | AC conc. | NaCl conc. | Flow rate | NaCl conc. | Flow rate |
| **Figure no.** | wt.% | g/L | mL/min | g/L | mL/min |
| *Influence of activated carbon concentration and slurry flow rate* | | | | | |
| **4.3 (a)** | 0-10 | 60 | 150 | 60 | 13 |
| **4.3 (b)** | 10 | 60 | 0-150 | 60 | 13 |
| *Influence of the salt concentration* | | | | | |
| **4.9 (a)** | 16 | 7-317 | 150 | 7-317 | 13 |
| **4.9 (b)** | 10 (graphite) | 0-60 | 75 | 0-60 | 13 |
| *Comparison of four activated carbons* | | | | | |
| **4.12 (a)** | 16 | 60 | 150 | 60 | 13 |
| *Prediction of desalination performance* | | | | | |
| **4.14 (a)** | 10, 15, 30, 35 | 60 | 175 | 60 | 2 |
| **4.14 (c)** | 17 | 60 | 175 | 60 | 2 |

### 4.2.6. Desalination experiments

A three-channel power supply (HM8143, HAMEG Instruments GmbH) was applied for the desalination measurements. The electrical conductivity (EC) of the aqueous solutions was measured using conductivity sensors (LTC 0,35/23; Sensortechnik Meinsberg). Additionally, product water samples were taken during steady state operation. The density of each sample was analyzed to verify the salt concentration of the samples. The diluate stream and the concentrate

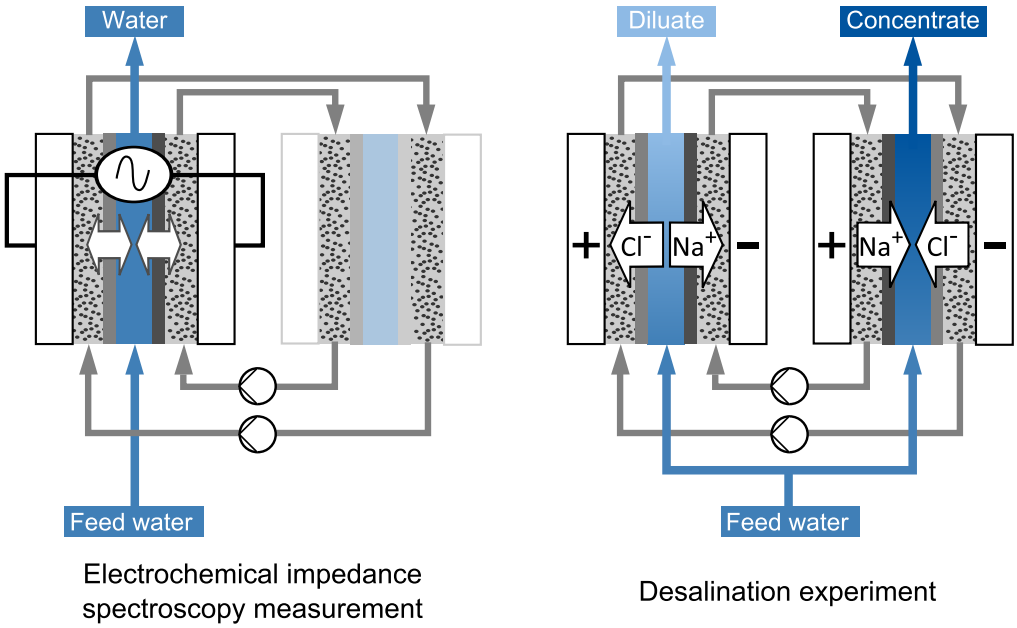


**Figure 4.2.:** Illustration of the FCDI system layout applied for (left) the electrochemical impedance spectroscopy measurements and (right) the desalination experiments. The EIS measurements were performed with the desalination cell only. The desalination experiments were performed with the continuous two-module FCDI layout described in previous publications [Rom2018a; Rom2018b].

stream were each treated in single-pass mode, while the flow electrodes were recirculated at a constant flow-rate. The experimental settings for the desalination experiments (Figures 4.14 (b) and (d)) equal the settings given in Table 4.2 for Figures 4.14 (a) and (c). All desalination experiments were performed at a constant voltage of 1.2 V, applied to each desalination and regeneration cell.

## 4.3. Results: EIS with parameter variations

As mentioned before, there are not many studies published in which the results of dynamic EIS measurements in an actual flow cell are described. For an initial understanding of the behaviour of such systems, parameter studies were performed, some results of which are plotted in Figure 4.3 (a) and (b). The experiments described in this section were performed with the activated carbon Carbopal SC11PG.

### 4.3.1. Influence of the activated carbon content

The activated carbon content was varied between 0-16 wt.%, while all other parameters were kept constant (Table 4.2). When considering the results plotted in Figure 4.3 (a), significant changes can be observed due to the addition of

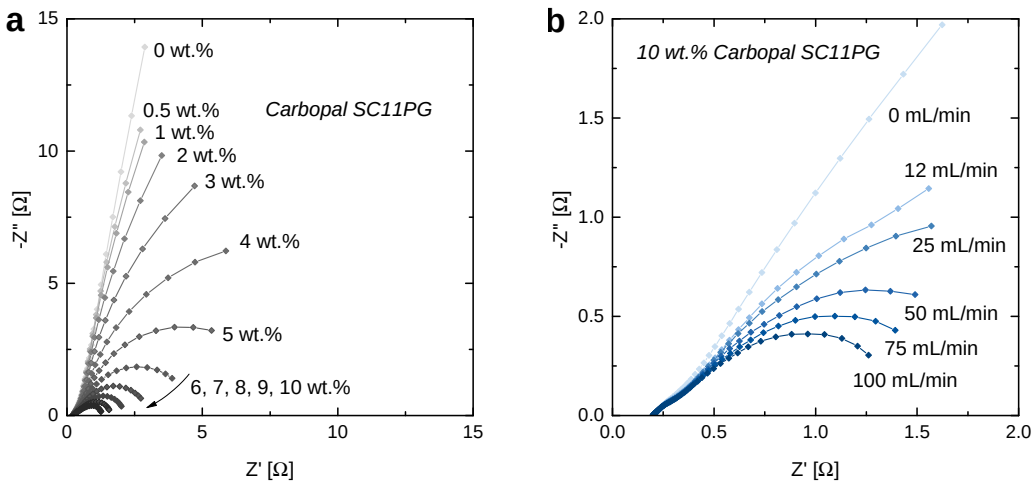


**Figure 4.3.:** Results of EIS measurements, cross-sectional area of the cell: 100 $cm^2$; (a) Variation of the activated carbon (AC) content with a constant NaCl concentration of 60 g/L in both water channel and flow electrode and a flow-electrode flow rate of 150 mL/min, and (b) Variation of the flow-electrode flow rate at a carbon loading of 16 wt.% (Carbopal SC11PG) and a 60 g/L NaCl concentration in both, water channel and flow electrode.

increasing amounts of activated carbon to the flow electrode. At 0 wt.% activated carbon only a small shoulder is seen in the plot at high frequencies and a more or less straight line at an angle of around 80° towards the low frequencies, which is in agreement with the behaviour of rough electrode surfaces (non-ideal capacitance). A slightly depressed semicircle develops in the lower frequency range with the addition of activated carbon. With increasing activated carbon content, this semicircle becomes smaller, which correlates with an increasing capacitance and a decreasing interfacial resistance within the flow electrode.

### 4.3.2. Influence of the flow-electrode flow rate

Next, the transition in the impedance of static flow electrodes to pumped flow electrodes was investigated by varying the flow-electrode flow rate between 0-100 mL/min. All other parameters were kept constant (Table 4.2). The results are plotted in Figure 4.3 (b). At first sight, the changes to the Nyquist plot when increasing the flow electrode flow rate look similar to the changes when increasing the activated carbon concentration. Without pumping, only a small shoulder is seen in the plot at high frequencies and a more or less straight line at an angle of around 55° towards the low frequencies, similar to the plot without activated carbon in the flow electrode. In both cases, 0 % activated carbon and 0 mL/min, the system acts like a static capacitor. The added activated carbon in the 0 mL/min case leads to a decrease of the line angle at low frequencies,

which can be explained by the influence of the activated carbon porosity. With increasing flow rate a slightly depressed semicircle forms at the lower frequency range, which correlates with an improved charge percolation. The hypotheses regarding these phenomena are discussed further in the following section.

## 4.4. Development of an equivalent electric circuit model

An equivalent circuit was developed, which can be used to fit and improve the understanding of the EIS data. The term ”equivalent circuit” refers to a system of electric circuit elements, in this case, which imitates the impedance behaviour of an electrochemical system (an FCDI cell in this case) over a wide range of frequencies. According to Fletcher et al. [Fle2014], this represents the ”electrochemist's way” of speaking.

In most EIS measurements with FCDI systems, mainly two semicircles were visible in the resulting Nyquist plots, which corresponds with two dominant time constants in the system (e.g. each one R-C element). In an FCDI system, we expect the EIS spectra to be influenced by both, diffusion limitation as well as the porous electrode material. In fact, the observed semicircles do not appear as perfect circles, but are rather depressed, which indicates an overlapping of the above mentioned physical effects. In the following, the thoughts which led to the development of the equivalent circuit model presented in this thesis are illustrated in more detail.

### 4.4.1. Convectional current - Formation of the low frequency semicircle

When transfering the understanding of faradaic systems and the understanding of the behaviour of classical capacitive systems (e.g. electrical double-layer supercapacitors) to capacitive flow electrodes, the formation of the ”larger”, low frequency, semicircle can be explained. One might assume at a first thought that capacitive flow electrodes in an FCDI cell, as applied in this study, would behave similar to a regular electrochemical double-layer capacitor (EDLC). This is the case for stagnant flow electrodes or an FCDI cell with water or salt solution pumped through the flow-electrode channels. In these cases, as sketched in Figure 4.6, a semicircle is visible at the higher frequency range, which changes into a more or less linear dependence at the lower frequencies, with a slope of different angles, depending on the experimental conditions. However, in case the flow-electrode channel contains an activated carbon suspension and is pumped, a

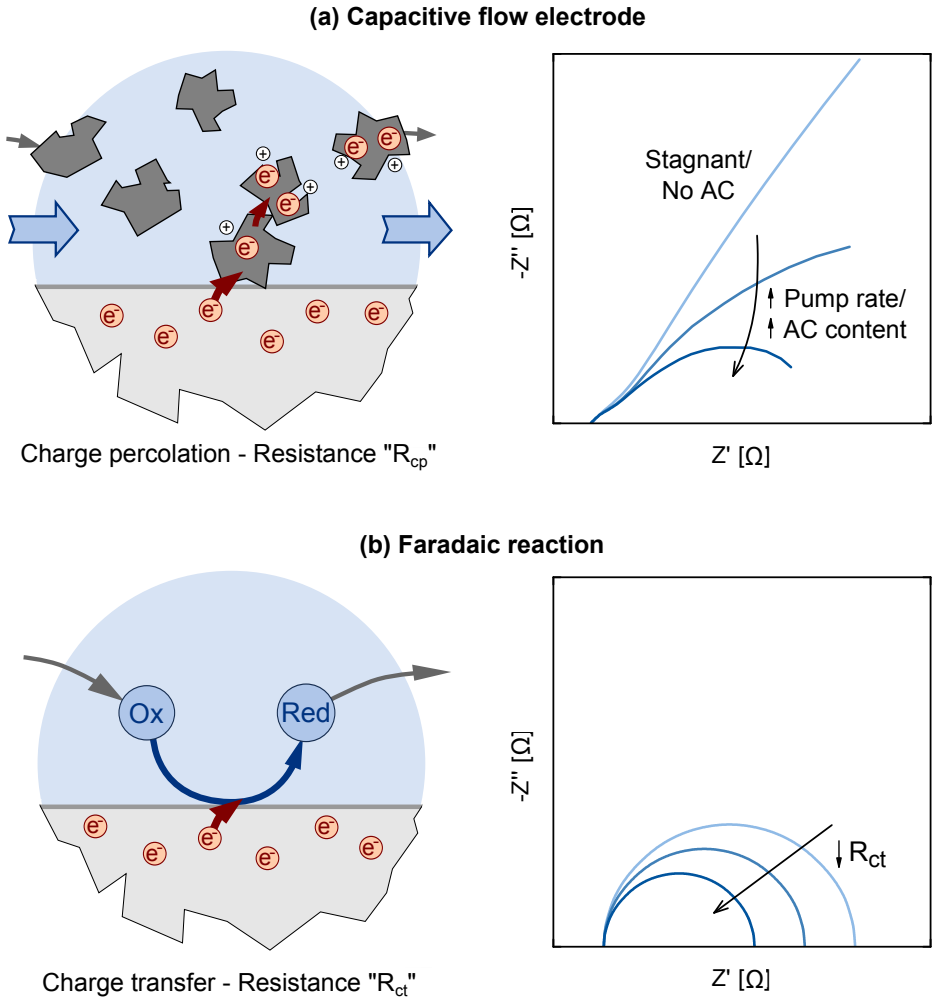


**Figure 4.4.:** Illustration of (a) the effect of an electric current induced by convection on EIS spectra of a system based on capacitive flow electrodes, and comparison to (b) an electrochemical system with faradaic reactions.

second semicircle appears in the low frequency region (Figure 4.4, Figure 4.3 (a) and (b)).

Such low-frequency semicircles are also visible in previously published work [Lia2017] and were also adressed by Hatzell et al. [Hat2015a]. In the latter work, it was suggested that this behaviour observed for flow electrodes results from increased electronical conductivity. Hoyt et al. [Hoy2018] mentioned this as "current induced by convection". I assume that this behaviour is induced by electron transfer, which also leads to a removal of electrons in form of charged electrical double layers at the carbon particle surface due to convective transport out of the cell in case of pumped flow electrodes, as illustrated in Figure 4.4. The formation of similar semicircles in impedance spectra can be observed in case of faradaic reactions, which involve a transfer of electrons and are usually modelled by a R-C element, where the resistor is usually termed charge transfer resistance.

In case of capacitive flow electrodes, when no potential bias is applied and when assuming ideal circumstances, no faradaic reactions should take place. The particles suspended in the salt solution are expected to be charged upon contact with the current collector or other charged particles (formation of charge percolation networks), which results in the adsorption of ions at the particle surface. This would usually result in the exhibition of a capacitive behaviour in the impedance spectra. In case of an activated carbon concentration of 0 % (Figure 4.3 (a)) this is the case, as only the current collector is charged and no electrons are removed by pumping. This is also the case for stagnant carbon flow electrodes. However, once the flow electrodes are pumped, the particles are charged and some of them will leave the cell in a charged state, without the ability to be discharged again directly, as illustrated in Figure 4.4. Although the charge is stored capacitively, the measuring system, thus, records an apparent electric current caused by the convective charge removal. Due to the apparent electron flow, this phenomenon can be modelled using a resistor. The value of this resistor, which is termed as "charge percolation resistance $R_{cp}$" from here onwards, decreases with increasing conductivity of the flow electrode. An increasing activated carbon content, for example, leads to an increased size of charge percolation networks [Hat2017] and an overall improved conductivity, which agrees with the discussion by Hatzell et al. [Hat2015a].

### 4.4.2. Charge transfer at current collector - Formation of the high frequency semicircle

Charge transfer phenomena at the current collector and insufficient contacting often lead to the observation of semicircles in the higher frequency range in Nyquist plots, for example in case of EDLCs [Lei2013; Dso2013]. In case of FCDI, charge transfer at the current collector may include the graphite plate itself, as well as activated carbon particles resting at the surface, which are in direct contact with the graphite plate, as illustrated in Figure 4.5.

The results of fitting the equivalent circuit model to the experimental results shown in Figure 4.3, given in Tables A.1 and A.2, support this hypothesis. Due to the direct contact of the particles with the current collector, short ways and comparably small electrically active surface area lead to a comparably low resistance and capacitance. The magnitude of the capacitance and resistance influences the time constant of a circuit element, which is in direct relation with the characteristic frequency of the related phenomenon. For simple R-C-circuits the time constant $\tau$ is defined as given in Equation 4.1, with R being the ohmic resistance and C being the capacitance of the correlating circuit elements [Bar2005].

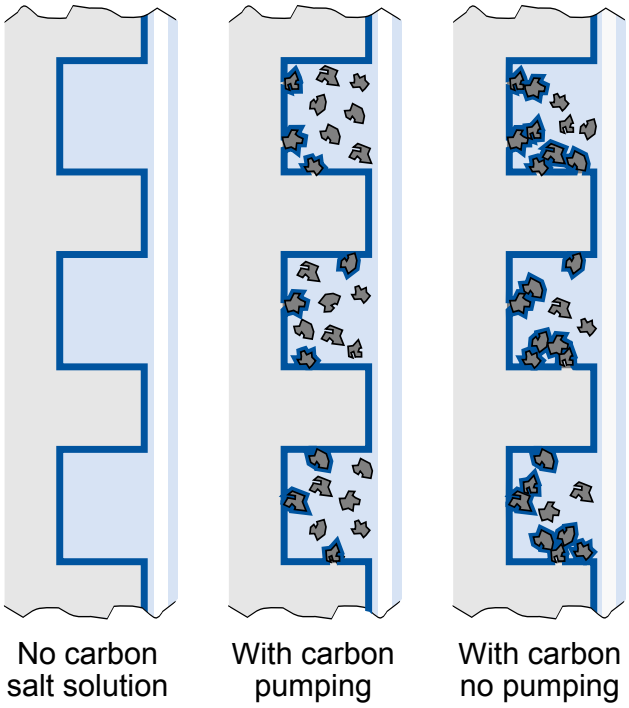


**Figure 4.5.:** Illustration of carbon particles in direct contact with the current collector in case of three different experimental conditions. Charged surfaces due to direct contact with the current collector are highlighted by the thick blue line. This leads to a change in the capacitance $C_{CC}$, as can be seen in the values fitted to experimental results (Tables A.1 and A.2).

$$\tau = R \cdot C \tag{4.1}$$

In case of a small resistance and a small capacitance, the time constant is small, which leads to a high characteristic frequency.

### 4.4.3. Diffusion and electrode porosity - Curve depression

We assume that the combined effect of diffusion and electrode porosity in the system lead to the non-ideal, depressed shape of the semicircles in the Nyquist plots of experimental results regarding FCDI systems obtained in this work. Distinction between diffusion and porosity is not feasible applying purely EIS measurements of the system at hand, as both phenomena cause a 45° line in impedance spectra in ideal cases. In many electrochemical systems the frequency range of porous electrode behaviour opposed to diffusion phenomena is sufficiently different to distinguish between the two phenomena. However, the system at hand consists of porous particles with internal diffusion, which may again form percolating particle networks, in which diffusion from the continuous phase to the particles as well as diffusion from the membrane into the depth of the flow-electrode channel

takes place. Hence, the fractal nature of the system at hand seems to prevent the development of distinct characteristic frequencies. This leads to an influence of internal and/or external diffusion over a wide frequency range, making it difficult to distinguish between the phenomena.

Due to the above discussed effect of the charge percolation resistance, this 45° line caused by internal and/or external diffusion results in depressed semi-circles in case of FCDI, as illustrated in Figure 4.6. While diffusion is usually modelled using Warburg elements [Ora2008], electrode porosity is often modelled using different types of ladder networks, or so-called transmission lines [Köt2000; Fle2014]. Robert de Levie [Lev1963; Lev1965] provided the basis for modelling the behaviour of rough and porous electrodes by introducing the concept of the so-called "RC transmission lines" in the 1960s [Lev1963; Lev1965]. Such transmission lines can be degenerated to models with ladder structures of different kinds, which can also model non-uniform porosity, as it occurs in materials based on natural raw materials, such as activated carbon [Fle2014]. Degenerate equivalent circuits are networks of electrical circuit elements with different structures, but the same total impedance behaviour over the investigated range of frequencies [Fle2014].

While these kinds of models also allow valuable insights, the disadvantage of such ladder structures is the high number of parameters, which need to be fitted. If the system is not well-known, the parameters need to be guessed, which hardly conveys an actual physical meaning. This, in combination with the fact that the observed flow electrodes not only exhibit porous behaviour, but also diffusive behaviour, led us to choose a constant phase element as simplified (and artificial) circuit element representing the systems porosity as well as diffusion behaviour. A constant phase element can, in fact, be seen as an infinite ladder network ranging over an infinite range of time constants [Fle2014].

However, in our measurements we often observed that an "unrestrained" constant phase element does not model the system very well, which leads to the conclusion that the system is not limited by porosity or diffusion at low frequency. To constrain this behaviour to a smaller frequency range we, thus, used a charge percolation resistance in parallel to the constant phase element, which leads to the behaviour illustrated in Figure 4.6.

### 4.4.4. The equivalent circuit model: Putting it together

By combining the above discussed observations, we developed the equivalent circuit illustrated in Figure 4.7. This equivalent circuit can be fitted to represent measurements with FCDI systems in a wide range of settings regarding different parameters such as activated carbon content and flow-electrode flow rate with a minimum of fitting parameters.

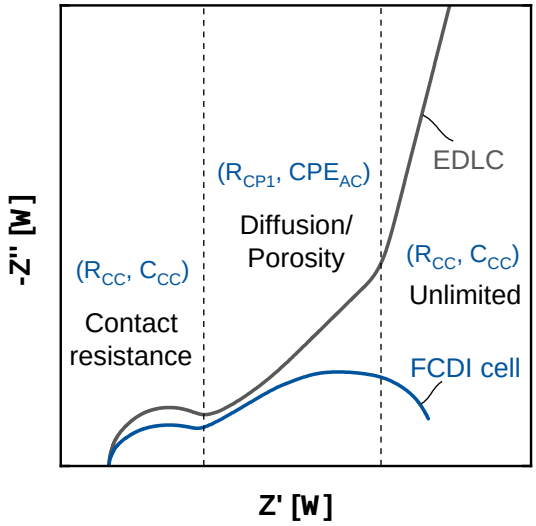


**Figure 4.6.:** Typical Nyquist plots of supercapacitors and capacitive flow electrodes and indicated physical behavioural regimes.

The circuit elements depicted in Figure 4.7 represent (1) the electron transfer at the current collector ($R_{CC}$ and $C_{CC}$), (2) the influence of diffusion and electrode porosity ($R_{cp1}$ and $CPE_{AC}$), (3) the capacitance and current induced by convection ($R_{cp2}$ and $C_{dl}$) and (4) the combined, serial resistance of solutions, membranes etc. ($R_S$).

## 4.5. Extended results and discussion

### 4.5.1. Fit results and observations based on the equivalent circuit model

The equivalent circuit model shown in Figure 4.7 was fitted to experimental results by using the software ZView 2 (Version 3.5b, Scribner Associates, Inc.). The square of the standard deviation of the resulting fits from experimental results was in the range of $10^{-4}$ in most cases. Tables A.1 and A.2 in Appendix A show results for the fit values of the different elements of the equivalent circuit model, fitted to the results shown in Figure 4.3 (a) and (b).

**Variation of the activated carbon content and flow-electrode flow rate** The circuit elements with the most significant changes due to a change in the activated carbon content are $C_{CC}$, $R_{cp1}$, $R_{cp2}$ and $C_{dl}$. The changes in $C_{CC}$ were discussed in Section 4.4.2 and illustrated in Figure 4.5. The values of $R_{cp1}$ are mostly similar to $R_{cp2}$. The electrode porosity/diffusion, modeled by the constant

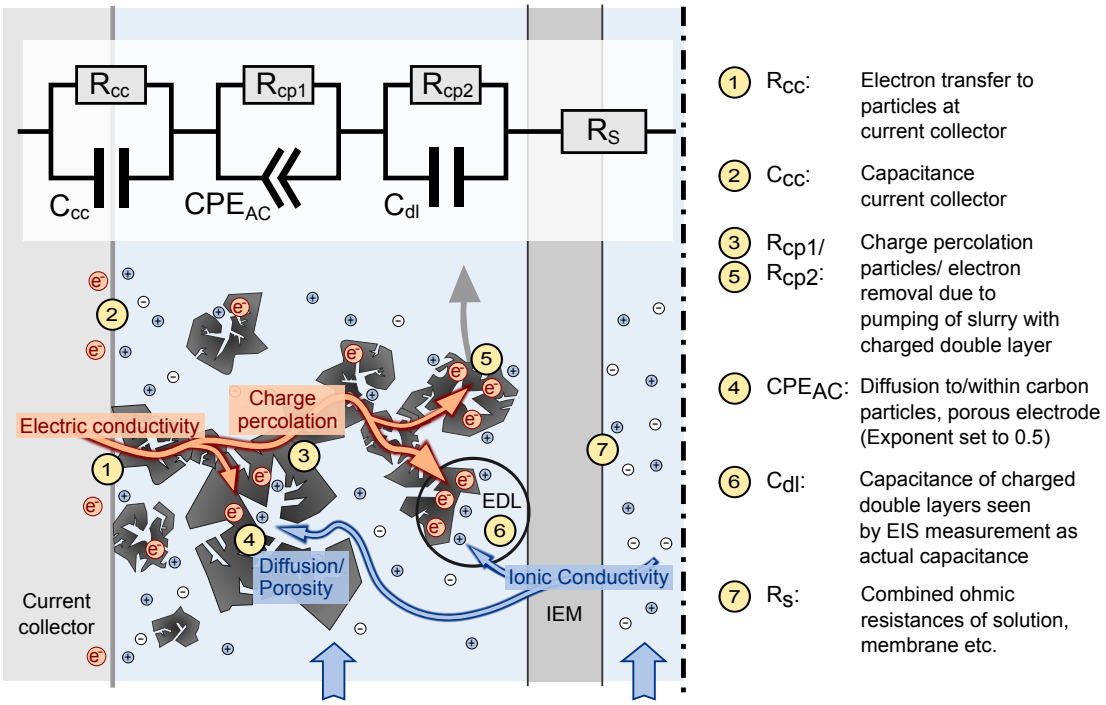


**Figure 4.7.:** Equivalent circuit model applied to fit experimental data.

phase element, has an influence over a major part of the investigated frequency spectrum, with a lower influence at low frequencies. In case of low activated carbon concentrations as well as low flow-electrode flow rate, the fitted values of $R_{cp1}$ increase disproportionally. In this case, the constant phase element dominates also at lower frequencies. The very high fit values for $R_{cp1}$ at low activated carbon concentrations and pump rates indicate an irrelevance of this type of conduction pathway under these conditions. When fitting an equivalent model with and without $R_{cp1}$ to the same experiments, the fit values for all other parameters were the same. Hence, $R_{cp1}$ was excluded from the model in case of low activated carbon contents and low flow-electrode flow rates.

With an increasing activated carbon content the size of the charge percolation networks increases [Hat2017], which leads to an improved exploitation of the activated carbons maximum salt adsorption capacity as well as an improved conductivity. A closer investigation of the trend of $C_{dl}$ over increasing activated carbon content, as plotted in Figure 4.8, reveals a slow increase of $C_{dl}$ at low activated carbon contents, and a sudden increase which passes into a linear increase of $C_{dl}$ at higher activated carbon contents above 8 wt.%.

We explain the slow increase at low activated carbon contents by an ineffective charge percolation, which leads to an incomplete use of the maximum salt adsorption capacity as not all carbon particles are charged. At higher activated carbon contents the percolation threshold is reached, above which the capacitance increases linearly with increasing activated carbon content due to an effec-

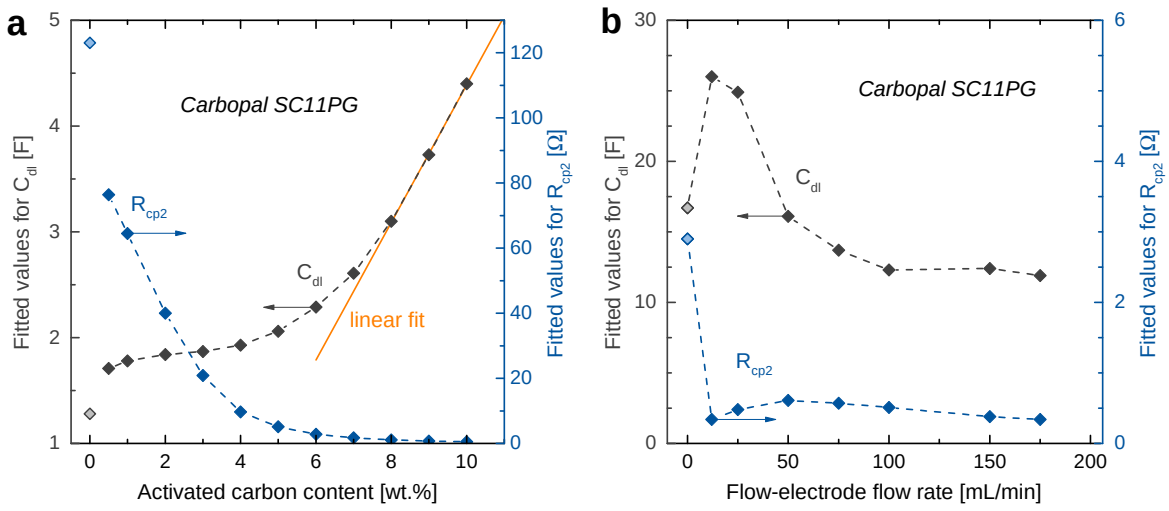


**Figure 4.8.:** Fitted values of $C_{dl}$ and $R_{cp2}$ using the equivalent circuit model, (a) fitted to results obtained at a varied activated carbon content in the flow electrodes, and (b) fitted to results obtained at a varied flow-electrode flow rate and constant activated carbon loading. Results of the corresponding experiments are plotted in Figure 4.3 (a) and (b), other fit values are listed in Appendix A, Table A.1 (second set of experiments) and Table A.2.

tive charge percolation. The formation of such conductive particle percolation networks has by now also been observed in a simulative study by Lohaus et al. [Loh2019].

The slope of the linear fit displayed in Figure 4.8 is 0.65 F/wt.%, which results in an effective capacitance of 2.7 F/g, considering the volume of the flow-electrode flow channels. This is a comparably low value considering literature values regarding the capacitance of activated carbons. For the Carbopal SC11PG sample we obtained a value for the maximum capacitance of 121.5 F/g considering the BET surface area and assuming a capacitance of 15 $\mu$F/cm$^2$ [Shi1996]. We explain this low capacitance value by the low residence time of the flow electrodes in the module, which only allows the use of a fraction of the maximum possible salt adsorption capacity by charging only the most easily accessible pores. This may also partially explain the high importance of mesopores for FCDI processes observed in this study. The advantages of using only a fraction of the maximum capacitance are the fast kinetics, which allow an efficient salt removal and thus the treatment of high salt concentrations.

The trend regarding the charge percolation resistance $R_{cp2}$ is in good agreement with the trend regarding $C_{dl}$. For low activated carbon contents a steep decrease in $R_{cp2}$ is visible, which passes into a very small decrease at very low charge percolation resistances at higher carbon loading. This supports the theory of effective charge percolation.

An open question is, whether the reduction in the charge percolation resistances $R_{cp1}$ and $R_{cp2}$ originates mainly from a reduction in the pathways for outer diffusion, or also from shortened inner diffusion pathways. At high activated carbon contents the increased volume fraction of particles leads to an improved charge percolation due to more frequent particle-particle and particle-electrode interactions. However, the increase of the activated carbon content also leads to an increase in the surface area per flow-electrode volume, which is available for adsorption. Therefore, a smaller fraction of the pore network is required to reach a certain desalination state, which leads to a reduced need for diffusion of ions into the pores. Thus, apart from the shortened outer diffusion pathways, the inner diffusion pathways are shortened as well due to an increased activated carbon content. A first attempt at understanding the contribution of both to the overall mass transport is made in a set of experiments in which the salt concentration in the flow electrodes was varied, as described in the following paragraph.

$C_{dl}$ increases with increasing activated carbon content in the flow electrode over the whole percentage range investigated. In case of an increasing flow-electrode flow rate, however, there is a sudden increase in $C_{dl}$ from 0 mL/min to 12 mL/min, while at further increasing flow rate $C_{dl}$ decreases again. In case of the stagnant flow electrode (0 mL/min), not all particles get in contact with the current collector. Some of the particles "rest" in the bulk of the flow electrode, not in contact with the current collector. When the flow electrodes are pumped, the particles are moved and, thus, brought into contact with the current collector. A larger fraction of the maximum salt adsorption capacity is used. At even higher flow rates the capacitance apparently decreases, due to the removal of charged particles by pumping. The charged particles removed from the system do not appear as a capacitance, but rather as current induced by convection, which leads to a decrease of $R_{cp2}$ at higher flow rates, while $C_{dl}$ stagnates. On the other hand, $C_{dl}$ may also be reduced at increasing flow-electrode flow rate due to a reduced residence time and, thus, an incomplete charging of the pores. The overlap of these effects may explain the maximum of $R_{cp2}$ at a flow rate of 50 mL/min.

**Variation of the salt concentration** Additional experiments were performed to investigate the influence of the electrode porosity/diffusion in capacitive flow-electrode systems. For this, EIS measurements were performed with varied NaCl concentrations at constant activated carbon concentration. The results are plotted in Figure 4.9 (a). Additionally, experiments were performed using flow electrodes based on graphite powder, the results of which are plotted in Figure 4.9 (b).

In case of activated carbon, at a low NaCl concentration a strong semicircle depression at low frequencies as well as a quasi-linear region at the higher fre-

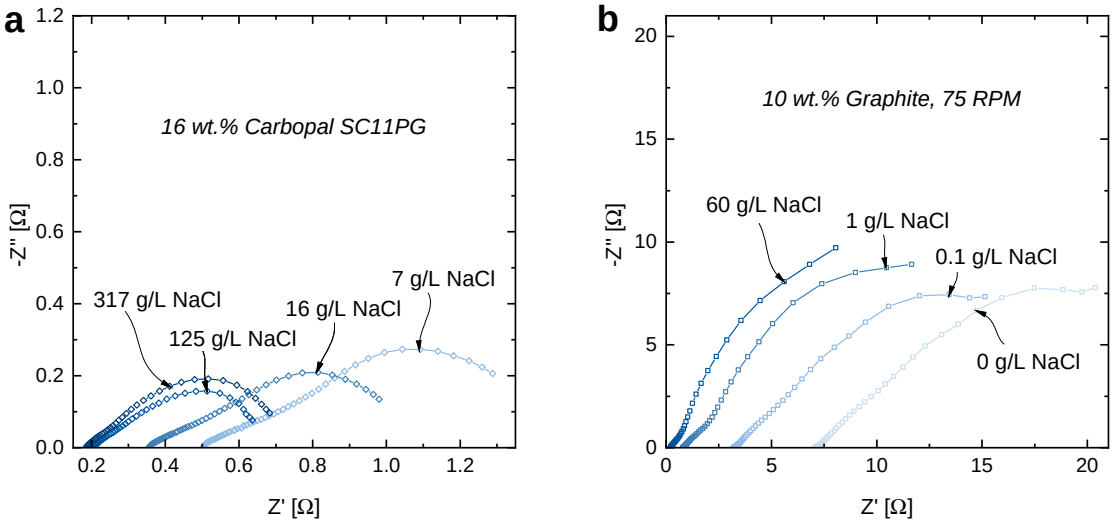


**Figure 4.9.:** Results of EIS measurements, cross-sectional area of the cell: 100 $cm^2$; Variation of the NaCl concentration at (a) a constant activated carbon content of 16 wt.% (Carbopal SC11PG) and a flow-electrode flow rate of 150 mL/min, (b) a constant graphite powder content of 10 wt.% flow-electrode flow rate of 75 mL/min.

quencies is visible, described as "quasi-steady porous electrode behaviour" by Hoyt et al. [Hoy2018]. We agree that this behaviour is caused by electrode porosity/diffusion, which we chose to model with a constant phase element and a parallel resistor ("charge percolation resistance"). This way of modelling enables an influence of the porosity/diffusion limitation of the whole spectrum of frequencies, which leads to a better fit in the lower frequency range at relatively low flow-electrode flow rates compared to the nice newly-developed model by Hoyt et al. [Hoy2018], which on the other hand allows additional insights such as the influence of steady-state boundary layers.

With increasing salt concentrations, the shape of the low frequency semicircles/shoulders changes to a closer approximation of an ideal semicircle, while at the same time the shoulders shift to higher frequencies. This effect may be explained by a reduced diffusion way at high salt concentrations and, thus, a faster charging, which shifts the characteristic frequency of the low-frequency semicircle to higher frequencies. This correlates well with the fit results given in Table A.4, Appendix A, which show a decreasing trend of the fit values of $R_{cp2}$ and additionally a reduction of $C_{dl}$. The latter may be explained by an increase in the convection-induced current at increasing salt concentrations, and thus a transport of charge out of the cell. Next to the improved ionic conductivity, the reduction of $R_{cp2}$ may also be caused by a change in particle-particle interactions due to attractive forces between the particles being altered by increasing salt concentrations. At very high salinities, the altered particle-particle interactions due

to an increased viscosity [Por2014] may also explain the performance decrease from 125 g/L to 317 g/L. At these high salt concentrations charge percolation becomes less efficient again, leading to increased charge percolation resistances $R_{cp1}$ and $R_{cp2}$ and a reduced capacitance $C_{dl}$.

The additional experiments performed with graphite powder flow electrodes, shown in Figure 4.9 (b), were performed to investigate the influence of inner and outer diffusion within the flow electrodes. The graphite powder has a negligible porosity, hence the outer porosity is expected to dominate the mass transport in the flow electrodes in this case. In case of graphite powder based slurries, the overall resistance of the flow electrodes is significantly larger compared to activated carbon at the same mass percentage. However, the general shape of the impedance spectra is comparable to the ones measured with activated carbon slurries at low carbon mass fractions. At medium to high frequencies, depending on the NaCl concentration, a linear area is visible, which passes into a semicircle/shoulder at low frequencies. The Nyquist plots of the graphite powder slurries are all in all steeper compared to activated carbon. This may be due to the lack of porosity within the particles, and therefore a lack of internal diffusion limitations.

The general trend with increasing salt concentrations is comparable to the trend visible for activated carbon based slurries. The linear area shifts to a higher range of frequencies, while the lower frequency area develops into a semicircle/shoulder. The overall ohmic resistance decreases with increasing salt concentration, considering the real part of the impedance at the x-axis subtracted from the real part of the impedance at the lowest measured frequency. The results demonstrate the importance of eliminating long diffusion ways to the particles as a limiting step for mass transport within the flow electrodes. This is in good agreement with the observations described by Yang et al. [Yan2016a], who suggested that increasing salt concentrations in the flow electrodes improve the mass transport by effectively shortening the diffusive pathways.

### 4.5.2. The influence of the particle size

In the following, we investigate the origin of the observed performance differences between the four activated carbon samples. A set of experiments was performed comparing the results of impedance measurements to results from desalination experiments, which were all performed with the same set of parameters.

Figure 4.10 (a) shows results of impedance measurements performed with the activated carbon Carbopal SC11PG and sieved particle size fractions of the same activated carbon. Figure 4.10 (b) shows results of the corresponding desalination experiments. While significantly different particle size fractions were chosen for the comparison, the difference in impedance as well as desalination performance is minute. The experiments performed with the size fraction of 40-50 $\mu$m show

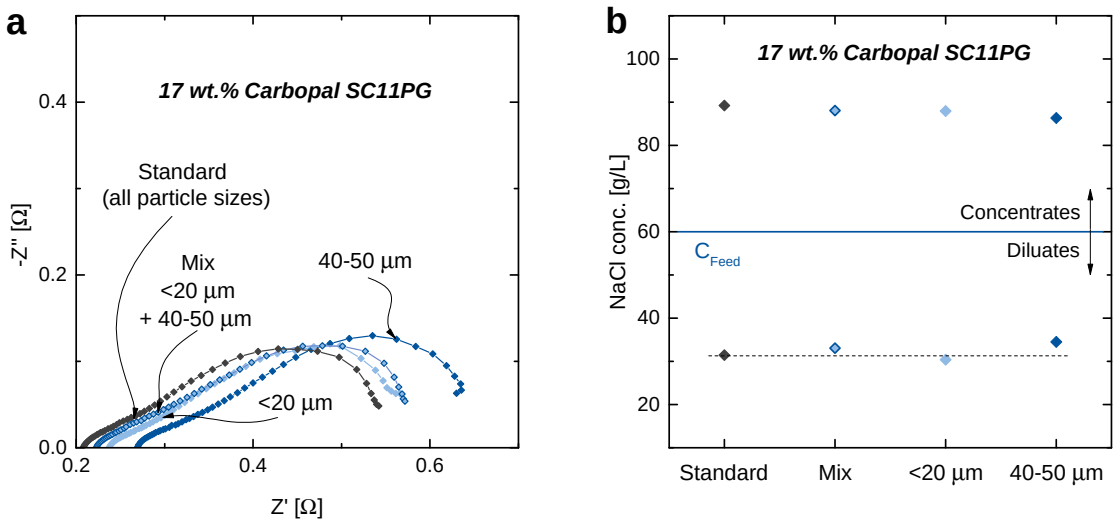


**Figure 4.10.:** Results of (a) EIS measurements (Nyquist plot) and (b) desalination experiments, cross-sectional area of the cell: 100 $cm^2$; A sample of the activated carbon Carbopal SC11PG was sieved into different particle size fractions. The standard sample was compared to the size fractions <20 $\mu$m and 40-50 $\mu$m of the same activated carbon and a mixture of the two sieved fractions. The EIS response at the same weight percentage was measured and compared to the desalination performance.

the most significant differences to the other measurements. The real as well as imaginary impedance are slightly increased, which matches the result of the desalination experiments, in which this fraction showed the lowest desalination rate. The microscopic images depicted in Figure 4.11 show significant differences between the different particle size fractions. However, in particle size fraction of 40-50 $\mu$m, for example, is still a significant number of small particles present, which may diminish the effect of sieving to a certain extent. All in all, the performance differences between the different size fractions are unexpectedly low, and cannot explain the significant differences observed in the performance of different carbon batches.

### 4.5.3. Comparison of four AC samples: The origin of the performance differences

To identify the activated carbon characteristics with the main influence on the desalination performance, we compared four different activated carbons, as listed in the "Materials and Methods" section. The four samples exhibited significantly different results regarding desalination performance and impedance behaviour, as plotted in Figure 4.12 (a).

At the same mass percentage, the activated carbon slurry prepared with "Car-

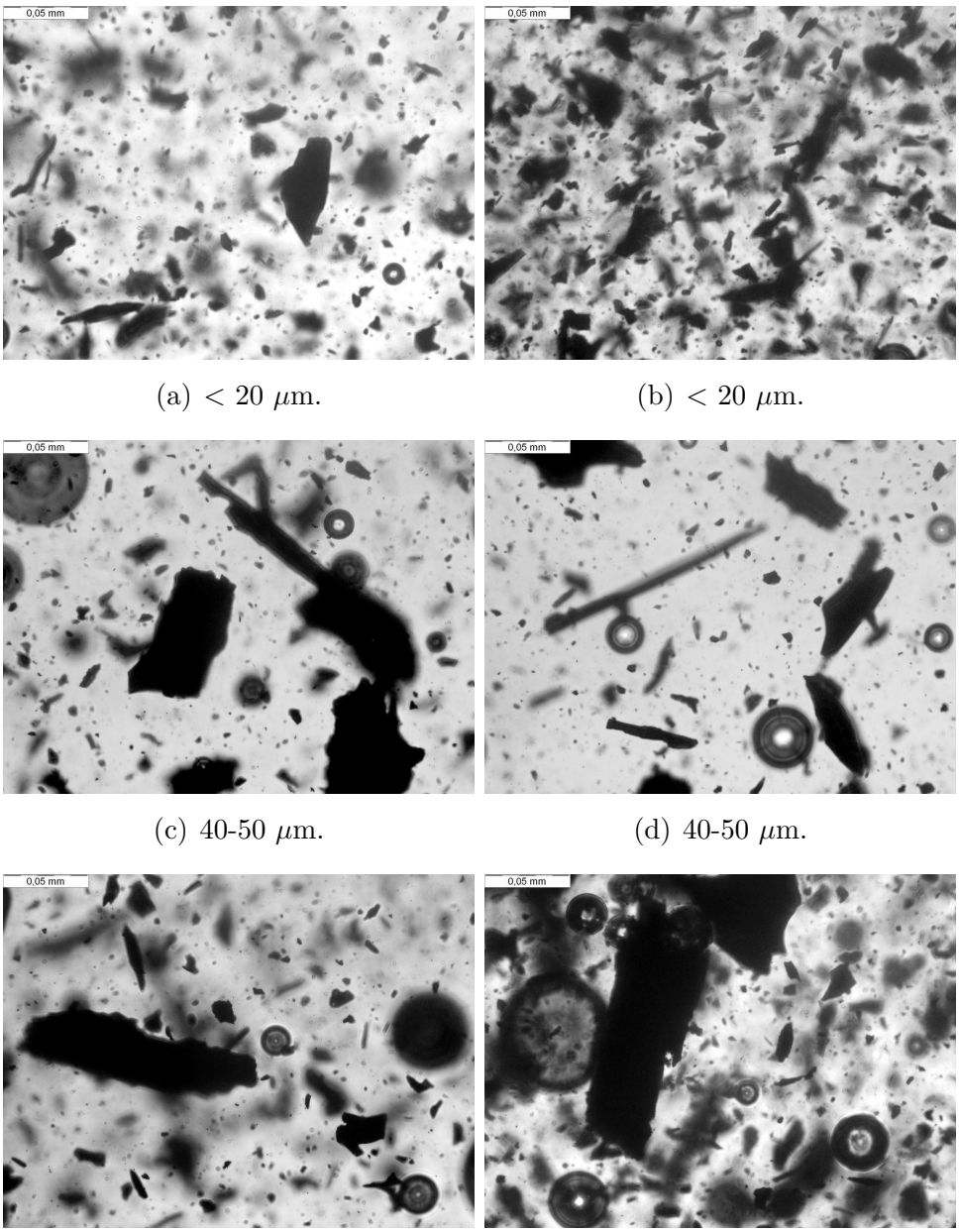


(a) $< 20$ $\mu$m. (b) $< 20$ $\mu$m.

(c) 40-50 $\mu$m. (d) 40-50 $\mu$m.

(e) Standard carbon mix. (f) Standard carbon mix.

**Figure 4.11.:** Microscopic images of Carbopal SC11PG activated carbon samples; (a) and (b): Sieve fraction $< 20$ $\mu$m, (c) and (d): Sieve fraction 40-50 $\mu$m, (e) and (f): Standard activated carbon, mix of all size fractions.

bopal SC11PG" showed a lower impedance and resistance by more than a factor of six, compared to the carbon sample with the highest impedance. The fit results for $C_{dl}$ and $R_{cp2}$, plotted in Figure 4.12 (b), show an inversed correlation between increasing capacitance and decreasing ohmic resistance. With decreasing resistance the capacitance increases, which may partially be due to an improved use of the available electrically active surface area. The results from gas adsorption measurements, plotted in Figures 4.12 (c) and (d), revealed the pore size distribu-

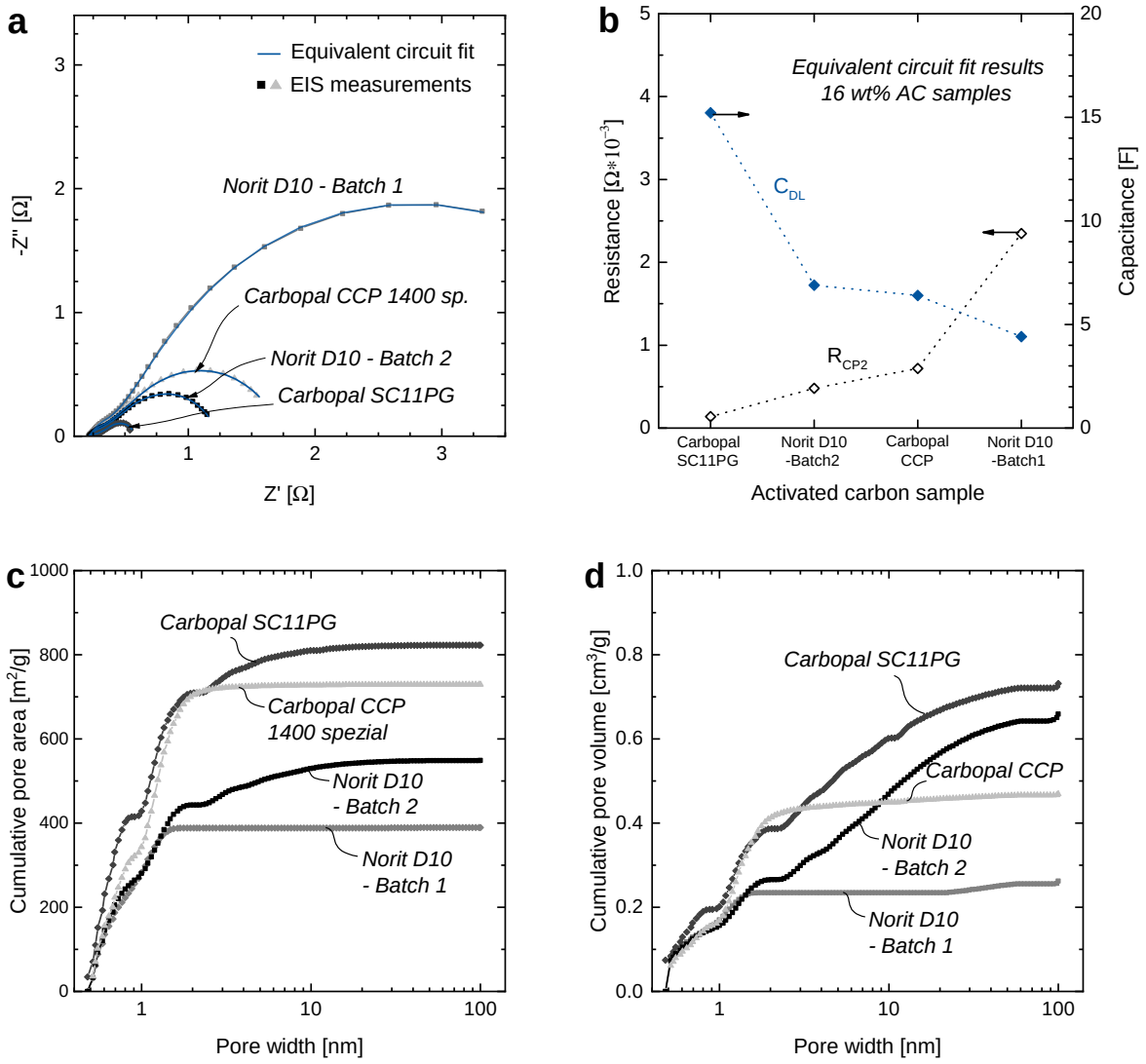


**Figure 4.12.:** Comparison of four different activated carbon samples, results of (a) EIS measurements (Nyquist plot) with 16 wt.% activated carbon sample including equivalent circuit fits, cross-sectional area of the cell: 100 $cm^2$, (b) fitted values using the equivalent circuit model, and (c)/(d) results of gas adsorption measurements to determine the pore size distribution.

tion as cause of the differences. The pore size distribution also appears to be the main difference between the two different batches of the same activated carbon type. The two best performing carbons have a significant amount of mesopores. Especially the cumulative pore volume, plotted in Figure 4.12 (d), correlates well with the desalination/impedance performance of the carbons, while the cumulative pore area does not. Two effects (Figure 4.13) can explain the improved desalination performance with the presence of mesopores: (1) An improved ion accessibility and transport and reduced transport resistance within mesopores and (2) a significantly increased outer particle volume, which leads to a signif-

icantly increased carbon volume fraction in the suspension at the same mass fraction. The increased "outer particle" volume fraction leads to a significant improvement in the charge percolation between particles, and a thus improved desalination performance. The increased viscosities observed in carbon slurries prepared with mesoporous carbons supports this hypothesis, as an increased volume fraction will also increase inner friction in the suspension. However, both effects may play an important role in the performance boost due to the presence of a significant amount of mesopores.

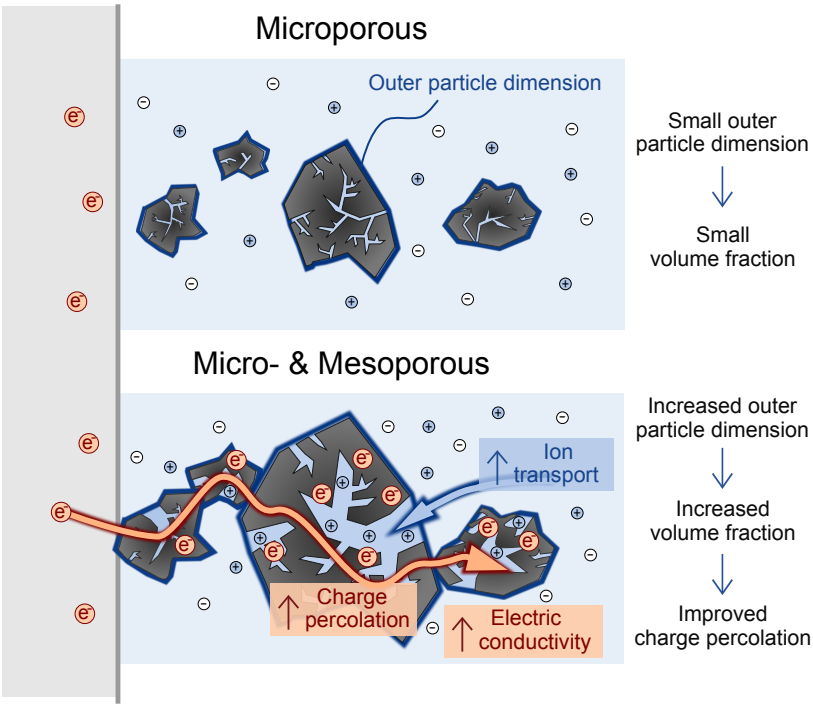


**Figure 4.13.:** Charge and ion transport in carbon suspensions of microporous carbons and carbons with additional mesopores at equal carbon mass percentages.

Based on the above described observations, we have two theories which can explain the significant difference between the two samples of Norit D10, which were taken from two different vessels marked with the same LOT-number: (1) Demixing/layering of the activated carbon during transport and/or storage, caused by varied particle sizes or varied overall densities of particles having different pore size distributions, and (2) variations of the carbon quality throughout the process.

### 4.5.4. Inner and outer diffusion

In further works, the influence of internal and external diffusion should be investigated in more depth. Based on the available data, it is difficult to differentiate between inner and outer diffusion, as most parameter variations influence both. An increasing activated carbon content leads to a better charge percolation, as

well as a larger available surface area. An increasing salt concentration leads to a shorter diffusion ways in case of both inner and outer diffusion. A change in the pore size distribution to a carbon type with a larger fraction of mesopores leads to an improved charge percolation, due to an increase of the particle volume fraction in the flow electrode, as well as to an improved diffusion within the (meso-)pores. The experimental results indicate the importance of both inner and outer diffusion. A more detailed equivalent circuit model could help to differentiate between the mass transport limitations caused by the diffusion within the particle (internal diffusion) and the diffusion to the particle (outer diffusion). This would provide further scientific insight into the transport mechanisms in porous slurry electrodes and their contribution to the overall resistance and desalination performance and could therefore help to further simplify the search for an optimized carbon material.

## 4.6. Prediction of the desalination performance

A final set of experiments aimed at demonstrating the possibility to predict the desalination performance of a carbon slurry by using EIS. We prepared flow-electrode suspensions using two activated carbons with significantly different characteristics, one being mainly microporous (Norit D10, Batch1, "Carbon A"), while the other also contains a significant amount of mesopores (Carbopal SC11PG, "Carbon B"). We adjusted the carbon content of the flow electrodes to achieve a similar impedance behaviour with the two different carbon types at two concentration ranges. The results of this set of experiments are shown in Figure 4.14 (a). Finally, we demonstrated the relevance of the impedance results for the desalination performance by performing continuous desalination experiments with the two-module setup illustrated in Figure 4.2 (right side). Results of the desalination experiments are plotted in Figure 4.14 (b). Figure A.2, Appendix A, shows the correlating electrical currents. Currents between 1.2 A and 1.9 A were measured at an applied voltage of 1.2 V. This corresponds to resistances between 0.63 Ω and 1 Ω, which matches the low frequency resistance of the impedance spectra displayed in Figure 4.14 (a) well.

We achieved a good match in the impedance behaviour of Carbon A and Carbon B for the mass fractions of the sets 10 wt% A / 30 wt% B and 15 wt% A / 35 wt% B (Figure 4.14 (a)). The carbon slurries also showed matching results in the corresponding desalination experiments (Figure 4.14 (b)). In case of the higher percentage set of carbon slurries, 15 wt% A / 35 wt% B, a slightly more pronounced deviation was observed between the desalination performances of the matched flow electrodes. The 15 wt% slurry of Carbon B reached a somewhat better desalination compared to the 35 wt% slurry prepared with Carbon A. The

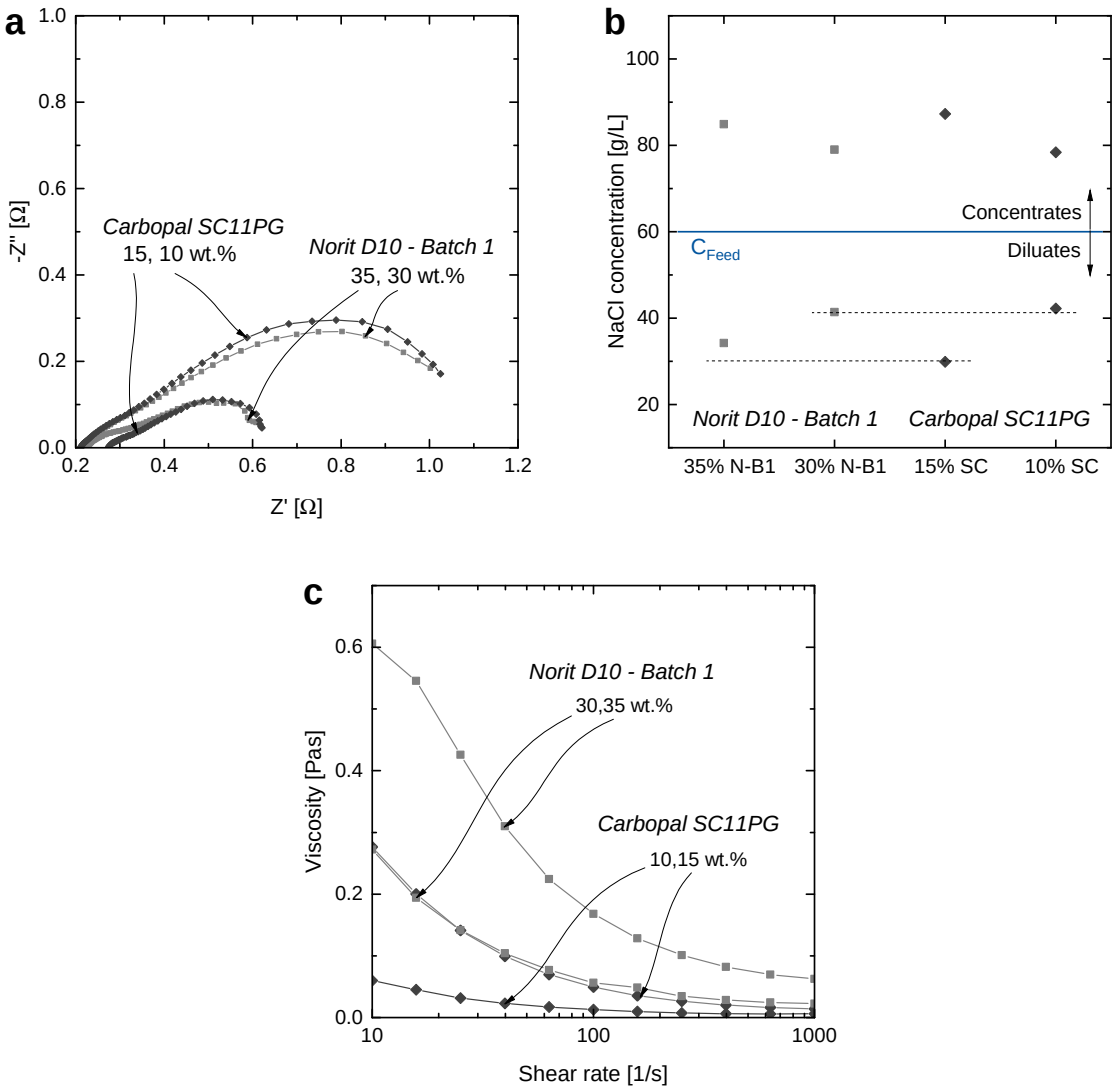


**Figure 4.14.:** Results of (a) EIS measurements (Nyquist plot), (b) desalination experiments and (c) viscosity experiments, cross-sectional area of the EIS/desalination cell: 100 $cm^2$; Suspensions based on two different activated carbons were matched regarding their EIS response to obtain the same performance at two different mass fraction values, next the corresponding desalination performance was tested.

curve representing the 15 wt% slurry of Carbon B intersects the x-axis at a higher ohmic resistance than the curve representing the 35 wt% slurry prepared with Carbon A, while the resistances at low frequencies are nearly the same. This results in a small difference in the overall real impedance of around 0.034 Ω, which may explain the small difference in desalination performance between the two carbon slurries. However, all in all the results for the matched slurries matched well.

Figure 4.14 (c) shows results of a viscosity investigation performed with the above described carbon slurries, which were adapted in weight percentage in

a way to exhibit a similar electrochemical performance. While the desalination performance of the two pairs of slurries match very well, the rheological behaviour appears to be significantly different. The slurries made of the Carbopal SC11PG carbon have a significantly lower viscosity, while reaching the same desalination performance. Hence, a combination of electrochemical impedance spectroscopy with rheological measurements is well suited for a screening study for activated carbons with optimum performance in FCDI processes.

## 4.7. Conclusions and outlook

Effective electronic and ionic charge transfer and transport, as well as effective mass transport, are vital for flow-electrode based systems. The experimental results presented in this chapter demonstrate the applicability of electrochemical impedance spectroscopy as a predictive characterization method for flow-electrode materials, especially in the context of water treatment. An equivalent circuit model is developed, based on the observed influence of different system parameters on the EIS response, which can be fitted to match all results we obtained experimentally. The findings allow insight into the charge transfer mechanisms in capacitive flow electrodes, such as the presence of a charge percolation threshold, above which an effective charge transfer leads to an improved salt adsorption.

The influence of different activated carbon characteristics is investigated. Unlike the particle size distribution, the pore size distribution is identified to have a major influence on the desalination performance. The carbon samples with a significant amount of mesopores, additional to micropores, showed an overall improved performance. The activated carbons with the highest cumulative pore volume showed the best desalination performance, which is concluded to be due to an increased volume fraction of the activated carbon. An increased carbon outer volume fraction leads to an improved charge percolation and thus an improved desalination.

Finally, the possibility to use electrochemical impedance spectroscopy measurements to adjust the performance of flow electrode suspensions made of different activated carbons is demonstrated. The desalination performance of the matched flow electrodes showed a very good congruence. Herewith, this study establishes a foundation for an application of EIS as predictive characterization method for flow-electrode materials, e.g. for incoming goods inspection. The combination of EIS measurements with viscosity measurements provides and effective screening method for optimal carbon materials for flow electrodes.

The results presented in this chapter are valuable for application as carbon characterization method for application in technologies using flow electrodes. EIS may be applied for on-line process monitoring and control of the flow-electrode performance in various processes. It can also serve as direct, easy in-line method for the characterization of carbon suspensions in general, considering the actual wetting and agglomeration conditions in-situ.

In future works, further scientific insight could be achieved by developing a more detailed equivalent circuit model, which could help to distinguish between the influence of internal and external diffusion. A thorough understanding of the charge and ion transfer within flow electrodes will help in designing efficient and cost-effective cells and finding the optimal carbon material.

For the experiments described in the following chapter, Chapter 5, the activated carbon Norit D10 was used, as the experiments took place at the same time and earlier than the experiments described here. The studies described in Chapter 6 and following already profited from the use of a more suitable activated carbon.

# 5

# System design and energy recovery

Parts of this chapter have been published:

Alexandra Rommerskirchen, Christian J. Linnartz, Daniel Müller, Lisa Kathrin Willenberg and Matthias Wessling. "Energy Recovery and Process Design in Continuous Flow-Electrode Capacitive Deionization Processes" in: *ACS Sustainable Chemistry & Engineering* 6/10 (2018), pp. 13007-13015. (citation: [Rom2018a])

## 5.1. FCDI for brine treatment: Research questions

The work presented in Chapters 5 to 7 focuses on the treatment of high salinity solutions (brines) using FCDI processes. The aim is to gain further understanding of whether FCDI processes can be used to treat high salinity solutions, and how they need to be designed to function efficiently. The main research questions are:

- Can FCDI be used to desalinate and concentrate brines? How high are the water recoveries reachable at high concentrations?
- What are the limiting factors of FCDI processes and how can they be overcome? How can we influence the ion and water transfer?
- What is the energy demand for treating brines with FCDI processes and how can it be tuned? Is it possible to reach an energy demand competitive with established processes?

The Chapter at hand, Chapter 5, focuses on the influence of the process design on the performance and energy demand of FCDI processes. The possibility to recover energy during the regeneration step of the flow electrodes is investigated. The study presented in Chapter 6 focuses on the impact of different driving forces on the salt and water transfer during the treatment of high salinity solutions using continuous FCDI processes. In Chapter 7 concepts are presented, which focus on the module and material design to overcome limitations and achieve a competitive process performance and energy demand.

## 5.2. Introduction, motivation and objectives

The increasing world population and living standards lead to a need to close material cycles to avoid the discharge of excess chemicals and salts into the environment [Eli2011; Ton2016]. In the most extreme case, this would lead to zero liquid discharge (ZLD). ZLD is a wastewater management strategy which completely avoids the emission of any liquid waste [Ton2016], which is the aim of many present studies [Ore2010; Ton2016]. To achieve ZLD a range of technologies is needed as a toolbox, which enable tailor-made processes for each application case. In some cases, a simple concentration of a pure salt stream may be required, while in other cases a process, industrial or domestic wastewater may contain a mixture of salts, which may also contain a variety of polar or non-polar organic components. Some water streams may have a low salinity, while others have a high salinity. Reverse osmosis is very efficient for the desalination of seawater and lower salinities. Thermal processes are also able to handle higher salinities. However, the energy demand for the treatment of high salinities is still relatively high. Additionally, all these processes are not selective. Many attempts at ZLD currently lead to a production of vast amounts of mixed salts, which usually cannot be directly recycled and often need to be disposed of.
The limitations of established processes present potential for the application of electrically driven processes for achieving ZLD, such as electrodialysis (ED) [Ton2016; Mac2017; Pér2012; Ore2010; Tur2009; McG2014] and flow-electrode capacitive deionization (FCDI), which has before been demonstrated for salinities in seawater range [Jeo2013; Jeo2014; Yan2016a].

Based on the characteristics of FCDI, four potential application areas seem adequate: (1) desalination of higher salinity brackish water, (2) brine treatment, (3) treatment of water streams with a high fouling and scaling potential (e.g. food industry, similar to ED [Str2010]) and (4) "special" applications such as salt metathesis [Lin2017] or (selective) removal of specific ionic species other than sodium chloride [Zha2018b]. The work presented here focuses on the treatment of high salinity solutions (brines) using FCDI processes. The findings can, of course, be transferred to other potential application areas of FCDI processes.

The energy demand of established brine desalination processes, such as mechanical vapor compression (MVC), strongly depend on the salinity and water recovery rate [Thi2015]. A study by McGovern et al. [McG2014] indicates a similar energy demand for brine treatment with ED compared to MVC, but potentially lower costs in case of ED. FCDI has the potential to reach high water recoveries [Gen2014; Rom2015] and a low energy demand [Jeo2014] even at high salinities, which could be advantageous compared to established processes, also for achieving ZLD.

**Continuous operation of FCDI processes and regeneration strategies.** In the literature, different electrode regeneration strategies were proposed. Jeon et al. [Jeo2013; Jeo2014] proposed regeneration by simple mixing of the two oppositely charged flow electrodes and demonstrated a possible energy recovery from charged slurries in a separate regeneration step, and thus, in a discontinuous manner. Hatzell et al. [Hat2014] proposed an FCDI process without ion-exchange membranes which includes a filtration step. Following this, a fully continuous operation was demonstrated in an FCDI system in two-module configuration, in which the electrodes are regenerated in a separate FCDI module [Gen2014]. Subsequently, continuous operation was demonstrated in single-module configuration, in which a single flow electrode is regenerated in a second, oppositely charged, electrode compartment [Rom2015]. Later, Doornbusch et al. [Doo2016] demonstrated a fully continuous FCDI system based on slurry-mixing in combination with a brine overflow tube, by which the carbon particles are separated from the concentrated salt solution through sedimentation.

When analyzing these process schemes, it becomes apparent that for regeneration and fully continuous operation three functions need to be provided in the regeneration step: (1) discharge of the carbon particles by electron transfer, (2) ion release and transfer, so electroneutrality is fulfilled and (3) separation of the discharged carbon particles from the (concentrated) salt solution. Step one, electron transfer, can be achieved either by mixing or by contact with a current collector, which both lead to a transfer of electrons and, thus, charge equalization. Step two, ion transfer, can be achieved by mixing or by allowing ion transfer via a porous membrane or a membrane with ion-exchange properties. Step three, separation of carbon particles, can be achieved by standard unit operations such as settling or filtration. Having this in mind, a wide variety of continuous FCDI processes may be designed.

**Objectives of this chapter.** The available literature regarding the energy demand of desalination processes primarily focused on state-of-the-art methods or CDI in general [And2010; Eli2011]. M.C. Hatzell and K.B. Hatzell discussed trade-offs and influences on the energy demand while considering CDI and FCDI processes as thermodynamic cycles [Hat2018], but did not calculate the energy required for FCDI processes specifically. There is an awareness that pumping slurry requires additional energy [Hat2015b], but only some studies investigated the additional energy required for pumping flow electrodes in FCDI [Hat2015b; Por2014]. The possibility to recover up to 83 % of the energy from charged electrodes in CDI [Dłu2013] and around 20 % in FCDI [Jeo2014] has been demonstrated in discontinuous, cyclic operation. However, the recovery of energy from flow electrodes in continuous operation of an FCDI system has not been demon-

strated previously.

Thus, the aims of the study presented in this chapter are to (1) show that continuous energy recovery is possible in continuous FCDI systems and is not restricted to a specific process layout, (2) investigate the performance and specific energy demand of FCDI systems in different process layouts, including the energy required for pumping flow electrodes, and finally (3) discuss the potential of FCDI systems compared to state-of-the-art desalination methods regarding the energy demand and the influence of specific process parameters, focusing on the treatment of high salinity brines.

## 5.3. Continuous FCDI and energy recovery - Experimental

The experiments presented in this chapter were performed with three different FCDI process layouts, illustrated in Figure 5.1. All three layouts enable fully continuous operation, i.e. a continuous production of a desalinated stream and a concentrated stream from salt water. Charge-discharge cycles are not required. When the systems reach steady state, two product streams of constant salt concentrations are produced at constant water and flow-electrode flow rates.

The FCDI modules applied for the study presented in this chapter were the same as described in Chapter 4. To avoid abrasion, PTFE foils were placed on the membrane surface at the inlets in this case.

### 5.3.1. Continuous operation of FCDI systems

A three-channel power supply (HM8143, HAMEG Instruments GmbH) was applied, which can be operated as power supply as well as electronic load. The flow electrodes were recirculated through the FCDI systems using a peristaltic pump (Ismatec MCP process drive, Masterflex two-channel pump head Easy-Load II, Norprene tubing). The feed water was supplied by a second peristaltic pump (Ismatec Reglo ICC peristaltic pump with three independent channels). The electrical conductivity of the aqueous solutions was measured using conductivity sensors (LTC0,35/23; Sensortechnik Meinsberg).

The feed water for most experiments presented in this chapter consisted of a 60 g/L sodium chloride solution prepared with purified water. The flow electrodes were prepared using the same sodium chloride solution and 20 wt% or 25 wt% AC powder (Norit D10, "Batch 1", as in Chapter 4). The flow-electrode suspensions were stirred overnight before use. In most systems, the flow electrodes were recirculated at a flow rate of 200 mL/min. Feed water was supplied to the desalination

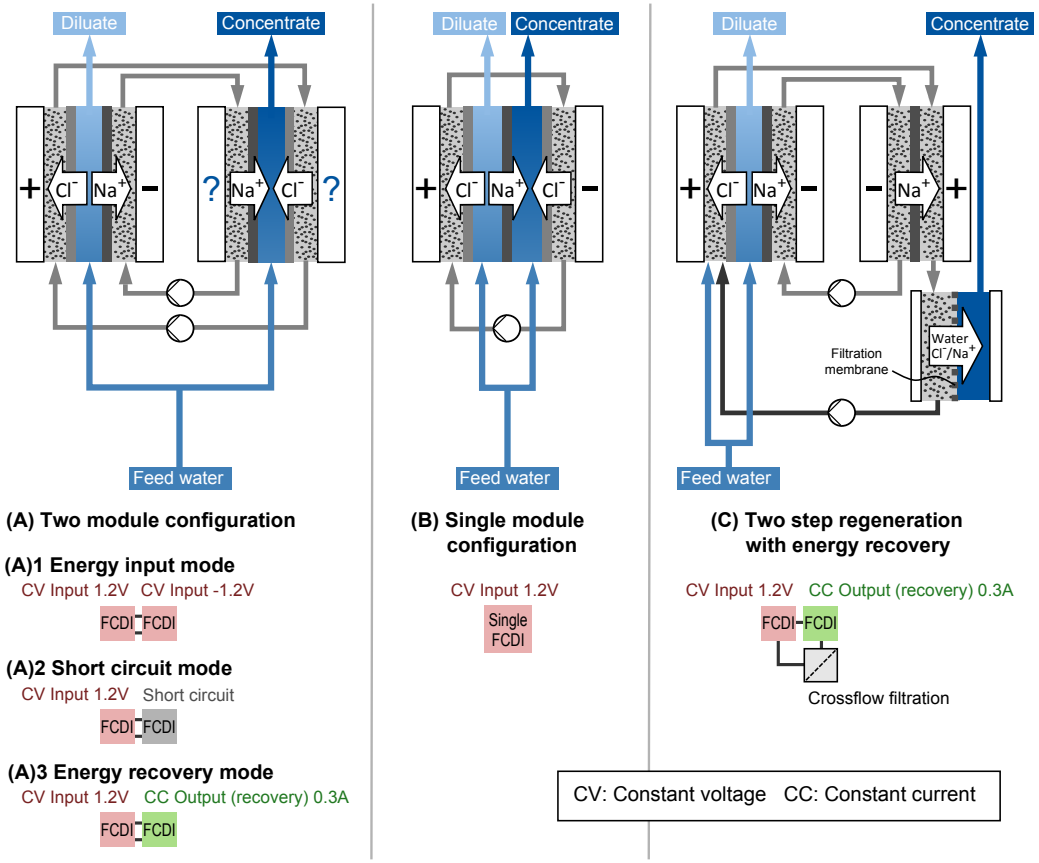


**Figure 5.1.:** Overview of continuous FCDI process layouts: (A) Two-module configuration in three different operational modes of the regeneration/concentration module: 1) energy input 2) short circuit 3) energy recovery. (B) Single-module configuration in constant voltage at 1.2 V in energy input mode. (C) Two-step regeneration configuration in energy recovery mode.

module/compartment to produce a diluate stream in single-pass at a constant flow rate of around 1.2 mL/min and to the regeneration module/compartment to produce a concentrate stream in single-pass at a constant flow rate of 1 mL/min. In case of the experiments performed for the results shown in Figure 5.3, solutions and suspensions with lower salinities of 1 g/L (0 g/L in electrode) and 10 g/L (10 g/L in electrode) were used, at product stream flow rates of 1.3 mL/min each. The experiments were performed with varied current densities to achieve average values allowing conclusions about the energy recovery possible at different feed salinities.

During the start-up of each FCDI system the following steps were carried out: (1) Filling the system with solutions/suspensions, degasing of the module(s), (2) recirculation without applied potentials for 30 minutes and (3) start of the power supply to the FCDI cells. In case of the energy recovery mode this is conducted in two separate steps: (A) start to supply a constant voltage of 1.2 V to the desalination module, charging of the electrodes for 30 minutes, and (B)

starting to draw a constant current via the power supply operated as electronic load at a constant current of 0.3 A. The constant current was chosen according to the maximum value allowing continuous operation, which was determined in preliminary tests. During the initial phase the observed currents and product water conductivities change, until steady-state is reached.

Additional to conductivity measurements, product water samples were taken during steady state operation of each system. In case of the 60 g/L feed concentration, the density of each sample was analyzed at 20°C (DMA 46, Anton Paar GmbH) to verify the salt concentration. In case of the 1 and 10 g/L feed concentration, the samples were analyzed using HPLC.

### 5.3.2. Two-module configuration (system A)

The first system, system A (Figure 5.1), was set up in the same way as described by Gendel et al. [Gen2014] using two before described "standard" FCDI cells. In this case, the two-module FCDI configuration (system A) was operated in three modes as indicated in Figure 5.1.

The first mode, operational mode 1, in the following termed "energy input mode", was introduced previously [Gen2014]. Both desalination and regeneration (concentration) modules are operated at a constant voltage (CV) of 1.2 V provided by the power source, as indicated in Figure 5.1. The resulting electrical currents were measured.

In operational mode 2, in the following termed "short circuit mode", only the desalination module was operated at a constant voltage of 1.2 V. The second module used for regeneration of the flow electrodes was short-circuited.

In operational mode 3, in the following termed "energy recovery mode", only the desalination module was operated at a constant voltage of 1.2 V. The second module was connected to the power supply operated as electronic load, to investigate the possibility to recover energy. This way a constant current (CC) of 0.3 A was supplied by the second FCDI module, which originates from the charged flow electrodes. The resulting voltage was measured to calculate the electrical energy recovered during regeneration of the charged flow electrodes.

**Investigating the system stability- Step experiment** Apart from the above described experiments, an additional experiment was performed to investigate the system stability and interaction and dependency of the desalination and regeneration step. In this experiment, the two-module system was operated in "energy input mode". The experiments were performed using 60 g/L NaCl as feed solution and as continuous phase for the preparation of the flow electrodes. The flow-electrode suspensions were prepared using 25 wt.% activated carbon (Norit D10, "Batch 1", as described in Chapter 4), which were recirculated at

a flow rate of 200 mL/min each. The diluate and concentrate streams passed each cell a single at a flow rate of 1.3 mL/min. The test procedure timing and settings for the step experiment are listed in Table 5.1. In an initial step, the system was operated without an applied electrical field. Diminutive changes in the concentrations during the first step are in the range of the measurement error. Following, 1.2 V were applied to both desalination and regeneration cell, which is the same setting as applied during the above described "energy input mode". Following this, the regeneration module is switched from constant voltage operation to constant current operation. In the first step, the highest current of 1.0 A is applied to the regeneration cell. In the subsequent steps, which also last 2.5 h each, the constant current applied to the regeneration cell is reduced stepwise and the system behaviour monitored.

**Table 5.1.:** Step measurement test procedure, energy input mode.

| **Step duration** | *30 min* | *2.5 h* | *2.5 h* | *2.5 h* | *2.5 h* | *2.5 h* | *2.5 h* |
|---|---|---|---|---|---|---|---|
| **Desalination** | - | 1.2 V | 1.2 V | 1.2 V | 1.2 V | 1.2 V | 1.2 V |
| **Regeneration** | - | 1.2 V | 1.0 A | 0.9 A | 0.7 A | 0.5 A | 0.3 A |

### 5.3.3. Single-module configuration (system B)

The second system, system B as illustrated in Figure 5.1, was set up similar to the system described in the article introducing the single-module configuration FCDI layout. A single FCDI cell constructed similar to the above described "standard" FCDI cell was used. In this case, an additional anion-exchange membrane and mesh spacer were placed in the FCDI cell [Rom2015]. This way, a diluate and concentrate water stream can be produced in a single cell, while using only a single flow-electrode circuit. The single FCDI cell was operated at a constant voltage of 1.2 V.

The experiment for the configuration comparison was operated with 25 wt% activated carbon (AC) suspensions at a flow rate of 200 mL/min. Apart from this, a second set of experiments was performed in single-module configuration, in which the flow-electrode composition (20-30 wt.%), the flow-electrode flow rate (100-200 mL/min) and the activated carbon type (Norit D10, "AC 1"/"Batch 1" and "AC 2"/"Batch 2", as named in Chapter 4) were varied. The flow-electrode suspensions were stirred overnight before use. The acquired data help to investigate the correlation of the flow-electrode composition and flow rate with the desalination performance, desalination energy and pumping energy requirement, as the previous chapter already indicated a strong correlation of the FCDI system performance with the activated carbon suspension characteristics.

### 5.3.4. Two-step regeneration (system C)

The third system, system C as illustrated in Figure 5.1, is a novel continuous FCDI process layout, published first in 2018 [Rom2018a]. Similar to the two-module configuration, the desalination takes place in a "standard" FCDI cell at 1.2 V. The charged flow electrodes are then regenerated in a two-step process. The first step allows a transfer of ions and electrons so that the ions previously stored in the electrical double layer are desorbed from the surface of the suspended carbon particles and are now present in the continuous phase, as a free salt solution. This is performed in a simplified "standard" FCDI cell, which contains only a single CEM, as indicated in Figure 5.1, system C. This allows the sodium ions to pass the CEM into the anode compartment, while the electric charge is equalised via the current collectors, enabling the recovery of energy. The use of a single AEM instead of the CEM may also be possible. After passing this simplified FCDI module, a mixture of salt water and (mostly) regenerated carbon particles is present in the flow-anode cycle. This mixture can be separated in a second step, for example a settler or cross-flow filtration. In this case, a simple cross-flow filtration module with filtration paper (MN 615 1/4, Macherey-Nagel) with a single flow channel (∼0.8 cm x ∼13,5 cm) was used to separate the salt concentrate from the carbon slurry. Hence, a concentrated saline stream is produced. The concentrated slurry is then diluted with feed salt solution to adjust the carbon content back to the initial value.

### 5.3.5. Pressure drop measurements

The pressure drop measurements were performed with a syringe pump (PHD Ultra, Harvard Apparatus) to avoid pressure fluctuations. Suspensions with AC concentrations of 20 wt.% and 25 wt.% of "AC 1", and of 30 wt.% of "AC 2" with NaCl concentrations of 60 g/L were pumped through the flow-electrode channel of an FCDI half-cell at flow rates ranging between 50 and 200 mL/min. The relative static pressures were measured at points before and behind the cell by two pressure sensors (WIKA, Type A-10, pressure range 0 - 1.6 bar). The pressure drop of suspensions of "AC 2" could not be measured at different mass fractions, as there was no sample of the same quality available anymore. However, the conducted measurements are valuable and are hence presented here.

# 5.4. Continuous FCDI and energy recovery - Results and discussion

## 5.4.1. System operation and stability - Step experiment

The two-module system in modes A(2) and A(3) (short circuit and energy recovery) is set up in a way that the desalination current can adapt itself due to the CV operation of the desalination module. The desalination current will automatically adapt a value very close to the CC value set for the regeneration module, so that the mass balances are kept. Thus, the systems are self-balancing and stable.

To demonstrate this behaviour, a step experiment was performed as described in Section 5.3.2. The results of this experiment are plotted in Figure 5.2. Figure 5.2 (a) shows the electrical current applied to the regeneration module as well as the electrical current measured at the desalination module. For each step, the desalination current shows an immediate reaction to changes in the regeneration current, and then a gradual convergence towards the current applied in the regeneration current. This demonstrates the close dependency of the desalination performance on the regeneration performance. An inefficient regeneration of the flow electrodes will result in an immediate deterioration of the desalination performance.

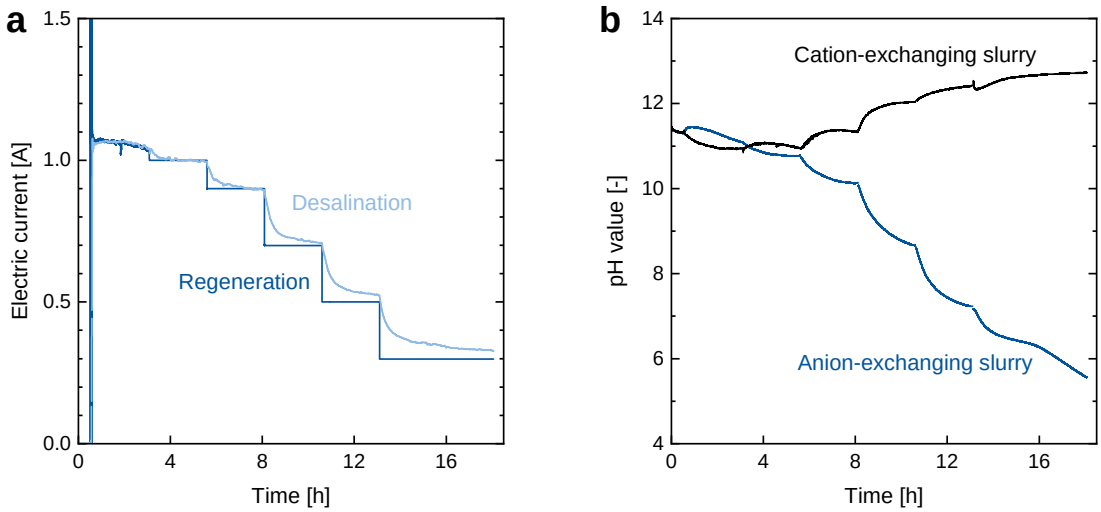


**Figure 5.2.:** Step experiment conducted in a two-module configuration FCDI setup in energy input mode to investigate the system stability and interaction between desalination and regeneration step. The current applied to the regeneration module was altered during the course of the experiment, as listed in Table 5.1. The graphs show (a) the electric current applied to the regeneration module and measured in the desalination module and (b) the pH values measured in the two flow-electrode circuits.

Figure 5.2 (b) shows the trends of the pH values measured in the cation exchanging slurry (cathode in desalination module) and the anion exchanging slurry (anode in desalination module). During the initial phase, during which the system was operated at a constant voltage and self-regulating current and then at a high regeneration current, the measured pH value is stable at around 11 in both flow-electrode suspensions. As soon as the regeneration current is limited to a lower value, the pH values of both flow electrodes start to drift apart. The anion exchanging slurry drifts towards lower pH values, while the cation exchange slurry drifts towards higher pH values, which becomes more pronounced with each further reduction of the regeneration current. This behaviour matches the trends described in FCDI [Nat2017] and CDI [Cho2014] literature well. During batch operation of a CDI or FCDI process, it is usually observed that the anode electrolyte pH value shifts towards acidic values, while the cathode electrolyte shifts towards basic pH values [Cho2014].

**pH values and faradaic reations in continuous FCDI.** In the usual continuous FCDI experiment operated with continuous regeneration either in two-module or single-module configuration, the flow electrodes reside in each current collector only a few seconds. The electrodes are charged and adsorb ions to counter the charge and are quickly recirculated to the oppositely charged current collector, where the flow electrode is regenerated. In this case, the system is in a stable steady state, the desalination and regeneration are well balanced. There are two ways to explain this behaviour of continuously regenerated FCDI systems: (1) There are no faradaic reactions taking place, or only to a very small extent, due to the adsorption of ions on the carbon surface being preferred over faradaic reactions. While faradaic reactions require a certain overpotential, plenty of activated carbon surface area is present, which is continuously renewed by pumping. Or (2) there are faradaic reactions taking place to a similar extent as observed in FCDI batch experiments by Nativ et al. [Nat2017], which assist the FCDI process also during these very low residence times and fast adsorption/removal of ions. In this case, the pH change may still not be visible due to the operation in a well balanced system, in which each pH change during the pass of a current collector is again equilibrated by an pH value change in the opposite direction during the passing of the oppositely charged current collector.

**pH values and faradaic reations in batch-mode FCDI.** In case of the experimental results plotted in Figure 5.2 (b), however, the limitation of the regeneration current leads to a partial charging of both flow electrodes, which goes hand in hand with (unwanted) faradaic side reactions. In this case, the desalination will initially be in excess, due to the available electrode potential, which leads to

a partial charging of the flow electrodes, similar to a batch operation, and hence a change of the pH values. At some stage after a change in the regeneration current, the desalination current and regeneration current equilibrate, the system is balanced again and hence the pH values in the flow electrodes stabilize. This experiment illustrates the interactions and interdependencies of separate FCDI modules connected by flow-electrode circuits well. While well-balanced systems can be operated at stable pH values in the electrodes, the flow electrodes acting as a stable connection between modules or oppositely charged current collectors, the system immediately reacts with an excess charging and pH shift to a system imbalance, which buffers imbalances to a certain extent.

**System stability towards changes in the feed flow rate.** A second experiment illustrated the system stability towards changes in the feed flow rate in case of a constant voltage operation. In this experiment the feed water pumps were stopped temporarily. After stopping the feed pumps, the currents will soon reduce to zero, while the flow electrodes are still recirculated and constant voltages are applied to the system. However, without making any changes to the system, it was observed that the electric currents automatically recover to the original values when restarting the pumps.

## 5.4.2. System comparison

Continuous desalination experiments were performed with the systems illustrated in Figure 5.1. The system performances regarding desalination, current efficiency and specific energy input were observed. The results are given in Figure 5.3 (a) - (d).

### Desalination performance

Figure 5.3 (a) shows the desalination and concentration performance of each system normalized by the feed concentration, which is indicated by the grey line. The corresponding desalination rates, electric current densities and current efficiencies are plotted in Figure 5.3 (b). The observed current efficiencies are low compared to values from our previous publications [Gen2014; Rom2015] due to the high salinity of the feed water, which leads to a reduced selectivity of the ion-exchange membranes.[Ton2002; Nag2006; Sad2009] The two-module system in energy input mode shows the best desalination performance, followed by the single-module system and the two-module system in short circuit mode. The two systems with continuous energy recovery have a similar, comparably low desalination rate.

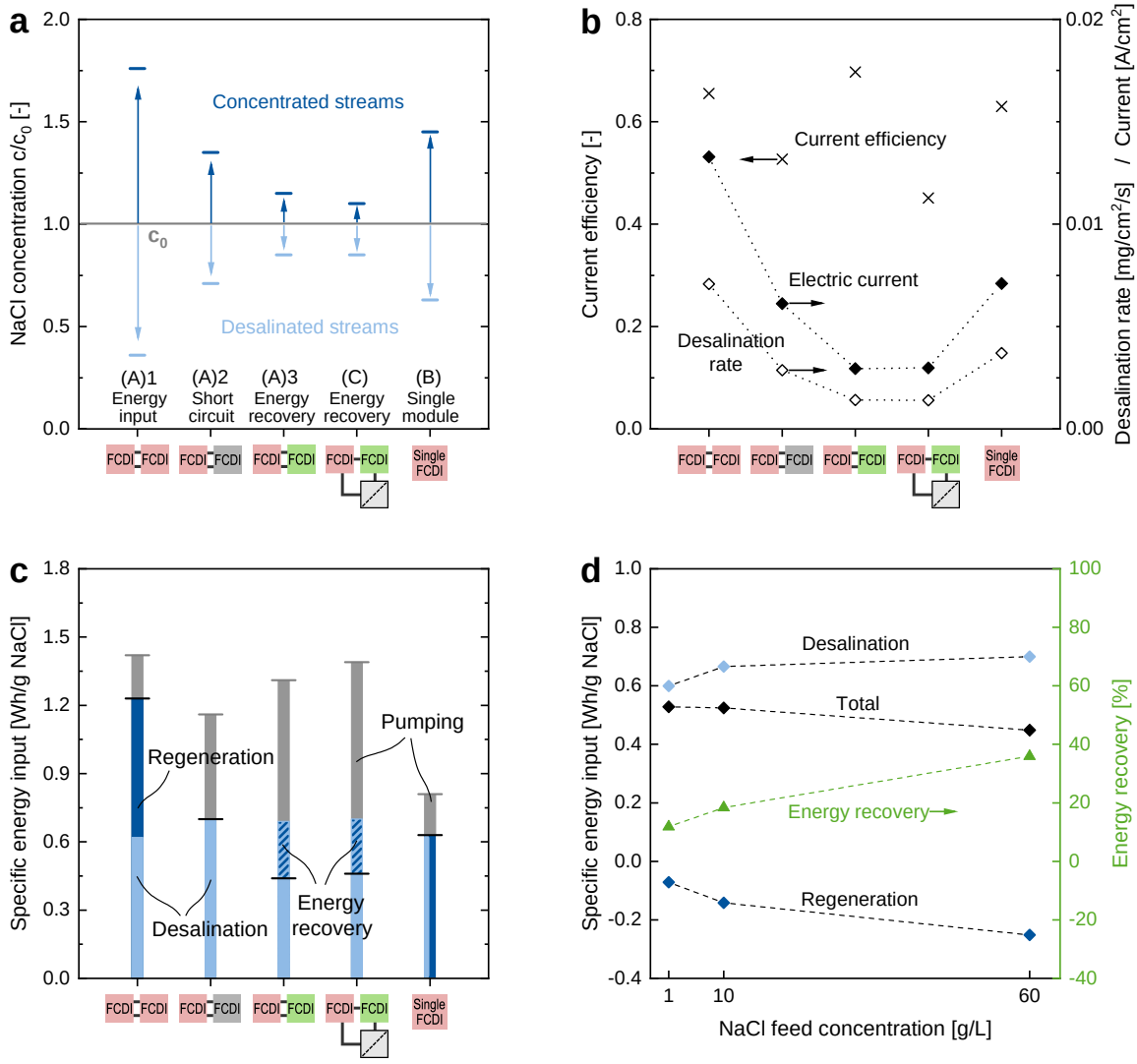


**Figure 5.3.:** Comparison of continuous FCDI system configurations (symbols given in Figure 5.1); All experiments in (a)-(c) were performed with 25 wt.% AC and 60 g/L NaCl in the flow electrodes, flow-electrode flow rates of 200 mL/min, diluate feed flow rates of 1.2 mL/min and concentrate feed flow rates of 1 mL/min. (a) Normalized NaCl concentrations of desalinated and concentrated streams. (b) Current efficiencies, electric currents and desalination rates. (c) Specific energy input: desalination (light blue), regeneration (dark blue) and pumping energy (grey). Energy recovery (striped bars) is subtracted and the net energy input for desalination marked (black lines). (d) Comparison of energy input and recovery at different NaCl feed concentrations, performed in the energy recovery mode in two-module configuration (A3) at flow rates of 1.3 mL/min (diluate and concentrate).

The observed desalination rates for the energy recovery and short circuit systems can be explained by the way the current of the desalination module adjusts to the regeneration current in a two-module system. As described before, the two modules show a direct dependence from each other. The desalination current can-

not be significantly higher compared to the regeneration current once the system is in steady state, as in this case the mass balance would not be kept. The driving force for the regeneration in short circuit and energy recovery mode is the electric charge stored in the flow electrodes, which is recovered in the recovery module. The recovery module, operated in CC mode, reaches lower voltages compared to the constant 1.2 V applied in the energy input mode. Hence, lower currents are reached in short circuit mode and energy recovery mode compared to the energy input mode in the regeneration, and hence also in the desalination. Thus, the overall desalination performance of the system is limited by the electric current achievable in the regeneration module. To improve the overall system performance the recovery current needs to be increased. This may be possible by using larger membrane areas or counter-flow for flow electrodes and concentrate water stream. However, it was chosen to keep these values constant and comparable in this initial study.

### Energy input

Figure 5.3 (c) shows the energy input for each system during steady state operation. The electrical energy for the desalination and the regeneration steps were calculated separately. The electric energy required for desalination was calculated from the measured electric current and the applied potential. It was normalized by (1) the volume of the treated water in $m^3$, as plotted in Figure 5.5 (a), and (2) the mass of the transferred salt, as plotted in Figure 5.3 (c).

The hydraulic energy which has to be applied by pumping, as included in the bar charts of Figures 5.3 (c) and 5.5 (a), was determined by measuring the pressure drop in a flow-electrode flow channel of an FCDI half-cell. The results or the pressure drop measurements are shown in Figure 5.4. The results show, as is to be expected, a strong dependency of the pressure drop on the activated carbon content in the flow electrode and the activated carbon type. This correlates well with the findings regarding the viscosities of the different activated carbon batches presented in Chapter 4.

The pumping power required for the recirculation of the flow electrodes was calculated based on the measured pressure drop $\Delta p$, the volumetric flow rate $\dot{V}$ and the number of FCDI half-cells $n_{cell}$ in the system (Equation 5.1).

$$P_{pump} = \Delta p \cdot \dot{V} \cdot n_{cell} \tag{5.1}$$

A single-module system has two half-cells, a two-module system has four half-cells. The pump efficiency and electrical efficiency were neglected as well as the length of the tubing outside the FCDI cells, since it is much shorter than the flow channels inside the FCDI cells. The energy required for pumping the feed water was neglected. Based on the pumping power the specific pumping energy

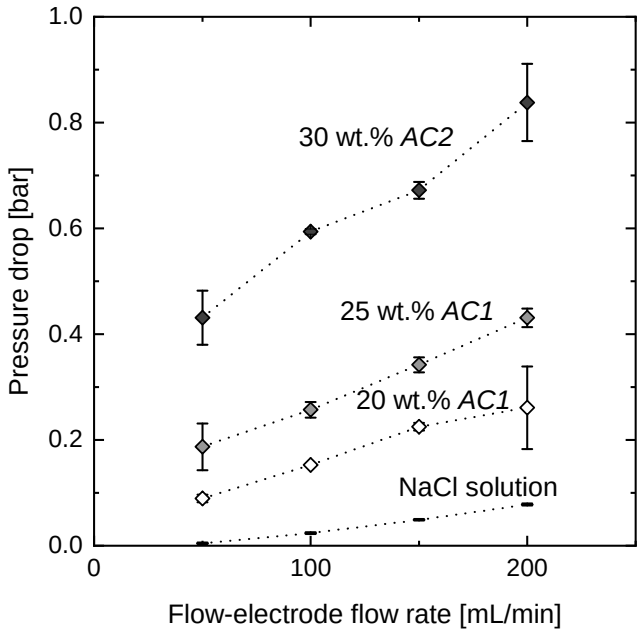


**Figure 5.4.:** Pressure drop measured in the flow-electrode channel of a single FCDI half-cell.

can be calculated, which was normalized by (1) the volume of the treated water (diluate) in $m^3$ and (2) the transferred salt in gram.

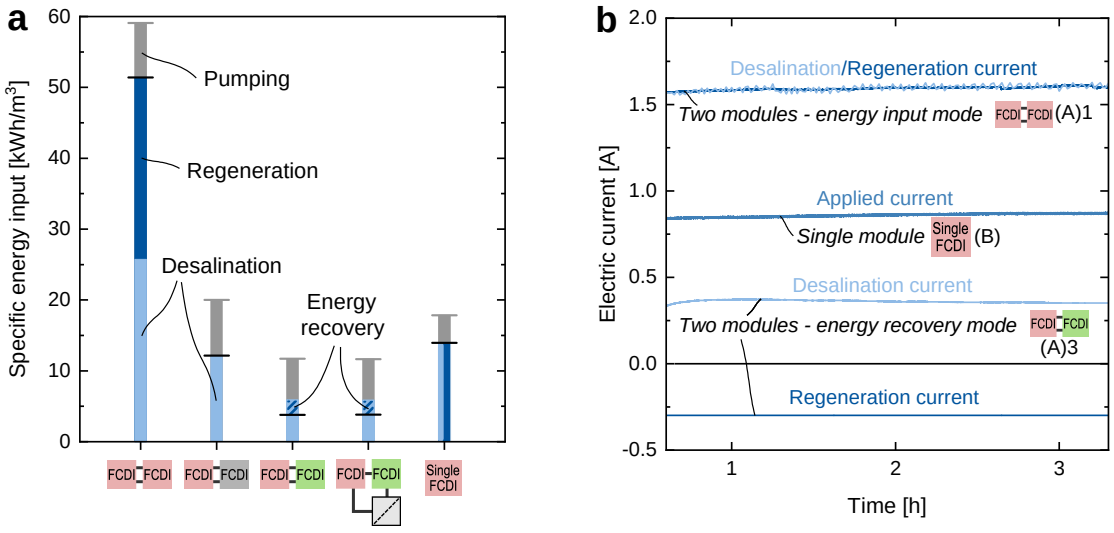


**Figure 5.5.:** Comparison of continuous FCDI system configurations (symbols given in Figure 5.1); All experiments performed with 25 wt.% AC carbon powder and 60 g/L NaCl in the flow electrodes, flow-electrode flow rates of 200 mL/min, diluate feed flow rates of 1.2 mL/min and concentrate feed flow rates of 1 mL/min. (b) Measured electric currents over time during sample experiments in energy input mode, single-module configuration and energy recovery mode during steady state operation of FCDI systems.

Figure 5.3 (c) compares the required energy input for the different system configurations and operational modes. The black lines represent the overall electrical energy required for desalination. In literature [Ton2016; Al-2013], the energy requirement of desalination systems is often compared in kWh/m$^3$ (Figure 5.5 (a)). In this case (unlike Figure 5.9 (a) and (b)), the values were not recalculated to represent full desalination. The dimension kWh/m$^3$ does not take the amount of removed salt into account, which often differs significantly from case to case. This is also the case here, as can be seen in Figure 5.3 (a) and (b). Values of the initial salt content and final salt content are often omitted in context of given values for the energy demand in literature. Especially in case of electrically driven processes a comparison of energy demands normalized by the amount of product water is questionable, when the feed and product salinities as well as the water recovery rates are not considered as well. It is usually preferable in this case to use values for the energy requirement normalized either by the moles of the salt or mass of the salt which has been removed or transferred. In this work, a normalization by mass was chosen to compare the different systems, leading to the dimension Wh/g. In all cases it should be clearly stated how a given energy demand of a desalination system was determined and calculated, as the values can vary significantly depending on the system conditions and salinities.

When comparing the values in Wh/g given in Figure 5.3 (c) for the four different systems, it becomes apparent that the energy requirement for the desalination step (light blue bars) is similar in each case. It is independent from the desalination performance, reaching values of around 0.6x Wh/g NaCl. Summing the electrical energy requirement for desalination and regeneration, the systems with energy recovery reach the lowest values of 0.44 and 0.46 Wh/g NaCl. This equates to energy recovery percentages of 36.2 % and 34.3 %, respectively, without considering the pumping energy required for the flow electrodes. The relatively high values compared to results published by Jeon et al. [Jeo2014] may result from reduced ohmic losses in the system due to a higher salinity. To investigate this, additional experiments were performed at lower salinities (Figure 5.3 (d)), which show an increasing energy recovery at increasing salt concentrations.

Figure 5.5 (b) shows the measured electric currents over time during CV operation of three different systems. Only in case of the energy recovery system the operational mode was set to a constant current of 0.3 A for the regeneration module. The measured electric currents were fairly constant during steady state operation. The results demonstrate that a stable operation is possible in case of all continuous systems presented here.

When comparing the energy demand of the different FCDI systems presented here in this way, it also becomes clear that the pumping energy is quite significant for the systems with energy recovery when normalized by the transferred

mass of salt, as in this case lower salt transfer rates are accomplished. Due to this, the overall energy required in Wh/g NaCl is actually comparable to the first two systems. The lowest overall energy requirement among the compared systems of 0.81 Wh/g NaCl is reached by the system in single-module configuration. Hence, the single-module configuration is a very promising candidate for further developments, which are presented in Chapter 7, as it combines a good desalination performance with low energy requirements and lower capital investment needed for building a new system. The results indicate that in FCDI module and process design the aim should be to reach high currents and current densities at low correlated pressure drops in the flow-electrode channels. This way, it should be possible to reduce the required pumping energy in relation to the transferred salt. On the other hand, the two-module configuration offers more design freedoms and might be advantageous in specific cases. It may be possible to significantly improve the desalination performance by increasing the module size for the regeneration step. At the same time, the pressure drops measured here, and thus the required pumping energy, will most probably not scale linearly with module size and may be reduced significantly by choosing a different AC type, an improved module and flow channel design or a reduced flow-electrode flow rate. Hence, the energy requirement in Wh/g NaCl for desalination, as well as pumping, would also decrease significantly. A significant improvement is expected when using a better suited activated carbon, such as discussed in Chapter 4. The experiments presented in the following chapter, Chapter 7, which includes a further discussion of how to influence the energy demand, were performed with the Carbopal SC11PG carbon investigated in Chapter 4. Even more suitable carbons may exist, may lead to an even better performance, and can be identified using the method presented in Capter 4.

The results presented in this chapter show that FCDI should be considered as a new type of unit operation or platform technology, which may be tailored to the process needs in each specific case. Advantages and disadvantages of specific process configurations might change depending on the application, and can be tailored accordingly.

### 5.4.3. Impacts on energy demand - Single-module configuration

**Impact of activated carbon content and flow-electrode flow rate.** Further FCDI experiments were conducted in single-module configuration to investigate the impact of other process parameters on the energy requirement. In Figure 5.6 (a) and Figure 5.6 (b) the desalination performance and specific energy requirement is compared for an FCDI single-module setup, which is operated

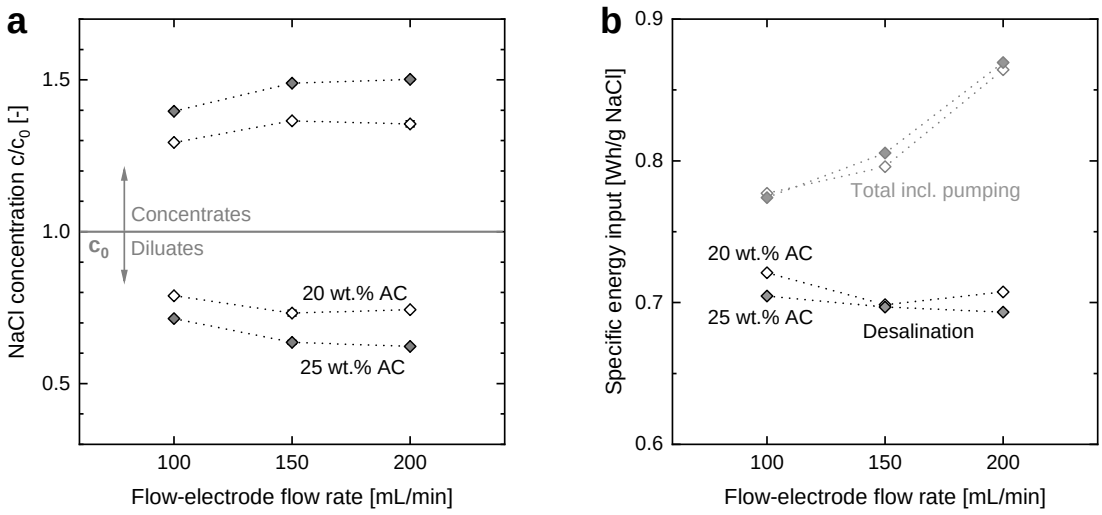


**Figure 5.6.:** System performance of a continuous FCDI system in single-module configuration at varied flow-electrode flow rates and varied activated carbon concentration in the flow electrodes.

with varied flow-electrode flow rates and varied flow-electrode compositions of 20 wt.% AC and 25 wt.% AC1 (Norit D10, Batch "AC1"). Otherwise, all process parameters were kept as described before.

As reported before [Por2014; Hat2015b; Rom2018b], the results plotted in Figure 5.6 (a) show an increasing desalination rate with increasing flow-electrode flow rate and increasing AC content. In the presented experiments, the increase of the AC content improves the desalination rate more significantly than the increase of the flow-electrode flow rate. Interesting is that the specific electrical energy requirement for desalination, given in Wh/g NaCl in Figure 5.6 (b), is very similar for all cases. However, the specific pumping energy increases significantly with increasing flow-electrode flow rate, which indicates that energetically an increase of the flow-electrode flow rate is not sensible, although it leads to an increase of the desalination rate. At the same time, the specific pumping energy is nearly the same for the two different AC concentrations. The increase of the AC content leads to an improved charge percolation [Hat2017] and conductivity. This improves the desalination performance so much that the increased pressure drop, which needs to be overcome by the pumps, is balanced by the improved desalination rate, which overall leads to the same specific energy input when expressed in Wh/g.

**Impact of the activated carbon characteristics.** Generally, trade-offs such as the desalination performance versus the rheological behaviour should be considered when designing FCDI systems. A low pressure drop is desirable, while

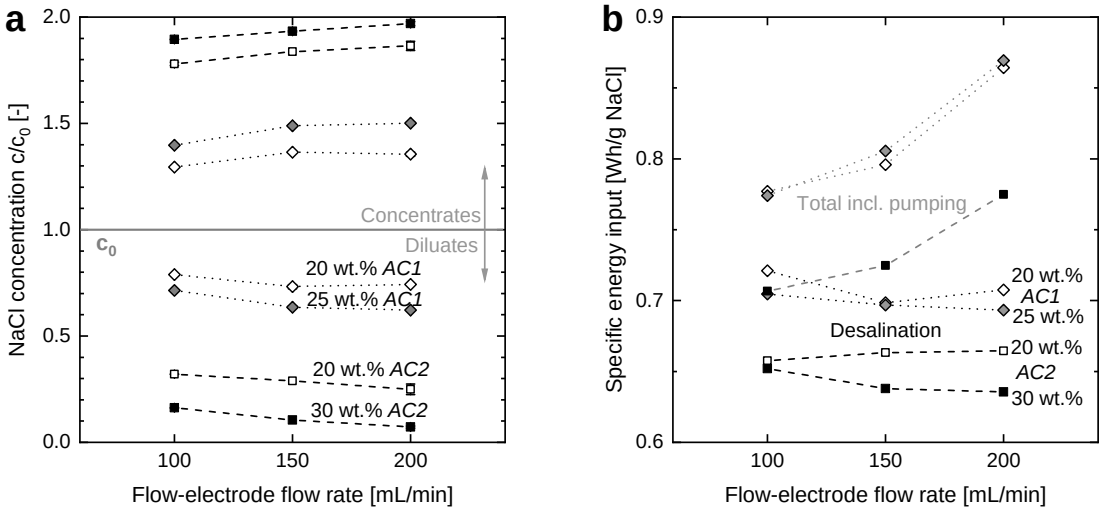


**Figure 5.7.:** System performance of the two different activated carbon batches "AC 1" and "AC 2" (same as investigated in Chapter 4) in a continuous FCDI system in single-module configuration at varied flow-electrode flow rates and varied activated carbon concentration in the flow electrodes.

achieving a high desalination rate at the same time, as previously discussed by Hatzell et al. [Hat2015b] and Chapter 4. This may be achieved by an increase of the AC content, if possible, or a further improvement/better choice of the flow-electrode materials and composition in general, as approached by several research groups [Hat2015b; Par2016; Yan2017; Lia2017] and in the previous Chapter 4.

The aim of a second set of experiments was to investigate the influence of the activated carbon characteristics on the energy demand. The experiments were conducted with a different batch of activated carbon, "AC 2" (same as "Norit D10-Batch 2" in Chapter 4). Apart from the activated carbon choice, the same settings as used for obtaining the experimental results plotted in Figure 5.6 (a) and (b) were used for this second set of experiments. The results for the second set of experiments are plotted in Figure 5.7 (a) and (b), which also show the results from Figure 5.6 (a) and (b) for easier comparison.

The graph in Figure 5.7 (a) shows the desalination performance and the graph in Figure 5.7 (b) shows the specific energy requirement for the two activated carbon batches in comparison, tested using the same process conditions in an FCDI single-module setup. The results plotted in Figure 5.7 (a) are in good agreement with the findings presented in Chapter 4. The desalination performance of FCDI systems, even in case of the single-module configuration as is the case here, depends strongly on the activated carbon characteristics. When comparing the two experiments using a 20 wt.% flow electrode, the system operated with the batch AC 2 removes with 70 % significantly more NaCl compared to AC 1,

which only removes about 20 % of the present NaCl from the feed solution. This significant difference in desalination performance and current density also has an impact on the energy demand. The energy demand for desalination reduces significantly when using the better-suited batch AC 2, which contains a significant amount of mesopores. This can be explained by the reduced ohmic resistance of the flow electrode based on AC 2, which leads to an increase in the current density. The normalized pumping energy, however, hardly changes depending on the activated carbon. The increase of the total required pumping energy, due to the increased pressure drop, balances the current density increase (and hence improved desalination performance).

These findings correlate well with the observations regarding the activated carbon content and illustrate the importance of optimizing the flow-electrode characteristics for an actual application. These findings are in good agreement with the predictions obtained from the simplified FCDI process model and the corresponding experimental results published previously [Rom2018b].

## 5.5. Theoretical energy demand: Can FCDI compete?

FCDI technologies are still in an early stage of development, and still have a high potential for further developments regarding module design, flow-electrode composition, membrane fabrication and process layout, which the above described experiments illustrate. For assessing the economic feasibility of FCDI processes, the energy requirement will play a crucial role, apart from other factors such as desalination rate per membrane area. Thus, results of theoretical calculations regarding the main influencing factors for the energy demand of FCDI processes, as plotted in Figure 5.8 and Figure 5.9 (a), are of major interest to evaluate the potential of the technology and to understand the crucial parameters which can make FCDI competitive.

Figure 5.8 shows the theoretical minimum energy demand of FCDI processes in Wh/g NaCl (equal to kWh/kg) depending on the current efficiency (CE) and the applied voltage (Equation 5.2).

$$E_{el/mass} = \frac{F \cdot n_{NaCl} \cdot U}{CE} \tag{5.2}$$

Here, $E_{el/mass}$ represents the mass-specific electrical energy required for desalination in a single-module or two-module FCDI system with short circuit regeneration (Mode A1, Figure 5.1), $F$ is the Faraday constant, $n_{NaCl}$ is the molar amount of transferred sodium chloride, $U$ is the applied voltage, and $CE$ is the current efficiency. Accordingly, the energy demand increases in a hyperbolic manner with decreasing current efficiency and linearly with increasing voltage. This

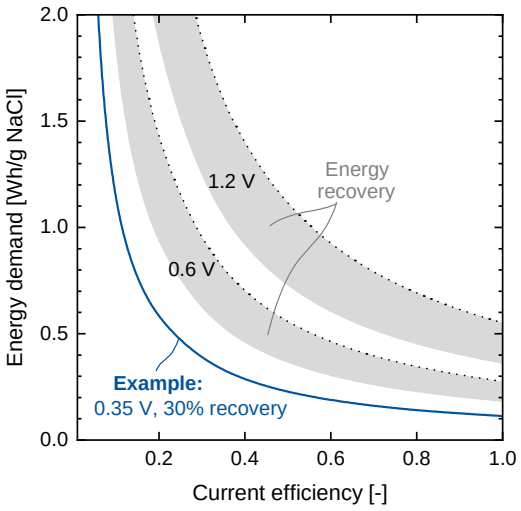


**Figure 5.8.:** Theoretical minimum energy demand for the complete desalination of NaCl solutions using FCDI processes, depending on the current efficiency and voltage given in Wh/g NaCl.

corresponds well with findings presented in electrodialysis literature, such as the increase in energy consumption at increasing current densities (and thus applied potentials) and increasing NaCl concentrations [Ton2002; Nag2006; Sad2009]. The latter is likely caused by decreasing current efficiencies due to a reduced efficiency of the Donnan exclusion, which leads to decreasing selectivities of ion exchange membranes at high salt concentrations. This illustrates the importance of (1) the membrane quality, to achieve high current efficiencies, and (2) the minimization of unwanted potential drops, to decrease the required voltage for the same desalination performance. The latter may be achieved by an improved module design (flow electrode and spacer channels), reduced membrane resistance (material and thickness) and flow-electrode composition, to achieve a low voltage and pressure drop together with good charge transfer and ion storage capacity. A further investigation of this is presented in Chapter 7.

Figure 5.9 (a) illustrates the influence of the NaCl concentration and voltage (sample values for 1.2 V and 0.6 V) on the theoretical minimum energy demand of an FCDI process in kWh/m$^3$. The volume specific electrical energy $E_{el/vol}$ can be calculated from $E_{el/mass}$ (Equation 5.2) by multiplication with the salt concentration in the solution (Equation 5.3).

$$E_{el/vol} = E_{el/mass} \cdot c_{NaCl} \tag{5.3}$$

Hence, the energy demand increases linearly with increasing difference between feed and product stream salinity. The graph also includes experimental results reported in this work, recalculated for full desalination by linearly scaling the electric current, which would be required to achieve full desalination.

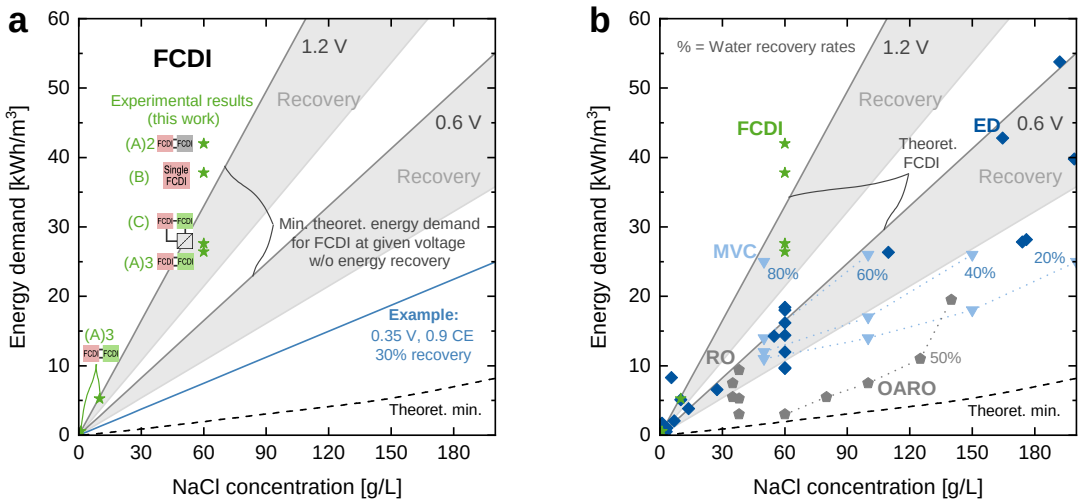


**Figure 5.9.:** Energy demand for complete desalination depending on the NaCl feed concentration (ED/FCDI values scaled to represent full desalination), (a) using FCDI processes. Dotted lines: theoretical values reachable in modes (A)2 or (B) (Figure 5.1). Grey areas: energy recovery of up to 35 %. Dashed line: minimum work of separation at a water recovery of 50% [Are2017]. Values do not account for pumping energy. (b) Results comparing FCDI and literature values (RO, [Ng2015; Avl2003] OARO [Bar2017], ED, [Tur2004; Cas2012; Dem2003; McG2014; Rei2014; Ort2005; Gma2017; Che2017] MVC [Thi2015]). ED: electrode losses often not included [Cas2012; Rei2014].

Figure 5.9 (b) gives an overview of the energy demand for selected established and novel desalination methods in kWh/m$^3$ treated water, and includes the results plotted in (a), the results regarding FCDI achieved in this chapter. In case of the electrically driven methods, ED and FCDI, the values were calculated to represent full desalination, based on (literature) values normalized by the transferred salt. The state-of-the-art technology for seawater desalination is currently reverse osmosis (RO) [Wer2016; Al-2013; Ton2016]. RO is energy efficient, but can typically treat saline streams with concentrations of only up to 70 g/L [Ton2016]. Additionally, the effect of RO brines on the environment remains unclear, due to increased salt levels and chemicals added for pretreatment [Fer2005; Eli2011; Mez2011]. This is why many studies focus on the utilization of brines, e.g. RO brines from seawater, and zero liquid discharge. In many cases, researchers focused on ED in combination with crystallization or evaporation for such applications [Rei2014; Yan2014; Tan2003; Cas2012; Ore2010; Tur2004]. Apart from this, a new RO process design called osmotically assisted reverse osmosis (OARO) enables the treatment of high salinity brines. However, even this new concept reaches only limited water recoveries of up to 50% [Bar2017].

The treatment of saline brines is a possible application field for the FCDI technology, which, unlike CDI, enables a fully continuous operation and electrode

regeneration [Gen2014]. This enables flow-electrode capacitive deionization to treat high salinity aqueous solutions. For brine treatment, FCDI will have to compete with established processes such as different temperature driven (distillation) processes, including vapor compression and membrane distillation (MD) [Mac2017; Des2018], and ED processes, as discussed in other works [Al-2013; Eli2011; And2010]. MVC is relatively energy efficient, compared to other temperature driven desalination and concentration processes. Values regarding the energy demand of MVC are reported mostly between 7-41 kWh/m$^3$, depending on the salinities and water recovery rates [Al-2013; Thi2015]. However, the capital costs of MVC units are also comparably high [Ton2016]. MD is currently still less efficient than multi-effect distillation and multi-stage flash, but may be sustainable due to the possible valorization of low-grade or waste heat, or renewable energy sources [Mac2017; Des2018].

Another potential application area for FCDI processes is the treatment of higher salinity brackish water, where FCDI will have to compete with ED and RO processes. A study by Choi et al. [Cho2017b] indicates the potential of hybrid processes in this area, such as FCDI combined with nanofiltration.

## 5.6. Summary and conclusions

The results presented in this chapter were an initial study focusing mainly on the possibility to treat brine solutions with FCDI, including a first comparison to literature values. It was shown before that ED processes may be an alternative for MVC for brine treatment [McG2014]. ED processes for NaCl concentration reported in literature reached values regarding the energy consumption of as low as 0.12-0.38 kWh/m$^3$, for the determination of which the electrode potentials were neglected in some cases, however [Rei2014; Tur2004; Yam1969]. The research so far indicated at this point that FCDI may be able to reach comparable or even better values when improved according to the parameters discussed in this chapter. One advantage of FCDI processes identified in the literature review presented here is the possibility to desalinate and concentrate brine streams significantly in a single pass, while many ED processes described in the literature treated brine streams in many steps.

The values presented in this chapter cannot compete with literature values. However, the comparison helped to understand the crucial factors to make FCDI competitive. These findings were motivation enough to continue this research and conduct further studies focusing on understanding the mass transport and the development of different approaches to reduce the energy demand of FCDI processes, as presented in the following chapters.

# 6

# Water and ion transfer in FCDI processes for the treatment of high salinity solutions

In this chapter, an experimental study is presented, which focuses on developing further understanding of the salt and water transfer in continuous FCDI processes aimed at the treatment of high salinity solutions. The possible desalination performance and achievable water recovery rates at high salt concentrations and concentration gradients are investigated, including the influence of system layout and experimental parameters on the desalination and concentration performance. These findings are the basis for a newer FCDI process model version, which is presented in Chapter 8, which includes a range of improvements compared to the first model published in 2018 [Rom2018b]. The newer process model version is now, unlike the older version, suitable for simulating FCDI processes at high salt concentrations.

## 6.1. Challenges in brine concentration via FCDI

The treatment of highly saline brines leads to several challenges in ion-exchange membrane based FCDI processes: (1) decreased membrane selectivities due to an ineffective charge exclusion of ion-exchange membranes at high salinities and (2) increased osmotic and electroosmotic water transfer rates.

During initial experiments aiming at reaching high water recoveries and, hence, high salt concentrations in the concentrate, a significant deviation in the mass balances was observed. A change of the product flow rates after applying an electrical potential to the cells was soon identified as the reason for the deviations in the mass balance. The diluate product stream flow rates were significantly smaller than the diluate feed flow rates, causing a concentration increase of the diluate. At the same time, the concentrate product stream flow rates were larger than the concentrate feed flow rates, causing a dilution of the concentrate. This is caused by a water transfer from diluate to concentrate stream due to osmosis and electroosmosis, which is also described in the electrodialysis and ion-exchange membrane literature.

Based on this observation, the role of water transfer in continuous FCDI processes for brine concentration and how it is influenced by the system layout was investigated. The hypothesis is that the water transfer may be reduced due to

the application of flow-electrodes. The flow-electrodes may reduce the osmotic pressure by adding an intermediate stream (the flow-electrode) between diluate and concentrate stream, which effectively reduces the concentration gradients. Excess ions are stored in electrical double layers, and do not necessarily influence the salt concentration in the continuous phase around the carbon particles. In electrodialysis processes, diluate and concentrate streams are only separated by a single membrane, which may promote an unwanted water transfer. An attempt to quantify the contributions of osmosis and electroosmosis on the water transfer in FCDI processes is presented.

## 6.2. Experimental

The experiments presented in this chapter were performed in two different continuous FCDI process layouts, the two-module configuration and the single-module configuration, as described in Chapter 5. The same type of FCDI modules, membranes, spacers and pumps were used, which were all assembled and operated in co-flow regarding water and slurry streams. Unlike the previous work, two Keysight power supplies (Keysight Technologies Inc., E3466A) were applied to achieve higher electrical currents. A digital multimeter (Voltcraft, VC270 Green-Line) was used to verify the actual voltage applied to the graphite current collectors. Additionally, the pumps, power supplies and conductivity sensors (LTC 0,35/23; Sensortechnik Meinsberg) were connected to a custom-made measuring system "ZUMO-FUMS" (ZUMOLab GbR, Wesseling, Germany), which was used to control the pumps and power supplies as well as record the experimental data. Whenever an FCDI module was newly assembled, fixed amounts of water were recirculated separately through each flow-electrode, diluate and concentrate compartment for several hours to rule out internal and external leakages.

### 6.2.1. System layout

Unlike the single-module systems applied in previous work (Chapter 5 and [Rom2015; Rom2018a]), the system layout differed regarding the flow electrode handling. As illustrated in Figure 6.1, the flow electrode was recirculated from a single beaker in this case ("single vessel layout"). In the original layout, the flow electrodes passed the oppositely charged current collectors one after another, with each one storage vessel designed as drip chamber in between. The disadvantage of this layout are small difference in the pressure drop on each side, due to differences in tubing length or wear. These pressure drop differences lead to differences in the flow rates and hence changing fluid levels in the flow-electrode vessels. This can be avoided when using the single vessel layout.

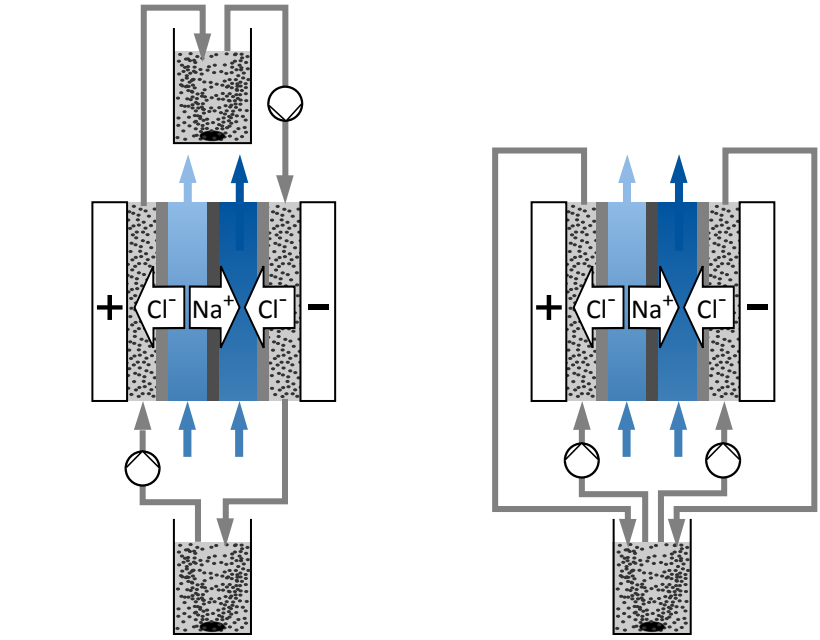


(A) Single-module configuration
- Original layout
(Reality: Flow-electrodes in co-flow)

(B) Single-module configuration
- Single-vessel layout

**Figure 6.1.:** Layout and flow electrode handling in single-module configuration FCDI systems in (A) previous works (Chapter 5 and [Rom2015; Rom2018a]) and in (B) experiments described in the current chapter.

## 6.2.2. Experimental procedure

Table 6.1 gives an overview of the experimental settings. All experiments described in this section were performed with activated carbon slurries as flow electrodes prepared at weight percentages ranging from 12-18 wt.% Carbopal SC11PG (Donau Carbon GmbH) in a NaCl solution with a concentration of 60 g/L (Sodium chloride ≥99.8%, VWR Chemicals). The slurries were stirred overnight before use. For each flow-electrode circuit a volume of 200 mL slurry was recirculated through the system at a flow rate ranging from 120-180 mL/min. The slurry storage beakers were continuously stirred using magnetic stirrers.
In the first two sets of experiments the general possibility to desalinate and concentrate brines with continuous two-module and single-module FCDI systems is investigated. The activated carbon content and flow rate of the flow electrode were varied. In the third and fourth set of experiments the salt and water transfer was investigated in more detail. To determine the contributions of osmosis and electroosmosis to the overall water transfer, two types of experiments were performed: ”desalination experiments” and ”osmosis experiments”.

**Table 6.1.:** Overview of experimental parameter settings (Chapter 6).

| | **Cell** | **Slurry** | | **Feed water** | |
|---|---|---|---|---|---|
| | Voltage | AC | Flow rate | NaCl | Flow rate |
| **Description** | V | wt.% | mL/min | g/L | mL/min |
| *Desalination experiments - carbon mass fraction variation* | | | | | |
| **Both systems** | 1.2/1.2 | 12 | 150 | 60 | D:1/C:0.04 |
| ” | 1.2/1.2 | 15 | 150 | 60 | D:1/C:0.04 |
| ” | 1.2/1.2 | 18 | 150 | 60 | D:1/C:0.04 |
| *Desalination experiments - flow-electrode flow rate variation* | | | | | |
| **Both systems** | 1.2/1.2 | 15 | 120 | 60 | D:1/C:0.04 |
| ” | 1.2/1.2 | 15 | 150 | 60 | D:1/C:0.04 |
| ” | 1.2/1.2 | 15 | 180 | 60 | D:1/C:0.04 |
| *Water transfer - desalination experiments* | | | | | |
| **Two modules** | 1.2/1.2 | 15 | 150 | 60 | D:1/C:0.04 |
| **Single module** | 1.2 | 15 | 150 | 60 | D:1/C:0.04 |
| *Water transfer - osmosis experiments* | | | | | |
| **Two modules** | - | 15 | 150 | D: 4.9/C:239.6 | D:1/C:0.04 |
| **Single module** | - | 15 | 150 | D:16.8/C:217.3 | D:1/C:0.04 |

**Desalination experiments.** Initially, continuous (steady-state) desalination and concentration experiments were performed in two-module and single-module configuration (Figure 6.2 (a) and (b)) using the above described settings.

The flow rates of the diluate (1 mL/min) and concentrate (0.04 mL/min) streams exiting the FCDI module(s) were measured and adjusted during the initial recirculation and pumping of all liquid/suspension streams through the system, without the application of an electrical voltage. The low value of the concentrate stream flow rate was chosen to achieve a high concentration factor and thus a high water recovery rate. Subsequently, a voltage of 1.2 V was applied to the graphite plates of each FCDI module. The electrical conductivity of the product streams, as well as the electrical current flowing through each FCDI cell was monitored. Once steady-state was reached, several samples of the diluate and concentrate stream were taken and the density measured to obtain the NaCl concentration, as described in the previous chapter. Additionally, the flow rates of the diluate and concentrate product streams were measured during steady-state operation with applied electrical voltage to determine a change in flow rates due to water crossover during desalination/concentration in case of the water transfer experiments.

**Osmosis experiments.** In an attempt to quantify the osmotic water crossover in the continuous two-module and single-module FCDI configuration, a set of

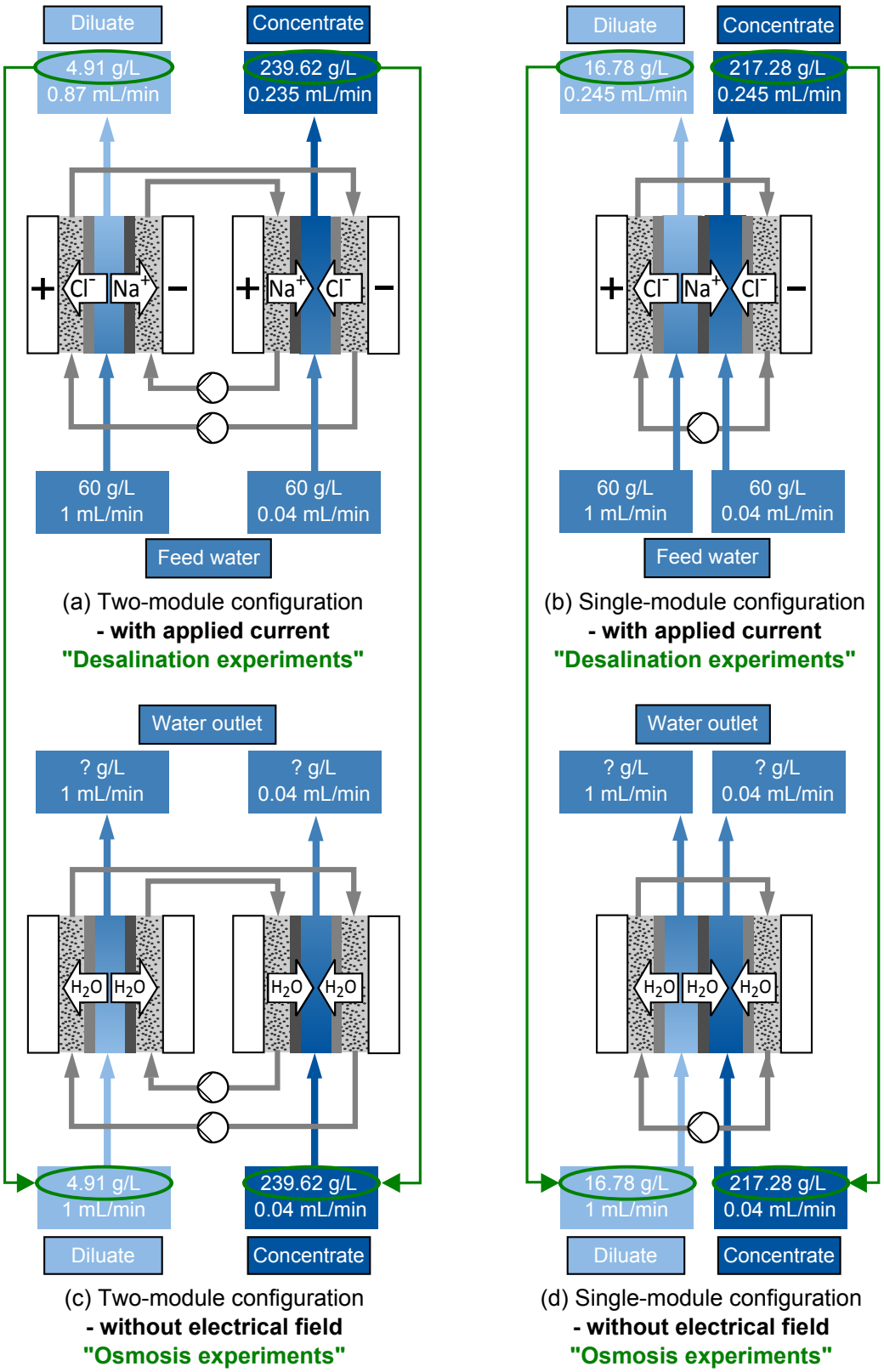


**Figure 6.2.:** Layout and experimental settings used for (a)/(b) desalination experiments and (c)/(d) osmosis experiments comparing (a)/(c) the continuous two-module configuration and (b)/(d) the continuous single-module configuration as described in this section.

experiments was conducted without the application of an external electrical voltage. The general procedure and system layout are same as described previously and is illustrated in Figure 6.2 (c) and (d). In this case, the concentrations of the diluate and concentrate streams exiting the FCDI cell(s) during a desalination experiment were chosen as inlet concentrations, as indicated by the green arrows in Figure 6.2. In these experiments the transfer of ions the water crossover caused by hydration shells (electroosmosis) can mainly be avoided due to the missing electrical field as driving force. The driving force for the transfer of salt and water in the osmosis experiments were concentration differences. Due to this, the time until steady state was reached in each osmosis experiment increased significantly to around 20 hours compared to only a few hours (depending on the flow rate and tubing length) in case of the desalination experiments. Due to the smaller amount of water and salt crossover, the vessels containing feed and product solutions were additionally weighed before and after each experiment to confirm the actual flow rates.

## 6.3. Results and discussion

In the following, the results of the above described experiments are presented and discussed. In the first part, the possibility of using FCDI for brine desalination and concentration is investigated, while in the second part the significant water crossover observed at high salt concentration differences is analyzed.

### 6.3.1. General influences

Figure 6.3 shows the results of experiments comparing the two-module configuration and single-module configuration at varied flow-electrode flow rates and activated carbon contents during the treatment of artificial solutions with high NaCl content.

Figure 6.3 (a) shows results for the experiments with medium settings, which are 150 mL/min flow-electrode flow rate and 15 wt.% AC content in the flow electrodes. The concentrations of diluate and concentrate streams are plotted over time. A significant difference in the desalination/concentration performance of the two-module and single-module system is apparent. While the two-module system is able to remove more than 94 % of the NaCl present in the feed stream, the single-module system removes only 75 % of the present NaCl. The behaviour regarding the concentration is similar. The highest concentrate concentration of 245 g/L is reached by the two-module system.

The obvious reason seems to be the increased resistance of the single-module system. A voltage of 1.2 V was applied to all FCDI modules, while the single-

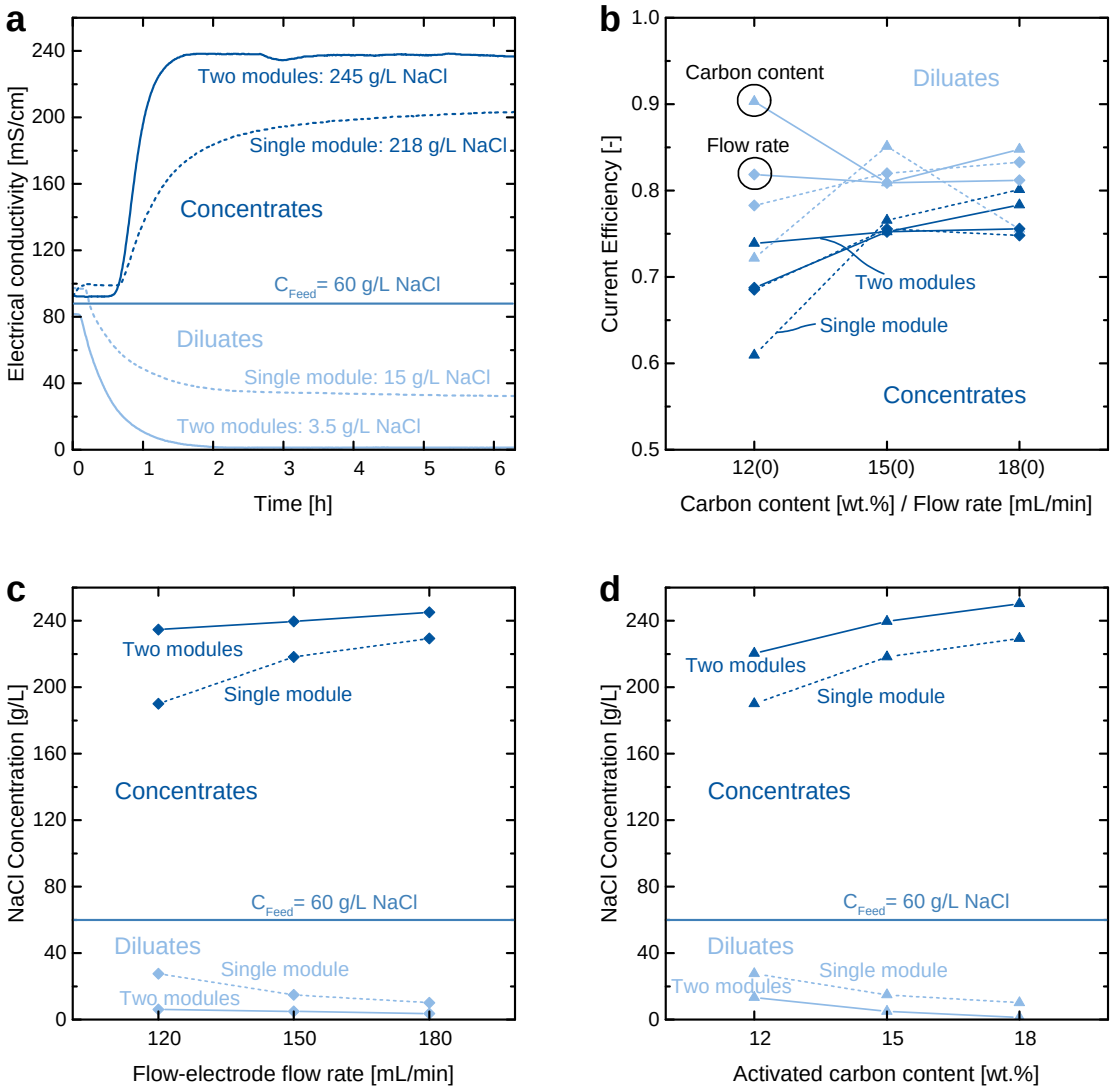


**Figure 6.3.:** Results of desalination/concentration experiments with a feed concentration of 60 g/L NaCl comparing the continuous two-module configuration to the continuous single-module configuration. The graphs show results for (a) the electrical conductivity over time, including steady state NaCl concentrations of diluates and concentrats, (b) the current efficiencies calculated for the diluate and concentrate mass balance, (c) the concentrations depending on the flow-electrode flow rate and (d) the concentrations depending on the activated carbon content in the flow electrode.

module contains one additional membrane and one additional feed spacer. An estimation of the ohmic resistance increase due to one additional spacer and membrane reveals that this cannot be the only reason. This was confirmed with an additional experiment, in which a two-module FCDI configuration was operated at a reduced voltage. The resulting current was still significantly higher.

Another reason for the significant difference in performance may be back diffusion of ions, which may occur to a higher extent in the single-module system due

to the high concentration gradient over the middle membrane. This should be expressed in reduced current efficiencies. Figure 6.3 (b) shows the current efficiencies calculated for the diluate and concentrate stream mass balances separately, for both systems and all parameter variations. The mass balance for the diluate streams seems to be favourable in nearly all cases. The current efficiency is slightly better for the two-module system compared to the single-module system, but not significantly.

Figures 6.3 (c) and (d) show the NaCl concentration of diluate and concentrate for both systems depending on (c) a varied flow-electrode flow rate and (d) a varied activated carbon content. In all cases, the two-module system performs best. The performance of the single-module system in the best cases is comparable to the performance of the two-module system in the worst cases. However, the parameter variation seems to have a more significant (positive) impact for the single-module configuration compared to the two-module configuration, especially in case of the varied flow-electrode flow rate. In case of a system optimization this is an interesting finding, as the pumping energy for the flow electrode will not influence the overall energy demand as significantly as in the two-module system, due to the recirculation of only a single flow electrode.

Three effects, which were not mentioned above, may help to explain the significant performance difference between the two-module and single-module configuration: (1) an increased water transfer in the single-module system due to the high concentration difference over the central membrane, (2) the high (adverse) concentration gradient between diluate and concentrate causing an increased resistance, and (3) an increased membrane resistance, as described by Geise et al. [Gei2013], for IEM separating solutions with significant concentration differences. In the following paragraph, the influence of the first effect is investigated and quantified. The second effect is investigated via the improved FCDI process model presented in Chapter 8.

### 6.3.2. Water transfer

Figure 6.4 shows the results of experiments comparing the water crossover in the two-module configuration and the single-module configuration in case of desalination experiments and osmosis experiments.

Figure 6.4 (a) shows results for the water flow rates at inlet and outlet of the FCDI cell(s) during desalination experiments performed with both systems. Additionally, the difference between the inlet and outlet flow rate is plotted on the right, for both diluate and concentrate streams in case of both systems. In all cases the flow rate of the diluate stream is reduced, while the flow rate of the concentrate stream is increased. The differences between ingoing and outgoing streams match relatively well for diluate and concentrate streams, the mass bal-

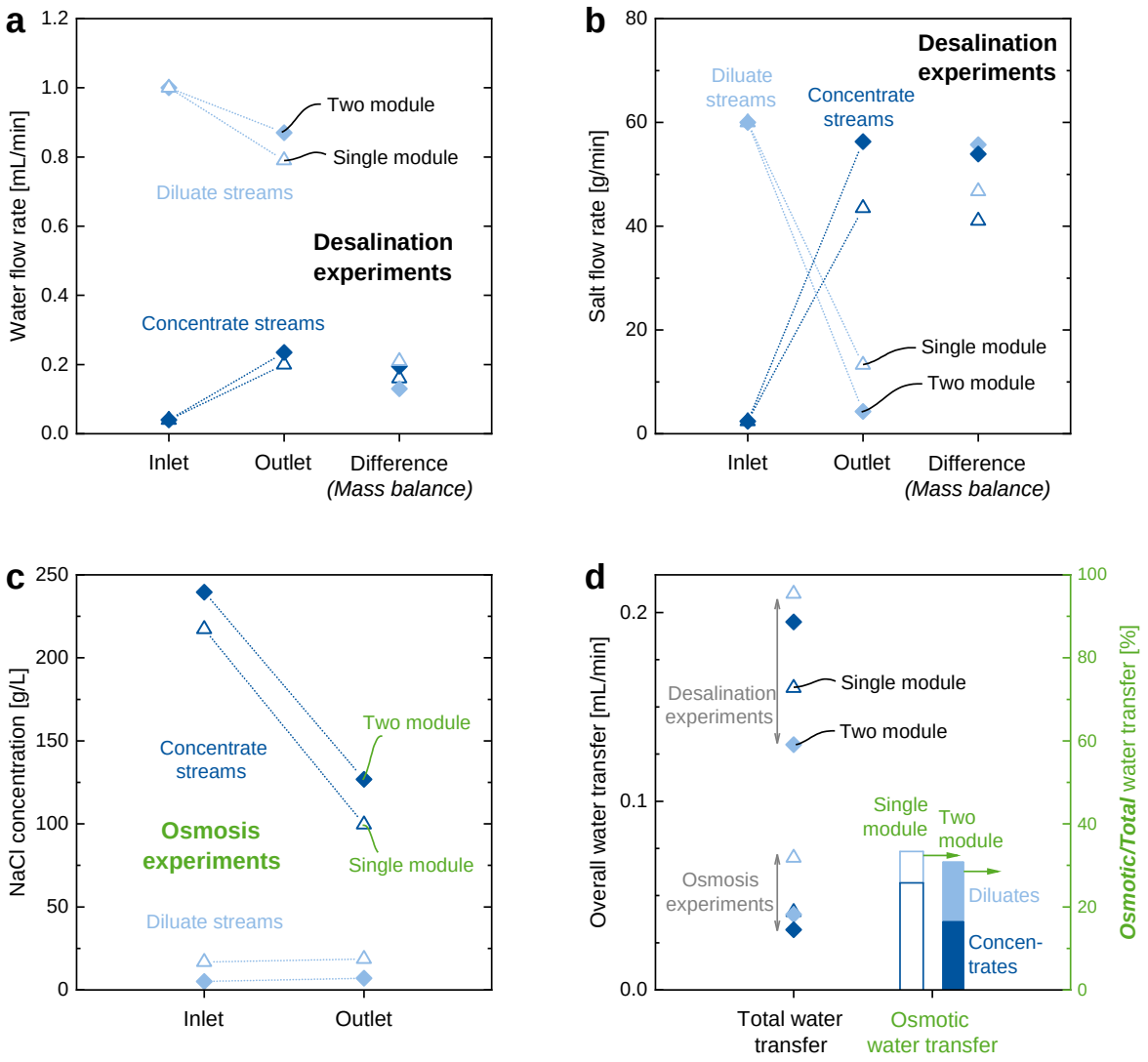


**Figure 6.4.:** Results of desalination and osmosis experiments comparing the continuous two-module configuration to the continuous single-module configuration. The graphs show results for (a) the water flow rate into and out of the cell during desalination experiments, (b) the salt flow rate into and out of the cell during desalination experiments, (c) the concentrations of inlet and outlet streams during osmosis experiments and (d) a comparison of the water transfer in desalination and osmosis experiments including the percentages of osmotic water transfer (overestimated) to electroosmotic transfer.

ance is complete. The water crossover seems to be slightly more pronounced in case of the single-module system. This trend is not very significant at first sight and cannot explain the significant difference in the overall system performance to the full extent.

The salt flow rates entering and exiting both systems in form of the diluate and concentrate streams are plotted in Figure 6.4 (b). Most of the salt is removed from the diluate stream and transferred to the concentrate stream while passing

through the FCDI cell(s). Again, the difference in the salt flow rate between inlet and outlet is plotted on the right. Here, a significant difference between two-module and single-module configuration is visible. The single-module configuration has a much smaller (desired) salt crossover compared to the two-module configuration. This corresponds with the previously discussed observations of reduced desalination performance and increased resistances, which result in reduced electrical currents. Having this significantly smaller salt transfer from diluate to concentrate in the single-module system in mind, the previously described data regarding the water transfer needs to be reconsidered. A smaller salt transfer also leads to a reduced electroosmotic water transfer. Hence, the difference in the water transfer between the two systems is actually much higher than it seems at first sight when considering Figure 6.4 (a).

In Figure 6.4 (c) results of the osmosis experiments are plotted. The NaCl concentration in diluate and concentrate streams is plotted for inlet and outlet in case of both systems. While the concentration of the diluate streams changes only very little, the concentration of the concentrate streams changes drastically. This may be explained by the increased residence time in the concentrate channel compared to the diluate channel, due to a significant difference in the feed flow rate. In this case, the inlet concentration for the single-module system was chosen lower compared to the two-module system, according to the concentrations reached during the desalination experiments. Although the concentration difference between the two inlet streams is significantly lower in case of the single-module system, the change in the NaCl concentration is slightly higher compared to the two-module system. Hence, the osmotic water transfer in the single-module system is higher.

Figure 6.4 (d) compares the osmotic to the overall water transfer in both systems. In case of the osmosis experiments, the concentration change while passing the cell is significantly lower compared to the desalination experiments. This means the osmotic water crossover is overestimated in these experiments. However, the experiments still indicate the scale of the contribution of osmotic and electroosmotic effects to the overall water crossover. In case of both systems, the osmotic transfer contributes to around 30 % of the total water crossover. The osmotic water transfer is more pronounced in case of the single-module system, even at smaller concentration differences. The reason for this is likely the system layout: the diluate and concentrate stream are only separated by a single membrane in case of the single-module system. This may be a hindrance to achieving a better desalination and concentration performance, especially at high desalination/concentration rates and the resulting high concentration differences.

## 6.4. Summary and conclusion

In summary, the in-depth analysis demonstrates the advantages of using flow electrodes for the desalination and concentration of brine solutions. The flow electrodes separate the diluate and concentrate streams, leading to reduced concentration differences over the IEMs and thus a decreased water transfer and improved performance. This becomes apparent when comparing the desalination/concentration performance of the two-module and single-module system. In the single-module system the water transfer in relation to the salt transfer is higher than in the two-module system. The findings from the experiments presented in this chapter helped to develop an improved version of the original process model published in 2018 [Rom2018b], as presented in Chapter 8.

The reduction of the water transfer may be a possible advantage over ED processes, in which many channels of alternating concentrations are separated by only a single ion-exchange membrane. However, this advantage is compensated to a certain extent, due to the overall significantly better performance of the single-module layout when considering the energy demand and investment costs, as discussed in Chapter 5. The possible reduction of the water transfer and further reduction of the energy demand in FCDI systems is investigated in the following Chapter 7.

# 7

# Influencing the energy demand

Parts of this chapter have been published:

Alexandra Rommerskirchen, Christian J. Linnartz, Franziska Egidi, Sefkan Kendir and Matthias Wessling. "Flow-electrode capacitive deionization enables continuous and energy-efficient brine concentration" in: *Desalination* 490 (2020) 114453.

As shown in Chapter 5, the values regarding the energy demand of FCDI processes cannot yet compete with literature values. However, the comparison in Chapter 5 in combination with the findings presented in Chapter 6 help to understand the crucial factors which need to be met to make FCDI competitive for the treatment of high salinity solutions, which are: (I) good desalination performance combined with high water recovery rates, (II) low energy demand, and (III) low investment and operation costs.
It is clear that many factors influence the performance of an FCDI system. In this chapter, different approaches for reducing the energy demand are presented and tested.

## 7.1. An analysis: How can we reduce the energy demand further?

The electrical power, and hence the electrical energy demand without considering the required pumping energy, is determined by the electrical current and the applied voltage. While the electrical current depends on the number of ions transferred within the system, the required electrical voltage depends on the electrical resistance of a system and can be adjusted accordingly.

### 7.1.1. Electrical resistances in an FCDI cell

For a better understanding of the contribution of individual electrical resistances in an FCDI cell, theoretical estimations of the individual resistances are presented in the following. Figure 7.1 shows the electrical resistance of specific parts of an FCDI cell depending on the electrical conductivity of the diluate product stream.

The calculations are based on the following assumptions:

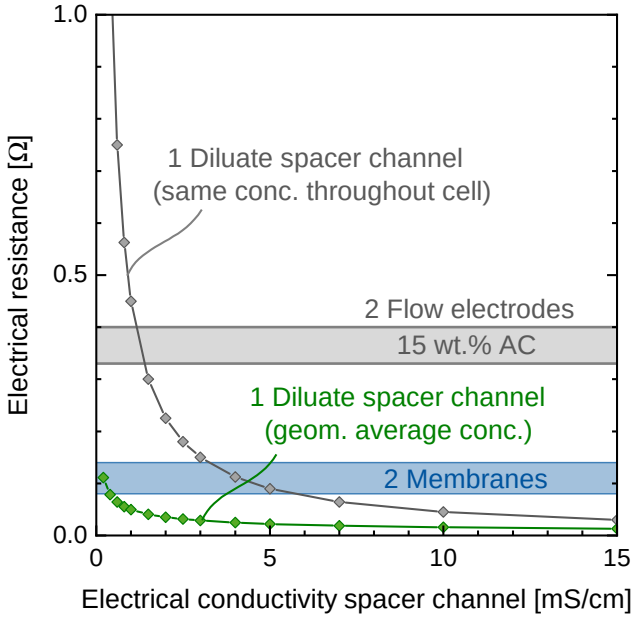


**Figure 7.1.:** Results of theoretical calculations regarding the influence of the NaCl concentration/electrical conductivity of the diluate stream on the electrical resistances in an FCDI cell. Assumptions: Constant diluate flow rate of 1 mL/min, diluate concentration constant throughout cell (overestimated resistances/cell voltage), no consideration of laminar boundary layers, desalination up to the required concentration (varied electrical current).

- NaCl feed: 60 g/L NaCl at a diluate feed flow rate of 1 mL/min.
- Resistance of membranes and flow electrodes constant throughout cell.
- The required electrical current is calculated based on the desalination down to the respective diluate concentration, leading to lower energy demands at higher diluate concentrations even at constant resistance.
- (Depleted) laminar boundary layers are not considered.
- Ideal pumping energy: pump efficiency is not considered.
- The diluate channel resistance was calculated using the geometric average between inlet and outlet concentrations.
- A current efficiency of 1 is assumed.
- Flow-electrode resistance $R_{Fe}$: based on total resistance $R_{total}$ and combined solution/ membrane resistance $R_S$ from EIS measurements presented in Chapter 4 and [Rom2019]. The combined solution and membrane resistance $R_S$ was subtracted from the total ohmic resistance, $R_{Fe} = R_{total} - R_S$.

As is to be expected from the significant influence of the carbon slurry quality on the desalination performance, described in Chapter 4, the resistance of the

flow electrodes at 0.33-0.4 Ω for an AC content of 15 wt. % presents a large fraction of the overall cell resistance.

The next largest resistance in the cell at most diluate concentrations is presented by the membranes. Two ion-exchange membranes of the type fumatech FAB/FKB with PEEK reinforcements account for around 0.08-0.14 Ω of the total cell resistance, based on the manufacturers data. The resistance of the diluate channel varies significantly depending on the outlet concentration, ranging between 0.02-0.1 Ω. The sum of the membrane resistance and the resistance of the diluate spacer channel should be equal to the resistance $R_S$ from the equivalent circuit model represented in Chapter 4. $R_S$ was usually found to be in the range of 0.2-0.27 Ω, which is in good agreement with the estimations presented here. In case of most diluate concentrations, the membrane resistance dominates over the solution resistance, especially when considering three membranes in an FCDI single module configuration. At very low concentrations, the solution resistance is in a similar range as the membrane resistance. However, the solution resistance in this case is likely underestimated, as the laminar boundary layers are not considered.

Based on this analysis, the reduction of resistances in FCDI cells should be prioritized in the following order: (1) Flow electrodes, (2) Membranes and (3) Diluate channel. Depending on the aimed at diluate product concentration and the depletion of the diluate boundary layers, the reduction of the diluate channel resistance should be prioritized over the membrane resistance in specific cases.

### 7.1.2. Concepts for reducing the energy demand

During the analysis of the desalination/concentration experiments presented in Chapter 6, the major influence of the water crossover became clear. When illustrated, as shown in Figure 7.7 (b), the two key factors for reducing the energy demand become apparent: (1) Reducing the electrical resistances (and hence the applied voltage, which is a main driver regarding the energy demand), and (2) reducing the water crossover. In the following, four strategies focusing on the module design and membrane materials are presented, which may help to reduce the overall energy demand of continuous FCDI processes. The four concepts and their key hypotheses/aims are illustrated in Figure 7.2.

The first concept, illustrated in Figure 7.2 (a), aims at reducing the influence of the resistance of the diluate channel. The hypothesis is that the ion transport can be promoted by replacing the standard net spacer by an ion conductive material, such as ion exchange resins.

Next to the improvement of the flow-electrode material and slurry composition,

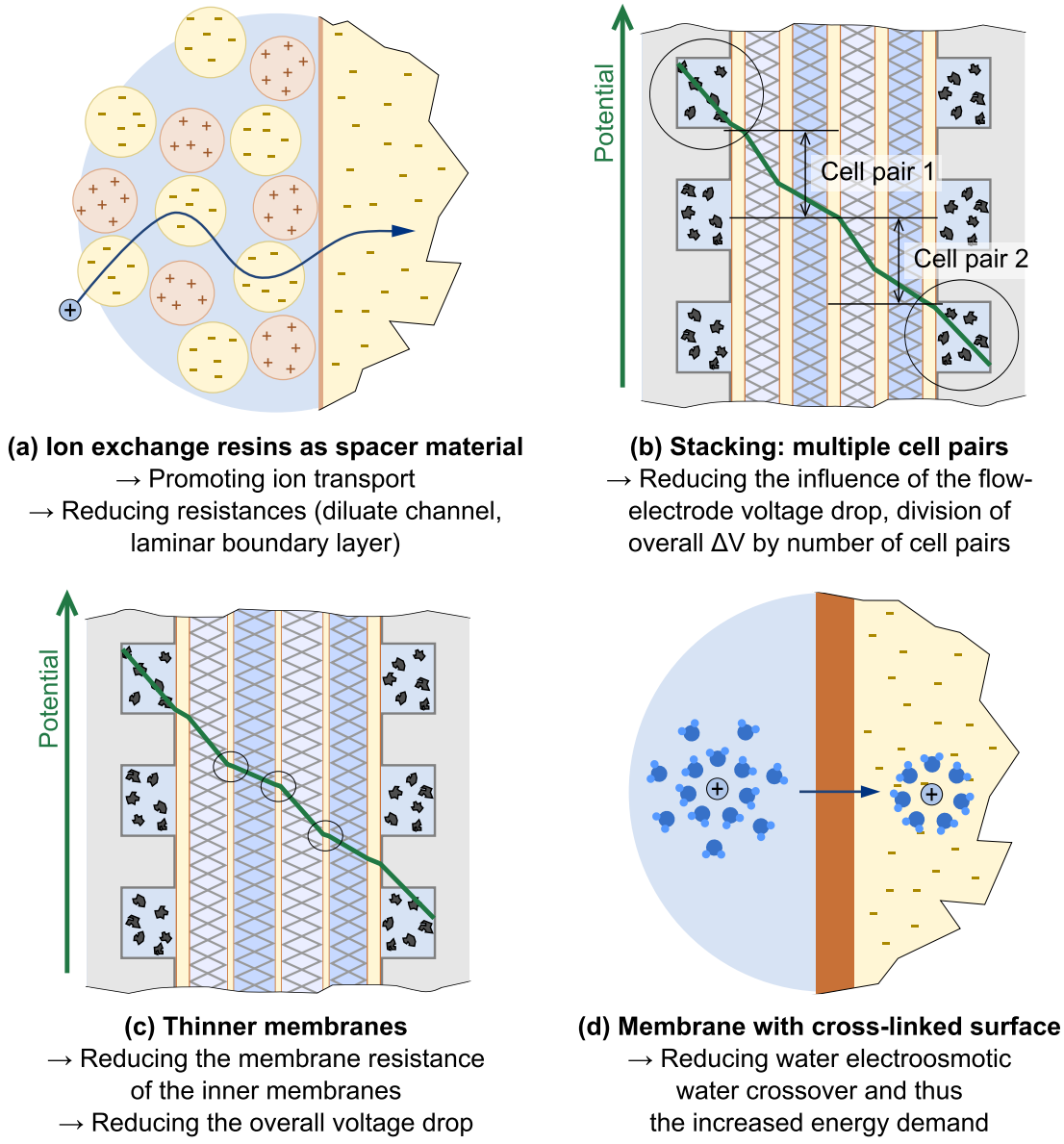


**(a) Ion exchange resins as spacer material**
→ Promoting ion transport
→ Reducing resistances (diluate channel, laminar boundary layer)

**(b) Stacking: multiple cell pairs**
→ Reducing the influence of the flow-electrode voltage drop, division of overall ΔV by number of cell pairs

**(c) Thinner membranes**
→ Reducing the membrane resistance of the inner membranes
→ Reducing the overall voltage drop

**(d) Membrane with cross-linked surface**
→ Reducing water electroosmotic water crossover and thus the increased energy demand

**Figure 7.2.:** Illustration of the four concepts for reducing the energy demand of continuous FCDI processes investigated in this chapter.

it is possible to reduce the impact of the voltage drop over the electrodes by changing the module design. In the second concept, illustrated in Figure 7.2 (b), the influence of the voltage drop over the electrodes is reduced by introducing additional cell pairs (each 1 diluate and 1 concentrate channel, two membranes). This way, the flow rate of the desalinated stream is multiplied by the number of cell pairs, while the energy loss due to the ohmic resistance of the flow electrodes is divided by the number of cell pairs. The hypothesis is that the number of desalination units per unit flow electrode should be increased in order to reduce the relative contribution of the flow electrodes to the total resistance.

The theoretical estimations plotted in Figure 7.1 show that the flow electrodes make up for a major part of the overall resistance in an FCDI cell, making the use of multiple cell pairs promising. Figure 7.3 shows results of theoretical calculations regarding the energy demand and expected required cell voltage for the desalination down to the desired diluate concentration (x-axis) in an FCDI system with one, two and three cell pairs. The calculations are based on the same assumptions stated in the list above.

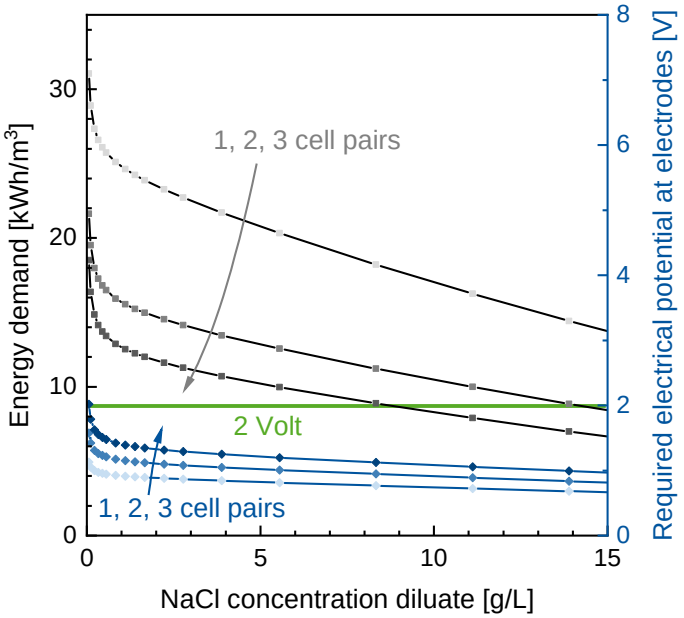


**Figure 7.3.:** Results of theoretical calculations regarding the influence of the NaCl concentration/electrical conductivity of the diluate stream on the energy demand and required cell potential in an FCDI cell with 1, 2 and 3 cell pairs. Assumptions: Constant diluate flow rate of 1 mL/min, diluate concentration constant throughout cell (overestimated resistances/cell voltage), no consideration of laminar boundary layers, desalination up to the required concentration (varied electrical current).

The calculations predict a steep decrease in the energy demand with increasing number of cell pairs, the most significant decrease being expected when introducing the second cell pair. Limitation for the number of cell pairs is the voltage applied to the graphite current collectors. At high voltages, unwanted faradaic reactions (e.g. carbon oxidation) may occur. In this work, a maximum of 2 V was applied in longer lasting experiments, indicated by the green line. At this voltage, no visible deterioration of the graphite plates was observed. Apart from the voltage drop, the use of multiple cell pairs will also reduce the specific pumping energy required. In this case, the absolute pumping energy will stay the same, while the amount of product stream is multiplied by the number of cell pairs.

The third concept is based on concept two, the use of multiple cell pairs. When using multiple cell pairs, the inner membranes may be replaced by thinner, less mechanically stable, membranes, as illustrated in Figure 7.2 (c). These membranes have a lower ohmic resistance, due to which the influence of the membrane resistance on the energy demand may be reduced.

The fourth concept, illustrated in Figure 7.2 (d), aims at reducing the water crossover. As shown in Chapter 6, the water crossover is mainly caused by electroosmosis. A reduction of the amount of water transferred through the ion-exchange membranes together with the salt ions would significantly reduce the overall water transfer. The use of membranes with a strongly cross-linked surface may hinder the transfer of the hydration shells by retaining part of the hydration shells in the diluate channel.

In the following sections, the above described concepts for reducing the energy demand of continuous FCDI processes for brine desalination and concentration are implemented, tested, and their performance is evaluated.

## 7.2. Materials and methods

All FCDI experiments presented in the following sections were performed using a continuous single module configuration, as described in Chapter 6. The standard module layout is based on the design described in Chapter 5, comprising anion-exchange membranes adjacent to the flow electrodes and a central cation-exchange membrane. In this case, however, the module was assembled in cross-flow mode, as illustrated in Figure 7.5. This module design enables the addition of several cell pairs. The standard "single module" layout with three membranes and two spacer channels, one for the diluate and one for the concentrate stream, is in the following referred to as module with one cell pair (1 CP). This layout uses the before mentioned electrodialysis net spacers (size ED-100, Fumatech BWT GmbH). The general experimental procedure is the same as described in the previous Chapter 6. The water crossover was monitored in all experiments. Table 7.1 gives an overview of the experimental settings.

All experiments described in this section were performed with activated carbon slurries used as flow electrodes, which were prepared from 15 wt. % Carbopal SC11PG (Donau Carbon GmbH) in a NaCl solution with a concentration equaling the feed concentration, either 60 g/L or 120 g/L (Sodium chloride $\geq$99.8 %, VWR Chemicals). The slurries were stirred overnight before use. For each flow-electrode circuit the slurry was recirculated through the system at a flow rate of 150 mL/min. The slurry storage beakers were continuously stirred using magnetic stirrers. The same feed flow rates as in the experiments described

**Table 7.1.:** Overview of parameter settings for desalination experiments.

| | **Cell** | **Slurry** | | **Feed water** | |
|---|---|---|---|---|---|
| | Voltage | NaCl | Flow rate | NaCl | Flow rate |
| **Description** | V | g/L | mL/min | g/L | mL/min |
| *Ion exchange resins (IER) as spacer material for promoting ion transport* | | | | | |
| **Net spacer** | 0.6 & 1.2 | 60 & 120 | 150 | 60 & 120 | D:1/C:0.04 |
| **IER** | 0.6 & 1.2 | 60 & 120 | 150 | 60 & 120 | D:1/C:0.04 |
| *Stacking: Multiple cell pairs (CP) for reducing the voltage per cell pair* | | | | | |
| **1 CP** | 1.2 | 60 | 150 | 60 | D:1/C:0.04 |
| **1 CP** | 1.2 & 1.4 | 120 | 150 | 120 | D:1/C:0.04 |
| **2 CP** | 1.2 | 60 | 150 | 60 | D:1/C:0.04 |
| **2 CP** | 1.2&1.4&1.8 | 120 | 150 | 120 | D:1/C:0.04 |
| **3 CP** | 1.2 | 60 | 150 | 60 | D:1/C:0.04 |
| **3 CP** | 1.4 & 1.8 | 120 | 150 | 120 | D:1/C:0.04 |
| *Thinner membranes for reducing internal resistances* | | | | | |
| **3 CP - ref** | 1.4 & 1.8 | 120 | 150 | 120 | D:1/C:0.04 |
| **3 CP - thin** | 1.4 & 1.8 | 120 | 150 | 120 | D:1/C:0.04 |
| *Crosslinked membrane coating to reduce water transfer* | | | | | |
| **Reference** | 1.2 | 60 & 120 | 150 | 60 & 120 | D:1/C:0.04 |
| **Mod. CEM** | 1.2 | 60 & 120 | 150 | 60 & 120 | D:1/C:0.04 |

in Chapter 6 were used for the diluate feed (1 mL/min) and the concentrate feed (0.04 mL/min). During steady-state operation, several samples of the diluate and concentrate stream were taken and the density measured to confirm the NaCl concentration.

**Ion exchange resins (IER) for promoting ion transport.** The possibility to promote ion transport in the diluate channel was tested by replacing the inner part of the spacer mesh in the diluate channel of a module in single module configuration (crossflow) with mixed-bed ion exchange resins. Equal amounts of anion-exchange resin (Lewatit MonoPlus M 500, Cl- form, Sigma-Aldrich) and cation-exchange resin (Lewatit MonoPlus SSP 112, Na+ form, Sigma-Aldrich) were mixed. Figure 7.4 illustrates the location of the ion exchange resins in the cell.

**Stacking: Multiple cell pairs.** The FCDI experiments with several cell pairs were performed in cross-flow mode. For each added cell pair, two net spacers (ED-100, Fumatech BWT GmbH), one anion-exchange membrane (AEM) (Fumasep FAB-PK-130, ED-100, Fumatech BWT GmbH) and one cation-exchange membrane (CEM) (Fumasep FKB-PK-130, ED-100, Fumatech BWT GmbH) were

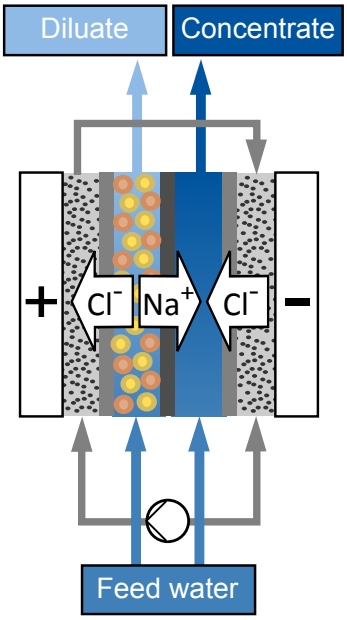


**Figure 7.4.:** Illustration of the location of the ion-exchange resins in the FCDI cell in a single-module FCDI system. The ion-exchange resins replace the spacer mesh of the diluate channel.

added between the central CEM and the AEM adjacent to the flow electrode on the concentrate side, as illustrated in Figure 7.6. Experiments were performed with one, two and three cell pairs, as indicated in Table 7.1. In case of the experiments with several cell pairs, the feed flow rates were multiplied by the number of cell pairs, to achieve comparable hydrodynamic conditions within the cell. Hence, overall flow rates of 1, 2 and 3 mL/min were applied for the diluate feed and 0.04, 0.08 and 0.12 mL/min were applied for the concentrate feed.

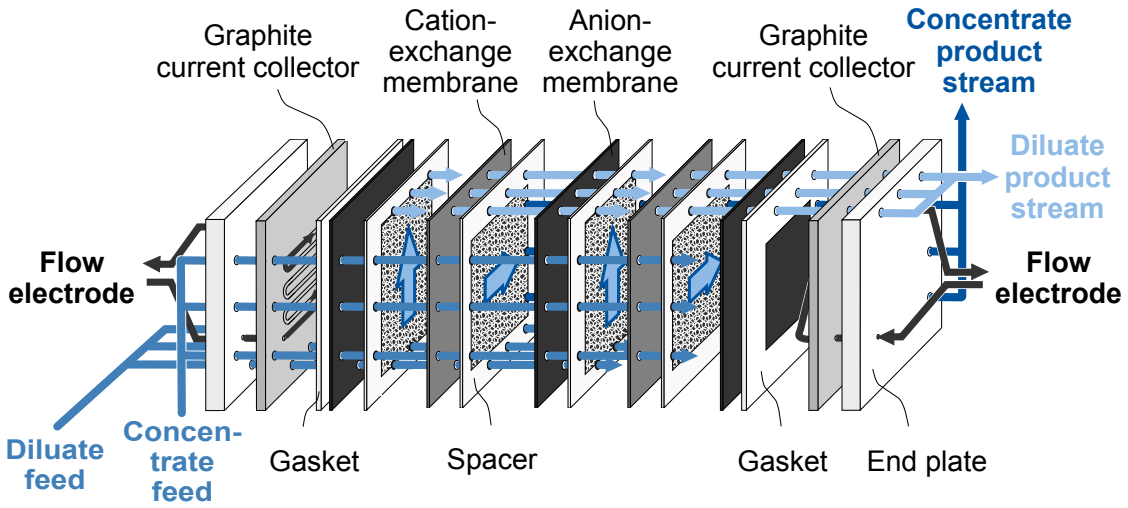


**Figure 7.5.:** Illustration of the cross-flow module layout applied for multiple cell pair experiments. In this example a module with two cell pairs is illustrated.

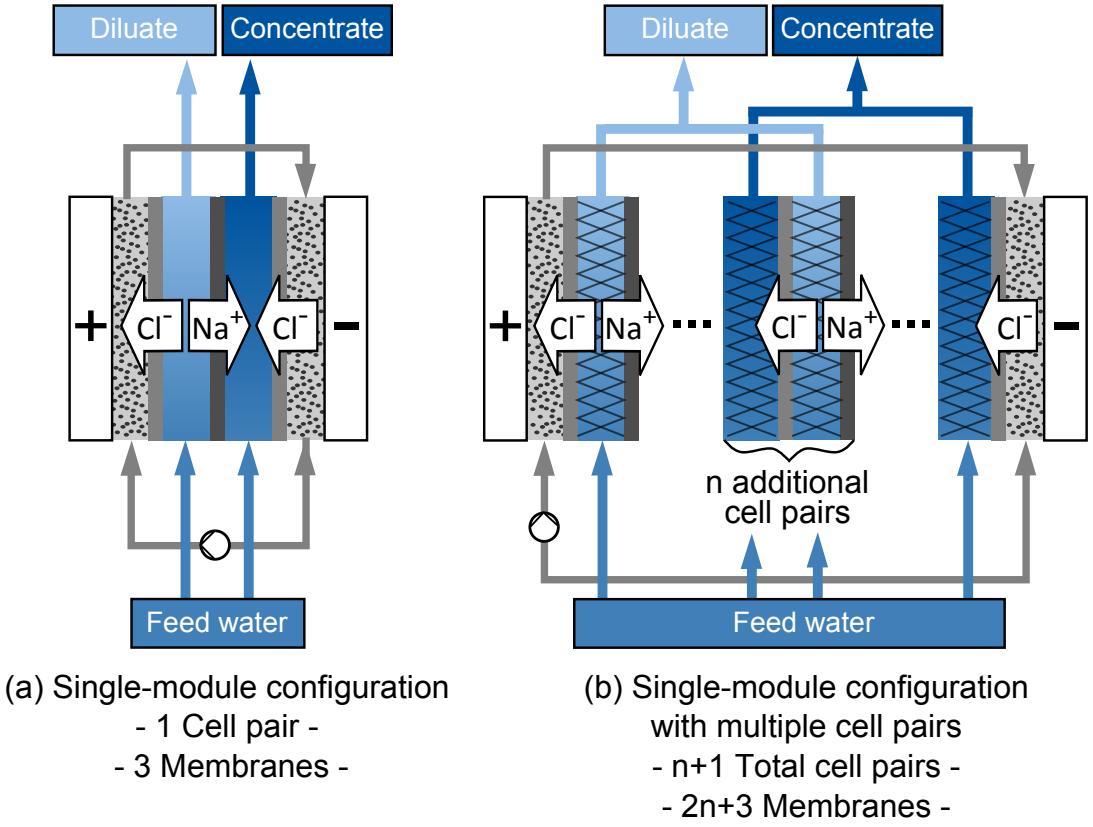


**Figure 7.6.:** Layout of continuous single module FCDI systems with (a) one cell pair (standard layout), (b) multiple cell pairs (1 cell pair + n additional cell pairs).

The experiments were conducted at constant voltage. While the addition of additional cell pairs leads to an increased overall cell resistance, only a moderate desalination was chosen. The concentrations in the diluate product stream did not fall below 29.5 g/L. Hence, the cell resistance for additional cell pairs was similar in all experiments with the same NaCl feed concentration, although the diluate concentration varied. In this range (e.g. 29.5 g/L in case of one cell pair and 33.5 g/L in case of three cell pairs), the differences in electrical resistance arising from concentration differences in the diluate stream have a negligible influence of around 0.002 Ω, which ensures the comparability of the experiments.

**Thinner membranes.** To investigate whether a reduction of the membrane thickness and resistance can improve the system performance, experiments were performed with unreinforced membranes (Fumasep FKB-ED-100, 30 $\mu$m, and Fumasep FAB-ED-100, 30 $\mu$m). A crossflow FCDI cell with three cell pairs was used, in which the unreinforced membranes replaced the inner five membranes. The anion-exchange membranes adjacent to the flow electrodes were kept the same as in the previously described experiments due to the better mechanical stability of the reinforced membranes.

**Crosslinked membrane coating.** For testing the concept of using membranes with a strongly cross-linked surface for reducing the electroosmotic water crossover, experiments were performed with coated membranes. The experimental parameters of the FCDI experiments are given in Table 7.1 ("Mod. CEM"). The same membranes as in the previously described experiments (Fumasep FKB-PK-130/ED-100 and Fumasep FAB-PK-130/ED-100) were built into a crossflow cell in single module configuration. Before the cell assembly, the central cation-exchange membrane was coated with an additional cross-linked layer according to the procedure described in the following.

Before the coating procedure, the membrane is rinsed and soaked in DI-water for at least 24 h. Following this, the membrane is fixed in the frame of a coating cell designed in-house, which uses o-rings to seal the cell on the sides to enable a one-sided coating of the membrane surface. Then, 10 mL of an aqueous piperazine (>99 %, Sigma Aldrich) solution containing 1.5 wt.% piperazine are applied on the membrane surface. After an exposure time of 1 h, the piperazine solution is removed and the membrane surface rinsed with 12 mL water to remove excess piperazine. The membrane is dried in the fume hood for 30 min. As a next step, a 10 wt.% solution of trimesoyl chloride (TMC, >98 %, Sigma Aldrich) in hexane (>99 %, Carl Roth GmbH & Co.KG) is applied to the membrane. After an exposure time of 15 min, the solution is removed and the membrane rinsed with 12 mL pure hexane. After leaving the membrane in the fume hood for another 15 min, the remains of the hexane have evaporated and the membrane is removed from the coating cell. The coated membrane is then heated to a temperature of 40 °C in a convection oven and left overnight.

**Current-voltage characteristics** The current-voltage characteristics (IV-curves) of the different systems were investigated by a step-wise change of the applied voltage in a range between 0 V and 2.5 V in steps of 0.1 V. After each change in voltage, the voltage was kept constant for 10 minutes, which corresponds to about two times the residence time. The steady-state electrical current was measured for each step.

During the measurements, the diluate feed flow rate was kept constant at 1 mL/min. To shorten the time until equilibrium is reached, the concentrate flow rate was also kept at 1 mL/min. To test the influence of the concentrate feed flow rate on the current-voltage characteristics of the system, one experiment was performed at a concentrate feed flow rate of 0.04 mL/min. The activated carbon content in the flow electrodes was 15 wt. %.

# 7.3. Assumptions and terminology

## 7.3.1. Impact of the system boundaries

When analyzing the energy demand of FCDI desalination and concentration experiments as described in the previous chapters, it becomes apparent that the way the system boundary is chosen is crucial, as illustrated in Figure 7.7 (a).

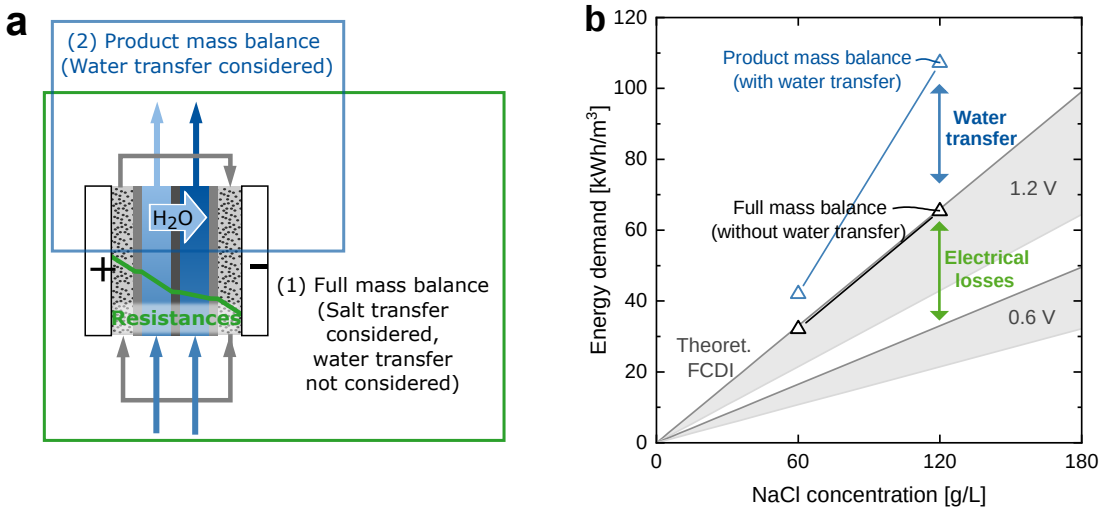


**Figure 7.7.:** Illustration of (a) the key factors increasing the energy demand in an FCDI process: water crossover and resistances, which increase the overall cell voltage, and (b) their impact on the electrical energy demand (per $m^3$ diluate). As illustrated in (a), it depends on the chosen mass balance, whether the water transfer, which leads to a salination of the diluate and a dilution of the concentrate, is considered or not.

The first option is to consider all feed and product water flow rates and the salt concentrations of the corresponding streams. Based on this, the salt transfer can be determined as indicated by the green line in the illustration. In this case, the actual overall salt transfer is considered. This system boundary is useful for the analysis of the salt transfer and the back diffusion of salt, as expressed in the current efficiency. This means, the energy demand for overcoming the electrical losses/resistances in the system is considered.

However, due to the additional transfer of water molecules with the ions, as well as the osmotic transfer, the dilution of the diluate stream and concentration of the concentration stream is not as high as expected when purely considering the salt transfer. Hence, the system performance is overestimated and the energy demand underestimated. The energy demand calculated in Wh/g salt is, of course, correct in this case. The amount of salt is transfered in the system. However, this value should not be used to calculate the energy demand in $kWh/m^3$ product

stream, as in this case the energy demand would be significantly underestimated, as illustrated in Figure 7.7 (b), due to the diluate concentration and concentrate dilution.
In case of the second option, marked by the system boundary in blue in Figure 7.7 (a), only the product water flow rates are considered in combination with the feed and product salt concentrations. It is assumed that the volumetric flow rate of the water streams stays constant when passing the cell. This way, the actually applied electrical power, calculated from the applied voltage and the measured current, can be set in relation to the product water streams. Thus, the negative effect of diluate concentration and concentrate dilution due to water crossover is considered in the energy demand, as illustrated in Figure 7.7 (b).

### 7.3.2. Energy demand per cubic meter diluate product stream

As described above, the choice of mass balance applied for a calculation results in the consideration or neglect of the influence of water transfer. In the following, the assumptions made for the current efficiency (CE) and the energy demand calculations are elucidated, which are the basis for several graphs presented further below in this chapter. In addition to the difference between product and full mass balance, disparities between the mass balances around the diluate and around the concentrate stream were observed.

**Neglect of water transfer $E_{dil,noWT}$.** When calculating the energy demand based on the full salt mass balance, the water transfer is neglected. The salt stream which is transferred from the diluate stream to the concentrate stream can be calculated in two ways: (1) via the salt mass balance around the diluate stream, which results in Equation 7.1 for the energy demand $E_{dil,D,noWT}$, and (2) via the salt mass balance around the concentrate stream, which results in Equation 7.2 for the energy demand $E_{dil,C,noWT}$. The average between the two energy demands $E_{dil,D,noWT}$ and $E_{dil,C,noWT}$ is in the following termed $E_{dil,noWT}$ (Equation 7.3).

$$E_{dil,D,noWT} = \frac{c_{Feed} \cdot I \cdot V}{n_{cp} \cdot (c_{Feed,D} \cdot \dot{V}_{Feed,D} - c_{Diluate} \cdot \dot{V}_{Diluate})} \tag{7.1}$$

$$E_{dil,C,noWT} = \frac{c_{Feed} \cdot I \cdot V}{n_{cp} \cdot (c_{Conc} \cdot \dot{V}_{Conc} - c_{Feed,C} \cdot \dot{V}_{Feed,C})} \tag{7.2}$$

$$E_{dil,noWT} = \frac{E_{dil,D,noWT} + E_{dil,C,noWT}}{2} \tag{7.3}$$

In these equations, $I$ stands for the electric current and $V$ for the cell voltage. $c_{Feed}$ and $\dot{V}_{Feed}$ are the NaCl concentration and volumetric flow rate of the feed

stream, in which the subscripts $D$ and $C$ stand for the diluate and concentrate stream, respectively. $n_{cp}$ stands for the number of cell pairs.

The consideration of the full salt mass balance allows the calculation of the actually transferred salt amount. However, the additional transfer of water due to hydration shells and osmotic effects leads to a reduction of the actual desalination and concentration performance. The concentrate is diluted and the diluate stream concentrated due to the transfer of water. This effect is not considered when calculating the energy demand via the full salt mass balance.

**Consideration of water transfer $E_{dil,withWT}$.** When calculating the energy demand based on the product salt mass balance, however, the water transfer is considered. By using only the volumetric flow rate of the product streams, the actual energy demand for the production of a specific volume of product (diluate or concentrate) of a certain desired concentration can be calculated, as given in Equation 7.4 for the energy demand $E_{dil,D,withWT}$, and in Equation 7.5 for the energy demand $E_{dil,C,withWT}$. The average between the two energy demands $E_{dil,D,withWT}$ and $E_{dil,C,withWT}$ is in the following termed $E_{dil,withWT}$ (Equation 7.6).

$$E_{dil,D,withWT} = \frac{c_{Feed} \cdot I \cdot V}{(c_{Feed,D} - c_{Diluate}) \cdot n_{cp} \cdot \dot{V}_{Diluate}} \tag{7.4}$$

$$E_{dil,C,withWT} = \frac{c_{Feed} \cdot I \cdot V}{(c_{Conc} - c_{Feed,C}) \cdot n_{cp} \cdot \dot{V}_{Conc}} \tag{7.5}$$

$$E_{dil,withWT} = \frac{E_{dil,D,withWT} + E_{dil,C,withWT}}{2} \tag{7.6}$$

By applying the above described equations, the additional electrical current required to reach exactly the concentration of 0 g/L NaCl in the diluate product stream is considered. Additional resistances within the desalination cell, especially due to the change of the diluate stream conductivity and the additional resistance of depleted laminar boundary layers at the membrane surface, are not considered by this. This means the values for "full desalination" given in this chapter are not realistic and mostly serve as a base for comparing the different module layouts.

A full desalination is likely not possible using a single cell and single pass FCDI system at feed concentrations of 60 g/L NaCl. A (nearly) full desalination may be achieved when using an optimized cell design, for example by using ion-conductive spacers, similar to continuous electrodeionization systems. A desalination to a low concentration of $<$ 1g/L is possible, however. For practical applications, the actual energy demand for a separation task should be determined by an experiment in which the desired concentrations are reached. Only this way it can be ensured that all the interlocking physical and chemical effects are considered.

To address this issue, a process model is being developed, as described in the following Chapter 8, which enables the consideration of many occuring effects. This may enable the realistic determination of energy demands and achievable process performances in the future.

**Mass balances diluate vs. concentrate.** Example results for the four different ways to calculate the energy demand are plotted in Figure 7.8 (a). The results for the average energy demand per cubic meter diluate without consideration of the water transfer, $E_{dil,noWT}$, and with consideration of the water transfer, $E_{dil,withWT}$, are plotted in Figure 7.8 (b).

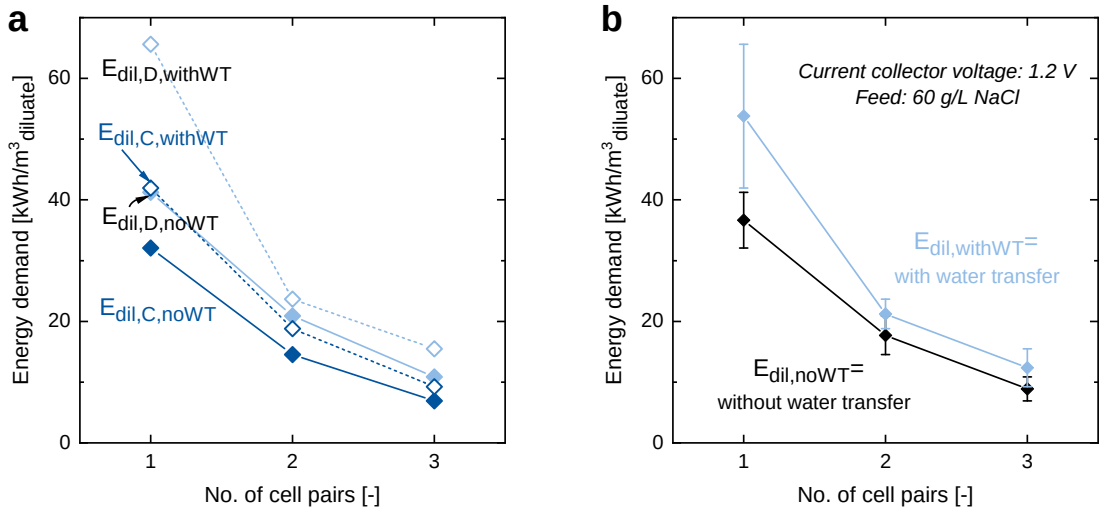


**Figure 7.8.:** Illustration of the averaging regarding the energy demand calculations in this chapter. The sample graphs show results of desalination experiments comparing modules with one, two and three cell pairs with a NaCl feed concentration of 60 g/L and a cell voltage of 1.2 V. The graphs show the energy demand calculated per diluate product stream, based on (a) the results for the individual mass balances of diluate and concentrate stream and (b) the average of the two mass balances. The values are recalculated to represent full desalination. Values do not account for pumping energy.

When considering the different curves in Figure 7.8 (a), it is striking that in all cases of this example the energy demand was higher when calculated for the diluate stream, compared to the calculation via the concentrate stream. However, a sighting of data collected over a longer period of time revealed experiments in which the opposite was the case. The reason for these deviations are most probably experimental and/or measurement errors. An example for a possible systematic error in the data, which leads to a higher tendency of the energy demand being higher when calculated via the diluate mass balance, may for example be the evaporation of water from the water samples during or after the

collection of water samples. This would lead to an increased concentration of the concentrate (and hence a performance improvement), as well as a concentration increase of the diluate (and hence a performance reduction and an increased energy demand).

In the following sections, only the average results between diluate and concentrate mass balance are plotted, similar to Figure 7.8 (b). This averaging based on two mass balances within the same experiment reduces the impact of experimental and measurement errors and allows a more reliable estimation of the energy demand required per cubic meter diluate product stream.

### 7.3.3. Energy demand per cubic meter concentrate product stream

The calculated energy demand values are more realistic when determining the energy demand based on the product mass balance, which leads to the consideration of the water transfer. Due to this, the energy demand per cubic meter concentrate product stream is only plotted including the water transfer in the following sections. To ensure a comparability between the experimental results, the energy demand was recalculated for a concentration up to 260 g/L NaCl concentration in the concentrate, according to the following equation:

$$E_{conc260} = \frac{(260\ g/L - c_{Feed,C}) \cdot I \cdot V}{(c_{Conc} - c_{Feed,C}) \cdot n_{cp} \cdot \dot{V}_{Conc}} \tag{7.7}$$

By using this equation, the additional/reduced current required to reach exactly the concentration of 260 g/L NaCl in the concentrate is considered. The change in resistances and back diffusion due to changes in the concentration gradients are not considered. To identify the actual energy demand for this specific task, an experiment in which these actual concentrations are reached would be required, due to the many interlocking physical and chemical effects.

### 7.3.4. Current efficiency

Similar to the energy demand, also the current efficiency (CE) can be calculated based on different mass balances. In case of FCDI processes, the current efficiency brings the transferred salt into relation with the required electric current:

$$CE = \frac{F \cdot \dot{n}_{Salttransfer}}{I} \tag{7.8}$$

In Equation 7.8, $F$ stands for the Faraday constant, $\dot{n}_{Salttransfer}$ for the molar amount of salt transferred from the diluate to the concentrate stream, and $I$

stands for the electric current. The salt flux $\dot{n}_{Salttransfer}$, and hence the current efficienty, can be calculated based on the full mass balance:

$$CE = \frac{F \cdot (c_{Feed,D} \cdot \dot{V}_{Feed,D} - c_{Diluate} \cdot \dot{V}_{Diluate})}{I \cdot M_{NaCl}} \tag{7.9}$$

Or based on the product mass balance:

$$CE_{eff} = \frac{F \cdot \dot{V}_{Diluate} \cdot (c_{Feed,D} - c_{Diluate})}{I \cdot M_{NaCl}} \tag{7.10}$$

In Equations 7.9 and 7.10, $M_{NaCl}$ represents the molar mass of the transferred salt, which is NaCl in this case. The first version of the current efficiency, based on the full mass balance, represents the physically correct current efficiency. The full salt mass balance gives information on how much salt was actually transferred. The CE based on the full mass balance hence represents the actual number of ion pairs transferred per electron and allows conclusions regarding the membrane selectivity. However, as discussed before, this does not represent the apparent current efficiency observed in a real application. In reality, the current efficiency will also be reduced by water transfer, which is why the term "effective current efficiency", $CE_{eff}$, is introduced here in case the CE is calculated based on the product mass balance.

## 7.4. Results and discussion

### 7.4.1. Current-voltage characteristics

For an initial comparison of the performance of the different energy demand reduction concepts, the current-voltage characteristics were investigated as described above. The results for NaCl concentrations of 60 and 120 g/L in feed and flow electrodes are plotted in Figure 7.9 in form of IV-curves.

Similar to IV-curves of electrodialysis processes, the FCDI IV-curves show an ohmic region at low voltages, in which the electric current increases linearly with increasing potential. At higher potentials, in case of the curves at hand usually around 1-2 V, the curves transcend to a limiting current region. The ohmic resistances and limiting currents differ significantly between the different systems. The ohmic resistance are listed in Table 7.2.

The standard FCDI system with three ion-exchange membranes (AEM, CEM, AEM) in cross-flow mode has an ohmic resistance of 0.927 Ω. At around 1.2 V the system starts to transcend to a limiting region, reaching a limiting current ranging around 1.4-1.5 A. The same system operated at a low concentrate flux, which would enable a high concentration factor in a desalination experiment, exhibits a very similar current-voltage behaviour. The two curves and ohmic resistances are

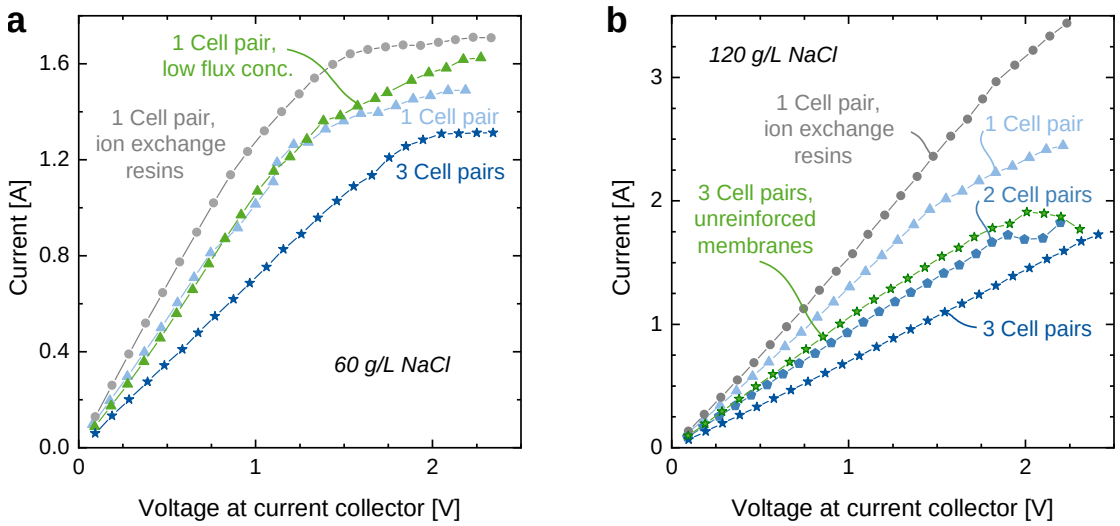


**Figure 7.9.:** IV-curves for the different FCDI conceptual systems at (a) 60 g/L NaCl, comparing the standard system to systems with ion exchange resins, with high and low concentrate flux, and a system with three cell pairs, and at (b) 120 g/L NaCl, comparing the standard system to systems with ion exchange resins, systems with two and three cell pairs, and a system with unreinforced membranes.

very similar, a small difference can be observed in the limiting region, in which the current of the low concentrate flux curve has a slightly higher slope, reaching currents of close to 1.6 A in the same voltage range. This insignificant difference may be caused by an increasing conductivity in the concentrate channel, due to the reduced flow rate.

In case of the standard FCDI system with one cell pair at 120 g/L the overall behaviour is similar to the system at 60 g/L, while the increased conductivity of the 120 g/L feed solution and flow-electrode electrolyte concentration leads to a significantly lower ohmic resistance (0.789 Ω). Additionally, the limiting current and the voltage at which the limiting region sets in are increased significantly. Concluding from this, one would expect improved ion transport rates at 120 g/L compared to 60 g/L.

Striking is the unusually flat ”limiting current region” in case of many IV-curves plotted here. The reason for this is likely that, unlike in IV-curves of electrodialysis processes, the effect causing the ”limiting current” region is a different one in case of these FCDI IV-curves. The electric current required for the full desalination of a 60 g/L NaCl solution at a feed flow rate of 1 mL/min, assuming a CE of 1, is 1.65 A. The maximum current achieved in an FCDI IV-curve with a 60 g/L feed is exactly in this range. This indicates that the limiting current observed here is simply the maximum current reachable, based on the salt ions available in the feed stream. Having this in mind, the IV-curves can be discussed

**Table 7.2.:** Overview of ohmic resistances derived from IV-curves.

| | *Experimental parameters* | | *Analysis results* |
|---|---|---|---|
| | **Slurry** | **Feed water** | **Ohmic resistances** |
| **Description** | wt. % AC | mL/min | Ω |
| *IV-curves with 60 g/L NaCl in Feed and Slurry* | | | |
| **1 CP, Standard** | 15 | D:1/C:1 | 0.927 |
| **1 CP, low flux concentr.** | 15 | D:1/C:0.04 | 0.994 |
| **1 CP, ion exchange resins** | 15 | D:1/C:1 | 0.739 |
| **3 CP** | 15 | D:1/C:1 | 1.411 |
| *IV-curves with 120 g/L NaCl in Feed and Slurry* | | | |
| **1 CP, Standard** | 15 | D:1/C:1 | 0.789 |
| **1 CP, ion exchange resins** | 15 | D:1/C:1 | 0.671 |
| **2 CP** | 15 | D:1/C:1 | 1.056 |
| **3 CP** | 15 | D:1/C:1 | 1.447 |
| **3 CP, unreinf. membr.** | 15 | D:1/C:1 | 0.960 |

under a different light.

The IV-curves of the various FCDI systems in which the above described concepts for energy reduction were tested are discussed in the following corresponding sections, together with an analysis of the desalination performance and energy demand.

### 7.4.2. Ion conductive spacers

The replacement of the net spacer in the diluate channel by ion exchange resins leads to a reduction of the ohmic resistance of about 20 % to 0.739 Ω, as can be seen from the results displayed in Figure 7.9 and Table 7.2. This can be explained by the improved ionic conductivity of the ion exchange resins. The voltage at which the limiting region starts is similar to the system without ion exchange resins at 60 g/L. The limiting current, however, is increased to close to 1.7 A. This indicates that a close to full desalination is achieved in this region. This is most likely possible due the improved conductivity of the resins and possibly the occurence of water splitting occuring in the mixed bed, similar to continuous electrodeionization processes. At 120 g/L, the incorporation of ion exchange resins leads to a significant reduction of the ohmic resistance. In this case, there is no clearly visible limiting region at voltages below 2.5 V. At around 1.9 V, the resistance seems to increase slightly, but not significantly.

Concluding from these initial results, the incorporation of ion exchange resins seems a promising concept for reducing the ohmic resistance and increasing the limiting current of FCDI systems.

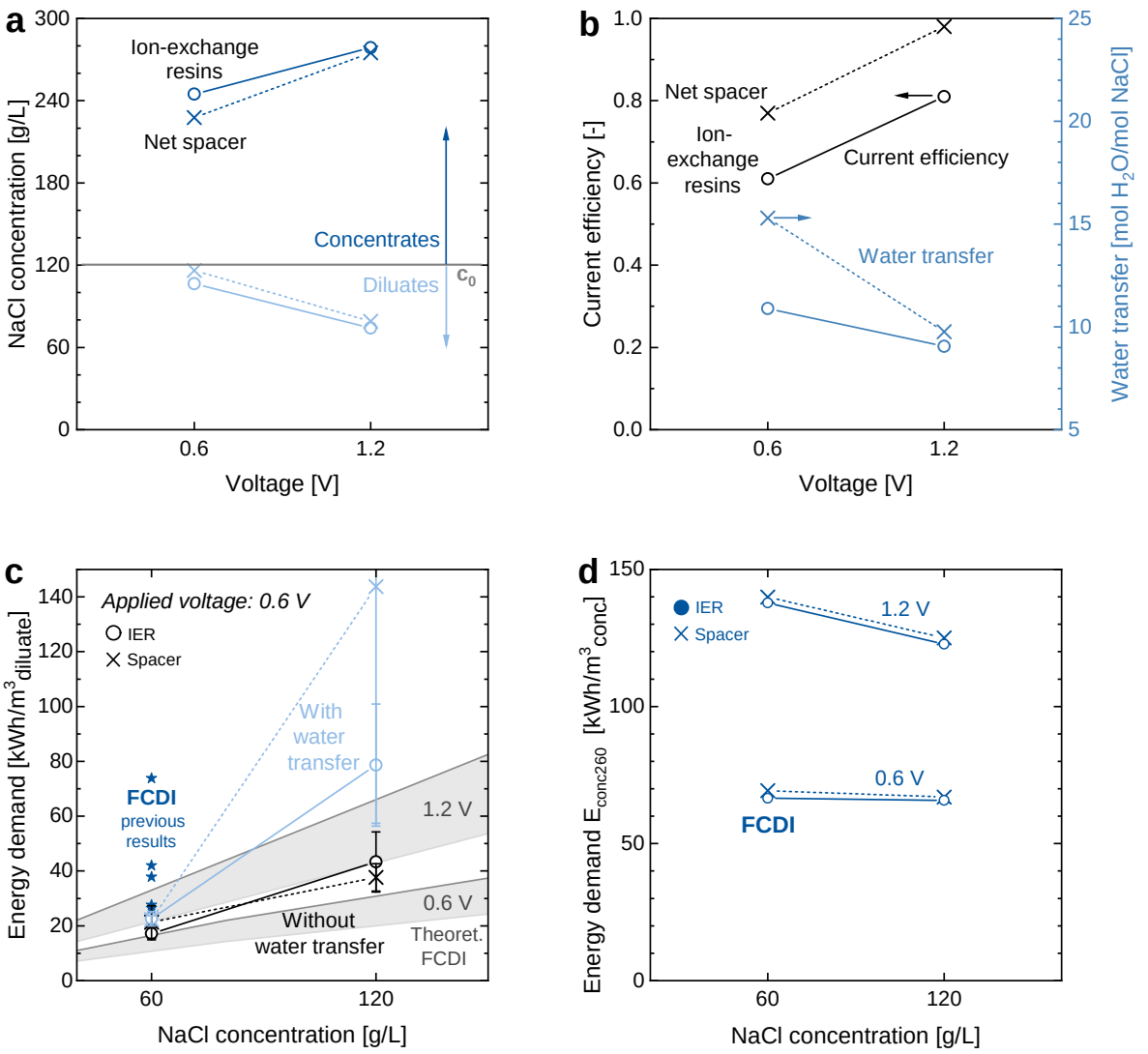


**Figure 7.10.:** Results of desalination experiments comparing modules with net spacers to modules with ion exchange resins. (a) NaCl concentrations of diluate and concentrate streams over the applied voltage at a feed concentration of 120 g/L, (b) current efficiencies (full mass balance) and water transfer rates over the applied voltage at a feed concentration of 120 g/L, (c) energy demand per $m^3$ diluate over the NaCl feed concentration at an applied voltage of 0.6 V (values recalculated to represent full desalination), dark blue stars: values for FCDI with energy recovery, as published in [Rom2018a], dark grey lines: theoretical values, grey areas: values reachable by energy recovery of up to 35 %. Values do not account for pumping energy. Error bars represent $1\sigma$ interval, calculated from average between diluate and concentrate mass balance. (d) Energy demand $E_{conc260}$ for concentration up to 260 g/L.

Figure 7.10 shows results of desalination experiments performed with the experimental conditions given in Table 7.1. Figure 7.10 (a) shows a plot of the NaCl concentrations of the diluate and concentrate product streams depending on the

voltage applied to the graphite plates for a feed concentration of 120 g/L. The experiments with ion exchange resins instead of spacers show a small improvement in the desalination and concentration performance, especially at the lower voltage of 0.6 V. However, the difference is not significant. When analyzing the results plotted in Figure 7.10 (b), the reasons for the insignificant improvement become clear: while the water transfer is reduced, especially at the lower voltage of 0.6 V, the current efficiency is decreased. The strongly cross-linked ion exchange resins may reduce the water crossover due to a partial retention of the hydration shells when ions enter the resin matrix. The reduction of the current efficiency, on the other hand, is unexpected at such high feed concentrations. While measurement inaccuracies should not be excluded as an explanation, a reason could be an improved transfer of membrane coions through the diluate, as mixed cation and anion exchange resin particles are used.

Figure 7.10 (c) shows the energy demand per diluate product stream when applying a voltage of 0.6 V for the desalination of 60 and 120 g/L NaCl solutions. The resulting energy demand based on both diluate and concentrate stream mass balances does not diff significantly when comparing the modules with net spacer and ion exchange resins. A significantly elevated energy demand is visible at 120 g/L feed concentration for the net spacer. This may be caused by a significant performance decrease at this low voltage. However, the large error bars could also be an indication for a measuring error in this case.

Figure 7.10 (d) shows the energy demand per concentrate product stream when applying a voltage of 0.6 V and 1.2 V for the treatment of 60 and 120 g/L NaCl solutions using modules with either mesh spacer or ion exchange resins in the diluate channel. While the ion exchange resins only make a marginal difference in the energy demand, recalculated for concentration up to 260 g/L, the voltage has a significant influence on the energy demand, as expected. This reduction of the energy demand by reducing the voltage, however, also leads to a significant reduction of 40-60 % in the current density. While a reduction of the cell voltage leads to significantly reduced operating costs, the required membrane area would be increased, which leads to a significant increase of the capital costs. An optimum between operation expenditure and capital expenditure needs to be found depending on the application case, as discussed in Chapter 5.

All in all, the use of ion exchange resin does not seem to be advantageous at these high salt concentrations and the low voltage range applied in these experiments so far. However, it may be advantageous to apply ion exchange resins in the diluate channel when the aim is to produce diluate streams with very low salinities. In the IV-curves currents very close to the theoretical maximum current were reached, which indicates a close to full desalination. At very low concentrations in the diluate product stream, the resistance of the diluate channels

will increase the required voltage significantly. This would lead to an elevated energy demand and reduced current densities, which may be avoided by using ion exchange resins or other ion-conductive spacers. This should be investigated in further works.

### 7.4.3. Multiple cell pairs

The introduction of additional cell pairs into an FCDI cell leads, as is to be expected, to an increased ohmic resistance. This is visible in the results displayed in Figure 7.9 and Table 7.2. In case of the 60 g/L NaCl concentration, the resistance increases from 0.927 Ω (1 cell pair) to 1.411 Ω (3 cell pairs). This would be equal to around 0.242 Ω per cell pair. The limiting current decreases slightly with increasing numbers of cell pairs, while the voltage at which the limiting current is reached increases significantly, due to the increased cell resistance. Presuming the reason for the observed "limiting current" is really the maximum desalination in this case, as described above, the cause for the reduced limiting current density in this case may be a maldistribution of the flow between the different cell pairs. In case of small differences in the volumetric flow rate between the different cell pairs the cell pair with the lowest flow rate would reach full desalination at the lowest current density and hence limit the further desalination of the other cell pairs. This hypothesis should be investigated further in future works.

The trends at a NaCl concentration of 120 g/L are similar to the trends observed at NaCl concentrations of 60 g/L in the feed solution. In this case, however, the ohmic resistance increases more significantly with the addition of the third cell pair. The reason for this is not clear, a possible explanation may be measurement inaccuracies or an unproportional increase of the resistance when bordered with salt solutions of significantly different concentrations [Gei2013]. A further analysis of FCDI systems with multiple cell pairs, including their desalination performance and energy demand, is attempted in the following.

Figure 7.11 shows results of desalination experiments performed with the experimental conditions given in Table 7.1. Figure 7.11 (a) shows a plot of the NaCl concentrations of the diluate and concentrate product streams at a feed concentration of 60 g/L and a constant potential of 1.2 V applied to the graphite plates. The grey line indicates the feed concentration $c_0$. Figure 7.11 (b) shows the results of desalination/concentration experiments at a feed concentration of 120 g/L. In this case, the constant potential applied to the graphite plates was varied between 1.2 V and 1.8 V.

In both cases, the NaCl concentration was reduced by about 30 g/L at the same feed flow rate, leading to a diluate product stream concentration of around 30 g/L NaCl in case of the 60 g/L feed stream and about 90 g/L NaCl in the

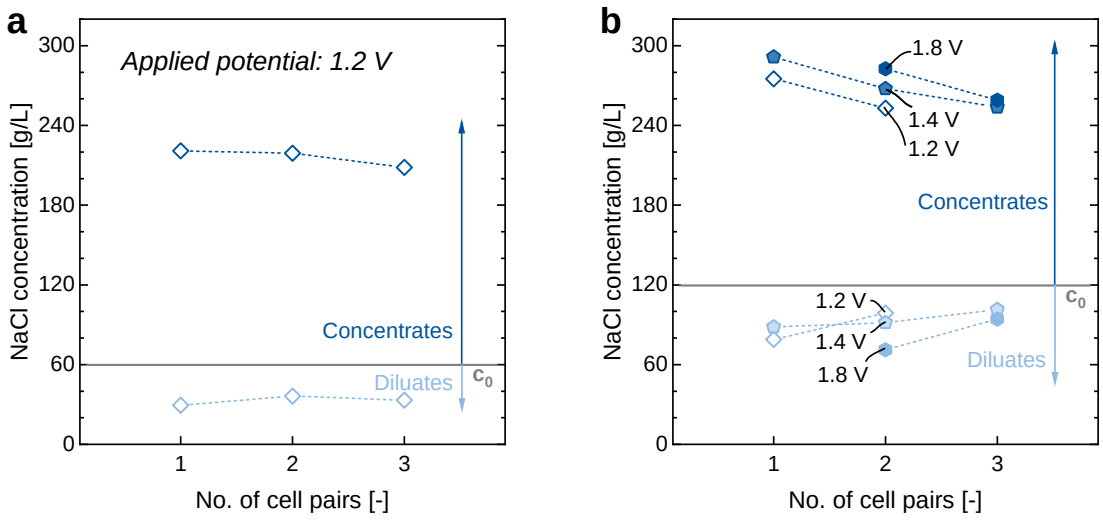


**Figure 7.11.:** Results of desalination experiments comparing modules with one, two and three cell pairs. The graphs show the NaCl concentrations of feed, diluate and concentrate streams depending on the number of cell pairs at NaCl feed concentrations of (a) 60 g/L and (b) 120 g/L. The potential applied to the current collectors was 1.2 V in case of the 60 g/L experiments and was varied between 1.2 V and 1.8 V in case of the 120 g/L experiments.

diluate product stream in case of the 120 g/L feed stream in case of the 1.2 V cell voltage. The NaCl transfer rates in g NaCl/min calculated for these experiments are in a similar range for both feed concentrations. The reason for this is most likely that in this concentration range the additional increase in conductivity has only a small effect, corresponding well with results presented by Yang et al. [Yan2016a]. The small effect it has is likely countered by a decreasing membrane selectivity at increasing salt concentrations, which results in a decreasing current efficiency and higher back-diffusion rates.

In case of both feed concentrations, the desalination and concentration performance decreases when adding additional cell pairs due to the increased resistance with increasing number of cell pairs. This trend can be avoided to a certain extent by increasing the applied voltage, as shown in Figure 7.10 (b). However, as faradaic reactions such as carbon oxidation are to be avoided in FCDI, the applicable voltage is limited. Due to this, the maximum voltage applied in this work did not exceed 2 V in longer experiments and 2.5 V in shorter experiments such as the measurement of IV-curves.

The energy demand corresponding to the results shown in Figure 7.11 (a) is plotted in Figure 7.12. Figure 7.12 (a) shows the energy demand per cubic metre diluate product stream, determined according to the equations described in Section 7.3 (Assumptions and Terminology). The energy demand with and without

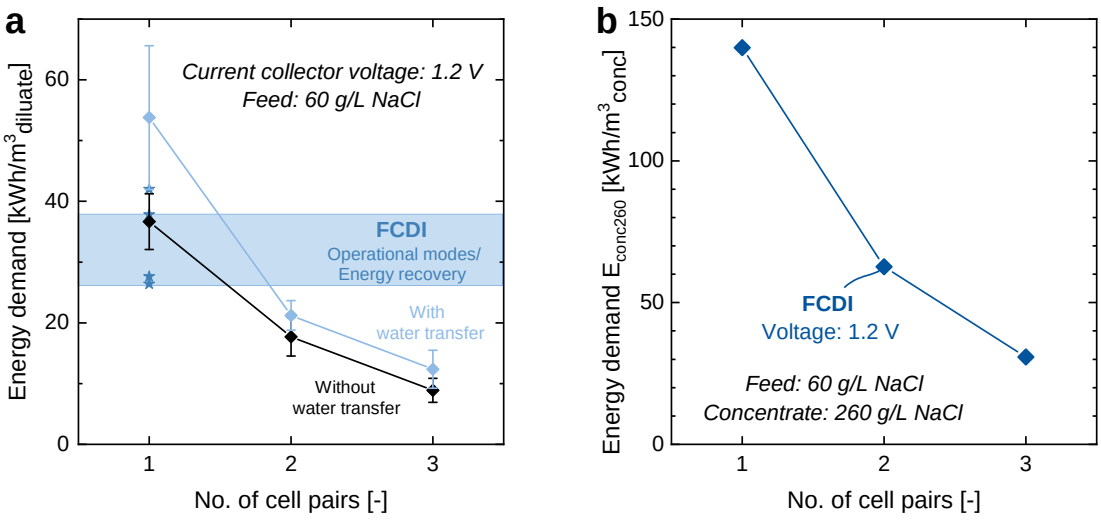


**Figure 7.12.:** Results of desalination experiments comparing modules with one, two and three cell pairs with a NaCl feed concentration of 60 g/L and a cell voltage of 1.2 V. The graphs show the energy demand calculated (a) per diluate product stream and (b) per concentrate stream. The values are recalculated to represent full desalination in case of (a) and concentration up to 260 g/L NaCl in case of (b). Values do not account for pumping energy.

consideration of the water transfer decreases significantly with increasing number of cell pairs. Comparing these results to the results presented in Chapter 5, indicated by the blue area in Figure 7.12 (a), the use of multiple cell pairs can reduce the energy demand of an FCDI process more efficiently than the partial energy recovery achievable using a second regeneration module. With energy recovery the energy demand for the desalination of a 60 g/L NaCl solution was reduced to around 25 kWh/m$^3$ diluate, while a value of only 15.5 kWh/m$^3$ diluate was reached using an FCDI module with three cell pairs.

The same trend is visible in Figure 7.12 (b), which shows the energy demand per cubic metre concentrate product stream. In this figure, all values consider the water transfer, which leads to a dilution of the concentrate. The use of three cell pairs leads to a reduction of the energy demand by more than 70 %, compared to using only a single cell pair.

Figure 7.13 shows the energy demand per cubic metre concentrate product stream, which corresponds to the desalination performances plotted in Figure 7.11 (b). The results for the concentration of a 120 g/L NaCl solution at varied cell voltages are compared to the results achieved for the concentration of a 60 g/L NaCl solution. All in all, the desalination and concentration of a 120 g/L NaCl solution at a cell voltage of 1.2 V worked well when using a single cell pair. However, when

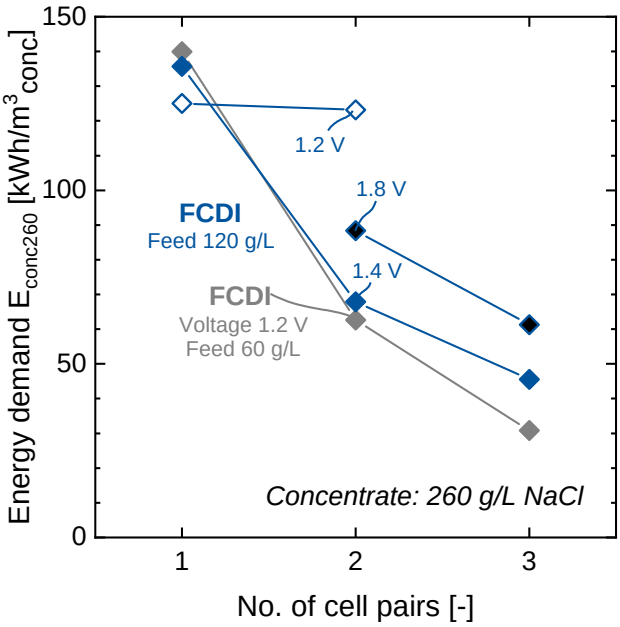


**Figure 7.13.:** Results of desalination experiments comparing modules with one, two and three cell pairs with a NaCl feed concentration of 120 g/L and a constant cell voltage, which was varied between 1.2 V and 1.8 V. The graphs show the energy demand calculated per cubic meter concentrate product stream. The values are recalculated to represent concentration up to 260 g/L NaCl. Values do not account for pumping energy.

increasing the number of cell pairs to two, the energy demand hardly decreased when applying a voltage of 1.2 V. When applying a voltage of 1.4 V or higher, the energy demand decreases significantly with increasing number of cell pairs, similar to the results observed for a feed concentration of 60 g/L NaCl. A reason for this is possibly a strong back diffusion and increased resistance, which requires the application of a higher voltage. Whether this is a measurement artefact or a real behaviour should be investigated further in the future. When the applied voltage is increased further to 1.8 V, the desalination performance improves further. However, the energy demand also increases further, while the overall energy demand is still lower compared to a single cell pair system. This will be an optimization task for an actual application. While increasing the voltage leads to higher current densities, and hence reduced capital cost, it also leads to a higher energy demand and increased operation costs.

Surprising is that at a constant voltage of 1.4 V, the energy demand for the concentration up to 260 g/L NaCl is nearly the same for a 60 g/L feed solution as for a 120 g/L feed solution. This is a distinct difference to thermally driven processes, in which the feed concentration has a major effect on the energy demand when aiming at the same concentrate concentration. Hence, an advantage of FCDI processes compared to thermally driven processes may be the ability to

bridge this wide concentration range with a moderate energy demand.

**Cell pair resistances and pumping energy** The use of multiple cell pairs in an FCDI module has several potential advantages, as indicated in Subsection 7.1.2. The theoretical calculations presented above in Figure 7.3 illustrate the advantages in more detail. Figure 7.14 illustrate the fractions of the energy demand caused by the different resistances and the pumping energy in case of one and three cell pairs. The theoretical calculations are based on the same assumptions as presented in Subsection 7.1.1. The energy demand calculated for pumping the flow electrodes is based on pressure drop measurements in flow electrodes continuously pumped by a peristaltic pump through a circuit with a dampening vessel to even out pressure fluctuations, and was determined using the same approach as described in Chapter 5. The theoretical estimations are compared to actual experimental results.

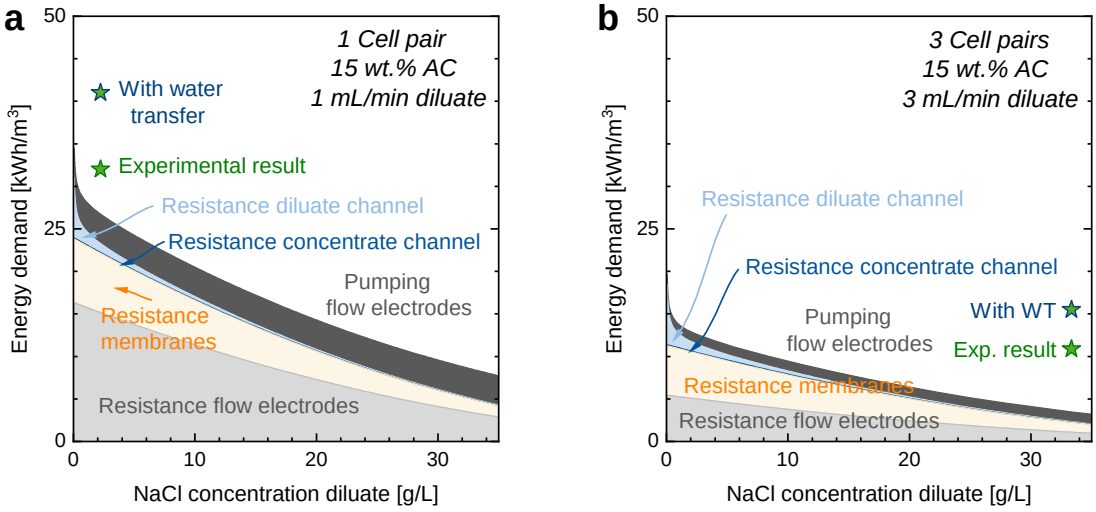


**Figure 7.14.:** Comparison of results of theoretical calculations and results obtained from laboratory experiments. Starshaped markers: Experimental results, energy demand calculated with and without considering the water transfer. Curves: Results of theoretical calculations regarding the influence of the NaCl concentration of the diluate stream on the energy demand and its causes in an FCDI cell with (a) 1 cell pair and (b) 3 cell pairs. Assumptions: Constant diluate flow rate of 1 mL/min, diluate concentration constant throughout cell (overestimated resistances/cell voltage), no consideration of laminar boundary layers, desalination up to the required concentration (varied electrical current).

As can be seen from the calculation results plotted Figure 7.14 (a), the resistance of the flow electrodes is a major driver of the energy demand in case of a single cell pair. Depending on the required diluate concentration, either the membrane resistance or the flow electrode pumping energy make up a larger part

of the total energy demand. By introducing multiple cell pairs, here represented by the example of three cell pairs, the fraction of the flow-electrode resistance and pumping energy, which are two major drivers of the energy demand, can be reduced significantly. This makes the membrane resistance a key factor for reducing the energy demand further. Hence, in the following sections the influence of the membranes is investigated in more detail.

When considering the results of laboratory experiments to the theoretical calculations, the energy demand in the experiments is significantly higher than the estimations. This indicates that not all phenomena are accounted for. Some of these, of course, lie in the nature of the estimation itself: non-ideal behaviour is not considered, such as a reduced current efficiency and back diffusion. These lead to increased currents in reality. Additionally, laminar boundary layers are not considered, which may increase the required voltage. A study by Geise et al. [Gei2013] also indicates a more than ten times increased membrane resistance at high concentration gradients across the membrane, which may be an explanation for increased cell resistances. The absolute concentration difference across the membrane is in this case at least 170 g/L NaCl. The question is, whether this increased resistance only occurs when one of the bordering concentrations is very low, as described in the study by Geise et al., or when there is generally a large concentration gradient. These phenomena may explain why the deviation between experimental and theoretical results is especially significant in case of the three cell pair system. The higher number of membranes in the system may increase the overall effect of the not-considered non-idealities in this calculation.

### 7.4.4. Influence of the membranes

The results of the theoretical calculations presented above indicate a significant influence of the membranes on the overall cell resistance. Hence, different membrane types were tested, which have potential to improve an FCDI system.

**Unreinforced membranes** Figure 7.9 shows results regarding the current-voltage characteristics of the system when the inner membranes are replaced by unreinforced membranes of reduced thickness in a three cell pair FCDI cell. In this case, the ohmic resistance decreases significantly, reaching a value lower than the system with two cell pairs, as can be seen from the results given in Table 7.2. Generally, the IV-curve for the system with unreinforced membranes is quite similar to the system with two cell pairs. At a first sight, this system is a very promising candidate for the reduction of the energy demand by avoiding losses high electrical resistances of the membranes. Figure 7.15 shows the results of FCDI experiments comparing a three cell pair FCDI stack to a three cell pair FCDI stack, in which the inner membranes were replaced by unreinforced mem-

branes. The experiments were performed at two different constant voltages and a feed concentration of 120 g/L using the settings given in Table 7.1.

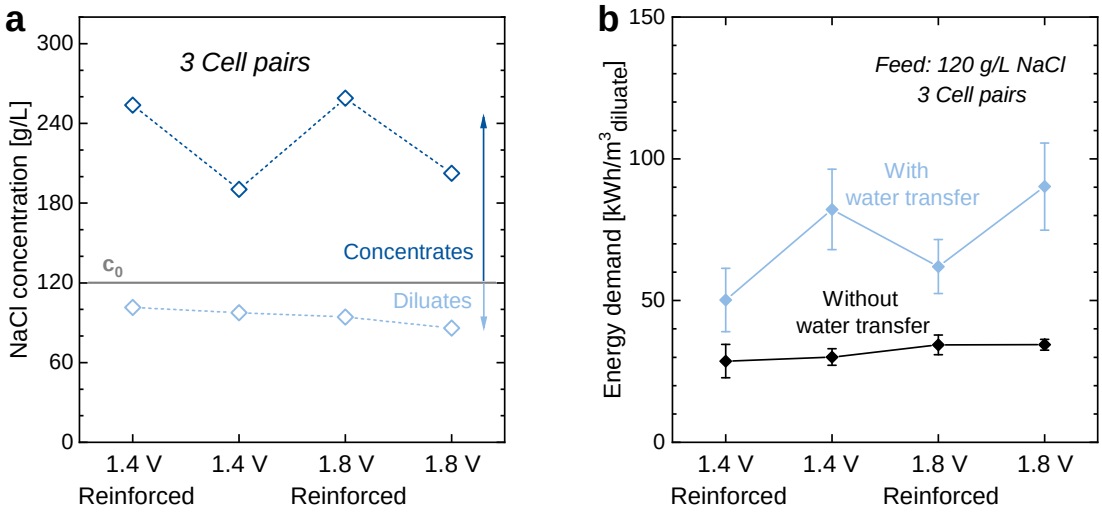


**Figure 7.15.:** Results of desalination experiments with three cell pair modules comparing reinforced with unreinforced membranes for the inner flow channels at voltages of 1.4 V and 1.8 V. The graphs show the (a) the desalination performance and (b) the energy demand for a NaCl feed concentration of 120 g/L. The values are recalculated to represent full desalination. Values do not account for the required pumping energy.

The results are very clear. While the desalination performance is nearly the same, the use of unreinforced membranes leads to a significant reduction in the concentration performance of the FCDI system, as can be seen from the results plotted in Figure 7.15 (a). Whenever unreinforced membranes were used, the NaCl concentration of the concentrate product stream dropped significantly. Considering the energy demand per cubic meter diluate, as plotted in Figure 7.15 (b), the reason for this becomes clear. When considering the energy demand for the full mass balance, disregarding the water transfer, the energy demand for the two different membranes is very similar. However, when considering the water transfer, the system based on the unreinforced membranes requires significantly more energy. When calculating the amount of transferred water per transferred salt, the same trend becomes visible. The water transfer increases significantly when using the here applied unreinforced membranes.

In conclusion, the unreinforced membranes tested in this case are not feasible for use in an FCDI system aiming at salt recovery and concentration. Although they exhibit a reduced resistance, the water transfer increases significantly, leading to a reduction in the concentration performance. Reasons for these are likely a combination of the following: (1) the reinforcing mesh may present an additional barrier for the water transfer, (2) the reinforced membranes are thicker,

which may represent an additional barrier for the water transfer, and (3) the ion-exchange material of the reinforced membranes is different to the ion-exchange material of the unreinforced membranes and likely more hydrophobic compared to the material of the unreinforced membranes. Especially at the low concentration side the membrane material may swell significantly, and hence the network of polymer chains may be expanded significantly, as described by Mackie and Meares [Mac1955a]. In this case, a thicker membrane may be of advantage. The increased thickness may allow a better adjustment to the local conditions at the two opposite sides of a membrane. Generally, the results are in good agreement with results recently presented by Porada et al. [Por2018].

**CEM with crosslinked surface coating** In an attempt to further reduce the water transfer rate of the reinforced membranes used as a standard in most parts of this work, an additional cross-linked coating was applied to the membranes, as described in the materials and methods section.

Figure 7.16 shows the results of experiments comparing the results when using a coated membrane to the results when using a standard membrane in a single-module FCDI layout with a single cell pair. Figure 7.16 (a) shows IV-curves measured at feed concentrations of 60 g/L NaCl and 120 g/L NaCl. While the coated membranes exhibit a nearly identical ohmic resistance, the main difference between the membranes seems to be the increased limiting current density. This result is surprising. Due to the addition of a coating layer an increased ohmic resistance would seem likely. A reason for this could be the increased concentrate concentration in case of the experiments with coated membranes, which go hand in hand with a reduced current efficiency. This may explain the apparently increased limiting current, while the actual salt transfer stays similar.

The results of desalination experiments plotted in Figures 7.16 (b), (c) and (d) show a reversed trend compared to the unreinforced membranes. The use of the surface coating leads to a significant reduction in the water transfer rate, and hence an improved concentration performance. This is also visible in the reduced energy demand per cubic meter diluate and concentrate stream when considering the water transfer.

The simultaneous shift of the concentrations in the diluate and concentrate streams to higher concentrations in case of the experiments with coated membranes is a contradiction at first glance. A possible explanation for this is the diluate flow rate: due to the more pronounced water transfer in case of the uncoated membranes, the diluate flow rate is reduced from 1 mL/min to 0.79 mL/min in case of an experiment with a 60 g/L feed solution. During the same experiment with a coated membrane, the diluate flow rate was only reduced to 0.9 mL/min, due to the reduced water transfer. The overall salt transfer rate is very com-

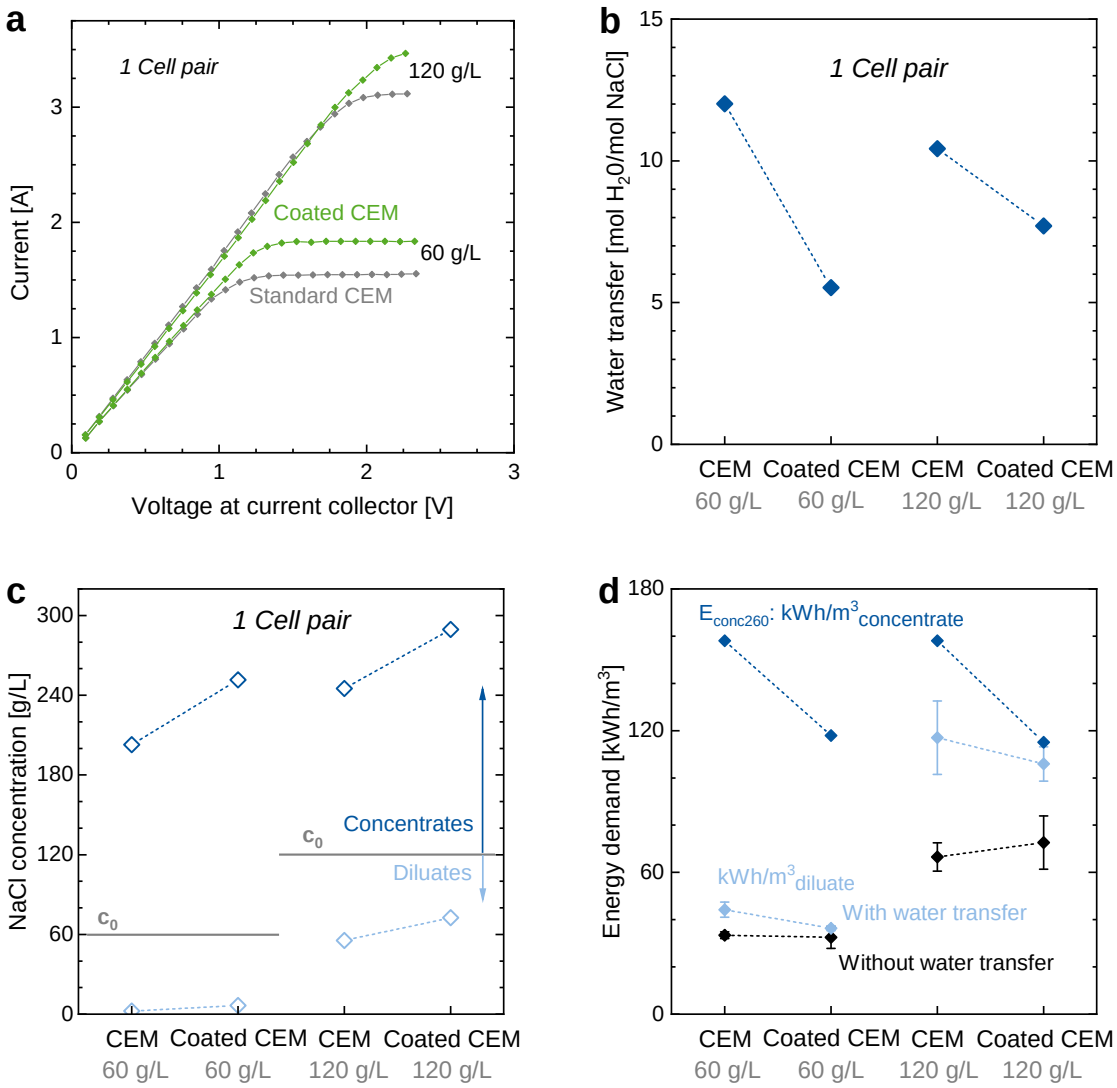


**Figure 7.16.:** Results of desalination experiments with one cell pair at 60 g/L and 120 g/L comparing modules assembled with the "standard" CEM to a module with a CEM with crosslinked surface coating. (a) IV-curves, (b) water transfer in mole water per mole salt, (c) NaCl concentrations of diluate and concentrate streams, and (d) Energy demand per $m^3$ product stream (for diluate with and without water transfer, and for concentration up to 260 g/L NaCl). Values do not account for pumping energy.

parable when using coated membranes, it is only slightly reduced. A similar salt removal rate together with an increased diluate flow rate hence leads to an increased diluate salt concentration measured at the outlet of the cell.

In conclusion, the application of this additional cross-linked coating is a promising approach to further improve the concentration performance of FCDI systems, while at the same time reducing the energy demand for concentration. Water transfer mainly leads to a dilution of the concentrate stream, making the membrane characteristics an essential factor for the successful application of FCDI for

salt recovery and concentration.

### 7.4.5. Effective current efficiency and diluate concentration

In some cases, extreme concentration gradients occur over a single ion-exchange membrane in the above described experiments. In literature, increased membrane resistances were observed for high concentration gradients [Gei2013]. Such concentration gradients are rarely reached in electrodialysis processes, due to the choice of higher flow rates and the treatment of lower salinities in most cases. A remaining question is how such high concentration gradients affect the membrane performance and selectivity. Does the current efficiency, for example, mainly depend on the concentration of the diluate stream ("low concentration") or the concentration of the concentrate stream ("high concentration")? The NaCl concentrations measured in diluate and concentrate product streams over the measured current efficiency, obtained from a number of experiments presented in Chapters 6 and 7, are plotted in Figure 7.17. The experiments were performed with high salinity feeds and various continuous FCDI process and cell configurations and different membrane types.

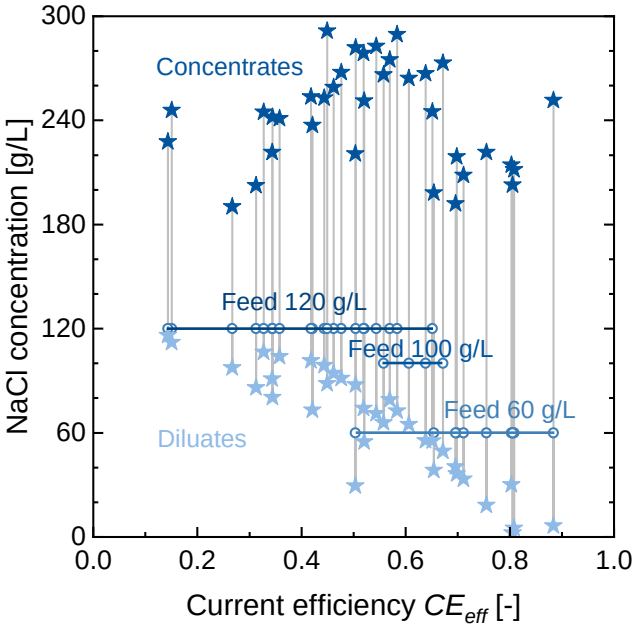


**Figure 7.17.:** Results for the NaCl concentration in diluate and concentrate product stream plotted over the effective current efficiency, $CE_{eff}$, which considers the water transfer within the system. The plot shows results from a high number of experiments performed with high salinity feeds and various continuous FCDI process and cell configurations and different membrane types, as presented in Chapters 6 and 7.

There is no clear trend visible for the NaCl concentration in the concentrate

streams and the current efficiency. This is surprising, as one may expect a relation due to reduced membrane selectivities at high salinities. However, a very clear trend is visible for the NaCl concentration in the diluate streams and the current efficiency. Low salinities in the diluate stream are clearly associated with high current efficiencies. There are two explanations for this, which may also occur in combination: (1) The low concentrations in the diluate product streams lead to a significant improvement of the membrane selectivity and hence the current efficiency. This would mean the lower concentration bordering an ion-exchange membrane determines the membrane selectivity. This would be a possible advantage for ion-exchange membrane processes aiming at high concentration gradients, in opposition to high throughputs aiming at the reduction of the impact of concentration polarization. (2) Low concentrations in the diluate are only reachable, when also a high membrane selectivity and hence a high current efficiency is achieved. A low membrane selectivity would lead to a stronger back diffusion of salt into the diluate stream and hence a higher salt concentration in the diluate product stream. This is to be investigated in the following chapter.

## 7.5. Summary and conclusions

In this chapter, different approaches for reducing the energy demand are presented and tested. While the incorporation of ion-exchange resins is only possibly promising in the desalination down to very low salinities, the use of multiple cell pairs is a very promising approach for reducing the impact of the voltage drop over the flow electrodes. The experimental results show a significant reduction in the energy demand. Open questions are, if the approach of multiple cell pairs also enables the high desalination rates down to very low salinities in a single step, which were demonstrated for the continuous two-module and single-module FCDI system before. A theoretical analysis demonstrated the possible potential of reducing the membrane resistance to further improve such multiple cell pair FCDI systems. This was investigated in the second half of this chapter.

The use of thinner, unreinforced membranes of reduced resistance, however, leads to a strongly increased water transfer. This negates the advantage of the reduced electrical resistance due to a significant deterioration of the concentration performance. The coating of the ”standard membranes” applied in this work on the other hand, leads to a significant improvement of the concentration performance due to a significant reduction of the water transfer. The presented coating is promising for the application in ion-exchange membrane processes aiming at the concentration of saline solutions, which especially suffer from pronounced water transfer.

It is clear that many factors influence the performance of an FCDI system. The interrelations of the different physical and chemical phenomena are complex. Hence, an improved process model is presented in the following Chapter 8, which may serve as a tool to systematically analyze and quantify the impact of the different phenomena and hence further improve the performance of FCDI processes.

# 8

# Modeling FCDI processes at high salinities

Preliminary work/parts of this chapter have been published:

Alexandra Rommerskirchen, Burkhard Ohs, Karl Arturo Hepp, Robert Femmer and Matthias Wessling. "Modeling continuous flow-electrode capacitive deionization processes with ion-exchange membranes" In: *Journal of Membrane Science* 546 (2018), pp. 188 - 196.

Alexandra Rommerskirchen, Michael Alders, Florian Wiesner, Christian J. Linnartz, Anna Kalde and Matthias Wessling. "Process model for high salinity flow-electrode capacitive deionization processes with ion-exchange membranes" In: *Journal of Membrane Science* 616 (2020) 118614.

## 8.1. Introduction

In 2018, our work group published a first simplified FCDI process model [Rom2018b]. Before this model, a number of experimental as well as modelling studies have been published regarding CDI and ion storage in porous electrodes [Bie2012; Zha2012; Has2017], which the principle of FCDI is based on. The main difference in FCDI compared to CDI is the use of capacitive electrodes in form of pumpable slurries, and the need for some kind of membrane, may it be porous [Hat2014] or dense and ion conductive [Jeo2013], to separate the slurries from the saline stream, which is to be desalinated.

The use of a process model can help to extend the understanding of the main influencing factors of FCDI, as well as reduce the need for time consuming experimental studies. Our first model, published in 2018 [Rom2018b], presented a great help in the recent years to develop further understanding of the physical dependencies and main influencing parameters of FCDI processes and lead to accelerated advancements. This simplified FCDI model combines equations for ion transport and charge storage in the electrical double layer and is only suitable for simulating the treatment of low salinity solutions. However, FCDI may be a good candidate for brine treatment and concentration, as discussed in the previous chapters. In this case, some assumptions made in the first process model are not valid.

In Chapter 6, an experimental study is presented, which provided a deeper understanding of influences on the water and salt transfer in FCDI processes

at high salinities. In the following, an extended FCDI process model version is presented, which includes a range of improvements. The newer version is now, unlike the older version, suitable for simulating FCDI processes at high salt concentrations.

## 8.2. Process model for high salt concentrations

In the following, the characteristics and differences between the two model versions are elucidated. Then, the framework equations and assumptions made in the newer model version presented in this chapter are described. Sensitivity analyses are performed to investigate the influence of various parameters on the simulation results. Finally, results of simulations are compared to experimental results to validate the new process model for high salinity feed solutions.

**Table 8.1.:** Characteristics and differences between the previously published [Rom2018b] process model and the process model presented here.

| | **Published model [Rom2018b]** | **Current model (this chapter)** |
|---|---|---|
| *General model characteristics* | | |
| **Type** | ◦ Steady state | ◦ Time dependent |
| **Structure** | ◦ Hierarchical (system, cell) | ◦ Hierarchical (system, cell) |
| | ◦ Cell model: one source code | ◦ Cell model: modular (liquid flow channels, membranes, flow electrodes) → Easily adjustable |
| **Simulatable systems** | ◦ Single pass FCDI systems, only desalination (e.g. [Jeo2013]) | ◦ Single pass FCDI systems, only desalination (e.g. [Jeo2013]) |
| | ◦ Continuous FCDI systems: Two modules [Gen2014] | ◦ Continuous FCDI systems: Two modules [Gen2014] Single module [Rom2015] |
| **Salinities** | ◦ Low salinities | ◦ Low and high salinities |
| *Considered physical phenomena and assumptions* | | |
| **Membrane** | ◦ Ideal selectivity | ◦ Coion transport considered |
| **Reactions** | ◦ No faradaic reactions | ◦ No faradaic reactions |
| | ◦ No pH changes | ◦ No pH changes |
| **Water transfer** | ◦ Not considered | ◦ Considered |
| **Model structure** | ◦ Direct connection | ◦ Recycled from storage vessel |

The published version of the process model, as well as the version of the process model presented in this chapter, can be used to simulate steady state FCDI processes such as single-pass configurations [Jeo2013] or a continuous two-module process [Gen2014]. Table 8.1 gives an overview of characteristics and differences

between the FCDI model version published in 2018 and the improved FCDI model version described in this chapter. The main difference between the two models is the possibility to simulate the treatment of high salt concentrations with the extended model, as well as the simulation of different process configurations, such as the continuous single-module configuration.

In the following, the model structure, framework equations and assumptions made in the newer model are presented.

## 8.2.1. Model structure and assumptions

Figure 8.1 shows the structure of the new FCDI process model at the example of an FCDI desalination module. In comparison to the model published previously [Rom2018b], this structure was designed with a hierarchical and more modularized approach, which allows modelling various FCDI process layouts, such as the continuous single-module configuration (Chapters 5 and 6). Even modelling multiple cell pairs is in principle possible, as presented in the experimental study in Chapter 7. Additionally, this structure allows the simple switching between different model versions. Different submodel versions considering ideal or non-ideal behaviour, such as the membranes, spacer channels or flow electrodes, can be easily exchanged in between simulations.

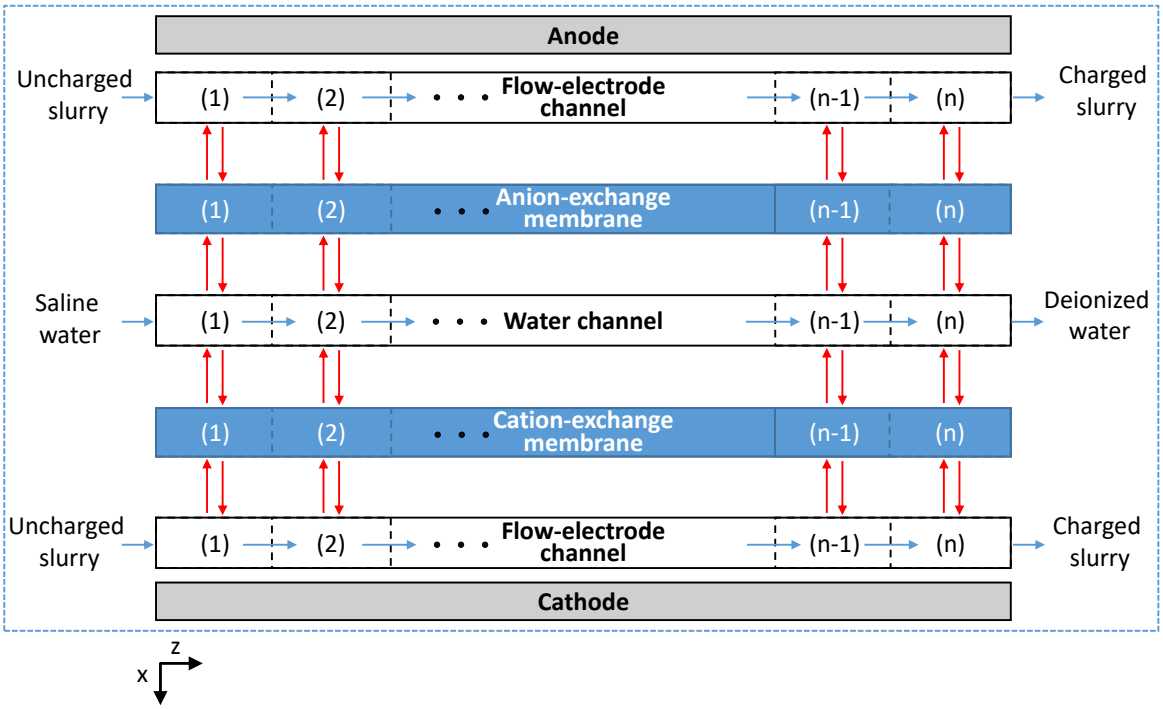


**Figure 8.1.:** Illustration of the model structure. Each submodel is discretized into n volumes. Blue arrows represent fluid flow through the flow-channels and red arrows represent ion flux through the ion exchange membranes.

Every FCDI cell is divided into several submodels in this model framework, such as the diluate and concentrate flow channels, the ion exchange membranes, and the flow-electrode channels, which are connected via data ports. Boundary layers of the fluids are currently not modelled in detail. However, in future work, new submodels for laminar boundary layers could easily be added between membrane and flow channel. The blue arrows in Figure 8.1 display the flow direction of the fluids, while red arrows represent ionic and electric currents being exchanged with other submodels. The latter are pointed in both directions, due to the consideration of coion and counterion transport in the model. Similar to the first model version, fluid flow (blue) is assumed to be much larger than diffusion in axial direction. Hence, convective flow is only considered in flow direction. Process quantities such as concentrations, conductivities and fluxes in flow channels are consequently considered to be constant perpendicular to the flow direction. Only for the ion concentrations in the ion-exchange membranes, linear concentration gradients are assumed.

Since fluid flow is only considered in positive axial direction, each array column can be calculated on its own and the necessary values are passed to the next element within the column, similar to a forward discretization method. Except for the solid outer electrodes, all submodels are again divided into instances of an array. The array structure functions as one dimensional discretization method over the cell length. This structure is a substitute for the internal discretization method of gProms, which was used in the previously published model. While the gProms discretization method is easier to use and implement, the new array structure has the major advantage of enabling the quick rearrangement of the cell composition.

Unlike the previous model, this process model is also discretized over the time. However, it is not yet aimed at investigating start-up processes. Several physical processes, such as time dependency and building up of boundary layers or membrane ion hold-up are not modeled, which would be necessary for a meaningful simulation of the start-up of FCDI processes. The model is aimed at investigating the steady-state behaviour of continuous FCDI processes, such as the two-module or single-module layout, or a single pass desalination module. However, in the future further time-dependent phenomena may be implemented to investigate start-up processes. A reason for the implemented time dependency is the improved convergence of the model, especially when considering coion transport.

Ionic transport is evoked by the electric driving potential (migration) and the concentration gradients (diffusion) in the membrane, unlike the previous model, in which the ion transport was calculated in the boundary layers between flow electrode and membrane. While regarding the membranes, ideal and non-ideal behaviour is implemented. In the following, only the version allowing coion

transport (non-ideal membrane behaviour) is described. The modeling of ideally permselective membranes is identical to the model version which was published previously [Rom2018b]. The transport of coions was modeled in a similar way as for example described in published electrodialysis models [Ted2015]. The limiting current density is calculated for each element in z-direction based on the local feed water concentration and thickness of the boundary layers. However, limiting current is not modeled explicitly in this model. A warning is given in case the limiting current density is exceeded at any point in the model.

Ions transported into the flow electrodes are stored in the electrical double layers (EDL), which are modeled exclusively in the micropores of the activated carbon particles. Outside the micropores, electroneutrality is assumed [Bie2011; Bie2012]. The modeling of EDLs is performed using the modified Donnan model known from CDI and MCDI literature [Por2013; Bie2011] and is described in more detail below. The driving potential for ionic transport is obtained from a potential balance, which is a central element of this model and is established for each infinitesimal element in flow direction. It accounts for potential drops and electrical double layer potentials as indicated in Figure 8.2 [Bie2011; Moo2004; Sal2010].

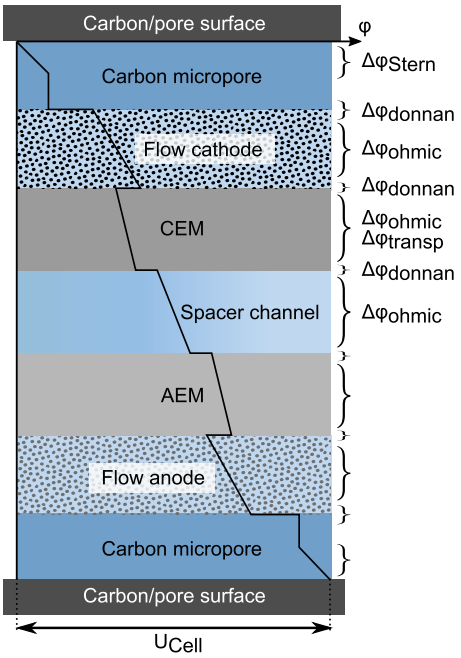


**Figure 8.2.:** Schematic distribution of the cell potential over the flow electrodes, membranes and spacer channel at one point/discrete element of an FCDI cell.

## 8.2.2. FCDI cell model

The cell model connects several submodels into a functioning model of an FCDI cell. In each cell model the transport potentials are calculated. The placement of this equation into the cell model is advantageous to an implementation in the submodels, since the main model has access to every parameter and variable of the submodels.

**Potential balance** An example for a potential balance in one discrete element of an FCDI cell in this model version is illustrated in Figure 8.2. The example shows a possible potential balance for an FCDI desalination cell with two ion exchange membranes.

In contrary to the ideal membranes assumed in the previously published process model, this model does not assume symmetry between both membranes and flow electrodes. Therefore, Donnan potentials of AEM and CEM do not always cancel each other out. Additionally, the transport potentials are calculated within the membrane submodel. The central potential balance is presented in Equation 8.1.

$$V_{cell} = \sum_{k} \Delta\varphi_{ohmic,k} + \Delta\varphi_{St}^{a/c} + \Delta\varphi_{Don}^{a/c} + \Delta\varphi_{trans} + \Delta\varphi_{Don}^{AEM} + \Delta\varphi_{Don}^{CEM} \quad (8.1)$$

In this equation, $\Delta\varphi_{ohmic}$ denotes all ohmic potential losses. The flow channels for water and flow electrodes, and the ion-exchange membranes in the FCDI cell, are regarded as a series of Ohmic resistances. $\Delta\varphi_{St}$ denotes the Stern potentials in the micropores with superscript $a$ and $c$ for anode and cathode. $\Delta\varphi_{Don}$ represents the Donnan potentials between micro- and macropores of anode and cathode ($a/c$) as well as on the edge of the ion exchange membranes (AEM & CEM). In the current model version the cell potential is fixed ("constant voltage"), hence the transport potential is calculated based on the other potentials. Since the transport potentials are not always evenly distributed, an equation was implemented to calculate the transport potential of each membrane. To solve this equation, an electroneutrality condition was implemented, which is described in the submodel for the water flow channels.

$$\Delta\varphi_{trans} = \sum_{i} \Delta\varphi_{trans,i} \quad (8.2)$$

## 8.2.3. Submodel: Water flow channels

The water flow channels are located between two ion-exchange membranes in all FCDI process layouts, which can be modeled using this model framework. The

central equations in this submodel are the mass balances, the ohmic resistance of the solution, and the electroneutrality condition.

**Species balance** The differential mass balance, Equation 8.3, accounts for the change of the number of ions in one discrete volume.

$$\frac{dn_i}{dt} = \dot{n}_{i,in} - \dot{n}_{i,out} + j_{i,in} - j_{i,out} + r_i \tag{8.3}$$

In this equation, $\dot{n}_{i,in}$ represents the incoming ion flow from the previous element in z-direction ("upstream"), $\dot{n}_{i,out}$ the outgoing ion flow to the next element in z-direction ("downstream"), while $i$ is the indicator of each ion. $j_{i,in}$ and $j_{i,out}$ denote incoming and outgoing ion flux through the membranes, and $r_i$ is the chemical reaction rate. Ion fluxes from right to left are assumed positive, while fluxes from right to left are assumed negative. It is assumed that no reactions take place in the cell, which sets the reaction rate $r_i$ to zero. Since this version of the process model considers time dependency, $\frac{\partial n_i}{\partial t}$ is not set to zero in this case and denotes the change in the amount of each ion species over time. The resulting equation can be used for every flow channel in the cell.

For further calculations, such as the determination of ohmic resistance and concentration gradients, the arithmetic mean (Equation 8.4) of the ionic concentration of anions and cations is calculated in each discrete volume.

$$c_i = \frac{c_{i,in} + c_{i,out}}{2} \tag{8.4}$$

**Mass balance water** The mass balance for the water in the flow channels does not consider time-dependent effects on the water flow rate ($\frac{\partial m_w}{\partial t} = 0$), since pressure differences or changes in the volume of the flow channels or tubing are not considered.

$$0 = \dot{m}_{w,in} - \dot{m}_{w,out} + \dot{m}_{w,membrane,left} - \dot{m}_{w,membrane,right} \tag{8.5}$$

In this equation, $\dot{m}_{w,in}$ describes the mass flow of water entering the element in z-direction and $\dot{m}_{w,out}$ describes the mass flow of water leaving each element in z-direction. $\dot{m}_{w,membrane,left}$ is the sum of the electroosmotic and osmotic flux through the neighbouring left membrane, which are implemented in the ion-exchange membrane submodel. $\dot{m}_{w,membrane,right}$ is the sum of all water fluxes through the neighbouring right membrane.

**Ohmic resistance** The calculation of the electric potential drop in each discrete volume of the flow channel (Equation 8.6), is based on Ohm's law. [Sch2012; Mel2007]

$$\Delta\varphi_{ohmic,k}(z) = \frac{h_k}{\kappa_k(z)} \cdot i(z) \tag{8.6}$$

The specific resistance is calculated by calculating its reciprocal value, the specific conductivity $\kappa$. The index $k$ represents the flow channels of feed water, anodic or cathodic flow electrodes. $h$ denotes the height of each channel, while $i$ denotes the current density in the discrete volume. The specific conductivity strongly depends on the concentration of dissolved ions. The combined specific conductivity of a solution $\kappa_{sol}$ is determined by Equation 8.7.

$$\kappa_{sol} = \sum_{i=1}^{n} c_i \cdot \lambda_i + \kappa_{water} \tag{8.7}$$

Here, $c_i$ is the concentration of each ion species in the solution, $\lambda_i$ the molar conductivity of each ion species, while $i$ denotes the indicator for each ion species. $\kappa_{water}$ denotes the specific conductivity of distilled water without any dissolved ions.

The molar conductivity of each ion species is obtained using Kohlrausch's law [Sch2012]. Kohlrausch's law (Equation 8.8) is an empirical, non-linear correlation between conductivity and concentration, which can be used to determine the molar conductivity for strong electrolytes.

$$\lambda_i = \lambda_i^{\infty} - K \cdot \sqrt{c_i} \tag{8.8}$$

In this equation, $\lambda_i$ denotes the molar conductivity of a fluid containing dissolved ions, $\lambda_i^{\infty}$ the molar conductivity at infinite dilution, which can be obtained experimentally or from literature, and $c_i$ the ion concentration. $K$ is called Kohlrausch coefficient and depends on the stoichiometry of each salt in solution. For the simulations, the parameters were fitted to data provided by Chambers et al. [Cha1956].

### 8.2.4. Submodel: Flow electrodes

The flow-electrode submodel can simulate anode as well as cathode. A conditional segment implemented in the submodel determines whether anode or cathode equations are used. Central equations in the flow-electrode submodel are the ohmic resistance (see Equation 8.6), the species balance in the flow channel (see Equation 8.3), the water mass balance (see Equation 8.5) and the equations describing the adsorption phenomena in the carbon pores.

**Species balance** The submodel of the flow electrodes considers an inner and an outer species balance. For all incoming and leaving ionic fluxes the outer

species balance is used, equivalent to Equation 8.3. The inner species balance is described in the following paragraph.

**Micro- and macropores** In the flow electrodes, a constant carbon loading is assumed. The carbon particles are modeled with well defined characteristics, such as specific micro- and macropore volumes, which were determined using the data for the Methylene blue and Iodine numbers provided in the data sheets of the manufacturer and the equations presented by Nunes and Guerreiro [Nun2011]. The formation of electrical double layers is assumed to occur in the micropores, pores smaller than 50 $\eta$m. No concentration gradients are assumed between the macropores and the bulk concentration of the fluid [Bie2012]. In order to calculate ion concentrations of the micropores, an inner mass balance between micropore, macropore and the flow channel as a whole is considered. Inside the macropores, local electroneutrality is assumed (Equation 8.9) [Bie2012]. Macropore concentrations of each ion species are denoted by $c_{macro,i}$ and the valence of each species is denoted by $z_i$.

$$\sum_i c_{macro,i} \cdot z_i = 0 \tag{8.9}$$

**Electrical double layers** Electrical double layers (EDLs) form at the interface between an electrode and the surrounding electrolyte solution, in which the electrical charge of the electrode is compensated by ions in the electrolyte. Over the years, various models for the mathematical description of EDLs were developed. The Helmholtz model only accounted for a stagnant non-diffusive double layer between electrode and electrolyte [Hel1853], while the Gouy-Chapman theory assumes diffuse electrical double layers with decreasing potential away from the electrode. The Gouy-Chapman-Stern (GCS) model merges the two individual theories. Within the pores of a carbon particle, the Gouy-Chapman-Stern (GCS) model would account for two simultaneously occurring double layers, which may overlap in case of very small pores. A newer, simplified model commonly used in CDI literature is the modified Donnan (mD) model [Jeo2011; Bie2010], which is more suitable to model overlapping EDLs. It combines a Stern layer with a Donnan equilibrium between macropores and micropores. Except for the Stern layers, it assumes a constant ion concentration and therefore a constant electric potential inside the micropores [Bie2012]. Equation 8.10 describes the Donnan potential $\Delta\varphi_Don$. This equation is similar to the Boltzmann relation used in the GCS theory, with the difference of the electric potential being no longer a function of the position away from the electrode, but constant, which is beneficial in terms of modeling.

$$c_{i,micro} = c_{i,macro} \cdot exp(\frac{-z_i \cdot \Delta\varphi_{Don}^{a/c}}{V_t}) \tag{8.10}$$

In this equation, $c_{micro}$ represents the concentration of each ion species in the micropores, with the subscript $i$ representing each species. $c_{macro}$ represents the ion concentration in the macropores and $z$ denotes the ion valence of each species. The Donnan potential is divided by the thermal voltage $V_t$ (Equation 8.11) to achieve a dimensionless potential. The equation is used in both, flow anode and flow cathode.

$$V_t = \frac{RT}{F} \tag{8.11}$$

The Stern layer and its Stern potential $\Delta\varphi_{St}$ are calculated using the Stern capacity $C_{Stern}$ and the charge density in the micropores $\sigma_{micro}$ (Equation 8.12). The Stern capacity influences the amount of ions, which can be stored in the micropores. It is a fixed value in the model and can be used to fit the simulation results to experimental data, as described for the previously published model [Rom2018b].

$$\sigma_{micro} \cdot F = -\Delta\varphi_{St} \cdot C_{Stern} \tag{8.12}$$

The charge density is the difference in ionic charge between anions and cations present in the micropores (Equation 8.13).

$$\sigma_{micro} = \sum_i c_{micro,i}^a \cdot z_i + \sum_j c_{micro,j}^c \cdot z_j \tag{8.13}$$

**Ohmic resistance** The ohmic resistances are calculated equivalent to the ohmic resistances in the water flow channels, as described above. In this submodel, the specific conductivity of the flow electrodes $\kappa_{sol}$ is determined by Equation 8.14. Compared to Equation 8.7, the specific conductivity of the water without solute ions ($\kappa_{water}$) is replaced with the specific conductivity of activated carbon $\kappa_{AC}$, which can be obtained from literature.

$$\kappa_{sol} = \sum_i c_i \cdot \lambda_i + \kappa_{AC} \tag{8.14}$$

### 8.2.5. Submodel: Ion-exchange membranes

Central equations in the ion-exchange membrane submodel are the equations describing the Ohmic resistances, as well as equations for the transport of ions and water through the membranes.

The ion-exchange membrane (IEM) submodel can be used two or more times in a model of an FCDI cell to model anion-exchange membranes (AEMs) and cation-exchange membranes (CEMs). The membrane submodels are connected to both the flow electrode and the water channel (diluate or concentrate) submodels via data ports. The ion flux between the diluate and the flow electrode is calculated in the membrane submodels, as well as the electric current and the water flux across the membrane.

**Ohmic resistance** Equation 8.15 enables the calculation of the ohmic potential losses in the ion-exchange membranes at each axial position $z$ depending on the local current density and the membrane resistance $r_{mem}$. The local current densities are calculated directly from the ionic fluxes.

$$\Delta\varphi_{ohmic,mem}(z) = r_{mem} \cdot i(z) \tag{8.15}$$

**Ionic transport** The assumption of ideally permselective membranes, as assumed in the model published in 2018 [Rom2018b], is reasonable for low salt concentrations. In this case, the membrane charge density is much higher than the salt concentration in the neighbouring solution. Additionally, low salt concentrations lead to long Debye lengths and overlapping electrical double layers in the nanoporous membrane materials. Hence, the charge based Donnan exclusion at the membrane surface works efficiently and leads to a high membrane selectivity and current efficiency.

However, one aim of this thesis is to investigate the use of FCDI processes for the treatment of high salinity (brine) solutions. To model the treatment of salt solutions with such high concentration, the assumption of ideally selective membranes by neglecting the coion transport is not valid. The permselectivity and current efficiency decreases significantly at high salt concentrations, as described in the experimental measurements described in the previous chapters. Hence, the ion-exchange membrane submodel was extended to now enable the simulation of coion transport in the membranes, which is described in the following.

In this model, Donnan potentials are calculated at each membrane/flow-channel interface.

Because of the fixed charge capacity ($X$) of the IEMs, ion concentrations in the electrical double layers (EDL) at the membrane/solution interfaces are significantly different to the ion concentrations in the adjacent solutions. Counterions, which are ions with opposite charge in respect to the fixed ions of the membrane, can cross the membrane freely. Coions, which have the same charge as the the fixed charge of the IEM, are hindered from entering the membrane. This effect is

called Donnan exclusion. Differences in ion concentrations imply electric potentials in equilibrium, hence Donnan potentials ($\Delta\varphi_{Don}$) can describe the difference in charge.

The co- and counterion concentrations and electric potentials in the IEM strongly depend on the ion concentrations in the solution near the membrane. This relationship can be described by the Boltzmann relation (Equation 8.16), which combines the Donnan potential with the ion concentration of one species in the IEM and the solution [Gal2013].

$$c_{i,mem} = c_{i,sol} \cdot exp(-z_i \Delta\varphi^k_{Don}/V_t) \tag{8.16}$$

In this equation, the concentrations of each ion species in membrane and solution is denoted by $c_{i,mem}$ and $c_{i,sol}$, respectively. The Donnan potential $\Delta\varphi_{Don}$ is divided by the thermal voltage ($V_t = RT/F$) to obtain a dimensionless form. The index $k$ represents the different membrane/solution interfaces. In this model, electroneutrality is assumed within the membranes (Equation 8.17).

$$0 = \sum z_i \cdot c_{i,mem} + \omega X \tag{8.17}$$

The ion-exchange capacity $X$ describes the amount of fixed ions in the membrane. $c_i$ denotes the ion concentration of each species in the membrane while $z_i$ is the valence of each ion species. $\omega$ represents the charge of the membrane (+1 for AEM, -1 for CEM) [Ted2016]. The ion-exchange capacity can be determined based on experimental data, as discussed in the following section.

The ionic flux of each ion species inside the ion exchange membranes is determined by Equation 8.18, the Nernst-Planck equation. In this model, convection is not considered.

$$j_i = -D_{i,mem} \cdot \frac{\Delta c_{i,mem}}{h_{mem}} + u_{i,mem} \cdot c_{i,mem,average} \cdot \frac{\Delta\varphi_{trans}}{h_{mem}} \tag{8.18}$$

The transport potential gradient $\frac{\Delta\varphi}{h_{mem}}$ is derived from the potential balance (Equation 8.2.2), which includes the Donnan potentials at the membrane/solution interfaces. $u_i$ and $D_i$ denote the mobility and diffusion coefficient of each ion in the ion exchange membranes, respectively.

The concentration gradient $\frac{\Delta c_{i,mem}}{h_{mem}}$ for each ion species is assumed to be linear and is calculated from the difference in concentrations between both membrane edges, divided by the thickness of the membrane $h_{mem}$. $c_{i,mem,average}$ is the average ion concentration in each membrane for each ion species, calculated as the arithmetic mean of the concentrations ($c_{i,mem}$) at each membrane interface. Limiting current densities and concentration polarization are not considered in this model, since these phenomena mainly occur at low salt concentrations or very high currents, which are not the focus of this model.

**Electrical current density and current** The current density is calculated as the sum of all ionic fluxes, taking into account their valence. Regardless of which membrane model is used, all ionic fluxes are calculated through the Nernst-Planck equation (Equation 8.18). The current density can be used to calculate ohmic potential losses over each flow-channel and membrane. The integration of the current density over the cell length results in the total electric current.

$$i = \sum_i j_i \cdot z_i \cdot F \tag{8.19}$$

**Water transfer** Since water transfer through ion-exchange membranes has significant impact on the desalination performance of FCDI processes, this model considers osmotic as well as electroosmotic water transfer. Electroosmotic water transport is coupled with ion transport, which entails a transport of hydration shells and a water flux created by the drag between moving ions/hydration shells and the solvent [Cam2019]. Due to the high salt transfer rates, electroosmosis dominates in FCDI systems under the relevant conditions, as was shown in the experiments described in Chapter 6. In this case, the resulting water flux through each membrane can be calculated via Equation 8.20.

$$\dot{V}_{electroosm} = \sum_i j_i \cdot h_i \cdot M_w/\rho_w \tag{8.20}$$

Here, $\dot{V}_{electroosm}$ represents the electroosmotic water flux through each membrane, while $j_i$ and $h_i$ denote the ionic flux and the hydration number of each ion species, respectively. $M_w$ and $\rho_w$ are the molar weight and the density of water. Due to the positive and negative signs of the various ion fluxes (counterions and coions in different directions), the water flux represents the net water transport through each membrane caused by electroosmosis.

The second most important water transport phenomenon is osmosis resulting from different ion concentrations at the left and right side of the membrane. This water transfer is calculated via Equation 8.21 [Cam2019; Kam2016a; Kin2018]:

$$\dot{V}_{osm} = A \cdot R \cdot T \cdot v \cdot (c_{sol,right} \cdot \varphi_{right} - c_{sol,left} \cdot \varphi_{left}) \tag{8.21}$$

Here, $\dot{V}_{osm}$ denotes the volumetric water flux in each membrane caused by osmosis, while $R$ and $T$ are the ideal gas constant and the temperature, respectively. $A$ describes the water permeance of the membrane. This parameter is different for each membrane type and needs to be obtained by experiments or literature. $v$ denotes the van't Hoff coefficient and $\varphi$ denotes the osmotic coefficient on each membrane side. It is depended on the salt and its concentration. $c_{sol,right}$

and $c_{sol,left}$ represent the salt concentration on each membrane side. [Cam2019; Kam2016a; Kin2018]

The net water transfer of each membrane is the sum of both $\dot{V}_{electroosm}$ and $\dot{V}_{osm}$. This value is used in each flow electrode and each spacer channel model as $\dot{m}_{w,membrane,left}$ or $\dot{m}_{w,membrane,right}$, respectively.

## 8.2.6. Modelling continuous FCDI systems

In order to simulate an FCDI system for continuous desalination and regeneration, such as the two cell or single cell configuration described in the previous chapters, the submodels can be connected as required. An example is shown in Figure 8.3. The properties of the slurry electrodes such as ion concentrations and potentials in EDLs are transferred between the flow-electrode channels and a flow-electrode storage vessel (reservoir) submodel. The flow-electrode reservoir submodel can, for example, connect either the two oppositely charged flow-electrode channels in a single-module configuration, as illustrated in Figure 8.3, or the two FCDI modules in a two-module configuration.

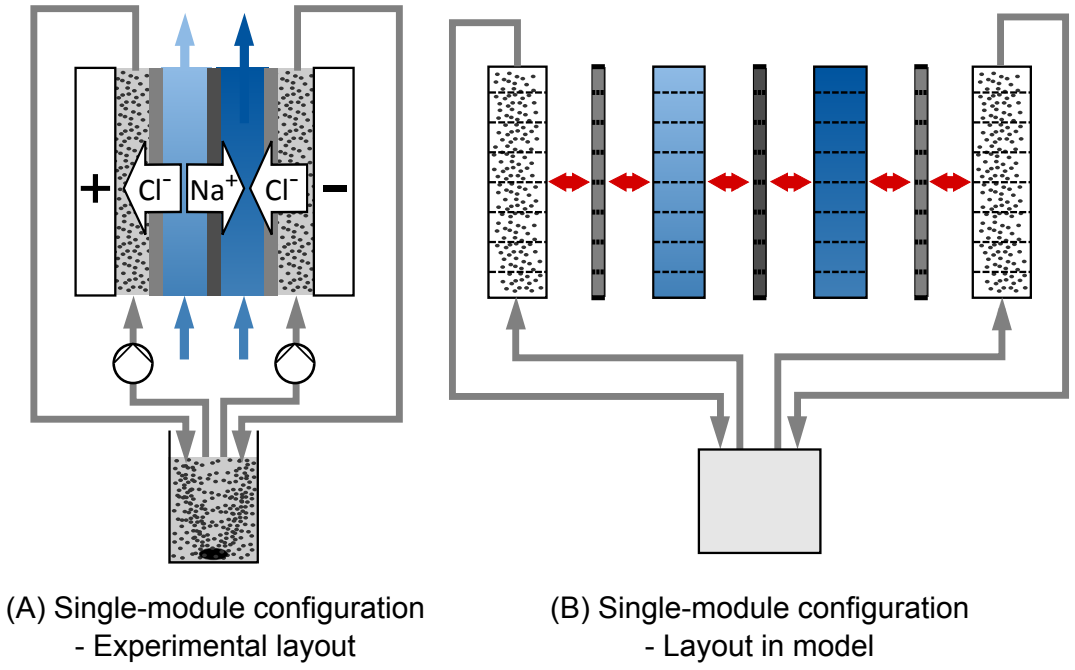


**Figure 8.3.:** Illustration of a continuous single cell FCDI system layout including flow-electrode circuits in (a) experiment and (b) the process model at hand.

**Submodel: Flow-electrode reservoir** Earlier experiments and simulations were performed with directly recirculated flow electrodes. The end of a flow-electrode channel was directly connected to the entrance of the next flow-electrode channel of the previous FCDI cell model. In recent experiments, the use of a slurry

reservoir was tested, as described in Chapter 6. In this case, a mixing tank between two flow-electrode channels is included. In experiments it was found that this layout does not influence the performance of the cell. In fact, it leads to a more stable performance, as liquid level fluctuations due to different pressure drops in the flow channels are avoided. With the slurry reservoir, the end of all flow-electrode channels lead into the reservoir, while the feed for each flow-electrode channel is pumped out of the reservoir.

To model the reservoir, three main equations are considered. The mass balance equation (Equation 8.22) calculates the time-dependent amount of ions for each ion species $i$, denoted by $n_{i,reservoir}$.

$$\frac{dn_{i,reservoir}}{dt} = \sum_{k} \dot{n}_{i,in,k} - \dot{n}_{i,out,k} \tag{8.22}$$

Here, incoming and leaving ion flow rates of each species are considered by $\dot{n}_{i,in}$ and $\dot{n}_{i,out}$. The index k denotes the number of flow electrodes. The concentration $c_{i,reservoir}$ of each ion species in the reservoir is calculated via Equation 8.23. The previously determined amount of each ion species in the reservoir is divided by the filling volume of the reservoir $V_{reservoir}$.

$$c_{i,reservoir} = \frac{n_{i,reservoir}}{V_{reservoir}} \tag{8.23}$$

The last equation defines which ion concentration leaves the reservoir and re-enters the flow electrodes. Since the flow-electrode outlet streams are mixed in the reservoir, the concentration re-entering each flow-electrode channel is equal for both anions and cations. Hence, the ion concentration $c_{in}$ at the beginning of each flow-electrode channel $k$ is set equal to the ion concentration in the reservoir (Equation 8.24). A side effect of this mixing is a discharge of the carbon particles. Therefore, a Donnan and Stern potential of 0 is assumed at the start of each flow-electrode channel.

$$c_{i,in,k} = c_{i,reservoir} \tag{8.24}$$

### 8.2.7. Simulation

The FCDI model was implemented in gProms ModelBuilder Version 5.0.1 and was fitted to experimental data for validation purposes. In order to reproduce the experimental results by the model, the influence of several parameters was analyzed, as described in the following section.

## 8.3. Model validation and sensitivity analyses

The simulation results depend on many input parameters, such as the membrane characteristics and the Stern capacity. Especially when simulating high feed salinities, which goes hand in hand with high concentration gradients, high fluxes, and significant non-idealities such as water transfer, these parameters can have a significant influence on the simulation results. The main input parameters of this model are:

- Flow channel, spacer and membrane geometries.
- Activated carbon and flow-electrode characteristics (pore volume, Stern capacity, activated carbon content).
- Membrane characteristics (diffusion coefficients, charge density, osmotic permeability coefficient, thickness, resistance).
- Other parameters (flow rates, salt concentrations, Kohlrausch parameters, hydration number of ions).

While some parameters are clearly determined by the chosen experimental settings or the material, some parameters vary depending on the assumptions and process conditions. To understand the influence of main input parameters, sensitivity analyses were performed as described in the following.

### 8.3.1. Ion diffusion coefficients in the membranes

In many process models for electrodialysis and other ion-exchange membrane based processes, simplified assumptions regarding the ion diffusion coefficients are made, such as the assumption of generalized diffusion coefficients in the membranes, which are ten times lower than in the solution [Ted2016]. However, many experimental and model-based studies show significant differences for the diffusion coefficients of (1) co- and counterions in ion-exchange materials [McH1969; Dem1979; Kam2016a], (2) depending on the ion type and the membrane materials [Mea1956; Yea1979; Li2005; Kam2016a], and (3) depending on the process conditions, such as the solution concentrations bordering the membrane [McH1969; Dem1979].

An alternative approach for modelling ion transport through ion-exchange membranes is the Maxwell-Stefan framework. In this case, the ion-ion, ion-water and ion-wall friction can be considered. While the Maxwell-Stefan approach considers more phenomena and is more complex, but it also requires input parameters. Tedesco et al. [Ted2017] showed that the extended Nernst-Planck equation can be deduced from the Maxwell-Stefan theory by neglecting ion-ion and ion-membrane friction. The model at hand is based on such a simplified approach

and shows good agreement with experimental results. However, for further works it may be interesting to consider the Maxwell-Stefan approach to investigate the impact of these neglections, as it may be especially relevant for a more accurate model of the water transport in FCDI systems.

In case of the Nernst-Planck equation, which is applied in this work, the Nernst-Einstein equation determines the relation between ion diffusion coefficients $D$ and ion mobilities $u$ [Kam2016a]. Hence, $D$ serves to determine the ion transport, albeit the driving force may be an electric field or a concentration gradient [Kam2016a]. In the following, the results of a sensitivity analysis are presented, which was performed to investigate the significance of the ionic diffusion coefficients within the ion-exchange membranes in this model under the relevant process conditions. Figure 8.4 shows the resulting diluate and concentrate product stream concentrations, total electrical currents and current efficiencies calculated by the model described above. The diffusion coefficients were varied in between values for $D$ in the solution, in the range of $10^{-8}$ to $10^{-9}$, and low values for $D$ from literature [Li2005].

In the first case, all four $D$ are kept equal, for counter- and coions in both AEM and CEM. The simulation results are plotted in Figures 8.4 (a) and (b). The results show an optimum for the desalination and concentration performance at around $2 \cdot 10^{-11}$. When considering the results for the total electric current and the current efficiency, it becomes clear why. While the overall current is very low at low values for $D$ due to an overall limitation of the mass transport, the current efficiency rapidly decreases at high values for D. In this case, all ion fluxes through the membrane, including the coion flux, increase to an extent that the selectivity is reduced. This leads to a reduced current efficiency and back diffusion/transport of coions back into the diluate. This results in a significant reduction of the desalination and concentration performance, while the total electric current is still high. The overall process becomes inefficient.

In the second case, plotted in Figures 8.4 (c) and (d), the values of $D$ for the counterions were kept at a constant value of $1.9 \cdot 10^{-11}$ in both membranes, while the value of $D$ for the coions in both membranes was varied. As is to be expected, this leads to a very good desalination and concentration performance, as well as a very good current efficiency in case of $D_{coion} < D_{counterion}$, due to the limited back diffusion of coions through the membrane. In case of $D_{coion} > D_{counterion}$, the desalination and concentration performance, as well as the current efficiency, rapidly decreases due to the increased coion transport.

For case three, as plotted in Figures 8.4 (e) and (f), the values for $D$ were kept equal for coions and counterions. The values for both $D$ in one membrane (AEM or CEM) were kept constant, while the values for both $D$ in the other membrane

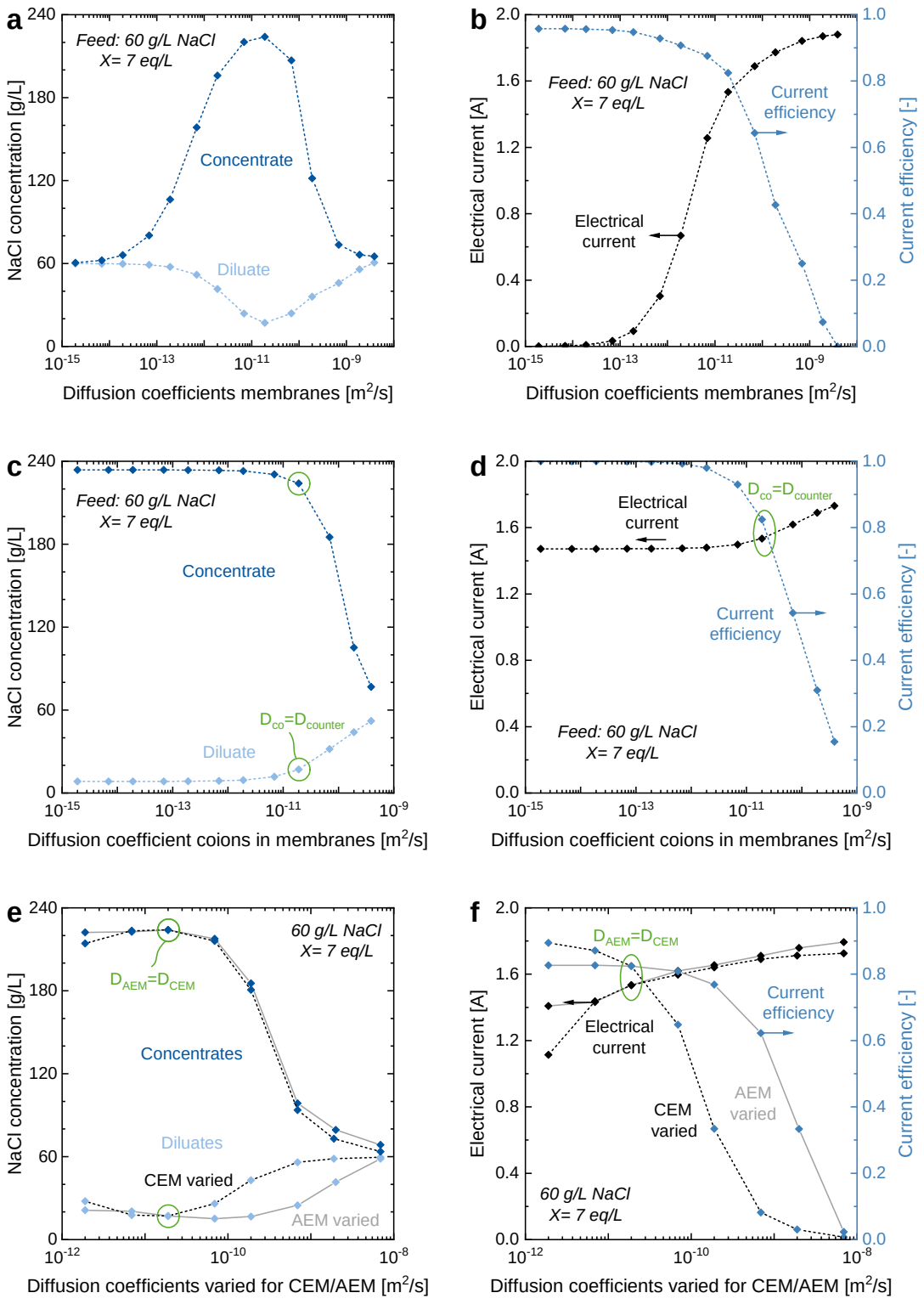


**Figure 8.4.:** Results of sensitivity analyses regarding the diffusion coefficients $D$ of ions in the ion-exchange membranes. The plots show results for the product stream salinities, the total electrical currents and the current efficiencies. The values for $D$ were varied while (a)/(b) $D_{Co,AEM}$=$D_{Counter,AEM}$=$D_{Co,CEM}$=$D_{Counter,CEM}$, (c)/(d) $D_{Counter}$=constant and $D_{Co}$=varied, and (e)/(f) $D_{Counter}$=$D_{Co}$, $D_{AEM}$ or $D_{CEM}$=constant and $D_{CEM}$ or $D_{AEM}$=varied.

(CEM or AEM) were varied. In both cases, in which either $D_{AEM}$ or $D_{CEM}$ were kept constant, the overall trends look similar. The differences probably result from small differences in diffusion coefficients in the solution and different sizes of hydration shells, or the simple fact that there are two AEMs present in the system and only a single CEM. Hence, the overall transport behaviour may differ for both ion and membrane types. The general trends are comparable to Figures 8.4 (c) and (d). A rapid decrease in desalination/concentration performance as well as current efficiency is seen in case one of the sets of Diffusion coefficients is significantly higher than the rest. At values around the values for $D$ in the solution, the overall performance of the process is poor, due to a lack of membrane selectivity.

Overall, the values for the ion diffusion coefficients $D$ in the membranes have significant influence on the process performance in this model. A decreasing current efficiency goes hand in hand with a decreasing desalination and concentration performance. Due to the water recover ratios/split ratios chosen in this work, this is most visible in the concentrate concentrations. This correlates well with observations made in experiments, which showed a significant influence of variation of different process parameters on the concentration performance.

**How can we determine the diffusion coefficients?** The observed significance of $D$ for the quality of the simulation results in the question: which $D$ is correct for each specific case, and how should $D$ be determined? As mentioned earlier, there are many different trends observed in the literature regarding the values for $D$ in case of co- and counterions in various membrane materials and depending on the surrounding solution concentration. In this work, it was chosen to determine $D$ based on a correlation for $D$ depending on the water content in an ion-exchange material, derived by Patrick Meares in 1956 [Mea1956; McH1969]:

$$D = D_0 \cdot \left( \frac{v_w}{2 - v_w} \right)^2 \tag{8.25}$$

In this equation, $D$ is the diffusion coefficient of an ion in an ion-exchange membrane, $D_0$ is the Fick diffusion coefficient of the respective ion in the adjacent solution, and $v_w$ is the water content (swelling degree) of the respective ion-exchange membrane.

This model assumes that diffusion occurs within the aqueous phase of an ion-exchange material along a tortuous path around the polymer chains [Mac1955a; Mea1956], and is hence based on the Karman-Cozeny equation, which describes the pressure drop in fluid flowing through a packed bed of solids. An advantage of this model is that it comprises no further adjustable parameters, and its validity has been demonstrated even in recent works. Kamcev et al. [Kam2016a]

compared the model predictions to a range of published experimental results and found a good correlation, especially for coion diffusion coefficients in charged, swollen polymers. In case of counterion diffusion, the model has been found to systematically overestimate the diffusion coefficients to a small extent. Attractive electrostatic interactions between counterions and fixed charge groups of the membrane are discussed as a possible reason for the reduction of counterion diffusion coefficients beyond the hindrance due to membrane tortuosity [Kam2016a].

Even though the counterion diffusion coefficients are undererstimated to a small extent by this model, this equation was tested and applied for determining coion as well as counterion diffusion coefficients in this work. Generally, a good agreement with experimental results was observed, as presented in Subsection 8.3.6.

**Diffusion coefficients and diluate concentration.** As in most models, the simulation results can be influenced significantly by the choice of parameters. Even when choosing parameters based on measured membrane characteristics and experimental settings, there is always a degree of uncertainty. During first simulations performed for model validation, certain discrepancies from experimental results were observed. When choosing the input parameters in a way that the simulation results matched the desalination and concentration performance very well, the overall electrical current was systematically overestimated and the current efficiency underestimated. When matching the input parameters to achieve the correct currents, the desalination degree was significantly lower than observed in experiments. The reason seemed to be a consistent underestimation of the achieved current efficiency.

In the experimental results described in Chapter 7, a significant dependence of the current efficiency on the salt concentration achieved in the diluate product stream was observed (Figure 7.17). This effect could also be the reason for the observed deviations of simulation from experimental results. The deviations were mainly observed in cases of experiments, which resulted in very high concentration gradients across the ion-exchange membranes. While the impact of high concentration gradients on the electrical resistance of IEM has been investigated previously [Gei2013; Gal2014], there is little literature available regarding the impact of concentration gradients on the selectivity or current efficiency of ion-exchange membranes and processes. However, it has been noted for example by Galama et al. [Gal2016] and Kristensen et al. [Kri2017] that the modeling approach applied here, often referred to as Teorell-Meyer-Sievers theory, is inaccurate in case of strong concentration gradients over the membrane. A potential alternative to this approach are space-charge models, which are applied in the respective research articles. In the following, a simple modification of the model at hand is presented, which leads to a significant improvement of the accuracy of

the model at hand without the use of a space-charge model.

**When and why is the unmodified modeling approach applied here inaccurate?** The experimental results presented in Chapter 7, together with the underestimation of the current efficiency in the model, indicate that the membrane selectivity for counter- over coions depends strongly on the lower concentrated solution adjacent to the membrane. A possible explanation for this is a gradually changing electrical double layer charge screening throughout the membrane, as illustrated in Figure 8.5.

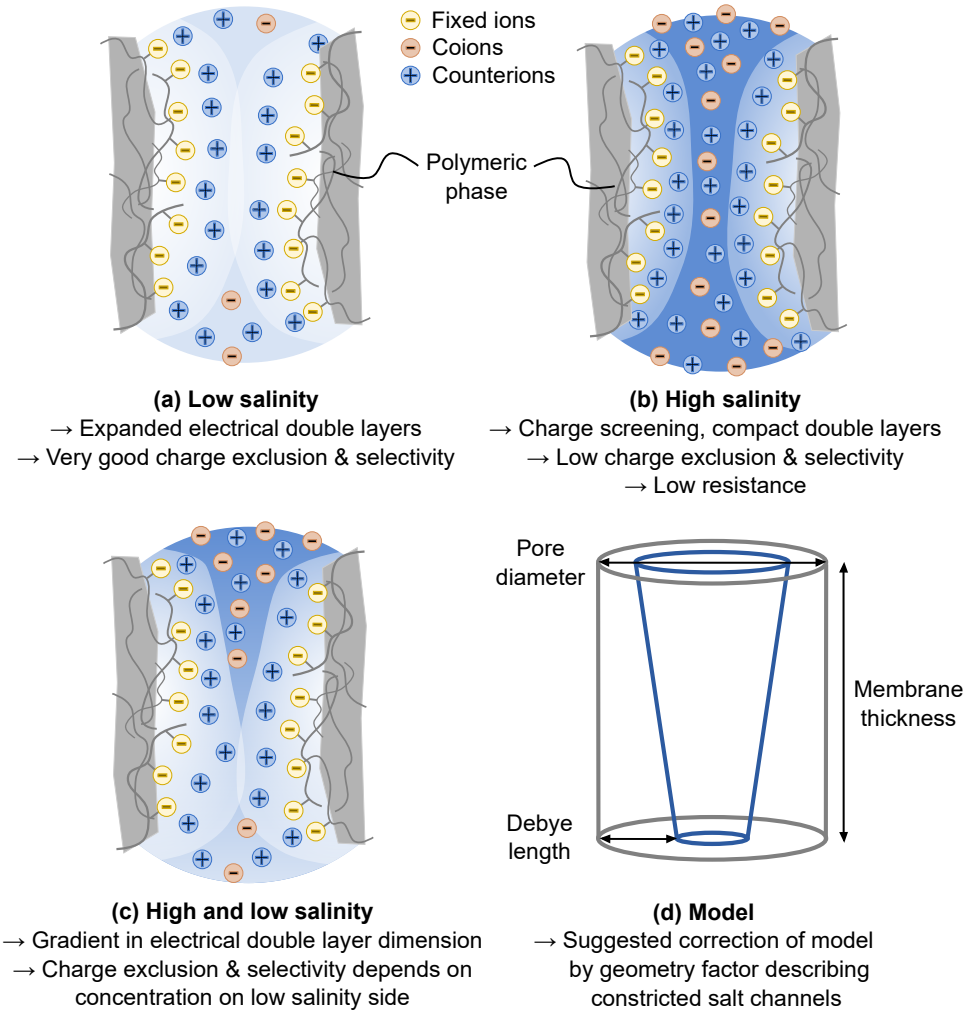


**Figure 8.5.:** Illustration of fixed charge screening within ion-exchange materials depending on the adjacent solution concentrations and its influence on membrane selectivities. (d) Illustration of the determination of the geometry factor for the reduced salt channel volume model.

The effective screening of fixed charges within the membrane material, as well as a strong swelling degree, may lead to the formation of regions within the membrane material, which contain "electrolyte at the same concentration as in

the external solution", as described by Mackie and Meares in 1955 [Mac1955a]. When these regions form a network within the polymer, the membrane looses selectivity. Co- and counterions can diffuse freely through such networks and are only hindered by the additional tortuosity and reduced volume of the channels. In the following, these are referred to as "salt channels". With increasing number of functional groups within an ion-exchange polymer, the ion-exchange capacity and water uptake increase, and hence the diffusion coefficients increase due to a larger fraction of salt channels [Li2005].

In case of low salt concentrations bordering the membranes on both sides, even a loosely crosslinked, highly charged polymer can have a very good selectivity. The fixed charges are countered by expanded, potentially overlapping electrical double layers, and will effectively block the transport of coions. This case is described well by the Donnan theory. The low solution concentration will lead to a very low coion concentration within the membrane, and hence a low coion transport rate and good membrane selectivity. For low salinities, a highly charged polymer is desirable, as it goes hand in hand with a low electrical resistance.

At high salinities, the fixed charges are screened and the membrane will loose selectivity. Coions as well as counterions can be transported through the tortuous salt channels, which is described well by the Nernst-Planck equation in combination with the Meares model for the diffusion coefficients, as described above. For high salinities, a less hydrophilic membrane with a high degree of crosslinking is desirable, which will offer a good selectivity even at high salinities, even if it comes with an increased resistance.

However, it appears that in case of very high concentration gradients, which occur in the continuous FCDI systems modeled here, the combination of Nernst-Planck equation with Donnan potentials and the Meares model applied here overestimates the coion back-diffusion through the membranes. The high concentration on one side of the membrane leads to a strong concentration gradient as driving force for the diffusive back transport. On the other hand, the improved selectivity due to expanded and potentially overlapping double layers on the side membrane bordering a low salinity solution is not considered adequately.

**A simple modification.** Hence, it is proposed here to introduce an additional geometry factor $\sigma$, to account for the diminished salt channels towards the low salinity side of the membrane, which are hypothesized to have a major effect especially on the transport of coions through the membrane. I suggest to calculate $\sigma$ based on the Debye length on both sides of the membranes and the average "pore" diameter within the membrane material, as illustrated in Figure 8.5 (d):

$$\sigma = \frac{\frac{h_{mem} \cdot \pi}{3} \cdot (r_{red,highC}^2 + r_{red,highC} \cdot r_{red,lowC} + r_{red,lowC}^2)}{h_{mem} \cdot \frac{d_{pore}^2 \cdot \pi}{4}} \tag{8.26}$$

In this equation, $h_{mem}$ is the thickness of the membrane, $r_{red,highC}$ and $r_{red,lowC}$ are the radii of the constricted salt channel model at the membrane side bordering the high and low salinity solutions, respectively. $d_{pore}$ is the average diameter of the porous network within the membrane. In this equation, $r_{red,highC}$ and $r_{red,lowC}$ can simultaneously be determined by the following equation:

$$r_{red,highC} = \frac{d_{pore}}{2} - \lambda_{D,highC} \tag{8.27}$$

$\lambda_{D,highC}$ and $\lambda_{D,lowC}$ represent the Debye lengths of the electrical double layers at the membrane-solution interface on the side bordering the high and low salinity solutions, respectively. Based on this, the salt channel volume $v_{sc}$ accessible to coions can be calculated, which depends on the water uptake $v_w$ of the membrane:

$$v_{sc} = \sigma \cdot v_w \tag{8.28}$$

The implementation of this correlation into the process model described here led to a significant improvement of the simulation results. With this modified Meares model, the results regarding desalination and concentration performance, as well as currents and current efficiencies, match the experimental results well, as presented in the validation subsections.

### 8.3.2. Membrane charge density

Apart from the diffusion coefficients, the charge density assumed in the membranes has a major influence on the simulation results of the model. When calculating the membrane charge density $X$ based on the ion exchange capacity, the question arises which reference volume is sensible: (1) the total volume of the membrane or (2) the water phase within the membrane. When considering an ion-exchange membrane, the material consists of polymer chains ("uncharged backbone") and charged functional groups, with pores in the low nanometer range. The water phase within the membrane, including the dissolved ions, is mainly in contact with the charged channels. Hence, the assumption of the water phase as reference volume seems logical.

To investigate the influence and validity of this assumption, a continuous FCDI process was simulated over a range of assumed charge densities in the membrane, which includes both ranges resulting from choosing the whole membrane or only the water phase in the membrane as reference volume. The results are presented in Figures 8.6 (a) and (b).

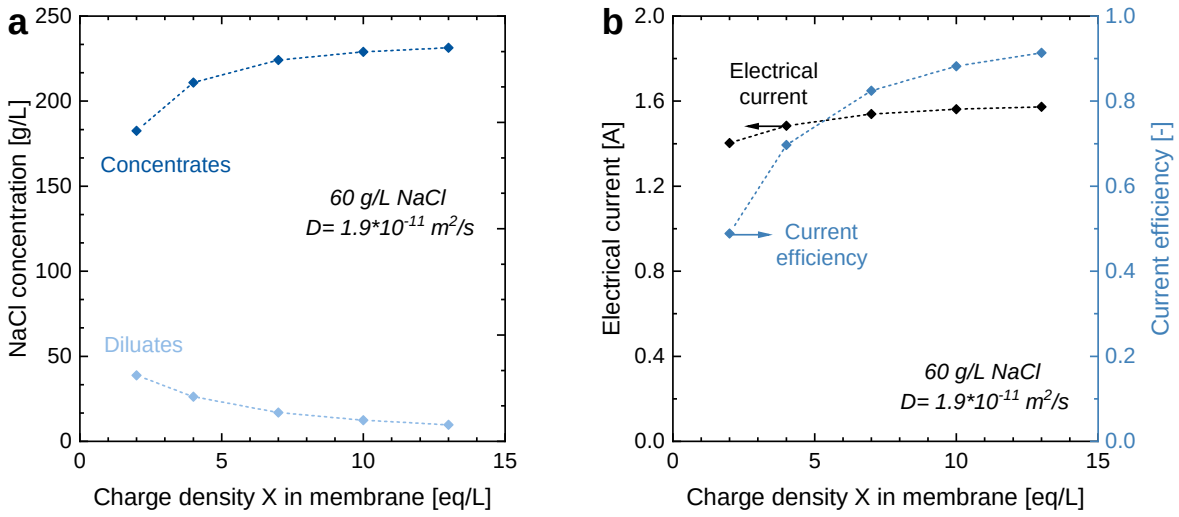


**Figure 8.6.:** Results of sensitivity analyses regarding the charge density $X$ assumed in the ion-exchange membranes. The plots show results for (a) the product stream salinities, and (b) the total electrical currents and current efficiencies.

The results show a significant decrease in the desalination and concentration performance at charge densities below 3 eq/L. This trend is most likely caused by a decreasing membrane selectivity due to an ineffective charge exclusion, which is consistent with the strongly decreasing current efficiency at decreasing charge densities. When calculating the charge densities for different ion-exchange membrane materials applied in our systems, one arrives at values below 2 eq/L when using the membrane dry mass as reference, and at values significantly higher than 2 eq/L when using the water phase within the membrane as reference. In some cases, values of up to 20 eq/L were determined, which is consistent with the values presented by Kingsbury et al. [Kin2018] for different commercial ion-exchange membranes.

The low desalination/concentration performances resulting from using the total membrane volume as reference volume are not in agreement with our experimental results. Our experimental results support the assumption of choosing the water phase as reference volume for the charge density. Galama et al. [Gal2013] came to the same conclusion in 2013, when they compared the validity of the two assumptions to experimental results. They found that a good fit to experimental data is only achievable when assuming the water phase as reference volume. Hence, the water phase is assumed as reference volume for the simulations presented in the following sections.

### 8.3.3. Stern capacity in the flow electrodes

Same as in the previously published model [Rom2018b], the Stern capacity $C_{St}$ is considered as a volumetric capacity. $C_{St}$ is a function of the micropore charge density, which was adapted conceptually from recent CDI literature [Zha2012].

In the previously published article, it was discussed that values of $C_{St}$ might allow conclusions about the effectiveness of charge percolation and carbon charging in general within the flow electrodes [Rom2018b]. To investigate the influence of the value of $C_{St}$ on the simulation result, a series of simulations was performed over a range of assumed Stern capacities $C_{St}$, as plotted in Figures 8.7 (a) and (b).

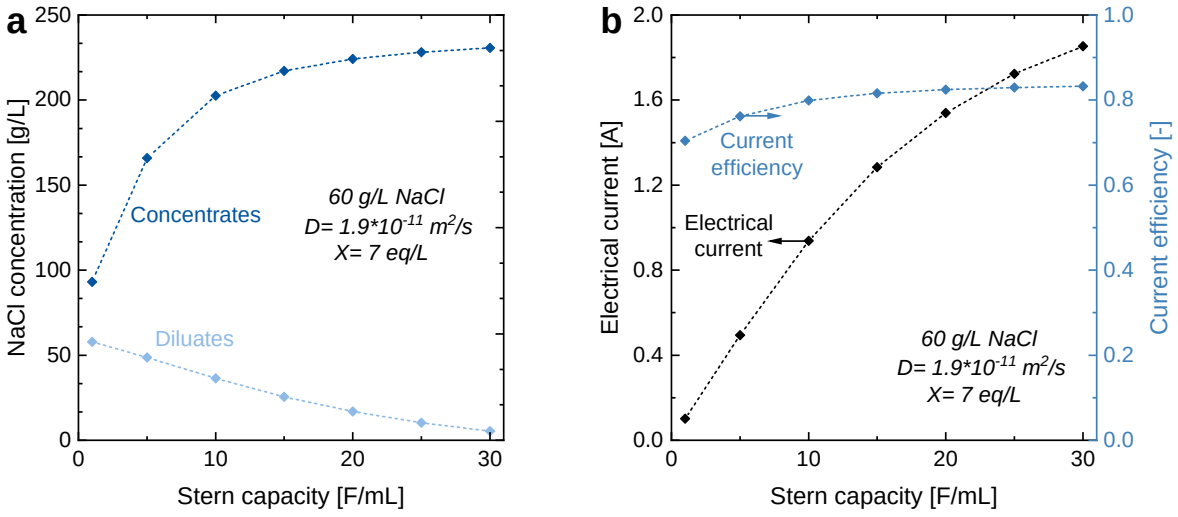


**Figure 8.7.:** Results of sensitivity analyses regarding the Stern capacity $C_{St}$ assumed in the pores of the carbon particles. The plots show results for (a) the product stream salinities, and (b) the total electrical currents and current efficiencies.

The plots show a strong dependence of the overall desalination and concentration performance on the Stern capacity. A low Stern capacity will lead to a small amount of ions being adsorbed inside the carbon particle pores, and hence a low desalination performance. While the current efficiency is relatively good over the whole range of tested $C_{St}$, a low $C_{St}$ leads to a low overall electrical current.

To match the experimental results, a relatively high $C_{St}$ of above 20 F/mL had to be assumed, while in our previous paper values for $C_{St}$ of 12 F/mL or lower were assumed to achieve good fit results. This indicates a more effective ion adsorption in the current experimental FCDI system compared to the previously operated experimental FCDI system. A reason for this may be the improved charge and mass transport within the flow electrodes, resulting from the impedance spectroscopy study presented in Chapter 4.

As was shown in the literature [Por2014; Hat2015b; Lia2017] and the results presented in Chapter 4, and the corresponding article [Rom2019], the carbon

content and quality has a major influence on the overall performance of flow electrodes. To adsorb ions, the suspended carbon particles need to acquire charge by interacting with either the charged current collector or other suspended particles, which are already charged. The effective charge percolation is not ensured at, for example, low carbon loadings in the flow electrode. A low carbon loading can result in the observation of low electrical double layer capacitances in impedance spectroscopy measurements [Rom2019]. Apart from this, the observations presented in Chapter 4 and the corresponding article [Rom2019] emphasize the importance of the pore size distribution and presence of mesopores in the carbon particles. All microscopic phenomena influence the inter- and intraparticle charge and mass transfer, and thus, have an influence on the value of the fitted "apparent" Stern capacity.

In case of an effective charge and mass transfer within the flow-electrode slurries, the apparent Stern capacity will be close to the maximum capacity. An uneffective charging performance will lead to low values for $C_{St}$. Uneffective charging was already discussed as a potential reason for significant differences between the $C_{St}$ values required for fitting literature data [Jeo2013] to our own previously published results [Rom2018b; Gen2014], in which flow electrodes at low carbon loadings of only 5 wt.% were applied. In more recent studies of our work group [Rom2018a; Rom2019], higher activated carbon contents and better suited carbon materials were applied. This results in the need for assuming higher $C_{St}$ values.

The results show that the apparent Stern capacity is, like in the previous model, still a governing parameter. However, due to the consideration of coion and water transport in this model, the membrane material characteristics such as the charge density and diffusion coefficients now add to the complexity of the interdependencies in this model and need to be chosen carefully.

### 8.3.4. Water transfer: Osmotic water permeance and electroosmosis

As demonstrated in Chapter 6 and described above, the water transfer through ion-exchange membranes has significant impact on the desalination performance of FCDI processes. The determination of the water transfer rate requires the assumption/determination of parameters, such as the osmotic water permeance $A$. The water permeance is defined as driving force normalized water flux through the membrane [Kam2016a; Kin2018]. $A$ depends not only on the material characteristics, but also on the membrane thickness. As membrane thicknesses are not always uniform and constant, for an evaluation of a membrane performance it is useful to apply a characteristic such as the water permeance [Kam2016a].

$A$ needs to be determined experimentally for a specific membrane material and thickness. As such measurements were not performed within this work, the sensitivity of the model at hand towards differences in the water permeance $A$ is investigated via a sensitivity analysis in the following. Simulation results based on varied values for $A$ are plotted in Figure 8.8.

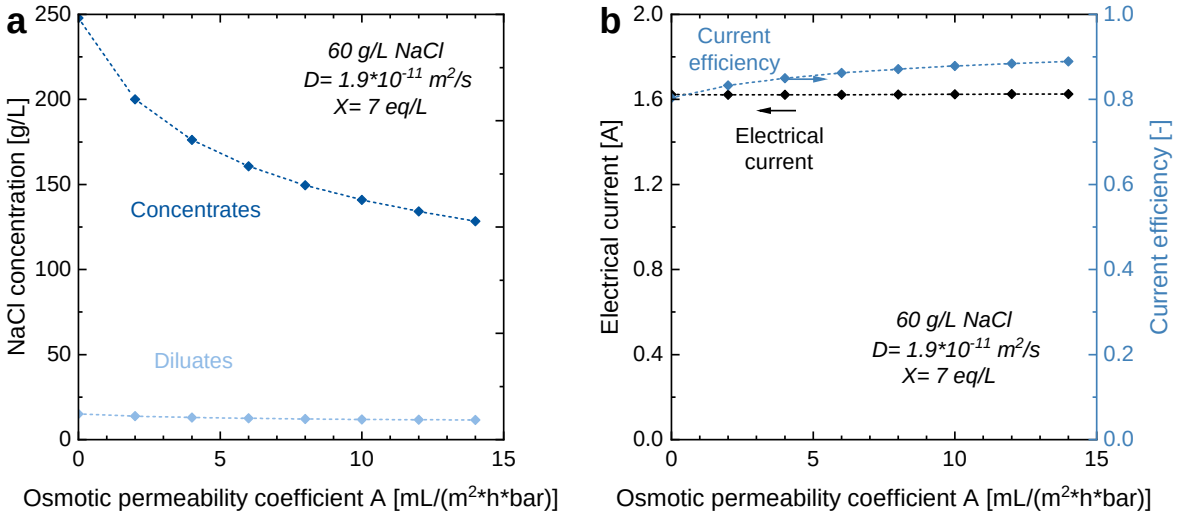


**Figure 8.8.:** Results of sensitivity analyses regarding the osmotic water permeance $A$ of the ion-exchange membranes. The plots show results for (a) the product stream salinities, and (b) the total electrical currents and current efficiencies.

The graph in Figure 8.8 (a) shows the impact of a varied water permeance $A$ on the desalination and concentration performance predicted by the process model at hand. While there is hardly an influence on the predicted diluate concentration, the concentrate concentration decreases significantly with increasing water permeance $A$. This is in good agreement with the observations described in Chapter 7 of the water transfer mainly having an impact on the concentrate product stream concentration.

In Figure 8.8 (b), the results regarding the predicted electrical current and current efficiency are plotted over the osmotic water permeance $A$. While $A$ exhibits close to no influence on the resulting electrical current, the predicted current efficiency increases with increasing water permeance. The reason for this is likely the decreased concentrate concentration, which leads to a more efficient charge exclusion, and hence a better membrane selectivity and an improved current efficiency.

A sensitivity analysis regarding the impact of the chosen electroosmotic water transfer rates on the model predictions revealed that the trends are similar to the impact of the osmotic water permeance. Due to the significant similarities to Figure 8.8 the results are not presented here to avoid redundancy. An increasing

electroosmotic water transfer mainly leads to a diluation/reduction of the concentrate product stream concentration and hence a slightly increasing current efficiency.

Overall, the results of the sensitivity analyses regarding the water transfer are in good agreement with trends observed in experimental measurements. The chosen parameter values have a main influence on the predicted concentrate concentration. Therefore, it is vital to choose the parameter settings well, to ensure the validity of the simulations. In this work, values presented by Kingsbury et al. [Kin2018], who published measurement results for 20 commercial ion-exchange membranes, were chosen as model input parameters. While not all membranes of exactly the same type as applied in this study were investigated by Kingsbury et al., very similar membranes based on the same material and/or similar thicknesses and reinforcement types were investigated. The relevant membranes exhibited comparable water permeance values in a small range. Therefore, the prediction uncertainty is in an acceptable range according to our sensitivity analysis.

### 8.3.5. Validation - Influence of the $\sigma$-factor

For validation of the modified Meares model with $\sigma$-factor representing hindered ion transport through ion-exchange membranes bordered by solutions of significantly different concentrations, the model was fitted to experimental results obtained for continuous FCDI systems in single-module configuration. All parameters were chosen based on the applied membrane and activated carbon materials and the assumptions described above. A list of the experimental and chosen simulation input parameters is given in Table 8.2. Most of the membrane related parameters are based on data obtained from manufacturer data sheets of the applied fumasep FAB-PK-130 and FKB-PK-130 membranes (fumatech BWT GmbH), while some are based on values published by Kingsbury et al. [Kin2018]. The pore diameter within the ion-exchange membranes was chosen according to the observations by Komarov et al. [Kom2010] in SPEEK membranes.

Apart from the chosen settings, Table 8.2 compares the results of two simulations to experimental results. In the first case ("Sim. 1"), the simulation was performed with the classical Meares model without the suggested $\sigma$-factor, which was set to $\sigma = 1$. In the second case ("Sim. 2"), the above described modified Meares model including the additional $\sigma$-factor to account for the altered diffusion characteristics of membranes being bordered by two solutions of significantly different salinity.

While there is a small deviation from the experimental results visible for Simulation 1, the results listed in Table 8.2 for Simulation 2, which includes the $\sigma$-factor, show a very good agreement with the experimental results. As intended

by the introduction of the $\sigma$-factor, the electrical current in the simulation is reduced and the current efficiency is improved and reaches values close to the extremely good current efficiency of around 1, which was achieved in this experiment. Apart from this, the results regarding the desalination and concentration performance, as well as the water transfer and the resulting product stream flow rates, the simulation results match the experimental results very well. By implementing the modified Meares model with $\sigma$-factor into the model, the diffusion coefficients for each ion type and membrane are calculated individually in each discrete element, and hence adjusted to the local condition. The results regarding $D$ given in the table are the values calculated at the very end of the FCDI cell and demonstrate the resulting different to the classical Meares model (Simulation 1). The calculated $\sigma$-factors ranged from 0.37 to 0.76 in this particular case. The values given in Table 8.2 are the values calculated each in the first and last element of the FCDI cell model.

The introduction of the $\sigma$-factor led to a significant improvement of the simulation results. Even better results may be achieved by implementing equations for determining the ion and water transport through the membrane based on the Maxwell-Stefan approach [Ted2017]. Alternatively, it may be interesting to apply the Manning condensation theory for the transport of ions through the ion-exchange membranes, as suggested by Kamcev et al. [Man1969; Kam2016b], which can also model non-ideal behaviour of ions in ion-exchange membranes. In most works, including this thesis, ideal activity coefficients of 1 are assumed, which is unlikely to be the case in reality. Recent works have found that Manning‘s model for counterion condensation on polyelectrolytes in solution can also be transferred to ion transport modeling in ion-exchange membranes and has been found to show remarkably good results [Kam2016b]. The further implementation of this model, however, was out of the scope of this work.

Regardless of possible further improvements of the process model presented here, the results already achieved in this still-simplified state are very good, as the further validation results illustrate, which are described in the following.

### 8.3.6. Validation - Influence of flow-electrode flow rate and activated carbon loading

For further validation, the model was fitted to experimental results obtained for continuous FCDI systems in two-module and single-module configuration, which are the same as described in Chapter 6. The parameters were chosen based on the applied membrane and activated carbon materials and the assumptions described

above. In Figure 8.9, experimental results for FCDI systems in two-module and single-module configuration are plotted, as well as the corresponding simulation results.

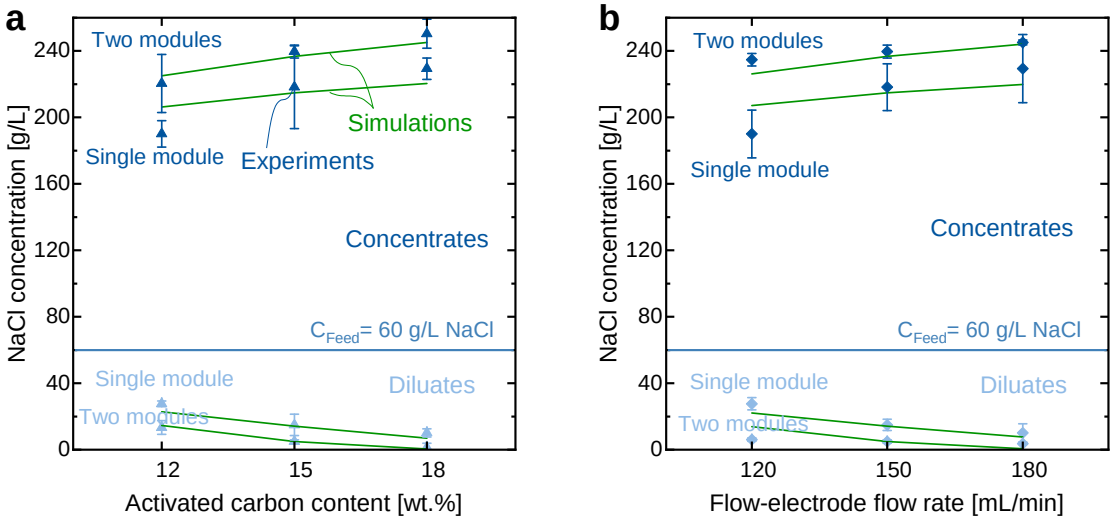


**Figure 8.9.:** Results of experimental measurements (blue symbols) in comparison to simulation results (green lines) for experiments in continuous FCDI systems in two-module and single-module configuration. Variation of (a) the activated carbon content in the flow electrodes and (b) the flow-electrode flow rate. The error bars indicate discrepancies in the mass balance between diluate and concentrate stream, as an indicator for experimental measurement inaccuracies.

The desalination and concentration performance displayed in Figure 8.9 increases with increasing activated carbon content and flow rate of the flow electrodes. This is the same trend identified with the previous model [Rom2018b]. For the simulations, the parameters were kept the same. Only for the differentiation between the single-module and two-module system the water transfer rate was adjusted to match experimental results. In general, the fits are relatively good especially for the diluate concentrations. The feed flow rates in the experiments as well as the corresponding simulations were chosen as 1 mL/min for the diluate and 0.04 mL/min for the concentrate, which leads to a high water recovery and high salt concentration in the concentrate product stream. The model predicted this well. The flow rates naturally lead to larger deviations in the concentrate product streams.

All in all, the trends are predicted correctly and the predicted current efficiencies and electrical currents are in the correct range. However, the slopes of the simulation curves do not exactly match the experimental results. Possible reasons for this are: (1) Measurement inaccuracies in the experiment: the error bars in Figure 8.9 indicate the range of deviations observed in the mass balance

between diluate and concentrate, (2) preparation inaccuracies regarding the carbon slurries: a slight deviation in the activated carbon percentage may lead to a significant deviation from the predicted results, and (3) changing conditions between the different experimental settings, which may have to be met by adjusted parameters. As an example: The simulation results at 12 wt.% activated carbon seem to excel all experimental results. This could be an indications for a less effective charge transfer in the actual experiment, which may have to be met by an adjustment of $C_{St}$ in the simulation.

## 8.4. Summary and conclusions

The transport phenomena in both, ion-exchange membranes and flow electrodes, are complex by itself, and are studied intensively. In FCDI, the combination of ion-exchange membranes and flow electrodes leads to complex interactions and dependencies, which are not yet fully understood. To extend our understanding of the potential of the FCDI technology, the use of a process model is vital. The process model presented in this chapter is an improved version of the model published by our work group in 2018 [Rom2018b]. The new model can simulate continuous FCDI processes with ion-exchange membranes, including the transport of coions and water through the membranes, and hence the treatment of concentrated salt solutions.

The model was verified using experimental results, and sensitivity analyses were performed to investigate the influence of different input parameters on the simulation results. The simulation results with input parameters based on experimental settings show good agreement with experimental results. The model can serve as a tool for extending the understanding of continuous FCDI processes, as well as for the target-oriented development and optimization of FCDI processes. Next to process parameters, the model can predict the performance of ion-exchange membranes with different characteristics in specific process settings, and hence can be of help in developing tailored ion-exchange membranes. In combination with experimental studies, this process model can pave the way towards the practical application of FCDI processes.

**Table 8.2.:** Model validation: Overview of experimental/simulation settings and results. Membrane parameters based on manufacturers data sheet (fumasep FAB-PK-130/FKB-PK-130) and values published by Kingsbury et al. [Kin2018].

| | | **Experiment FAB/FKB** | **Sim. 1 no $\sigma$** | **Sim. 2 with $\sigma$** |
|---|---|---|---|---|
| *Settings experiment/simulations and membrane characteristics* | | | | |
| **Feed** | mL/min | 60 | ” | ” |
| **Diluate feed** | mL/min | 1 | ” | ” |
| **Flow electrode** | mL/min | 180 | ” | ” |
| **Activated carbon** | wt.% | 15 | ” | ” |
| **Concentrate feed** | mL/min | 0.04 | ” | ” |
| **CV Potential** | V | 1.2 | ” | ” |
| **Water uptake** | wt.% | 5-30 | ” | ” |
| *Results experiments/simulations* | | | | |
| **Diluate** | mL/min | 0.785 | 0.806 | 0.794 |
| **NaCl Diluate** | g/L | 4.66 | 8.64 | 4.32 |
| **Concentrate** | mL/min | 0.24 | 0.24 | 0.25 |
| **NaCl Concentrate** | g/L | 229.3 | 224.1 | 228.1 |
| **Current** | A | 1.496 | 1.696 | 1.655 |
| **CE** | eff / real | 0.86 / 1 | - / 0.864 | - / 0.944 |
| **Water transfer** | mol/mol | 10.7 | set | set |
| *Simulation settings* | | | | |
| **Stern capacity** | F/mL | | 23.3 | 23.3 |
| **Permeance A** | | | 0.35 | 0.35 |
| **E.osmotic transfer** | mol/mol | | 10.5 | 10.5 |
| **AEM resistance** | $\Omega \cdot m^2$ | | 3.5 | 3.5 |
| **CEM resistance** | $\Omega \cdot m^2$ | | 2.5 | 2.5 |
| **Mem. thickness** | $\mu$m | | 110 | 110 |
| **X- AEM** | eq/L | | 14.5 | 14.5 |
| **X- CEM** | eq/L | | 12.1 | 12.1 |
| **Mem. pore diameter** | nm | | - | 3.5 |
| **AEM swelling factor** | nm | | 0.15 | 0.15 |
| **CEM swelling factor** | nm | | 0.2 | 0.2 |
| *Simulation results at cell outlet* | | | | |
| **$\sigma$-factor, AEM Diluate** | - | | 1 | 0.69 to 0.37 |
| **$\sigma$-factor, CEM** | - | | 1 | 0.70 to 0.42 |
| **$\sigma$-factor, AEM Conc.** | - | | 1 | 0.71 to 0.76 |
| **$D_{Cl-,AEM}$, Diluate** | $m^2/s$ | | $1.38 \cdot 10^{-11}$ | $1.38 \cdot 10^{-11}$ |
| **$D_{Na+,AEM}$, Diluate** | $m^2/s$ | | $8.55 \cdot 10^{-11}$ | $1.06 \cdot 10^{-12}$ |
| **$D_{Na+,CEM}$** | $m^2/s$ | | $1.60 \cdot 10^{-11}$ | $1.60 \cdot 10^{-11}$ |
| **$D_{Cl-,CEM}$** | $m^2/s$ | | $2.59 \cdot 10^{-11}$ | $4.14 \cdot 10^{-12}$ |
| **$D_{Cl-,AEM}$, Conc.** | $m^2/s$ | | $1.38 \cdot 10^{-11}$ | $1.38 \cdot 10^{-11}$ |
| **$D_{Na+,AEM}$, Conc.** | $m^2/s$ | | $8.55 \cdot 10^{-12}$ | $4.76 \cdot 10^{-12}$ |

# List of abbreviations and symbols, Chapter 8

| | | |
|---|---|---|
| **Parameters** | $[\kappa_{AC}]$Specific conductivity of activated carbon | $[S/m]$ |
| $\kappa_{water}$ | Specific conductivity of distilled water | $[S/m]$ |
| $\lambda^{\infty}$ | Molar conductivity at infinite dilution | $\left[m^2/mol \cdot \Omega\right]$ |
| $\omega$ | Membrane sign (+1 for AEM, -1 for CEM) | $[-]$ |
| $\rho$ | Mass density | $\left[kg/m^3\right]$ |
| $A$ | Water permeance of the membranes | $\left[m^3/(m^2 \cdot s \cdot Pa)\right]$ |
| $C$ | Stern capacity | $\left[F/m^3\right]$ |
| $D$ | Diffusion coefficient | $\left[m^2/s\right]$ |
| $D_0$ | Ion diffusion coefficient in solution | $\left[m^2/s\right]$ |
| $d_{pore}$ | Average membrane pore diameter | $[m]$ |
| $F$ | Faraday constant | $[J/(C/mol)]$ |
| $h$ | Height of channels | $[m]$ |
| $h$ | Number of hydrations per salt ion | $[-]$ |
| $h_{mem}$ | Membrane thickness | $[m]$ |
| $K$ | Kohlrausch coefficient | $\left[m^{3.5}/(mol^{1.5} \cdot \Omega)\right]$ |
| $M$ | Molar mass | $[Kg/mol]$ |
| $R$ | Ideal gas constant | $[J/(K \cdot mol)]$ |
| $r_{mem}$ | Ohmic resistance of the membrane | $\left[\Omega \cdot m^2\right]$ |
| $u$ | Ion mobility coefficient | $\left[m^2/s\right]$ |
| $v$ | van't Hoff coefficient | $[-]$ |
| $V_t$ | Thermal voltage | $[V]$ |
| $V_{cell}$ | Total cell potential | $[V]$ |
| $V_{reservoir}$ | Volume of the water reservoir | $\left[m^3\right]$ |
| $v_w$ | Water uptake of the membrane | $[-]$ |
| $X$ | Ion-exchange capacity | $\left[eq/m^3\right]$ |
| $z$ | Ion valence | $[-]$ |

**Sub- and superscripts**

| | |
|---|---|
| $a/c$ | Anode & Cathode |
| $AEM$ | Anion exchange membrane |
| $CEM$ | Cation exchange membrane |
| $Don$ | Donnan |

| | |
|---|---|
| *electroosm* | Electroosmotic |
| $i$ | Index for different ions |
| *in* | Incoming |
| $k$ | Index for different flow channels |
| *macro* | Macropore |
| *mem* | Membrane |
| *micro* | Micropore |
| *ohmic* | Ohmic |
| *osm* | Osmotic |
| *out* | Existing |
| *sol* | Solution |
| *St* | Stern |
| *trans* | Transport |
| $w$ | Water |

**Variables**

| | | |
|---|---|---|
| $\Delta\varphi$ | Potential difference | $[V]$ |
| $\dot{m}$ | Mass flow | $[kg/s]$ |
| $\dot{n}$ | Molar flow | $[mol/s]$ |
| $\dot{V}$ | Volumetric flowrate | $\left[m^3/s\right]$ |
| $\kappa$ | Specific conductivity | $[S/m]$ |
| $\lambda$ | Molar conductivity | $\left[m^2/mol \cdot \Omega\right]$ |
| $\lambda_D$ | Debye length inside the membrane's pores | $[m]$ |
| $\sigma$ | Charge density | $\left[eq/m^3\right]$ |
| $\sigma$ | Water uptake correction factor for coions | $[-]$ |
| $c$ | Molar concentration | $\left[mol/m^3\right]$ |
| $i$ | Current density | $\left[A/m^2\right]$ |
| $j$ | Ion flux across membrane | $[mol/s]$ |
| $n$ | Amount of ions | $[mol]$ |
| $r$ | Molar reaction rate | $[mol/s]$ |
| $r_{red,highC}$ | Reduced pore radius on the high concentration side | $[m]$ |
| $r_{red,lowC}$ | Reduced pore radius on the low concentration side | $[m]$ |
| $T$ | Temperature | $[K]$ |
| $t$ | Time | $[s]$ |
| $v_{sc}$ | Fraction of water channel inside membrane accessible for coions | $[-]$ |

# 9

# FCDI - The new alternative for water treatment? A compendium.

This chapter presents a summary of the results presented in this thesis, attempts a discussion of their relevance and impact, and outlines possible topics for further research and development.

## 9.1. Topics of this thesis: Summary and outlook

Effective electronic and ionic charge transfer and transport, as well as effective mass transport, are vital for flow-electrode based systems. Chapter 4 investigates the factors influencing the charge transfer and transport in suspension-based flow electrodes. An equivalent circuit model is developed, which can be fitted to all experimental results. A charge percolation threshold, above which an effective charge transfer leads to an improved salt adsorption, is evident. Unlike the particle size distribution, the pore size distribution of the activated carbon is found to have a major influence on the desalination performance. The carbon samples with a significant amount of mesopores, additional to micropores, showed an overall improved performance. A high cumulative pore volume is concluded to lead to an increased volume fraction of the activated carbon within the flow electrode. This leads to an increased carbon outer volume fraction, an improved charge percolation and hence an improved desalination.

Apart from this, the possibility to use electrochemical impedance spectroscopy (EIS) measurements to adjust the performance of flow-electrode suspensions made of different activated carbons is demonstrated. Herewith, this study establishes a foundation for an application of EIS as predictive characterization method for flow-electrode materials, e.g. for incoming goods inspection, especially in the context of water treatment. The combination of EIS measurements with viscosity measurements provides and effective screening method for optimal carbon materials for flow electrodes.

The results presented in this chapter are generally valuable for application as carbon characterization method for application in technologies using flow electrodes. EIS may be applied for on-line process monitoring and control of the flow-electrode performance in various processes. It can also serve as direct, easy in-line method for the characterization of carbon suspensions in general, consid-

ering the actual wetting and agglomeration conditions in-situ.

In Chapter 5, the possibility to continuously recover energy from charged flow electrodes is demonstrated in FCDI processes for the first time. It is demonstrated that continuous FCDI processes can desalinate and concentrate brine streams significantly in a single pass, while most electrodialysis (ED) processes described in the literature treated brine streams in many steps or in batch mode.

The performance and specific energy demand of FCDI systems in different process layouts, including the energy required for pumping flow-electrodes, is investigated. Among the tested FCDI systems, the continuous single-module layout was identified as the most energy efficient and most promising for an actual application. A first intermediary comparison to state-of-the-art desalination methods is attempted, which at the time served as a guidepost for further works aiming at developing a better understanding of FCDI processes and at making it competitive.

An experimental study is presented in Chapter 6, which focuses on developing a deeper understanding of salt and water transfer in the treatment of high salinity solutions using continuous FCDI processes. Two continuous FCDI process layouts, the two-module and single-module configuration, are directly compared regarding the water and salt transfer within the system. The results give an indication of the contribution of osmotic and electroosmotic effects to the overall water transfer.

Based on the observations made in Chapters 5 and 6, four concepts for achieving a further reduction of the energy demand of FCDI processes are presented and tested in Chapter 7. While the incorporation of ion-exchange resins is only possibly promising in the desalination down to very low salinities, the use of multiple cell pairs is a very promising approach to reduce the impact of the voltage drop over the flow electrodes. The experimental results show a significant reduction in the energy demand. Desalination down to very low salinities has been demonstrated for the continuous two-module and single-module FCDI system. An open question is, whether the approach of multiple cell pairs also enables desalination down to very low salinities in a single step. A theoretical analysis demonstrates the possible potential of reducing the membrane resistance to further improve such multiple cell pair FCDI systems.

The use of thinner, unreinforced membranes of reduced resistance, however, leads to a strongly increased water transfer. This negates the advantage of the reduced electrical resistance due to a significant deterioration of the concentration performance. The coating of the ”standard membranes” applied in this work, on the other hand, leads to a significant improvement of the concentration performance due to a significant reduction of the water transfer. The presented coating

is promising for the application in ion-exchange membrane processes aiming at the concentration of saline solutions, which especially suffer from pronounced water transfer.

It is clear that many factors influence the performance of an FCDI system. The interrelations of the different physical and chemical phenomena are complex. Hence, an improved process model is presented in Chapter 8, which may serve as a tool to systematically analyze and quantify the impact of the different phenomena and hence further improve the performance of FCDI processes. The model is suitable for the simulation of continuous FCDI processes for the treatment of high salinity solutions. The process model is verified using experimental results. Sensitivity analyses are performed to investigate the influence of different input parameters on the simulation results. A modified version of the Meares model is implemented for the determination of ion diffusion coefficients in ion-exchange membranes bordered by two solutions of significantly different salinities, which leads to an improved agreement with experimental results. The simulation results with input parameters based on experimental settings show a very good agreement with experimental results.

The model can serve as a tool for extending the understanding of continuous FCDI processes, as well as for the target-oriented development and optimization of FCDI systems. Next to process parameters, the model can predict the performance of ion-exchange membranes with different characteristics in specific process settings, and hence can be of help in developing tailored ion-exchange membranes. In combination with experimental studies, this process model, and hence this thesis, can pave the way towards the practical application of FCDI processes.

**Outlook.** Regarding the impedance spectroscopy study focusing on charge transfer in flow electrodes presented in Chapter 4, further scientific insight could be achieved by developing a more detailed equivalent circuit model in the future. An improved equivalent circuit model should distinguish between the influence of internal and external diffusion. A thorough understanding of the charge and ion transfer within flow electrodes will help in designing efficient and cost-effective cells and finding the optimal carbon material.

Several concepts were presented, which have the potential of improving the performance and reducing the energy demand of continuous FCDI processes. These concepts should be tested in application-oriented settings, with ”real” wastewater, to test the feasibility of the presented concepts. Depending on the case and aim of the application, combinations of the concepts may be advantageous. In case of the multiple cell pair approach, it should be investigated whether a stronger

desalination is possible. Additionally, it may be relevant to test the applicable, safe voltage window depending on the application, for example by using linear sweep voltammetry. A small extension of the voltage window may lead to the feasible application of additional cell pairs, and hence savings regarding the cost and energy demand. Finally, the presented process model can be a helpful tool for the optimization of FCDI processes. Although it is still based on simplified assumptions, it can already predict a large part of the complex interactions in FCDI processes.

Within the process model, the introduction of the $\sigma$-factor led to a significant improvement of the simulation results. Even better results may be achieved by implementing equations for determining the ion and water transport through the membrane based on the Maxwell-Stefan approach [Ted2017]. Alternatively, it may be instrumental to apply the Manning condensation theory for the transport of ions through the ion-exchange membranes, as suggested by Kamcev et al. [Man1969; Kam2016b]. This approach can also model non-ideal behaviour of ions in ion-exchange membranes. In most works, including this thesis, ideal activity coefficients of 1 are assumed, which is unlikely to be the case in reality. Recent works have found that Manning‘s model for counterion condensation on polyelectrolytes in solution can also be transferred to ion transport modeling in ion-exchange membranes and has been found to show remarkably good results [Kam2016b].

## 9.2. The overall energy demand - Comparing FCDI to state-of-the-art technologies

The following sections attempt to evaluate the current state of the FCDI technology and compare it to state-of-the-art technologies.

### 9.2.1. Comparing FCDI and mechanical vapor compression

The improvements achieved by the concepts presented in Chapter 7 are significant and illustrate the extant potential of the FCDI technology. Figure 9.1 gives an overview of the best results regarding the energy demand achieved using the proposed concepts presented in Chapter 7. The results are compared to literature values for mechanical vapor compression [Thi2015] and to results achieved by FCDI systems with energy recovery, as presented in Chapter 5.

The energy demand for the production of one cubic meter of desalinated water using different FCDI systems and mechanical vapor compression (MVC) is

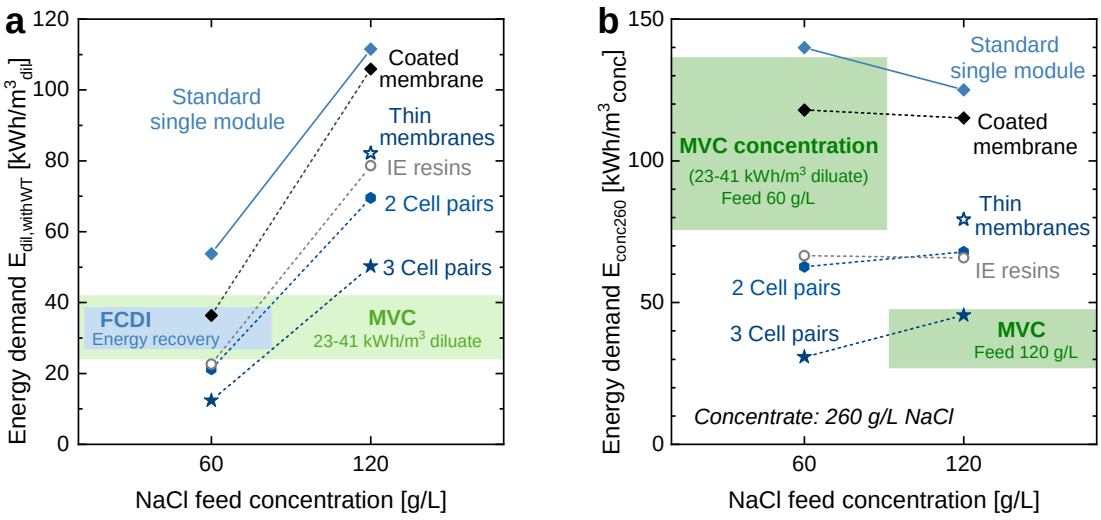


**Figure 9.1.:** Results of FCDI concept experiments in direct comparison with mechanical vapor compression (MVC) [Thi2015] and FCDI with energy recovery (Chapter 5, [Rom2018a]).

plotted in Figure 9.1 (a). Figure 9.1 (b) shows results for the energy demand when normalized per one cubic meter of produced concentrate at 260 g/L NaCl. All values consider the increased energy demand due to water transfer from the diluate to the concentrate channel.

The energy demand scales with increasing feed concentration in case of desalination, which is consistent for all desalination technologies driven by an electrical field. However, in case of FCDI the energy demand for concentration is fairly independent from the feed concentrations of 60 g/L or 120 g/L NaCl.

To achieve a reduced energy demand it is vital to reduce the cell voltage. This can be achieved by reducing the applied voltage, for example to 0.6 V, as is the case for the result for the ion-exchange resins. Another approach is to use two or more cell pairs, which leads to a division of the voltage drop over the flow electrode by the number of cell pairs. The electrical current stays relatively constant, while the product volume stream is doubled or tripled, leading to a significant reduction of the energy demand per product volume. A reduction of the cell voltage or the use of two cell pairs have a comparable effect regarding the energy demand, while the desalination performance reduces significantly in case of the reduced overall cell voltage.

Compared to FCDI with energy recovery, the use of multiple cell pairs is a more efficient approach, as it enables (1) a better desalination and concentration performance, (2) a higher current density, is (3) generally more stable and reliable in operation, and (4) enables a stronger reduction of the energy demand (Figure 9.1 (a)).

The use of ion-exchange resins does not make a significant difference in the chosen settings. However, it may be feasible to apply ion-exchange resins in the diluate channels when aiming at very low product salinities. While thinner, unreinforced membranes exhibited a reduced ohmic resistance, the water transfer was increased so significantly that the advantage of the lower resistance is lost. In fact, the overall performance was worse than the here applied "standard" membranes. The application of an additional crosslinked coating on the membrane, on the other hand, surprisingly led to only a barely measurable increase in the ohmic resistance, while enabling a measurable reduction of the water transfer. This leads to an improved concentration performance and reduced energy demand, which makes the presented membrane coating promising for the recovery and concentration of salts.

The results regarding continuous FCDI systems presented in this thesis are promising and show extant potential. When comparing the results to MVC, FCDI is competitive with MVC at the lower feed salinity of 60 g/L regarding the energy demand. At higher feed salinities, the energy demand for concentration via FCDI is barely able to reach values comparable to MVC. However, considering the given potential of FCDI, this may change in the future. An open question is, whether FCDI can become competitive with state-of-the-art technologies, such as MVC, regarding the investment and operating costs, and whether the approach of multiple cell pairs also allows the single-pass desalination of concentrates to very low salinities.

### 9.2.2. Comparing FCDI and electrodialysis

Electrodialysis (ED) is the most obvious technology, which the continuous FCDI processes presented in this thesis would be compared with. However, based on the data available in literature, a direct comparison is challenging. Hence, experiments were performed with the aim to collect directly comparable data for FCDI and ED experiments, as described in the following.

**Materials and methods.** For the experiments one FCDI and one ED cell were assembled, which each comprise three cell pairs, as described in Chapter 7 for FCDI systems. In this case, the membranes separating the feed streams from the electrolyte rinse solutions or flow electrodes were two cation-exchange membranes. The inner, alternating membranes separating the feed solutions were three anion-exchange membranes and two cation-exchange membranes. Both cells were based on the ED-100 layout distributed by the Fumatech BWT GmbH. The electrodialysis stack consisted of an ED-100 cell with three cell pairs, while the FCDI cell used the layout of endplates and graphite plates with flow channels

as described in the previous chapters of this thesis. The applied membranes were Fumasep FKB-PK-130/ED-100 and Fumasep FAB-PK-130/ED-100. Standard ED-100 mesh spacers with a thickness of 0.5 mm (Fumatech BWT GmbH) were used in both cells. The pumps and power sources were the same as described earlier in this thesis.

Two sets of experiments were performed with the above described settings. First, IV-curves were measured using the same procedure as described in Chapter 7. Second, desalination experiments with feed flow rates of 1 mL/min per diluate flow channel and 0.04 mL/min per concentrate flow channel were performed. The FCDI system was operated at a constant voltage of 1.2 V. For the electrodialysis system, the required voltage to achieve the same current as in the FCDI system was determined in a preliminary experiment, following which the desalination experiment was performed at a constant voltage of 3.67 V. The experimental parameters and results of the desalination experiments are given in Table 9.1. Samples were taken during steady-state operation of the systems to confirm the salinities of feed, diluate and concentrate solutions.

**Table 9.1.:** Settings and results of desalination experiments with an FCDI and an electrodialysis setup in direct comparison.

| | | **FCDI** | **Electrodialysis** |
|---|---|---|---|
| Electrical current | $A$ | 0.87 | 0.87 |
| **Potential at current collectors** | $V$ | 1.2 | **3.67** |
| Feed | $g/L\ NaCl$ | 60 | 60 |
| Diluate | $g/L\ NaCl$ | 33.3 | 35.6 |
| Concentrate | $g/L\ NaCl$ | 208.3 | 204.4 |
| Number of cell pairs | - | 3 | 3 |
| Feed Diluate (per flow channel) | $mL/min$ | 1 | 1 |
| Diluate | $g/L\ NaCl$ | 0.87 | 0.82 |
| Feed Concentrate (per flow channel) | $mL/min$ | 0.04 | 0.04 |
| Concentrate | $g/L\ NaCl$ | 0.25 | 0.18 |
| Current efficiency | - | 0.98 | 0.97 |
| **Energy demand desalination** (incl. water transfer) | $kWh/m^3$ | 14.93 | **53.01** |

**Results and discussion.** Figure 9.2 shows experimental results and theoretical calculations directly comparing FCDI and ED systems. Figure 9.2 (a) shows the resulting IV-curves of the elctrodialysis and the FCDI system. The results of theoretical calculations presented in Figure 9.2 (b) are based on the same assumptions as given in Paragraph 7.1.1.

The IV-curves plotted in Figure 9.2 (a) illustrate the main difference between

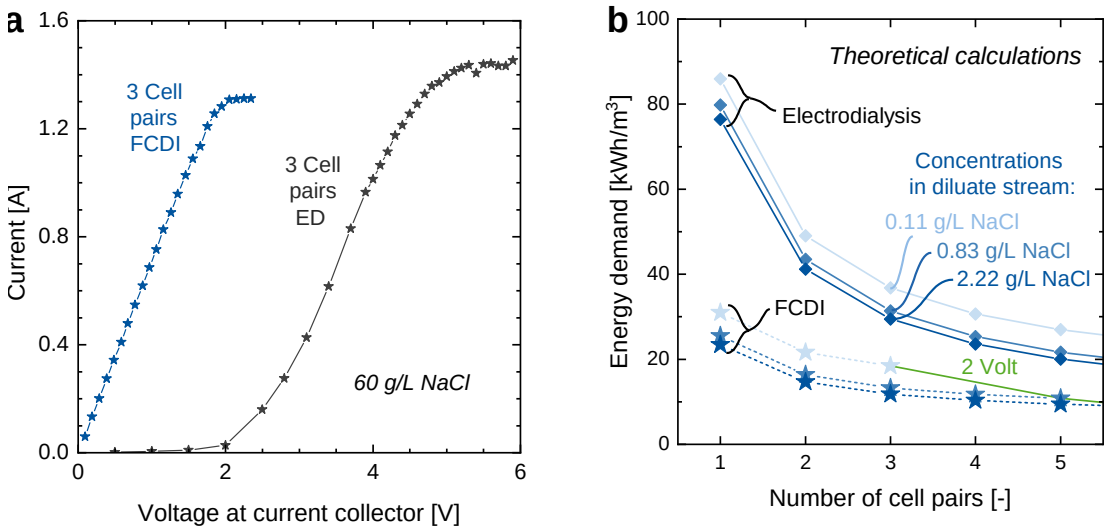


**Figure 9.2.:** Results of experiments directly comparing the performance of FCDI system and an electrodialysis (ED) using the same membrane type, spacer type, cell pair number and feed flow rates. (a) Current-voltage characteristics and (b) results of desalination experiments comparing the FCDI to the ED system.

FCDI and ED well. The slopes in the ohmic region are very similar and the systems reach a very similar limiting current density. However, while the FCDI system produces a linear IV-curve which goes through the origin in the Ohmic region at lower voltages, there is basically no electrical current flowing through the electrodialysis system at low voltages. At around 2 V, the electrical current starts to increase, passing over into a linear increase in the ohmic region. The reason for this is the overpotential required by the electrodes of the electrodialysis system. In contrast to the FCDI system, which relies on the capacitive adsorption of ions on the flow-electrode surface, the electrodes of the electrodialysis system require faradaic reactions to achieve the transition from ionic current to electrical current.

Table 9.1 shows the results of the desalination experiments directly comparing FCDI and ED. The results show that the FCDI and ED system were able to achieve nearly identical desalination and concentration results and current efficiencies when operated at the same electrical current density. The main difference is, as seen before in the IV-curves, the significantly higher voltage required to run the faradaic reactions at the electrodes. For this specific experiment, the ED system required a voltage increase of nearly 2.5 V in comparison to the FCDI system. This leads to a significant increase in the energy demand.

To reduce the impact of the electrode voltage drop, the electrodialysis stacks used for industrial applications usually consist of dozens or even hundreds of

cell pairs. This way, the voltage drop over the electrode does not have such a significant impact on the overall energy demand anymore. However, such large stacks suffer from different restrictions, such as ionic shortcut currents through feed and drain channels [Vee2008]. Due to this, it may be advantageous in some cases to be able to operate a desalination/concentration cell efficiently and economically even when using a low number of cell pairs, using a well-designed cell. The plots in Figure 9.2 (b), which show the energy demand for FCDI and ED systems depending on the number of cell pairs, illustrate this. For both systems, a significant reduction of the energy demand is achievable by increasing the number of cell pairs to more than one. In case of FCDI, the voltage drop over the electrodes is much smaller and does not require a starting potential, which leads to the significantly lower energy demand and the lower decrease with increasing number of cell pairs. As per the theoretical calculations, the increase to more than three cell pairs improves the energy demand only to a small extent. In case of electrodialysis, a much higher number of cell pairs is theoretically required to reach the same energy demand as FCDI. At a number of five cell pairs, the energy demand of the electrodialysis system is similar to the FCDI system at one cell pair, not accounting for the pumping energy.

Apart from this, electrodialysis stacks require electrochemical reactions at the electrodes to convert the electrical current in the outside circuits into the ionic current within the cell. Next to gas evolution and the associated safety risks, the chemical reactions occuring at the electrodes can lead to unwanted side reactions, which may be undesired in case of specific applications, e.g. involving susceptible chemicals or mixtures. In this regard, FCDI processes may be advantageous for certain applications.

**Concluding - Open questions.** In this thesis, it is demonstrated that FCDI can reach very high desalination and concentration rates. Even at high salinities of 60-120 g/L NaCl, continuous single-pass FCDI processes can reach high water recoveries of around 80 %. There are electrodialysis studies available, in which single-pass electrodialysis processes are applied for salt concentration up to very high salinities [Tan2003]. In Japan, electrodialysis is, or was, applied for salt production from seawater in combination with thermal concentration and crystallization [Yam1969; Tur2002]. The combination of salt production and desalination is challenging. Marian Turek [Tur2002] published a study attempting this in 2002. Several of his publications focused on the treatment of high salinity solutions using electrodialysis processes. However, reaching very low salinities in the diluate is challenging and limited by factors such as increased resistances and high concentration gradients across the membranes. Such processes do not

yet seem to be widely applied. The continuous FCDI processes presented in this thesis show potential for such applications. The question is, why are electrodialysis systems not yet widely applied for such applications? Is the reason a matter of possibility, are there economical reasons, or something else? And finally: can FCDI processes be advantageous over existing processes in practical applications, such as brine desalination and concentration?

During the comparison of the single cell pair FCDI system to multiple cell pair FCDI systems, a moderate desalination percentage was chosen for the initial study (Chapter 7) to be able to see differences well and not be limited by the simple absence of salt in the diluate stream towards end of the cell. In this case, only a small reduction of the desalination performance was observed when increasing to a higher number of cell pairs. However, as already indicated by the reduced limiting current densities visible in the IV-curves, there seems to be a limitation to multiple cell pair systems when aiming at higher desalination degrees. This may be the result of one or both of the following possible reasons:

- Unequal distribution of the feed flow between the different cell pairs, leading to unequal flow rates in the separate cell pairs and varying maximum currents. Hence, the overall current is limited by the cell pair with the lowest flow rate. Due to this, a multiple cell pair system may not reach the desalination degree of a single cell pair system.
- The beneficial effect of flow electrodes on the water and ion transfer in continuous FCDI systems is so significant that it is completely lost when using more than one cell pair. Back diffusion and water transfer due to the high concentration gradients over the inner membranes lead to a significant deterioration of the desalination performance.

Based on this, it may be a matter of possibility that there are only few electrodialysis studies demonstrating a good desalination and concentration performance in a single-pass system, close to the performance achieved for continuous FCDI systems presented in this thesis. On the other hand, the simultaneous desalination and concentration may have been investigated by some, but not published, and the achieved metrics such as the current density deemed too low to be able to operate such a system economically.

This thesis cannot give a final reply. However, the experimental results presented here, the improved understanding of the system interrelations, as well as the improved process model, can serve as a foundation to investigate this further. Possibly, this will lead to an extension of the industrial process engineering toolbox by a new process called flow-electrode capacitive deionization in the future.

# A
# Appendix

## A.1. Results: First EIS measurements in an FCDI cell

For an initial understanding of the behaviour of such systems a range of parameter studies were performed, as described in the main manuscript. Figure A.1 shows additional results obtained at higher activated carbon contents. The experiments described in this section were performed with the activated carbon Carbopal SC11PG.

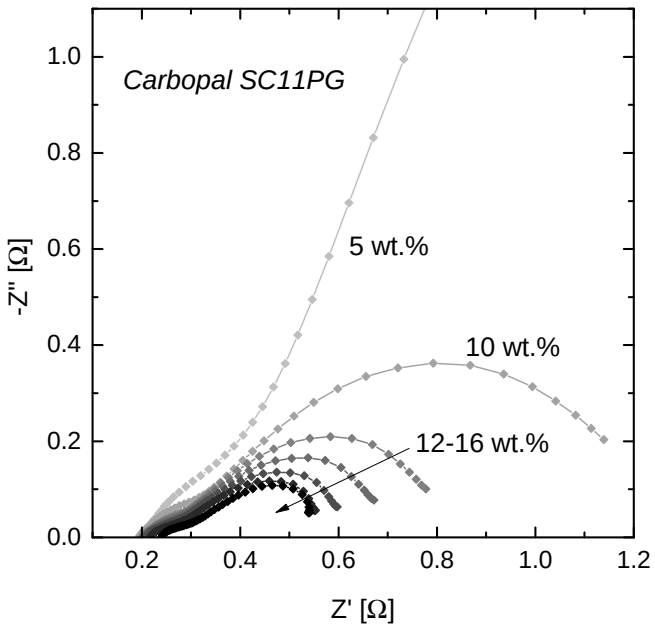


**Figure A.1.:** Results of EIS measurements; Variation of the activated carbon content with a constant NaCl concentration of 60 g/L in both water channel and flow-electrode and a flow-electrode pump rate of 150 mL/min.

# A.2. Results of fitting the equivalent circuit model to results of EIS measurements

### Influence of the activated carbon content

The activated carbon content was varied between 0-16 wt.%, while all other parameters were kept constant. The experiments were performed with a NaCl concentration of 60 g/L in flow-electrodes as well as the feed, the pump for the flow-electrodes was set to 150 mL/min and a salt water flow rate of 13 mL/min. Table A.1 gives an overview of EIS fit results fitted to the results of the above described experiments using the equivalent circuit model described in the main manuscript.
The corresponding experimental results are plotted in Figure 3 (a) of the main manuscript. The trends regarding $C_{dl}$ and $R_{cp2}$ are plotted in Figure 8 and discussed in the main manuscript.
The two sets of experiments were conducted several weeks apart. The cell has been used for several desalination experiments before the second set of experiments. The deposition of activated carbon in dead zones in the cell may explain the significant difference in $C_{cc}$ between the two sets of experiments, while the overall capacitance ($C_{cc}$ + $C_{dl}$) is very similar in both cases. The significant difference in $R_{cp2}$ at 0 wt.% and 0.5 wt.% between the two sets of experiments may be explained by the order the experiments were conducted. In the first set we reduced the weight percentage gradually. In the second set of experiments the cell was rinsed well before starting, and the weight percentage of carbon in the flow-electrode then increased gradually. The lower amount of activated carbon traces in the cell in case of the experimental set two led to a significantly increased $R_{cp2}$ at 0 wt.% and 0.5 wt.% activated carbon. At these concentrations carbon traces left in the dead zones of the cell from previous experiments would have the most significant influence.

**Table A.1.:** Overview of EIS fit results. Variation of activated carbon concentration in flow-electrode at constant pump rate of 150 mL/min.

| **AC conc.** | $\chi^2$ | $\mathbf{R}_{CC}$ | $\mathbf{C}_{CC}$ | $\mathbf{R}_{CP1}$ | **CPE -T** | **CPE -P** | $\mathbf{R}_{CP2}$ | $\mathbf{C}_{DL}$ | $\mathbf{R}_S$ |
|---|---|---|---|---|---|---|---|---|---|
| % | | Ω | F | Ω | | | Ω | F | Ω |
| **clean cell** | 0.00064 | 0.088 | 0.022 | - | 0.085 | 0.91 | - | - | 0.265 |
| **0** | 0.00011 | 0.081 | 0.86 | - | 1.9 | 0.5 | 77.5 | 2.29 | 0.216 |
| **0.5** | 0.00034 | 0.062 | 1.4 | - | 1.7 | 0.5 | 16.5 | 2.80 | 0.203 |
| **5** | 0.00047 | 0.071 | 0.68 | - | 2.4 | 0.5 | 6.0 | 3.82 | 0.197 |
| **5** | 0.00031 | 0.071 | 0.68 | $1.6{\cdot}10^{10}$ | 2.4 | 0.5 | 6.0 | 3.82 | 0.197 |
| **10** | 0.00026 | 0.037 | 0.43 | 0.60 | 2.4 | 0.5 | 0.47 | 7.62 | 9.194 |
| *Second set of experiments* | | | | | | | | | |
| **0** | 0.00025 | 0.099 | 3.9 | - | 2.1 | 0.5 | 123.1 | 1.28 | 0.212 |
| **0.5** | 0.00014 | 0.065 | 3.7 | - | 2.4 | 0.5 | 76.4 | 1.71 | 0.207 |
| **1** | 0.00016 | 0.063 | 3.2 | - | 2.3 | 0.5 | 64.5 | 1.78 | 0.207 |
| **2** | 0.00017 | 0.061 | 3.0 | - | 2.3 | 0.5 | 40.0 | 1.84 | 0.207 |
| **3** | 0.00027 | 0.063 | 3.3 | - | 2.1 | 0.5 | 20.9 | 1.87 | 0.208 |
| **3** | 0.00028 | 0.063 | 3.3 | $6.0{\cdot}10^{19}$ | 2.1 | 0.5 | 20.9 | 1.87 | 0.208 |
| **4** | 0.00015 | 0.085 | 3.4 | - | 2.1 | 0.5 | 9.7 | 1.93 | 0.219 |
| **4** | 0.00015 | 0.085 | 3.4 | $1.1{\cdot}10^{12}$ | 2.1 | 0.5 | 9.7 | 1.93 | 0.219 |
| **5** | 0.00010 | 0.082 | 3.1 | 6.2 | 2.0 | 0.5 | 5.1 | 2.06 | 0.220 |
| **6** | 0.00011 | 0.081 | 2.9 | 2.5 | 1.9 | 0.5 | 2.8 | 2.29 | 0.221 |
| **7** | 0.000097 | 0.071 | 2.8 | 1.4 | 1.8 | 0.5 | 1.7 | 2.61 | 0.221 |
| **8** | 0.00011 | 0.061 | 2.7 | 0.97 | 1.7 | 0.5 | 1.1 | 3.10 | 0.223 |
| **9** | 0.00016 | 0.051 | 2.8 | 0.76 | 1.5 | 0.5 | 0.71 | 3.73 | 0.225 |
| **10** | 0.00022 | 0.046 | 3.4 | 0.61 | 1.4 | 0.5 | 0.50 | 4.40 | 0.230 |

Abbreviations see Figure 4.7, Chapter 4.

### Influence of the flow-electrode pump rate

The flow-electrode flow rate was varied between 0-175 mL/min, while all other parameters were kept constant. The experiments were performed with a NaCl concentration of 60 g/L in flow-electrodes as well as the feed and an activated carbon content of 10 wt.% Carbopal SC11PG. The salt water flow rate was set to 13 mL/min. Table A.2 gives an overview of EIS fit results fitted to the results of the above described experiments using the equivalent circuit model described in the main manuscript. The corresponding experimental results are plotted in Figure 3 (b) of the main manuscript.

**Table A.2.:** Overview of EIS fit results. Variation of flow-electrode pump rate at constant activated carbon concentration of 10 wt% Carbopal SC11PG.

| **Pump rate** mL/min | $\chi^2$ | $\mathbf{R}_{CC}$ Ω | $\mathbf{C}_{CC}$ F | $\mathbf{R}_{CP1}$ Ω | **CPE -T** | **CPE -P** | $\mathbf{R}_{CP2}$ Ω | $\mathbf{C}_{DL}$ F | $\mathbf{R}_S$ Ω |
|---|---|---|---|---|---|---|---|---|---|
| **0** | 0.00029 | 0.023 | 2.0 | - | 2.5 | 0.5 | 2.9 | 16.7 | 0.202 |
| **12** | 0.00036 | 0.045 | 0.86 | - | 2.9 | 0.5 | 0.34 | 26.0 | 0.202 |
| **25** | 0.00023 | 0.035 | 0.82 | 5.3 | 2.7 | 0.5 | 0.48 | 24.9 | 0.203 |
| **50** | 0.00024 | 0.029 | 0.84 | 1.6 | 2.6 | 0.5 | 0.61 | 16.1 | 0.201 |
| **75** | 0.00018 | 0.024 | 0.88 | 1.1 | 2.4 | 0.5 | 0.57 | 13.7 | 0.200 |
| **100** | 0.00017 | 0.019 | 0.98 | 0.81 | 2.3 | 0.5 | 0.51 | 12.3 | 0.198 |
| **150** | 0.000094 | 0.019 | 0.98 | 0.73 | 2.2 | 0.5 | 0.38 | 12.4 | 0.200 |
| **175** | 0.00015 | 0.017 | 0.76 | 0.63 | 2.1 | 0.5 | 0.34 | 11.9 | 0.210 |

Abbreviations see Figure 4.7, Chapter 4.

### Influence of the activated carbon type

The performance of different activated carbon samples was compared at constant flow-electrode flow rate, activated carbon concentration, salt water flow rate and salt concentration. Table A.3 gives an overview of EIS fit results fitted to the results of the above described experiments using the equivalent circuit model described in the main manuscript. The corresponding experimental results are plotted in Figure 11 (a) of the main manuscript.

**Table A.3.:** Overview of EIS fit results. Comparison of different AC types at constant concentration and pump rate.

| **AC sample** | $\chi^2$ | $\mathbf{R}_{CC}$ Ω | $\mathbf{C}_{CC}$ F | $\mathbf{R}_{CP1}$ Ω | **CPE -T** | **CPE -P** | $\mathbf{R}_{CP2}$ Ω | $\mathbf{C}_{DL}$ F | $\mathbf{R}_S$ Ω |
|---|---|---|---|---|---|---|---|---|---|
| **CP** | 0.00023 | 0.015 | 0.16 | 0.15 | 3.6 | 0.5 | 0.14 | 15.2 | 0.206 |
| **N-B2** | 0.00022 | 0.028 | 0.55 | 0.54 | 1.9 | 0.5 | 0.48 | 6.89 | 0.222 |
| **CP sp.** | 0.00020 | 0.034 | 0.92 | 0.85 | 1.8 | 0.5 | 0.72 | 6.40 | 0.217 |
| **N-B1** | 0.000097 | 0.064 | 0.75 | 4.1 | 1.9 | 0.5 | 2.3 | 4.41 | 0.215 |

Abbreviations see Figure 4.7, Chapter 4.

### Influence of the NaCl concentration

In this series of experiments the NaCl concentration was varied, which was always kept the same in water channel and flow-electrodes. All other parameters such as flow-electrode flow rate, activated carbon concentration and salt water flow

rate were kept constant. Table A.4 gives an overview of EIS fit results fitted to the results of the above described experiments using the equivalent circuit model described in the main manuscript. The corresponding experimental results are plotted in Figure 9 of the main manuscript.

**Table A.4.:** Overview of EIS fit results at varied NaCl concentration at constant activated carbon concentration and pump rate.

| **AC sample** | $\chi^2$ | $\mathbf{R}_{CC}$ | $\mathbf{C}_{CC}$ | $\mathbf{R}_{CP1}$ | **CPE -T** | **CPE -P** | $\mathbf{R}_{CP2}$ | $\mathbf{C}_{DL}$ | $\mathbf{R}_{S}$ |
|---|---|---|---|---|---|---|---|---|---|
| | | Ω | F | Ω | | | Ω | F | Ω |
| **7 g/L** | 0.00096 | 0.031 | 0.04 | 0.45 | 1.4 | 0.5 | 0.43 | 13.9 | 0.507 |
| **16 g/L** | 0.00043 | 0.021 | 0.08 | 0.39 | 1.9 | 0.5 | 0.29 | 15.7 | 0.358 |
| **125 g/L** | 0.00019 | 0.004 | 2.62 | 0.32 | 3.4 | 0.5 | 0.18 | 15.9 | 0.203 |
| **317 g/L** | 0.970 | 0.006 | 3.73 | 0.36 | 4.0 | 0.5 | 0.23 | 13.1 | 0.184 |

Abbreviations see Figure 4.7, Chapter 4.

### Fits of experiments with varied particle size and matched desalination performance

In this series of experiments the performance of different particle size fractions was compared to the performance of the two mixed particle size fractions and the standard (unsieved) activated carbon. All other parameters such as flow-electrode flow rate, activated carbon concentration and salt water flow rate were kept constant. Table A.5 gives an overview of EIS fit results fitted to the results of the above described experiments using the equivalent circuit model described in the main manuscript. The corresponding experimental results are plotted in Figure 10 of the main manuscript.

**Table A.5.:** Overview of EIS fit results. Fits of experiments with varied particle size and matched desalination performance.

| **AC sample** | $\chi^2$ | $\mathbf{R}_{CC}$ | $\mathbf{C}_{CC}$ | $\mathbf{R}_{CP1}$ | **CPE -T** | **CPE -P** | $\mathbf{R}_{CP2}$ | $\mathbf{C}_{DL}$ | $\mathbf{R}_S$ |
|---|---|---|---|---|---|---|---|---|---|
| | | Ω | F | Ω | | | Ω | F | Ω |
| *Desalination experiments - matching two AC* | | | | | | | | | |
| **10% CP** | 0.00019 | 0.017 | 0.75 | 0.63 | 2.1 | 0.5 | 0.34 | 11.9 | 0.209 |
| **30% N** | 0.00020 | 0.0096 | 0.54 | 0.59 | 1.9 | 0.5 | 0.33 | 15.4 | 0.211 |
| **15% CP** | 0.00018 | 0.013 | 0.18 | 0.22 | 2.9 | 0.5 | 0.15 | 16.5 | 0.266 |
| **35% N** | 0.00034 | 0.023 | 0.14 | 0.24 | 2.2 | 0.5 | 0.15 | 22.0 | 0.227 |
| *Desalination experiments - comparison particle size fractions* | | | | | | | | | |
| **CP** | 0.00023 | 0.0093 | 0.46 | 0.20 | 3.3 | 0.5 | 0.16 | 15.0 | 0.203 |
| **<20 $\mu$m** | 0.00049 | 0.012 | 0.23 | 0.22 | 3.9 | 0.5 | 0.14 | 18.6 | 0.238 |
| **40-50 $\mu$m** | 0.00020 | 0.015 | 0.16 | 0.23 | 2.9 | 0.5 | 0.18 | 15.9 | 0.269 |
| **Mix** | 0.00035 | 0.0090 | 0.24 | 0.22 | 2.7 | 0.5 | 0.16 | 16.6 | 0.222 |

Abbreviations see Figure 4.7, Chapter 4.

## A.3. Results: Performance prediction of the desalination performance, electrical currents

Figure A.2 shows the measured electrical currents correlating with results shown in Figure 13 (b) of the main manuscript. Currents between 1.2 A and 1.9 A were measured at an applied voltage of 1.2 V. This corresponds to resistances between 0.63 Ω and 1 Ω, which match the impedance spectra displayed in Figure 13 (a) well.

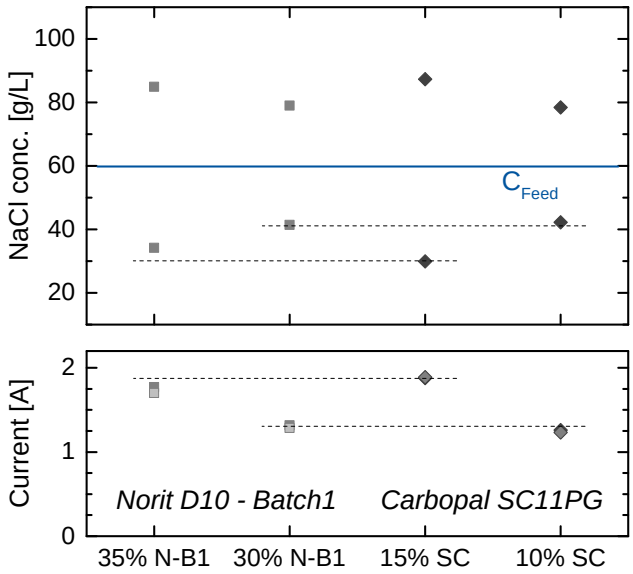


**Figure A.2.:** Average electrical currents recorded during desalination experiments described in main manuscript (Figure 13 (b) of main manuscript); Suspensions based on two different activated carbons were matched regarding their EIS response at two different mass fraction values and the corresponding desalination performance tested.

# Bibliography


[Akt2015] N. Akther, A. Sodiq, A. Giwa, S. Daer, H. A. Arafat, and S. W. Hasan. "Recent advancements in forward osmosis desalination: A review". In: *Chemical Engineering Journal* 281 (2015), pp. 502–522. DOI: 10.1016/j.cej.2015.05.080.

[Aku2017] B. Akuzum, L. Agartan, J. Locco, and E. C. Kumbur. "Effects of particle dispersion and slurry preparation protocol on electrochemical performance of capacitive flowable electrodes". In: *Journal of Applied Electrochemistry* 47.3 (2017), pp. 369–380. DOI: 10.1007/s10800-017-1046-5.

[Al-2013] Ali Al-Karaghouli and Lawrence L. Kazmerski. "Energy consumption and water production cost of conventional and renewable-energy-powered desalination processes". In: *Renewable and Sustainable Energy Reviews* 24 (2013), pp. 343–356. DOI: 10.1016/j.rser.2012.12.064.

[AlM2014] Faisal A. AlMarzooqi, Amal A. Al Ghaferi, Irfan Saadat, and Nidal Hilal. "Application of Capacitive Deionisation in water desalination: A review". In: *Desalination* 342 (2014), pp. 3–15. DOI: 10.1016/j.desal.2014.02.031.

[Amy2017] Gary Amy, Noreddine Ghaffour, Zhenyu Li, Lijo Francis, Rodrigo Valladares Linares, Thomas Missimer, and Sabine Lattemann. "Membrane-based seawater desalination: Present and future prospects". In: *Desalination* 401 (2017), pp. 16–21. DOI: 10.1016/j.desal.2016.10.002.

[And2010] Marc A. Anderson, Ana L. Cudero, and Jesus Palma. "Capacitive deionization as an electrochemical means of saving energy and delivering clean water. Comparison to present desalination practices: Will it compete?" In: *Electrochimica Acta* 55.12 (2010), pp. 3845–3856. DOI: 10.1016/j.electacta.2010.02.012.

[Are2017] Jason T. Arena, Jinesh C. Jain, Christina L. Lopano, J. Alexandra Hakala, Timothy V. Bartholomew, Meagan S. Mauter, and Nicholas S. Siefert. "Management and dewatering of brines extracted from geologic carbon storage sites". In: *International Journal of Greenhouse Gas Control* 63 (2017), pp. 194–214. DOI: 10.1016/j.ijggc.2017.03.032.

[Avl2003] S. A. Avlonitis, K. Kouroumbas, and N. Vlachakis. "Energy consumption and membrane replacement cost for seawater RO desalination plants". In: *Desalination* 157.1-3 (2003), pp. 151–158. DOI: 10.1016/S0011-9164(03)00395-3.

[Bal2010] J. Balster, D. F. Stamatialis, and M. Wessling. "Membrane with integrated spacer". In: *Journal of Membrane Science* 360.1-2 (2010), pp. 185–189. DOI: 10.1016/j.memsci.2010.05.011.

[Ban2015] Sebastian Bannwarth, Mariam Darestani, Hans Coster, and Matthias Wessling. "Characterization of hollow fiber membranes by impedance spectroscopy". In: *Journal of Membrane Science* 473 (2015), pp. 318–326. DOI: 10.1016/j.memsci.2014.09.001.

[Bar2001] Allen J Bard and Larry R. Faulkner. *Electrochemical Methods: Fundamentals and Applications*. 2nd ed. John Wiley & Sons, 2001, pp. 1–864. DOI: 10.1016/B978-0-08-098353-0.00003-8.

[Bar2005] Evgenij Barsoukov and J. Ross Macdonald. *Impedance Spectroscopy: Theory, Experiment, and Applications*. 2nd ed. John Wiley & Sons, Inc., 2005, pp. 1–606. DOI: 10.1002/0471716243.

[Bar2017] Timothy V. Bartholomew, Laura Mey, Jason T. Arena, Nicholas S. Siefert, and Meagan S. Mauter. "Osmotically assisted reverse osmosis for high salinity brine treatment". In: *Desalination* 421 (2017), pp. 3–11. DOI: 10.1016/j.desal.2017.04.012.

[Bia2019] Yanhong Bian, Xi Chen, Lu Lu, Peng Liang, and Zhiyong Jason Ren. "Concurrent Nitrogen and Phosphorus Recovery Using Flow-Electrode Capacitive Deionization". In: *ACS Sustainable Chemistry and Engineering* 7.8 (2019), pp. 7844–7850. DOI: 10.1021/acssuschemeng.9b00065.

[Bie2009] P M Biesheuvel. "Thermodynamic cycle analysis for capacitive deionization". In: *Journal of Colloid and Interface Science* 332.1 (2009), pp. 258–264. DOI: 10.1016/j.jcis.2008.12.018.

[Bie2010] P. M. Biesheuvel and A. van der Wal. "Membrane capacitive deionization". In: *Journal of Membrane Science* 346.2 (2010), pp. 256–262. DOI: 10.1016/j.memsci.2009.09.043.

[Bie2011] P. M. Biesheuvel, R. Zhao, S. Porada, and A. van der Wal. "Theory of membrane capacitive deionization including the effect of the electrode pore space". In: *Journal of Colloid and Interface Science* 360.1 (2011), pp. 239–248. DOI: 10.1016/j.jcis.2011.04.049.

[Bie2012] P. M. Biesheuvel, Y. Fu, and M. Z. Bazant. "Electrochemistry and capacitive charging of porous electrodes in asymmetric multicomponent electrolytes". In: *Russian Journal of Electrochemistry* 48.6 (2012), pp. 580–592. DOI: 10.1134/S1023193512060031.

[Blo1988] H. Block and J. P. Kelly. "Electro-rheology". In: *Journal of Physics D: Applied Physics* 21.12 (1988), pp. 1661–1677. DOI: 10.1088/0022-3727/21/12/001.

[Boc1998] John O'M. Bockris and Amulya K. N. Reddy. *Modern Electrochemistry - Volume 1, Ionics*. 2nd Editio. Kluwer Academic Publishers, 1998, pp. 1–770. DOI: 10.1007/b114546.

[Boc2002] John O'M. Bockris, Amulya K. N. Reddy, and Maria Gamboa-Aldeco. *Modern Electrochemistry - Volume 2A, Fundamentals of Electrodics*. 2nd Editio. Kluwer Academic Publishers, 2002, pp. 1–763. DOI: 10.1007/b113922.

[Boo2014] M. Boota, K. B. Hatzell, M. Beidaghi, C. R. Dennison, E. C. Kumbur, and Y. Gogotsi. "Activated Carbon Spheres as a Flowable Electrode in Electrochemical Flow Capacitors". In: *Journal of the Electrochemical Society* 161.6 (2014), A1078–A1083. DOI: 10.1149/2.072406jes.

[Cam2018] A. Campione, L. Gurreri, M. Ciofalo, G. Micale, A. Tamburini, and A. Cipollina. "Electrodialysis for water desalination: A critical assessment of recent developments on process fundamentals, models and applications". In: *Desalination* 434 (2018), pp. 121–160. DOI: 10.1016/j.desal.2017.12.044.

[Cam2019] Antonino Campione, Andrea Cipollina, I. David L. Bogle, Luigi Gurreri, Alessandro Tamburini, Michele Tedesco, and Giorgio Micale. "A hierarchical model for novel schemes of electrodialysis desalination". In: *Desalination* 465 (2019), pp. 79–93. DOI: 10.1016/j.desal.2019.04.020.

[Cas2012] S. Casas, C. Aladjem, J. L. Cortina, E. Larrotcha, and L. V. Cremades. "Seawater Reverse Osmosis Brines as a New Salt Source for the Chlor-Alkali Industry: Integration of NaCl Concentration by Electrodialysis". In: *Solvent Extraction and Ion Exchange* 30.4 (2012), pp. 322–332. DOI: 10.1080/07366299.2012.686849.

[Cha1956] J. F. Chambers, Jean M. Stokes, and R. H. Stokes. "Conductances of concentrated aqueous sodium and potassium chloride solutions at 25°". In: *Journal of Physical Chemistry* 60.7 (1956), pp. 985–986. DOI: 10.1021/j150541a040.

[Cha2019] Junjun Chang, Feng Duan, Hongbin Cao, Kexin Tang, Chunlei Su, and Yuping Li. "Superiority of a novel flow-electrode capacitive deionization (FCDI) based on a battery material at high applied voltage". In: *Desalination* 468 (2019), p. 114080. DOI: 10.1016/j.desal.2019.114080.

[Che2017] Karim M. Chehayeb, Daniel M. Farhat, Kishor G. Nayar, and John H. Lienhard. "Optimal design and operation of electrodialysis for brackish-water desalination and for high-salinity brine concentration". In: *Desalination* 420 (2017), pp. 167–182. DOI: 10.1016/j.desal.2017.07.003.

[Cho2014] Jae Hwan Choi. "Determination of the electrode potential causing Faradaic reactions in membrane capacitive deionization". In: *Desalination* 347 (2014), pp. 224–229. DOI: 10.1016/j.desal.2014.06.004.

[Cho2017a] Younghyun Cho, Ki Sook Lee, Seung Cheol Yang, Jiyeon Choi, Hong Ran Park, and Dong Kook Kim. "A novel three-dimensional desalination system utilizing honeycomb-shaped lattice structures for flow-electrode capacitive deionization". In: *Energy & Environmental Science* 10.8 (2017), pp. 1746–1750. DOI: 10.1039/c7ee00698e.

[Cho2017b] Seungyeon Choi, Barsa Chang, Ji Hyun Kang, Mamadou S. Diallo, and Jang Wook Choi. "Energy-efficient hybrid FCDI-NF desalination process with tunable salt rejection and high water recovery". In: *Journal of Membrane Science* 541 (2017), pp. 580–586. DOI: 10.1016/j.memsci.2017.07.043.

[Cho2017c] Ko Yeon Choo, Chung Yul Yoo, Moon Hee Han, and Dong Kook Kim. "Electrochemical analysis of slurry electrodes for flow-electrode capacitive deionization". In: *Journal of Electroanalytical Chemistry* 806 (2017), pp. 50–60. DOI: 10.1016/j.jelechem.2017.10.040.

[Cho2019] Younghyun Cho, Chung Yul Yoo, Seung Woo Lee, Hana Yoon, Ki Sook Lee, Seung Cheol Yang, and Dong Kook Kim. "Flow-electrode capacitive deionization with highly enhanced salt removal performance utilizing high-aspect ratio functionalized carbon nanotubes". In: *Water Research* (2019), pp. 252–259. DOI: 10.1016/j.watres.2018.11.080.

[Coh2016] Hagai Cohen, Shaked Ein Eli, Morten Jõgi, and Matthew E. Suss. "Suspension Electrodes Combining Slurries and Upflow Fluidized Beds". In: *ChemSusChem* 9.21 (2016), pp. 3045–3048. DOI: 10.1002/cssc.201601008.

[Dem1979] H. U. Demisch and W. Pusch. "Electric and electrokinetic transport properties of homogeneous weak ion exchange membranes". In: *Journal of Colloid And Interface Science* 69.2 (1979), pp. 247–270. DOI: 10.1016/0021-9797(79)90154-1.

[Dem2003] M. Demircioglu, N. Kabay, I. Kurucaovali, and E. Ersoz. "Demineralization by electrodialysis (ED)-separation performance and cost comparison for monovalent salts". In: *Desalination* 153.1 (2003), pp. 329–333. DOI: 10.1016/S0011-9164(02)01119-0.

[Den2014a] C. R. Dennison, M. Beidaghi, K. B. Hatzell, J. W. Campos, Y. Gogotsi, and E. C. Kumbur. "Effects of flow cell design on charge percolation and storage in the carbon slurry electrodes of electrochemical flow capacitors". In: *Journal of Power Sources* 247 (2014), pp. 489–496. DOI: 10.1016/j.jpowsour.2013.08.101.

[Den2014b] C. R. Dennison, Y. Gogotsi, and E. C. Kumbur. "In situ distributed diagnostics of flowable electrode systems: resolving spatial and temporal limitations". In: *Physical Chemistry Chemical Physics* 16 (2014), pp. 18241–18252. DOI: 10.1039/C4CP02820A.

[Des2018] Akshay Deshmukh, Chanhee Boo, Vasiliki Karanikola, Shihong Lin, Anthony P. Straub, Tiezheng Tong, David M. Warsinger, and Menachem Elimelech. "Membrane distillation at the water-energy nexus: Limits, opportunities, and challenges". In: *Energy and Environmental Science* 11.5 (2018), pp. 1177–1196. DOI: 10.1039/c8ee00291f.

[Dix2019] Marm B. Dixit, Daniel Moreno, Xianghui Xiao, Marta C. Hatzell, and Kelsey B. Hatzell. "Mapping Charge Percolation in Flowable Electrodes Used in Capacitive Deionization". In: *ACS Materials Letters* 1.1 (2019), pp. 71–76. DOI: 10.1021/acsmaterialslett.9b00106.

[Dłu2010] Piotr Długołecki, Piotr Ogonowski, Sybrand J. Metz, Michel Saakes, Kitty Nijmeijer, and Matthias Wessling. "On the resistances of membrane, diffusion boundary layer and double layer in ion exchange membrane transport". In: *Journal of Membrane Science* 349.1-2 (2010), pp. 369–379. DOI: 10.1016/j.memsci.2009.11.069.

[Dłu2013] Piotr Długołecki and Albert van der Wal. "Energy recovery in membrane capacitive deionization". In: *Environmental Science and Technology* 47.9 (2013), pp. 4904–4910. DOI: 10.1021/es3053202.

[Doo2016] G. J. Doornbusch, J. E. Dykstra, P. M. Biesheuvel, and M. E. Suss. "Fluidized bed electrodes with high carbon loading applied to water desalination by capacitive deionization". In: *Journal of Materials Chemistry A* 4 (2016), pp. 3642–3647. DOI: 10.1039/C5TA10316A.

[Dri2015] Enrico Drioli, Aamer Ali, and Francesca Macedonio. "Membrane distillation: Recent developments and perspectives". In: *Desalination* 356 (2015), pp. 56–84. DOI: 10.1016/j.desal.2014.10.028.

[Dso2013] Sonia Dsoke, Xu Tian, Corina Täubert, Steffen Schlüter, and Margret Wohlfahrt-Mehrens. "Strategies to reduce the resistance sources on Electrochemical Double Layer Capacitor electrodes". In: *Journal of Power Sources* 238 (2013), pp. 422–429. DOI: 10.1016/j.jpowsour.2013.04.031.

[Eli2011] Menachem Elimelech and William A Phillip. "The Future of Seawater and the Environment: Energy, Technology, and the Environment". In: *Science* 333 (2011), pp. 712–718. DOI: 10.1126/science.1200488.

[Fan2014] Frank Y. Fan, William H. Woodford, Zheng Li, Nir Baram, Kyle C. Smith, Ahmed Helal, Gareth H. McKinley, W. Craig Carter, and Yet Ming Chiang. "Polysulfide flow batteries enabled by percolating nanoscale conductor networks". In: *Nano Letters* 14.4 (2014), pp. 2210–2218. DOI: 10.1021/nl500740t.

[Fan2018] Kuo Fang, Hui Gong, Wenyan He, Fei Peng, Conghui He, and Kaijun Wang. "Recovering ammonia from municipal wastewater by flow-electrode capacitive deionization". In: *Chemical Engineering Journal* 348 (2018), pp. 301–309. DOI: 10.1016/j.cej.2018.04.128.

[Fer2005] Yolanda Fernández-Torquemada, J. L. Sánchez-Lizaso, and J. M. González-Correa. "Preliminary results of the monitoring of the brine discharge produced by the SWRO desalination plant of Alicante (SE Spain)". In: *Desalination* 182.1-3 (2005), pp. 395–402. DOI: 10.1016/j.desal.2005.03.023.

[Fle2014] Stephen Fletcher, Victoria Jane Black, and Iain Kirkpatrick. "A universal equivalent circuit for carbon-based supercapacitors". In: *Journal of Solid State Electrochemistry* 18.5 (2014), pp. 1377–1387. DOI: 10.1007/s10008-013-2328-4.

[Fri2007] C. Fritzmann, J. Löwenberg, T. Wintgens, and T. Melin. "State-of-the-art of reverse osmosis desalination". In: *Desalination* 216 (2007), pp. 1–76. DOI: 10.1016/j.desal.2014.10.039.

[Gal2013] A. H. Galama, J. W. Post, M. A. Cohen Stuart, and P. M. Biesheuvel. "Validity of the Boltzmann equation to describe Donnan equilibrium at the membrane-solution interface". In: *Journal of Membrane Science* 442 (2013), pp. 131–139. DOI: 10.1016/j.memsci.2013.04.022.

[Gal2014] A. H. Galama, D. A. Vermaas, J. Veerman, M. Saakes, H. H.M. Rijnaarts, J. W. Post, and K. Nijmeijer. "Membrane resistance: The effect of salinity gradients over a cation exchange membrane". In: *Journal of Membrane Science* 467 (2014), pp. 279–291. DOI: 10.1016/j.memsci.2014.05.046.

[Gal2016] A. H. Galama, J. W. Post, H. V.M. Hamelers, V. V. Nikonenko, and P. M. Biesheuvel. "On the origin of the membrane potential arising across densely charged ion exchange membranes: How well does the Teorell-Meyer-Sievers theory work?" In: *Journal of Membrane Science and Research* 2.3 (2016), pp. 128–140. DOI: 10.22079/jmsr.2016.20311.

[Gei2013] Geoffrey M. Geise, Andrew J. Curtis, Marta C. Hatzell, Michael A. Hickner, and Bruce E. Logan. "Salt Concentration Differences Alter Membrane Resistance in Reverse Electrodialysis Stacks". In: *Environmental Science and Technology Letters* 1.1 (2013), pp. 36–39. DOI: 10.1021/ez4000719.

[Gen2014] Youri Gendel, Alexandra K. E. Rommerskirchen, Oana David, and Matthias Wessling. "Batch mode and continuous desalination of water using flowing carbon deionization (FCDI) technology". In: *Electrochemistry Communications* 46 (2014), pp. 152–156. DOI: 10.1016/j.elecom.2014.06.004.

[Gma2017] Soumaya Gmar, Nawel Helali, Ali Boubakri, Ilhem Ben Salah Sayadi, Mohamed Tlili, and Mohamed Ben Amor. "Electrodialytic desalination of brackish water: determination of optimal experimental parameters using full factorial design". In: *Applied Water Science* 7.8 (2017), pp. 4563–4572. DOI: 10.1007/s13201-017-0609-2.

[Has2017] Armineh Hassanvand, George Q. Chen, Paul A. Webley, and Sandra E. Kentish. "Improvement of MCDI operation and design through experiment and modelling: Regeneration with brine and optimum residence time". In: *Desalination* 417 (2017), pp. 36–51. DOI: 10.1016/j.desal.2017.05.004.

[Hat2013] Kelsey B. Hatzell, Majid Beidaghi, Jonathan W. Campos, Christopher R. Dennison, Emin C. Kumbur, and Yury Gogotsi. "A high performance pseudocapacitive suspension electrode for the electrochemical flow capacitor". In: *Electrochimica Acta* 111 (2013), pp. 888–897. DOI: 10.1016/j.electacta.2013.08.095.

[Hat2014] Kelsey B. Hatzell, Etsuro Iwama, Anais Ferris, Barbara Daffos, Koki Urita, Théodore Tzedakis, Fabien Chauvet, Pierre Louis Taberna, Yury Gogotsi, and Patrice Simon. "Capacitive deionization concept based on suspension electrodes without ion exchange membranes". In: *Electrochemistry Communications* 43 (2014), pp. 18–21. DOI: 10.1016/j.elecom.2014.03.003.

[Hat2015a] Kelsey B. Hatzell, Muhammad Boota, and Yury Gogotsi. "Materials for suspension (semi-solid) electrodes for energy and water technologies". In: *Chem. Soc. Rev.* 44.23 (2015), pp. 8664–8687. DOI: 10.1039/C5CS00279F.

[Hat2015b] Kelsey B. Hatzell, Marta C. Hatzell, Kevin M. Cook, Muhammad Boota, Gabrielle M. Housel, Alexander McBride, E. Caglan Kumbur, and Yury Gogotsi. "Effect of oxidation of carbon material on suspension electrodes for flow electrode capacitive deionization". In: *Environmental Science and Technology* 49.5 (2015), pp. 3040–3047. DOI: 10.1021/es5055989.

[Hat2017] Kelsey B. Hatzell, Jens Eller, Samantha L. Morelly, Maureen H. Tang, Nicolas J. Alvarez, and Yury Gogotsi. "Direct observation of active material interactions in flowable electrodes using X-ray tomography". In: *Faraday Discussions* 199 (2017), pp. 511–524. DOI: 10.1039/c6fd00243a.

[Hat2018] Marta Hatzell and Kelsey Hatzell. "Blue Refrigeration: Electrochemical Separations for Water Deionization". In: *Journal of Electrochemical Energy Conversion and Storage* 15.1 (2018), 011009:1–6. DOI: 10.1115/1.4037907.

[Hel1853] Henrich Helmholtz. "Ueber einige Gesetze der Vertheilung elektrischer Ströme in körperlichen Leitern, mit Anwendung auf die thierisch-elektrischen Versuche". In: *Annalen der Physik und Chemie* 7 (1853).

[Hoy2016] Nathaniel C. Hoyt, Robert F. Savinell, and Jesse S. Wainright. "Modeling of flowable slurry electrodes with combined faradaic and nonfaradaic currents". In: *Chemical Engineering Science* 144 (2016), pp. 288–297. DOI: 10.1016/j.ces.2016.01.048.

[Hoy2018] Nathaniel C. Hoyt, Ertan Agar, Enoch A. Nagelli, Robert Savinell, and Jesse Wainright. "Editors' Choice—Electrochemical Impedance Spectroscopy of Flowing Electrosorptive Slurry Electrodes". In: *Journal of The Electrochemical Society* 165.10 (2018), E439–E444. DOI: 10.1149/2.0051810jes.

[Jeo2011] Byong Guk Jeon, Hee Cheon No, and Jeong Ik Lee. "Development of a two-dimensional coupled-implicit numerical tool for the optimal design of CDI electrodes". In: *Desalination* 274.1-3 (2011), pp. 226–236. DOI: 10.1016/j.desal.2011.02.021.

[Jeo2013] Sung-il Jeon, Hong-ran Park, Jeong-gu Yeo, SeungCheol Yang, Churl Hee Cho, Moon Hee Han, and Dong Kook Kim. "Desalination via a new membrane capacitive deionization process utilizing flow-electrodes". In: *Energy & Environmental Science* 6.5 (2013), pp. 1471–1475. DOI: Doi10.1039/C3ee24443a.

[Jeo2014] Sung-il Jeon, Jeong-gu Yeo, SeungCheol Yang, Jiyeon Choi, and Dong Kook Kim. "Ion storage and energy recovery of a flow-electrode capacitive deionization process". In: *Journal of Materials Chemistry A* 2.18 (2014), p. 6378. DOI: 10.1039/c4ta00377b.

[Kam2016a] Jovan Kamcev and Benny D. Freeman. "Charged Polymer Membranes for Environmental/Energy Applications". In: *Annual Review of Chemical and Biomolecular Engineering* 7.1 (2016), pp. 111–133. DOI: 10.1146/annurev-chembioeng-080615-033533.

[Kam2016b] Jovan Kamcev, Michele Galizia, Francesco M. Benedetti, Eui Soung Jang, Donald R. Paul, Benny D. Freeman, and Gerald S. Manning. "Partitioning of mobile ions between ion exchange polymers and aqueous salt solutions: Importance of counter-ion condensation". In: *Physical Chemistry Chemical Physics* 18.8 (2016), pp. 6021–6031. DOI: 10.1039/c5cp06747b.

[Kim2018] Choonsoo Kim, Pattarachai Srimuk, Juhan Lee, Mesut Aslan, and Volker Presser. "Semi-continuous capacitive deionization using multi-channel flow stream and ion exchange membranes". In: *Desalination* 425 (2018), pp. 104–110. DOI: 10.1016/j.desal.2017.10.012.

[Kin2018] R. S. Kingsbury, S. Zhu, S. Flotron, and O. Coronell. "Microstructure Determines Water and Salt Permeation in Commercial Ion-Exchange Membranes". In: *ACS Applied Materials and Interfaces* 10.46 (2018), pp. 39745–39756. DOI: 10.1021/acsami.8b14494.

[Kom2010] P. V. Komarov, I. N. Veselov, P. P. Chu, P. G. Khalatur, and A. R. Khokhlov. "Atomistic and mesoscale simulation of polymer electrolyte membranes based on sulfonated poly(ether ether ketone)". In: *Chemical Physics Letters* 487.4-6 (2010), pp. 291–296. DOI: 10.1016/j.cplett.2010.01.049.

[Köt2000] R. Kötz and M. Carlen. "Principles and applications of electrochemical capacitors". In: *Electrochim. Acta* 45.15-16 (2000), pp. 2483–2498. DOI: DOI:10.1016/S0013-4686(00)00354-6.

[Kri2017] Mette Birch Kristensen, Anders Bentien, Michele Tedesco, and Jacopo Catalano. "Counter-ion transport number and membrane potential in working membrane systems". In: *Journal of Colloid and Interface Science* 504 (2017), pp. 800–813. DOI: 10.1016/j.jcis.2017.06.010.

[Lei2013] Chunhong Lei, Foivos Markoulidis, Zenya Ashitaka, and Constantina Lekakou. "Electrochimica Acta Reduction of porous carbon / Al contact resistance for an electric double-layer capacitor ( EDLC )". In: 92 (2013), pp. 183–187. DOI: 10.1016/j.electacta.2012.12.092.

[Lev1963] Robert de Levie. “On porous electrodes in electrolyte solutions”. In: *Electrochimica Acta* 8.10 (1963), pp. 751–780. DOI: 10.1016/0013-4686(63)80042-0.

[Lev1965] Robert de Levie. “The influence of surface roughness of solid electrodes on electrochemical measurements”. In: *Electrochimica Acta* 10.2 (1965), pp. 113–130. DOI: 10.1016/0013-4686(65)87012-8.

[Li2005] Xianfeng Li, Zhe Wang, Hui Lu, Chengji Zhao, Hui Na, and Chun Zhao. “Electrochemical properties of sulfonated PEEK used for ion exchange membranes”. In: *Journal of Membrane Science* 254.1-2 (2005), pp. 147–155. DOI: 10.1016/j.memsci.2004.12.051.

[Lia2017] Peng Liang, Xueliang Sun, Yanhong Bian, Helan Zhang, Xufei Yang, Yong Jiang, Panpan Liu, and Xia Huang. “Optimized desalination performance of high voltage flow-electrode capacitive deionization by adding carbon black in flow-electrode”. In: *Desalination* 420 (2017), pp. 63–69. DOI: 10.1016/j.desal.2017.05.023.

[Lin2017] Christian Linnartz, Alexandra Rommerskirchen, Matthias Wessling, and Youri Gendel. “Flow-electrode capacitive deionization for double displacement reactions”. In: *ACS Sustainable Chemistry & Engineering* 5 (2017), pp. 3906–3912. DOI: 10.1021/acssuschemeng.6b03086.

[Loh2019] Johannes Lohaus, Deniz Rall, Maximilian Kruse, Viktoria Steinberger, and Matthias Wessling. “On charge percolation in slurry electrodes used in vanadium redox flow batteries”. In: *Electrochemistry Communications* 101 (2019), pp. 104–108. DOI: 10.1016/j.elecom.2019.02.013.

[Ma2016] Jinxing Ma, Di He, Wangwang Tang, Peter Kovalsky, Calvin He, Changyong Zhang, and T. David Waite. “Development of Redox-Active Flow Electrodes for High-Performance Capacitive Deionization”. In: *Environmental Science and Technology* 50.24 (2016), pp. 13495–13501. DOI: 10.1021/acs.est.6b03424.

[Ma2019] Jinxing Ma, Yumeng Zhang, Richard N. Collins, Sergey Tsarev, Noboru Aoyagi, Andrew S. Kinsela, Adele M. Jones, and T. David Waite. “Flow-Electrode CDI Removes the Uncharged Ca-UO2-CO3 Ternary Complex from Brackish Potable Groundwater: Complex Dissociation, Transport, and Sorption”. In: *Environmental Science and Technology* 53.5 (2019), pp. 2739–2747. DOI: 10.1021/acs.est.8b07157.

[Mac1955a] J. S. Mackie and P. Meares. “The diffusion of electrolytes in a cation-exchange resin membrane”. In: *Proceedings of the Royal Society of London. Series A. Mathematical and Physical Sciences* 232.1191 (1955), pp. 510–518. DOI: 10.1098/rspa.1955.0235.

[Mac1955b] J. S. Mackie and P. Meares. “The sorption of electrolytes by a cation-exchange resin membrane”. In: *Proceedings of the Royal Society of London. Series A. Mathematical and Physical Sciences* 232.1191 (1955). DOI: https://doi.org/10.1098/rspa.1955.0233.

[Mac2017] Francesca Macedonio and Enrico Drioli. “Membrane Engineering for Green Process Engineering”. In: *Engineering* 3.3 (2017), pp. 290–298. DOI: 10.1016/J.ENG.2017.03.026.

[Man1969] Gerald S. Manning. “Limiting laws and counterion condensation in polyelectrolyte solutions I. Colligative properties.” In: *Journal of Physical Chemistry* 51 (1969), pp. 924–933. DOI: 10.1021/j150611a011.

[McG2014] Ronan K. McGovern, Adam M. Weiner, Lige Sun, Chester G. Chambers, Syed M. Zubair, and John H. Lienhard V. “On the cost of electrodialysis for the desalination of high salinity feeds”. In: *Applied Energy* 136 (2014), pp. 649–661. DOI: 10.1016/j.apenergy.2014.09.050.

[McH1969] W. J. McHardy, P. Meares, and J. F. Thain. “Diffusion of Radiotracer Ions in a Cation-Exchange Membrane”. In: *Journal of The Electrochemical Society* 116.7 (1969), pp. 920–928. DOI: 10.1149/1.2412171.

[Mea1956] Patrick Meares. “The Conductivity of a Cation-Exchange Resin”. In: *Journal of Polymer Science* (1956), pp. 507–514.

[Mel2007] Thomas Melin and Robert Rautenbach. *Membranverfahren*. 3rd ed. Springer-Verlag Berlin Heidelberg, 2007, pp. 1–584. DOI: 10.1007/978-3-540-34328-8.

[Mez2011] Toufic Mezher, Hassan Fath, Zeina Abbas, and Arslan Khaled. “Techno-economic assessment and environmental impacts of desalination technologies”. In: *Desalination* 266.1-3 (2011), pp. 263–273. DOI: 10.1016/j.desal.2010.08.035.

[Moh2015] A. W. Mohammad, Y. H. Teow, W. L. Ang, Y. T. Chung, D. L. Oatley-Radcliffe, and N. Hilal. “Nanofiltration membranes review: Recent advances and future prospects”. In: *Desalination* 356 (2015), pp. 226–254. DOI: 10.1016/j.desal.2014.10.043.

[Moo2004] Paula Moon, Giselle Sandí, Deborah Stevens, and Riza Kizilel. “Computational Modeling of Ionic Transport in Continuous and Batch Electrodialysis”. In: *Separation Science and Technology* 39.11 (2004), pp. 2531–2555. DOI: 10.1081/SS-200026714.

[Mor2018] Daniel Moreno and Marta C. Hatzell. “Influence of Feed-Electrode Concentration Differences in Flow-Electrode Systems for Capacitive Deionization”. In: *Industrial and Engineering Chemistry Research* 57.26 (2018), pp. 8802–8809. DOI: 10.1021/acs.iecr.8b01626.

[Nag2006] R. K. Nagarale, G. S. Gohil, and Vinod K. Shahi. “Recent developments on ion-exchange membranes and electro-membrane processes”. In: *Advances in Colloid and Interface Science* 119.2-3 (2006), pp. 97–130. DOI: 10.1016/j.cis.2005.09.005.

[Nat2017] Paz Nativ, Yuval Badash, and Youri Gendel. “New insights into the mechanism of flow-electrode capacitive deionization”. In: *Electrochemistry Communications* 76 (Mar. 2017), pp. 24–28. DOI: 10.1016/j.elecom.2017.01.008.

[Nat2018] Paz Nativ, Ori Lahav, and Youri Gendel. “Separation of divalent and monovalent ions using flow-electrode capacitive deionization with nanofiltration membranes”. In: *Desalination* 425 (2018), pp. 123–129. DOI: 10.1016/j.desal.2017.10.026.

[Ng2015] Kim Choon Ng, Kyaw Thu, Seung Jin Oh, Li Ang, Muhammad Wakil Shahzad, and Azhar Bin Ismail. “Recent developments in thermally-driven seawater desalination: Energy efficiency improvement by hybridization of the MED and AD cycles”. In: *Desalination* 356 (2015), pp. 255–270. DOI: 10.1016/j.desal.2014.10.025.

[Nun2011] Cleiton a. Nunes and Mário C. Guerreiro. “Estimation of Surface Area and Pore Volume of Activates Carbons by Methylene Blue and Iodine Numbers”. In: *Química Nova* 34.3 (2011), pp. 472–476. DOI: 10.1590/S0100-40422011000300020.

[Ora2008] Mark E. Orazem and Bernard Tribollet. *Electrochemical Impedance Spectroscopy*. John Wiley & Sons, 2008, pp. 1–525. DOI: 10.1002/9780470381588.

[Ore2008] Yoram Oren. “Capacitive deionization (CDI) for desalination and water treatment - past, present and future (a review)”. In: *Desalination* 228.1-3 (2008), pp. 10–29. DOI: 10.1016/j.desal.2007.08.005.

[Ore2010] Y. Oren, E. Korngold, N. Daltrophe, R. Messalem, Y. Volkman, L. Aronov, M. Weismann, N. Bouriakov, P. Glueckstern, and J. Gilron. “Pilot studies on high recovery BWRO-EDR for near zero liquid discharge approach”. In: *Desalination* 261.3 (2010), pp. 321–330. DOI: 10.1016/j.desal.2010.06.010.

[Ort2005] J. M. Ortiz, J. A. Sotoca, E. Expósito, F. Gallud, V. García-García, V. Montiel, and A. Aldaz. “Brackish water desalination by electrodialysis: Batch recirculation operation modeling”. In: *Journal of Membrane Science* 252.1-2 (2005), pp. 65–75. DOI: 10.1016/j.memsci.2004.11.021.

[Par2016] Hong-ran Park, Jiyeon Choi, Seungcheol Yang, Sung Jo Kwak, Sung-il Jeon, Moon Hee Han, and Dong Kook Kim. “Surface-modified spherical activated carbon for high carbon loading and its desalting performance in flow-electrode capacitive deionization”. In: *RSC Adv.* 6.74 (2016), pp. 69720–69727. DOI: 10.1039/C6RA02480G.

[Par2017] H. Parant, G. Muller, T. Le Mercier, J. M. Tarascon, P. Poulin, and A. Colin. “Flowing suspensions of carbon black with high electronic conductivity for flow applications: Comparison between carbons black and exhibition of specific aggregation of carbon particles”. In: *Carbon* 119 (2017), pp. 10–20. DOI: 10.1016/j.carbon.2017.04.014.

[Pér2012] A. Pérez-González, A. M. Urtiaga, R. Ibáñez, and I. Ortiz. "State of the art and review on the treatment technologies of water reverse osmosis concentrates". In: *Water Research* 46.2 (2012), pp. 267–283. DOI: 10.1016/j.watres.2011.10.046.

[Per2018] Korcan Percin, Alexandra Rommerskirchen, Robert Sengpiel, Youri Gendel, and Matthias Wessling. "3D-printed conductive static mixers enable all-vanadium redox flow battery using slurry electrodes". In: *Journal of Power Sources* 379 (2018), pp. 228–233. DOI: 10.1016/j.jpowsour.2018.01.061.

[Pet2015a] T. J. Petek, N. C. Hoyt, R. F. Savinell, and J. S. Wainright. "Characterizing Slurry Electrodes Using Electrochemical Impedance Spectroscopy". In: *Journal of the Electrochemical Society* 163.1 (2015), A5001–A5009. DOI: 10.1149/2.0011601jes.

[Pet2015b] Tyler J. Petek, Nathaniel C. Hoyt, Robert F. Savinell, and Jesse S. Wainright. "Slurry electrodes for iron plating in an all-iron flow battery". In: *Journal of Power Sources* 294 (2015), pp. 620–626. DOI: 10.1016/j.jpowsour.2015.06.050.

[Pet2018] L. Peters, G. Linz, and M. Wessling. "Membrane based direct pH parametric pumping". In: *Journal of Membrane Science* 558 (2018), pp. 78–85. DOI: 10.1016/j.memsci.2018.02.056.

[Pet2019] Christian D. Peters and Nicholas P. Hankins. "Osmotically assisted reverse osmosis (OARO): Five approaches to dewatering saline brines using pressure-driven membrane processes". In: *Desalination* 458 (2019), pp. 1–13. DOI: 10.1016/j.desal.2019.01.025.

[Por2012] S. Porada, B. B. Sales, H. V M Hamelers, and P. M. Biesheuvel. "Water desalination with wires". In: *Journal of Physical Chemistry Letters* 3.12 (2012), pp. 1613–1618. DOI: 10.1021/jz3005514.

[Por2013] S. Porada, R. Zhao, A. van der Wal, V. Presser, and P. M. Biesheuvel. "Review on the science and technology of water desalination by capacitive deionization". In: *Progress in Materials Science* 58.8 (2013), pp. 1388–1442. DOI: 10.1016/j.pmatsci.2013.03.005.

[Por2014] S. Porada, D. Weingarth, H. V. M. Hamelers, M. Bryjak, V. Presser, and P. M. Biesheuvel. "Carbon flow electrodes for continuous operation of capacitive deionization and capacitive mixing energy generation". In: *Journal of Materials Chemistry A* 2.24 (2014), pp. 9313–9321. DOI: 10.1039/c4ta01783h.

[Por2018] S. Porada, W. J. van Egmond, J. W. Post, M. Saakes, and H. V.M. Hamelers. "Tailoring ion exchange membranes to enable low osmotic water transport and energy efficient electrodialysis". In: *Journal of Membrane Science* 552 (2018), pp. 22–30. DOI: 10.1016/j.memsci.2018.01.050.

[Pre2012] Volker Presser, Christopher R. Dennison, Jonathan Campos, Kevin W. Knehr, Emin C. Kumbur, and Yury Gogotsi. "The electrochemical flow capacitor: A new concept for rapid energy storage and recovery". In: *Advanced Energy Materials* 2.7 (2012), pp. 895–902. DOI: 10.1002/aenm.201100768.

[Qu2015] Yatian Qu, Theodore F. Baumann, Juan G. Santiago, and Michael Stadermann. "Characterization of Resistances of a Capacitive Deionization System". In: *Environmental Science and Technology* 49.16 (2015), pp. 9699–9706. DOI: 10.1021/acs.est.5b02542.

[Rat2019] Paula Ratajczak, Matthew E. Suss, Friedrich Kaasik, and François Béguin. "Carbon electrodes for capacitive technologies". In: *Energy Storage Materials* 16 (2019), pp. 126–145. DOI: 10.1016/j.ensm.2018.04.031.

[Rei2014] Mònica Reig, Sandra Casas, Carlos Aladjem, César Valderrama, Oriol Gibert, Fernando Valero, Carlos Miguel Centeno, Enric Larrotcha, and José Luis Cortina. "Concentration of NaCl from seawater reverse osmosis brines for the chlor-alkali industry by electrodialysis". In: *Desalination* 342 (2014), pp. 107–117. DOI: 10.1016/j.desal.2013.12.021.

[Rom2015] Alexandra Rommerskirchen, Youri Gendel, and Matthias Wessling. "Single module flow-electrode capacitive deionization for continuous water desalination". In: *Electrochemistry Communications* 60 (2015), pp. 34–37. DOI: 10.1016/j.elecom.2015.07.018.

[Rom2018a] Alexandra Rommerskirchen, Christian J. Linnartz, Daniel Müller, Lisa Kathrin Willenberg, and Matthias Wessling. "Energy Recovery and Process Design in Continuous Flow-Electrode Capacitive Deionization Processes". In: *ACS Sustainable Chemistry and Engineering* 6.10 (2018), pp. 13007–13015. DOI: 10.1021/acssuschemeng.8b02466.

[Rom2018b] Alexandra Rommerskirchen, Burkhard Ohs, Karl Arturo Hepp, Robert Femmer, and Matthias Wessling. "Modeling continuous flow-electrode capacitive deionization processes with ion-exchange membranes". In: *Journal of Membrane Science* 546 (2018), pp. 188–196. DOI: 10.1016/j.memsci.2017.10.026.

[Rom2019] A. Rommerskirchen, A. Kalde, C.J. Linnartz, L. Bongers, G. Linz, and M. Wessling. "Unraveling charge transport in carbon flow-electrodes: Performance prediction for desalination applications". In: *Carbon* 145 (2019), pp. 507–520. DOI: 10.1016/j.carbon.2019.01.053.

[Sad2009] Mohtada Sadrzadeh and Toraj Mohammadi. "Treatment of sea water using electrodialysis: Current efficiency evaluation". In: *Desalination* 249.1 (2009), pp. 279–285. DOI: 10.1016/j.desal.2008.10.029.

[Sal2010] B. B. Sales, M. Saakes, J. W. Post, C. J. N. Buisman, P. M. Biesheuvel, and H. V. M. Hamelers. "Direct power production from a water salinity difference in a membrane-modified supercapacitor flow cell." In: *Environmental Science & Technology* 44.14 (2010), pp. 5661–5665. DOI: 10.1021/es100852a.

[Sch2012] Volkmar M. Schmidt. *Elektrochemische Verfahrenstechnik: Grundlagen, Reaktionstechnik, Prozessoptimierung*. Wiley-VCH, 2012, pp. 1–688.

[Sha2013] Devin L. Shaffer, Laura H. Arias Chavez, Moshe Ben-Sasson, Santiago Romero-Vargas Castrillón, Ngai Yin Yip, and Menachem Elimelech. "Desalination and reuse of high-salinity shale gas produced water: Drivers, technologies, and future directions". In: *Environmental Science & Technology* 47.17 (2013), pp. 9569–9583. DOI: 10.1021/es401966e.

[Sha2015] Devin L. Shaffer, Jay R. Werber, Humberto Jaramillo, Shihong Lin, and Menachem Elimelech. "Forward osmosis: Where are we now?" In: *Desalination* 356 (2015), pp. 271–284. DOI: 10.1016/j.desal.2014.10.031.

[Sha2016] S. Shanbhag, J. F. Whitacre, and M. S. Mauter. "The Origins of Low Efficiency in Electrochemical De-Ionization Systems". In: *Journal of The Electrochemical Society* 163.14 (2016), E363–E371. DOI: 10.1149/2.0181614jes.

[Shi1996] Hang Shi. "Activated carbons and double layer capacitance". In: *Electrochimica Acta* 41.10 (1996), pp. 1633–1639. DOI: 10.1016/0013-4686(95)00416-5.

[Son2019] Jingke Song, Jinxing Ma, Changyong Zhang, Calvin He, and T. David Waite. "Implication of non-electrostatic contribution to deionization in flow-electrode CDI: Case study of nitrate removal from contaminated source waters". In: *Frontiers in Chemistry* 7 (2019), pp. 1–11. DOI: 10.3389/fchem.2019.00146.

[Str2004] Heiner Strathmann. *Ion-Exchange Membrane Separation Processes, Volume 9 (Membrane Science and Technology)*. 1st ed. Elsevier Science, 2004, pp. 1–348.

[Str2010] H. Strathmann. "Electrodialysis, a mature technology with a multitude of new applications". In: *Desalination* 264.3 (2010), pp. 268–288. DOI: 10.1016/j.desal.2010.04.069.

[Sus2012] Matthew E. Suss, Theodore F. Baumann, William L. Bourcier, Christopher M. Spadaccini, Klint a. Rose, Juan G. Santiago, and Michael Stadermann. "Capacitive desalination with flow-through electrodes". In: *Energy & Environmental Science* 5.11 (2012), p. 9511. DOI: 10.1039/c2ee21498a.

[Sus2013] Matthew E. Suss, Theodore F. Baumann, Marcus A. Worsley, Klint A. Rose, Thomas F. Jaramillo, Michael Stadermann, and Juan G. Santiago. "Impedance-based study of capacitive porous carbon electrodes with hierarchical and bimodal porosity". In: *Journal of Power Sources* 241 (2013), pp. 266–273. DOI: 10.1016/j.jpowsour.2013.03.178.

[Sus2015] Matthew Suss, Slawomir Porada, Xiaowei Sun, Maarten Biesheuvel, Jeyong Yoon, and Volker Presser. "Water desalination via capacitive deionization: what is it and what can we expect from it?" In: *Energy & Environmental Science* 8 (2015), pp. 2296–2319. DOI: 10.1039/C5EE00519A.

[Tan2003] Yoshinobu Tanaka, Reo Ehara, Sigeru Itoi, and Totaro Goto. "Ion-exchange membrane electrodialytic salt production using brine discharged from a reverse osmosis seawater desalination plant". In: *Journal of Membrane Science* 222.1-2 (2003), pp. 71–86. DOI: 10.1016/S0376-7388(03)00217-5.

[Tan2019] Kexin Tang, Sotira Yiacoumi, Yuping Li, and Costas Tsouris. "Enhanced Water Desalination by Increasing the Electroconductivity of Carbon Powders for High-Performance Flow-Electrode Capacitive Deionization". In: *ACS Sustainable Chemistry and Engineering* 7.1 (2019), pp. 1085–1094. DOI: 10.1021/acssuschemeng.8b04746.

[Ted2015] Michele Tedesco, Paolo Mazzola, Alessandro Tamburini, Giorgio Micale, I. David L. Bogle, Michael Papapetrou, and Andrea Cipollina. "Analysis and simulation of scale-up potentials in reverse electrodialysis". In: *Desalination and Water Treatment* 55.12 (2015), pp. 3391–3403. DOI: 10.1080/19443994.2014.947781.

[Ted2016] M. Tedesco, H. V.M. Hamelers, and P. M. Biesheuvel. "Nernst-Planck transport theory for (reverse) electrodialysis: I. Effect of co-ion transport through the membranes". In: *Journal of Membrane Science* 510 (2016), pp. 370–381. DOI: 10.1016/j.memsci.2016.03.012.

[Ted2017] M. Tedesco, H. V.M. Hamelers, and P. M. Biesheuvel. "Nernst-Planck transport theory for (reverse) electrodialysis: II. Effect of water transport through ion-exchange membranes". In: *Journal of Membrane Science* 531 (2017), pp. 172–182. DOI: 10.1016/j.memsci.2017.02.031.

[Thi2015] Gregory P. Thiel, Emily W. Tow, Leonardo D. Banchik, Hyung Won Chung, and John H. Lienhard V. "Energy consumption in desalinating produced water from shale oil and gas extraction". In: *Desalination* 366 (2015), pp. 94–112. DOI: 10.1016/j.desal.2014.12.038.

[Tia2017] Meng Tian, Yueqing Sun, Chuanfang (John) Zhang, Jitong Wang, Wenming Qiao, Licheng Ling, and Donghui Long. "Enabling high-rate electrochemical flow capacitors based on mesoporous carbon microspheres suspension electrodes". In: *Journal of Power Sources* 364 (2017), pp. 182–190. DOI: 10.1016/j.jpowsour.2017.08.001.

[Tog2019] Norihiro Togo, Keizo Nakagawa, Takuji Shintani, Tomohisa Yoshioka, Tomoki Takahashi, Eiji Kamio, and Hideto Matsuyama. "Osmotically Assisted Reverse Osmosis Utilizing Hollow Fiber Membrane Module for Concentration Process". In: *Industrial and Engineering Chemistry Research* 58.16 (2019), pp. 6721–6729. DOI: 10.1021/acs.iecr.9b00630.

[Ton2002] Xu Tongwen. “Electrodialysis processes with bipolar membranes (EDBM) in environmental protection - A review”. In: *Resources, Conservation and Recycling* 37.1 (2002), pp. 1–22. DOI: 10.1016/S0921-3449(02)00032-0.

[Ton2016] Tiezheng Tong and Menachem Elimelech. “The Global Rise of Zero Liquid Discharge for Wastewater Management: Drivers, Technologies, and Future Directions”. In: *Environmental Science and Technology* 50.13 (2016), pp. 6846–6855. DOI: 10.1021/acs.est.6b01000.

[Tur2002] Marian Turek. “Dual-purpose desalination-salt production electrodialysis”. In: *Desalination* 153 (2002), pp. 377–381. DOI: 10.1016/S0011-9164(02)01131-1.

[Tur2004] Marian Turek. “Electrodialytic desalination and concentration of coalmine brine”. In: *Desalination* 162.1-3 (2004), pp. 355–359. DOI: 10.1016/S0011-9164(04)00069-4.

[Tur2009] Marian Turek, Joanna Was, and Piotr Dydo. “Brackish water desalination in RO-single pass EDR system”. In: *Desalination and Water Treatment* 7.1-3 (2009), pp. 263–266. DOI: 10.5004/dwt.2009.710.

[Van2008] B. Van der Bruggen, M. Mänttäri, and M. Nyström. “Drawbacks of applying nanofiltration and how to avoid them: A review”. In: *Separation and Purification Technology* 63.2 (2008), pp. 251–263. DOI: 10.1016/j.seppur.2008.05.010.

[Vee2008] J. Veerman, J. W. Post, M. Saakes, S. J. Metz, and G. J. Harmsen. “Reducing power losses caused by ionic shortcut currents in reverse electrodialysis stacks by a validated model”. In: *Journal of Membrane Science* 310.1-2 (2008), pp. 418–430. DOI: 10.1016/j.memsci.2007.11.032.

[Wan2016] Miao Wang, Shujin Hou, Yong Liu, Xingtao Xu, Ting Lu, Ran Zhao, and Likun Pan. “Capacitive neutralization deionization with flow electrodes”. In: *Electrochimica Acta* 216 (2016), pp. 211–218. DOI: 10.1016/j.electacta.2016.09.026.

[Wel2005] T. J. Welgemoed and C. Frik Schutte. “Capacitive Deionization Technology™: An alternative desalination solution”. In: *Desalination* 183.1-3 (2005), pp. 327–340. DOI: 10.1016/j.desal.2005.02.054.

[Wer2016] Jay R. Werber, Chinedum O. Osuji, and Menachem Elimelech. “Materials for next-generation desalination and water purification membranes”. In: *Nature Reviews Materials* 1.no. 16018 (2016). DOI: 10.1038/natrevmats.2016.18.

[Xu2017] Xingtao Xu, Miao Wang, Yong Liu, Ting Lu, and Likun Pan. “Ultrahigh Desalinization Performance of Asymmetric Flow-Electrode Capacitive Deionization Device with an Improved Operation Voltage of 1.8 v”. In: *ACS Sustainable Chemistry and Engineering* 5.1 (2017), pp. 189–195. DOI: 10.1021/acssuschemeng.6b01212.

[Yam1969] Reiichi Yamane, Mutsumi Ichikawa, Yukio Mizutani, and Yasuharu Onoue. "Concentrated brine production from sea water by electrodialysis using ion exchange membranes". In: *Industrial and Engineering Chemistry Process Design and Development* 8.2 (1969), pp. 159–165. DOI: 10.1021/i260030a003.

[Yan2014] Yang Yang, Xueli Gao, Aiyong Fan, Lili Fu, and Congjie Gao. "An innovative beneficial reuse of seawater concentrate using bipolar membrane electrodialysis". In: *Journal of Membrane Science* 449 (2014), pp. 119–126. DOI: 10.1016/j.memsci.2013.07.066.

[Yan2016a] SeungCheol Yang, Jiyeon Choi, Jeong-gu Yeo, Sung-il Jeon, Hong-ran Park, and Dong Kook Kim. "Flow-Electrode Capacitive Deionization Using an Aqueous Electrolyte with a High Salt Concentration". In: *Environmental Science & Technology* 50.11 (2016), pp. 5892–5899. DOI: 10.1021/acs.est.5b04640.

[Yan2016b] SeungCheol Yang, Sung-il Jeon, Hanki Kim, Jiyeon Choi, Jeong-gu Yeo, Hong-ran Park, and Dong Kook Kim. "Stack Design and Operation for Scaling Up the Capacity of Flow-Electrode Capacitive Deionization Technology". In: *ACS Sustainable Chemistry & Engineering* 4.8 (2016), pp. 4174–4180. DOI: 10.1021/acssuschemeng.6b00689.

[Yan2017] SeungCheol Yang, Hong-ran Park, Jungjoon Yoo, Hanki Kim, Jiyeon Choi, Moon Hee Han, and Dong Kook Kim. "Plate-Shaped Graphite for Improved Performance of Flow-Electrode Capacitive Deionization". In: *Journal of The Electrochemical Society* 164.13 (2017), E480–E488. DOI: 10.1149/2.1551713jes.

[Yan2019] Fan Yang, Junjun Ma, Xudong Zhang, Xia Huang, and Peng Liang. "Decreased charge transport distance by titanium mesh-membrane assembly for flow-electrode capacitive deionization with high desalination performance". In: *Water Research* 164 (2019), p. 114904. DOI: 10.1016/j.watres.2019.114904.

[Yea1979] H. L. Yeager and B. Kipling. "Ionic diffusion and ion clustering in a perfluorosulfonate ion-exchange membrane". In: *Journal of Physical Chemistry* 83.14 (1979), pp. 1836–1839. DOI: 10.1021/j100477a008.

[Yoo2015] Hana Yoon, Hyung-Jin Kim, Jung Joon Yoo, Chung-Yul Yoo, Jun Hui Park, Yeong A. Lee, Woo Kyung Cho, Young-Kyu Han, and Dong Ha Kim. "Pseudocapacitive slurry electrodes using redoxactive quinone for high-performance flow capacitors: an atomic-level understanding of pore texture and capacitance enhancement". In: *Journal of Materials Chemistry A* 3 (2015), pp. 23323–23332. DOI: 10.1039/c5ta05403f.

[You2015] Mohamed Youssry, Lénaïc Madec, Patrick Soudan, Manuella Cerbelaud, Dominique Guyomard, and Bernard Lestriez. "Formulation of flowable anolyte for redox flow batteries: Rheo-electrical study". In: *Journal of Power Sources* 274 (2015), pp. 424–431. DOI: 10.1016/j.jpowsour.2014.10.076.

[Zha2012] R. Zhao, M. van Soestbergen, H. H M Rijnaarts, A. van der Wal, M. Z. Bazant, and P. M. Biesheuvel. "Time-dependent ion selectivity in capacitive charging of porous electrodes". In: *Journal of Colloid and Interface Science* 384.1 (2012), pp. 38–44. DOI: 10.1016/j.jcis.2012.06.022.

[Zha2018a] Changyong Zhang, Di He, Jinxing Ma, Wangwang Tang, and T. David Waite. "Faradaic reactions in capacitive deionization (CDI) - problems and possibilities: A review". In: *Water Research* 128 (2018), pp. 314–330. DOI: 10.1016/j.watres.2017.10.024.

[Zha2018b] Changyong Zhang, Jinxing Ma, Di He, and T. David Waite. "Capacitive Membrane Stripping for Ammonia Recovery (CapAmm) from Dilute Wastewaters". In: *Environmental Science and Technology Letters* 5.1 (2018), pp. 43–49. DOI: 10.1021/acs.estlett.7b00534.

[Zha2019a] Changyong Zhang, Jinxing Ma, and T. David Waite. "Ammonia-Rich Solution Production from Wastewaters Using Chemical-Free Flow-Electrode Capacitive Deionization". In: *ACS Sustainable Chemistry and Engineering* 7.7 (2019), pp. 6480–6485. DOI: 10.1021/acssuschemeng.9b00314.

[Zha2019b] Xudong Zhang, Fan Yang, Junjun Ma, and Peng Liang. "Effective removal and selective capture of copper from salty solution in flow electrode capacitive deionization". In: *Environmental Science: Water Research & Technology* (2019). DOI: 10.1039/c9ew00467j.